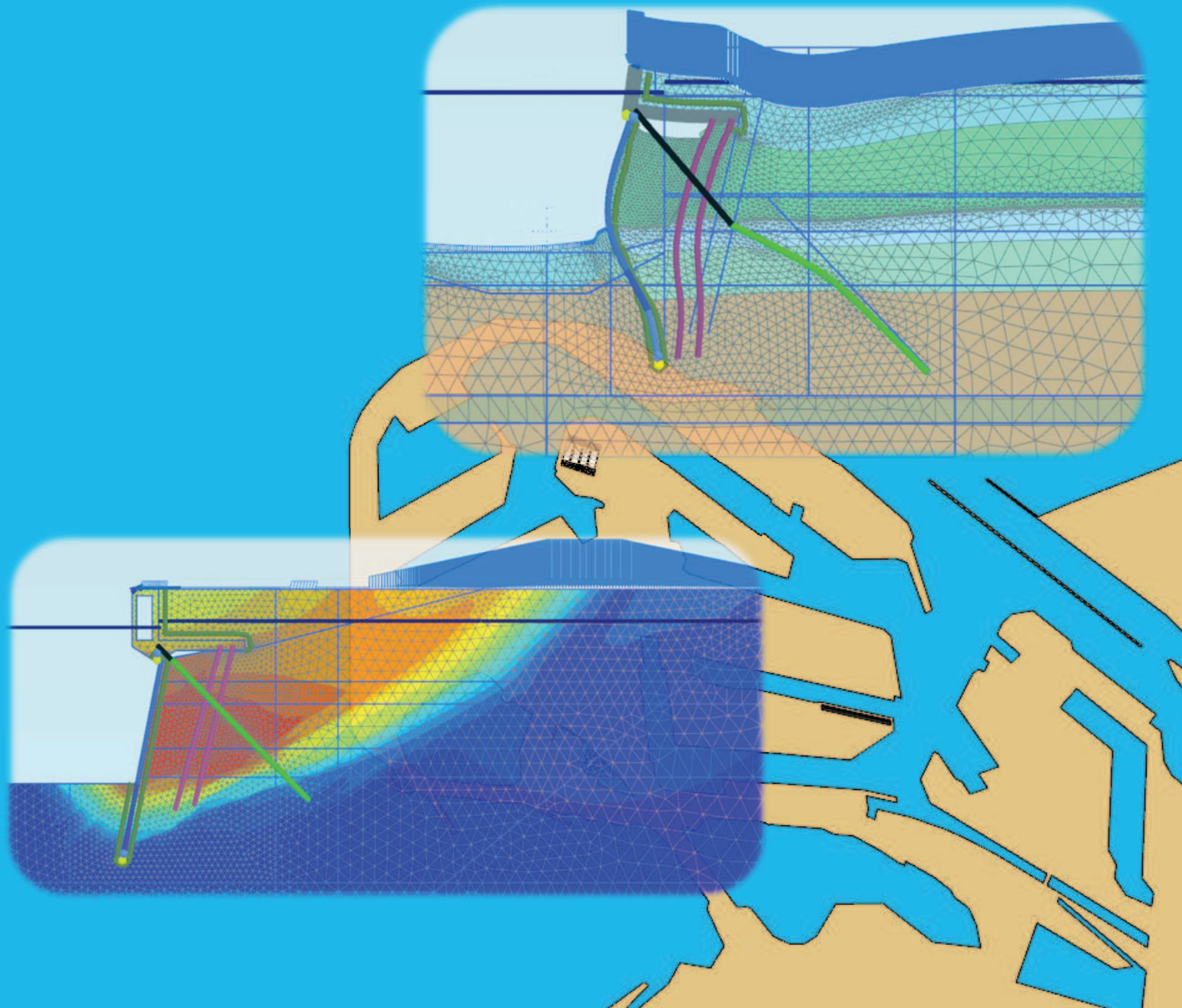


Test Loading of Quay Structures using FEM

A case study to determine the load capacity of the old Amazonehaven and the SIF quay structures



*"If you can't explain it simply, you don't understand it well enough."
Albert Einstein*

Test Loading of Quay Structures using FEM

A case study to determine the load capacity of the old Amazonehaven and the SIF quay structures

By

M. van Weringh

A thesis submitted in partial fulfilment of the requirements for the degree of

Master of Science

In

Civil Engineering

At the Delft University of Technology,

To be defended publicly on Wednesday the 29th of August, 2018 at 15:00

Title: Test Loading of Quay Structures using FEM
Subtitle: A case study to determine the load capacity of the old Amazonehaven and the SIF quay structures
Author: M. van Weringh, Mark
Student number: 4010922
Master program: Civil Engineering - Hydraulic Engineering
Specialization: Hydraulic Structures
Date: 10-08-2018
Place: Delft
Institution: Delft University of Technology & Municipality of Rotterdam

Assessment committee:

Chairman:	Prof. Dr. K.G. Gavin	TU Delft
Other:	Dr. Ir. J.G. de Gijt	TU Delft & Municipality of Rotterdam
	Dr. Ir. R.B.J. Brinkgreve	TU Delft & Plaxis bv
	Ir. H. Pacejka	Municipality of Rotterdam
	Ir. N.K.N. Mourillon	Municipality of Rotterdam
	Ir. E.J. Broos	TU Delft & Port of Rotterdam
	Ir. J. Putteman	SBE

Preface

This report contains the MSc thesis of Mark van Weringh. It was written to obtain the degree of Master of Science in the field of Civil Engineering.

The target audience of this thesis is people with a hydraulic engineering background.

Readers that are most interested in the results of this thesis and how these were obtained can find this in Chapters 9 and 10.

The author would like to express his sincere gratitude to the entire assessment committee for their input and guidance during his thesis. Especially to dr.ir. J.G. de Gijt for making this thesis possible and to dr.ir. R.B.J. Brinkgreve for his extensive feedback, especially regarding the FEM analysis.

Table of contents

Preface	i
Summary	vi
List of tables	xi
List of figures	xiii
Abbreviations	xvi
Nomenclature	xvii
1 Introduction	1
1.1 Background.....	1
1.2 Problem description	1
1.3 Objective	1
1.4 Research questions	1
1.5 Structure of this report	2
2 Literature study	3
2.1 Selected type of quay structure	3
2.2 Failure mechanisms.....	3
2.3 Soil characteristics	3
2.3.1 Relevant parameters	3
2.3.2 Stresses.....	4
2.4 Different modelling methods	7
2.4.1 Classical method	7
2.4.2 Beam on elastic foundation method	8
2.4.3 Finite Element Method	9
3 Quays of interest.....	10
3.1 Amazonehaven.....	10
3.1.1 Structural elements	10
3.1.2 Local conditions	13
3.1.3 Construction stages.....	15
3.2 SIF	16
3.2.1 Structural elements	16
3.2.2 Local conditions	18
3.2.3 Construction stages.....	21
4 Selection of the critical cross sections	22
4.1 Modifiable elements.....	22
4.2 Amazonehaven.....	23

4.2.1	Soil profiles	23
4.2.2	Water	24
4.2.3	Loads	24
4.2.4	Selected scenarios	25
4.3	SIF	28
4.3.1	Soil profiles	28
4.3.2	Water	29
4.3.3	Loads	29
4.3.4	Selected scenarios	29
5	Blum calculation	33
5.1	Amazonehaven 1	33
5.2	Amazonehaven 2	35
5.3	SIF 1	35
5.4	SIF 2	36
6	D-Sheet calculation	38
6.1	Challenges	38
6.2	Amazonehaven 1	38
6.3	Amazonehaven 2	40
6.4	SIF 1	40
6.5	SIF 2	42
7	Plaxis 2D calculation	43
7.1	Modelling of the original model of SIF 2	43
7.1.1	Soil layering	43
7.1.2	Structural elements	43
7.1.3	Loads	44
7.1.4	Water conditions	44
7.1.5	Meshing	45
7.1.6	Calculation phases	45
7.2	Sensitivity of the model	45
7.3	Amazonehaven 1	47
7.3.1	Soil layering	47
7.3.2	Structural elements	48
7.3.3	Loads	48
7.3.4	Water levels	48
7.3.5	Meshing	49

7.3.6	Calculation phases	49
7.3.7	Results.....	49
7.4	Amazonehaven 2.....	50
7.4.1	Soil layering	51
7.4.2	Structural elements	51
7.4.3	Remainder	51
7.4.4	Results.....	51
7.5	SIF 1	52
7.5.1	Soil layering	53
7.5.2	Structural elements	53
7.5.3	Calculation phases	54
7.5.4	Results.....	54
7.6	SIF 2	55
7.6.1	Soil layering	55
7.6.2	Structural elements	55
7.6.3	Calculation phases	55
7.6.4	Results.....	56
8	Model verification and validation.....	57
8.1	Comparison to other modelling methods.....	57
8.1.1	Amazonehaven.....	57
8.1.2	SIF	59
8.2	Comparison to field data.....	60
8.2.1	Deformations of the combined sheet pile wall.....	60
8.2.2	Head displacement of the M.V.-piles.....	61
8.3	Critical assessment.....	64
8.4	Conclusion	66
9	Test loading set-up	67
9.1	Respective scenarios.....	67
9.1.1	Amazonehaven.....	67
9.1.2	SIF	68
9.2	Relevant failure mechanisms	70
9.2.1	Failure of the M.V.-piles	70
9.2.2	Failure of the combined sheet pile wall	71
9.2.3	Failure of the bearing piles	72
9.2.4	Total instability.....	73

9.3	Expected results	73
9.3.1	Amazonehaven.....	73
9.3.2	SIF	74
10	Results of the test loading	75
10.1	Amazonehaven	75
10.1.1	Overview of the test loading	75
10.1.2	First failure mechanism	77
10.1.3	Second failure mechanism	78
10.1.4	Reflection with the expected results	79
10.2	SIF.....	79
10.2.1	Overview of the test loading	79
10.2.2	First failure mechanism	81
10.2.3	Second failure mechanism	82
10.2.4	Third failure mechanism	83
10.2.5	Reflection with the expected results	84
11	Discussion of the results	85
11.1	Amazonehaven	85
11.2	SIF.....	86
12	Conclusions	87
13	Recommendations	89
	References	90
	Appendices	91
A.	Maple - Reaction forces of the superstructures.....	92
B.	Maple - Blum calculations.....	101
C.	Evaluation of different modelling methods within Plaxis 2D	117
D.	Critical assessment of the Plaxis 2D models	125

Summary

Quay structures are essential for society. Through several design methodologies mankind has made structures that can withstand the forces of nature and that of mankind itself. Whether the assumptions that have been used in the design process have been just and if the boundary conditions have been correctly specified is still unknown. From this uncertainty the following question originated: How much load could the old quay structure of the Amazonehaven withstand, and how much can that of the current SIF structure withstand?

Physical load testing would be very expensive and failure of a quay structure would in most cases be unacceptable, therefore it was decided to model these structures in a FEM software. The way in which this question was treated is as follows. First a literature study was conducted to gain insight into the relevant fields of knowledge. Then, the specific quay structures were analyzed to determine the structural characteristics and local conditions. The normative cross sections of the structure were determined, after which these cross sections were used for several Blum, D-Sheet Piling, and Plaxis 2D calculations. The results of these calculations were used to further optimize the created FEM models. Next, the relevant failure mechanisms were further examined and the FEM test loading took place. The results of this test loading were then discussed, followed by the conclusions and recommendations.

During the literature study the functions and possible failure mechanisms of quay structures were determined. For the structures in question the most relevant failure mechanisms are structural failure, geotechnical failure, and overall instability. Insight was gained in the way in which surcharges are transmitted through the soil and the effect that a relieving platform (RP) has. Three different modelling methods have been considered, namely:

- A classical method – Blum;
- A beam on an elastic foundation method – D-Sheet Piling;
- A FEM – Plaxis 2D.

The old Amazonehaven structure was located on the Maasvlakte while the SIF structure is located on the Maasvlakte 2. Both quay structures consist of a combined sheet pile wall (CSPW), a reinforced concrete RP, M.V.-piles, and two rows of bearing piles. The CSPW is connected to the RP by means of a cast iron saddle. The table below specifies the structural elements and boundary conditions to some extent.

Element of interest	Amazonehaven	SIF
Primary tubular piles of the combined sheet pile wall	Ø1420 mm Length = 30-32 m Thickness = 15.4-22 mm C.t.c. = 2.980 m Inclination = 5:1	Ø1420 mm Length = 32-37 m Thickness = 21/23 mm C.t.c. = 3.294 m
Relieving platform	Height = 11 m Length = 18 m Width = 44.7 m	Height = 7.1 m Length = 18.1 m Width = 23.06 m
M.V.-piles	Length = 30-36 m C.t.c. = 2.060 m O = 1.72 m Inclination = 42.5° / 47.5°	Length = 52.2-58.5 m C.t.c. = 2.882/5.765 m O = 2.2 m Inclination = 42.5° / 47.5°
Concrete bearing piles	Length = 22-28 m Square prefab piles Width = 450 mm	Length = 29-35 m Screw injection piles Ø609/850 mm

	Inclination = 3.5:1/4:1	Inclination = 3.5:1/4:1
Construction depth	NAP-25.5 m	NAP-25 m
Ground level	NAP+5.0 m	NAP+5.1 m
Soil	Mostly moderately dense to dense sand with relatively thick soft soil layers at NAP-10 m and NAP-20 m	The same as the Amazonehaven
Surcharge	Triangular surcharge from 90 kN/m ² up to a maximum of 450 kN/m ² . 38-107 m from the edge of the RP	100 kN/m ² everywhere on the landside. 36 kN/m ² on the waterside (due to remolded soil as a result of spud can loading)

The construction process of the SIF structure included the replacement of a thick clay layer on the water side. To enable this replacement the groundwater level was lowered to NAP-6.0 m. In determining the cross sections that would be modelled it was decided to use the actual structures as a starting point. Based on the soil profiles and the acting loads, 2 different scenarios with 2 variations each were selected for both quay structures. For the Amazonehaven the soil profiles with the most and that with the least soft soil layers were selected. For the SIF the one with the thickest and the one with the smallest clay layer were chosen. The characteristics of the structural elements were found based on the location of the selected soil profiles.

The first modelling method that was applied was the Blum method. This method determined the needed embedded depth of the CSPW by using a set of boundary conditions. Based on this depth, the structural forces were determined. The total stress distribution on the CSPW was determined by combining the individual contributions of the water level difference, soil profiles, external loads, and effect of the bearing piles. This total stress distribution was processed in a Maple sheet which resulted in the structural forces. To make the scenarios compatible with the created Maple sheet and to not over complicate things, several adjustments were made. For the Amazonehaven structure the triangular surcharge was simplified to a rectangular one. For the SIF structure 55% of the remolded soil was present instead of a surcharge of 55% of the effective weight. For both structures it was assumed that the water level difference was present over the entire length of the CSPW. The total stress distribution was averaged over the length, resulting in a triangular distribution on the water side and both a rectangular and a triangular distribution on the land side.

The second modelling method that was applied was the software D-Sheet Piling. Within this method only vertical retaining walls could be modelled. It was assumed that the increase in both the active and passive soil pressure coefficients would somewhat cancel each other out. The RP was modelled by removing the chunk of soil and the loads that would work upon it. The M.V.-piles were modelled as translational springs, their stiffness was determined based on the acting load on a single M.V.-pile and the corresponding displacements that were found during load testing of these piles.

The final modelling method was the modelling in Plaxis 2D, a FEM software. At first an original model was created based on the structural properties of the respective scenarios. The boundaries of the model were chosen so that they did not create boundary disturbances. The finite element mesh was refined in the areas which were closer to the structure. The model was subjected to several modelling modifications to determine the sensitivity to each modification.

Next, the models were verified by comparing the results of the FEM models to that of the Blum and D-Sheet Piling methods, field data, and a subsection to a critical assessment. The comparison to other modelling methods showed both great similarities and some deviations, these deviations could however be explained by the assumptions that were needed to make the modelling methods compatible with the structures and the fact that the CSPW was calculated separately from the rest of the structure. The models were compared to field measurements regarding the deflection of the CSPW and test loading scenarios of actual M.V.-piles. The modelled displacements of the CSPW were a factor 2 larger than that of the field measurements. It is highly likely that this is due to the way in which the field measurements were performed and the fact that characteristic values were used for the soil parameters. The results of the M.V.-pile test loading were very similar to that of the actual field measurements. The critical assessment showed that the relevant failure mechanisms were incorporated into the models correctly. There is still too little data to determine whether drained or undrained soil conditions should be applied to the thicker clay layers in the models. This however has little effect on the performed analysis in regard to the field measurements since there was no surcharge on top of the soil at the time of the test loading. In this thesis drained soil conditions have been used.

Based on the initial results, one scenario was selected for both the Amazonehaven structure and the SIF structure, both scenarios contained relatively thick clay layers. It was decided to only increase the magnitude of the bulk surcharge of the scenarios. The most relevant failure mechanisms are that of the M.V.-piles (both structural and geotechnical), the normal stress capacity of the CSPW, and total instability.

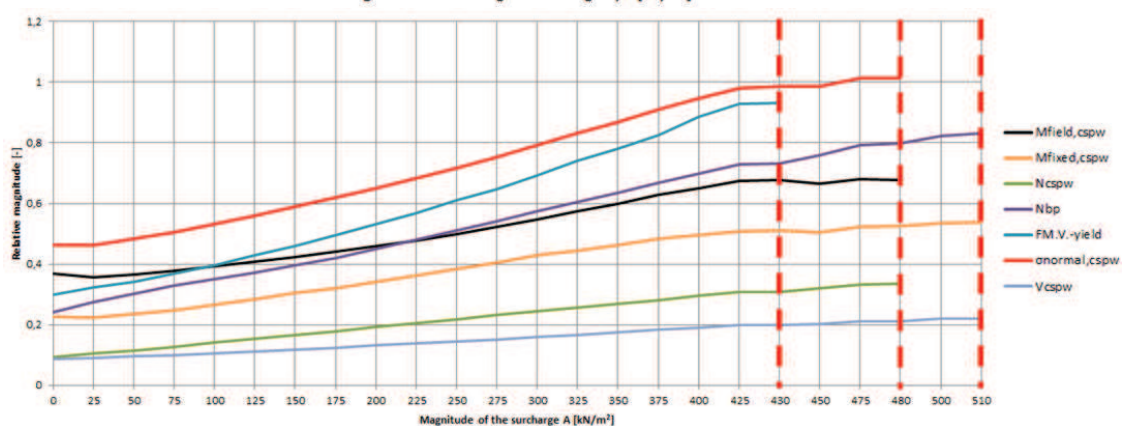
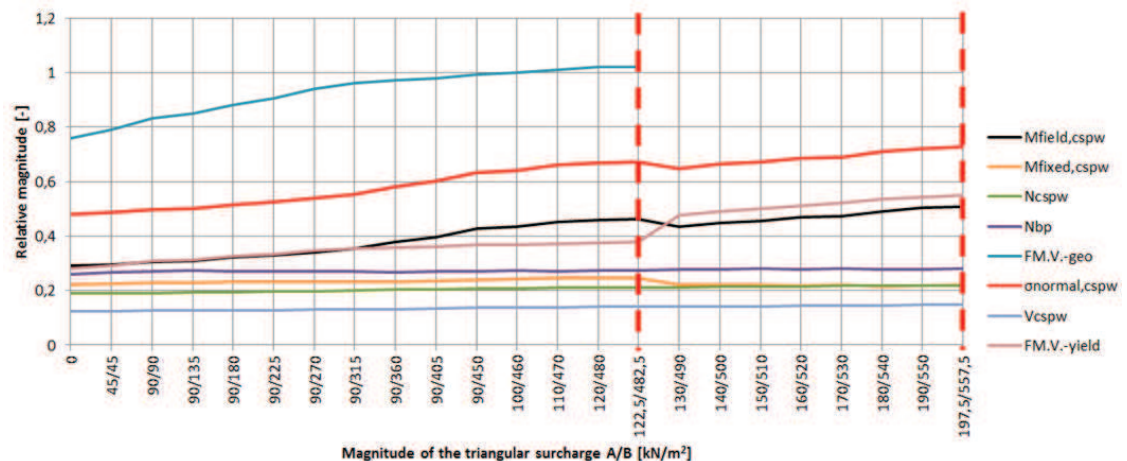
The first failure of the Amazonehaven model occurred at a load that was 32.5 kN/m^2 higher than the design load. The mechanism was induced by geotechnical failure of the M.V.-piles, which is largely dependent on the maximum allowable skin friction of the pile. The positive effect that the surcharge has on this skin friction has not been taken into consideration in this thesis. The final failure mechanism was a total instability one, it occurred at a load that was 107.5 kN/m^2 higher than the design load. For SIF the first failure of the model occurred at a surcharge of 430 kN/m^2 , this was induced by structural failure of the M.V.-piles. After this the model failed at 480 kN/m^2 due to structural failure of the CSPW, and at 510 kN/m^2 due to local geotechnical failure of a soil body on the waterside. The development of the structural forces in several structural elements was analyzed by post processing the results of the FEM models. To effectively represent the effect, the results have been normalized with respect to the values at which the structural elements would fail, should the structural force exceed it. The table below presents the structural capacities of the structural elements.

Variable	Description	Amazonehaven	SIF
$M_{\text{field,CSPW}}$ [kNm/m]	Maximum bending moment in the CSPW	5,451.8	7,614.2
$M_{\text{fixed,CSPW}}$ [kNm/m]	Maximum fixed end bending moment in the CSPW	5,018.4	7,276.0
N_{CSPW} [kN/m]	Maximum normal force in the CSPW	14,351.6	20,469.3
V_{CSPW} [kN/m]	Maximum shear force in the CSPW	4,331.9	6,046.0
N_{BP} [kN/m]	Maximum normal force in the bearing piles	6,795.3 kN/m	10,063.9
$F_{\text{M.V.-piles}}$	Maximum normal force in the	Geotechnical: 1,239.9	Geotechnical: 2,969.8

[kN/m]	M.V.-piles	Yielding: 3,360.4	Yielding: 2,904.5
--------	------------	-------------------	-------------------

In the figures below the normalized structural reactions to the test loading of the Amazonehaven (top) and the SIF (bottom) models are presented. The horizontal axis shows the magnitude of the bulk surcharge in kN/m^2 , the vertical axis represents the relative magnitude with respect to the structural capacities, e.g. a relative magnitude of 0.5 for $M_{\text{field,CSPW}}$ would mean that the maximum bending moment in the CSPW is equal to half the value at which it would fail. The vertical red dashed lines in the figures represent the point at which the model failed. The other plotted lines are the normalized results with respect to the structural capacities of:

- $M_{\text{field,CSPW}}$ = The maximum bending moment in the CSPW
- $M_{\text{fixed,CSPW}}$ = The fixed end bending moment in the CSPW
- N_{CSPW} = The maximum normal force in the CSPW
- N_{bp} = The maximum normal force in the bearing piles
- $F_{\text{M.V.-geo/yield}}$ = The maximum normal force in the M.V.-piles with respect to geotechnical bearing capacity/yielding capacity
- $\sigma_{\text{normal,CSPW}}$ = The normal stress capacity of the CSPW
- V_{CSPW} = The maximum shear force in the CSPW



At the surcharge that caused the models to fail the maximum horizontal deflection of the CSPW was in the order of 300 mm for the Amazonehaven model and in the order of 400 mm for the SIF model.

An understanding of the structure and the reaction that this would have to specific local conditions is critical in the validation of a model. The models were validated through comparison with field data, other modelling methods and a critical assessment. The results of

the different modelling methods with the FEM results in regard to $M_{\text{field,CSPW}}$ and T_{anchor} showed a deviation of ca. 20% for Amazonehaven and ca. 30% for SIF. These deviations could be explained through the assumptions and limitations that were needed to make the structures compatible with the other methods. One of the differences between FEM and the other modelling methods is the fact that the entire structure is coupled in FEM. Another major difference is the use of constitutive soil models that FEM allows for.

According to the FEM models, the Amazonehaven fails at a bulk surcharge of 122.5/482.5 kN/m² and the SIF at a bulk surcharge of 430 kN/m². For the Amazonehaven the M.V.-piles however reached their limit state before the design loading conditions had been reached. Even though the model had not yet failed at the design loading conditions, it was deemed unacceptable for a structural element to have reached its limit state itself. It was therefore concluded that the Amazonehaven could not withstand its design loading conditions. If the effect of the surcharge on the geotechnical bearing capacity of the M.V.-piles had been implemented, the first failure of the model might have occurred at a larger surcharge. The SIF structure however could withstand its design loading conditions.

More research should be done into 3D effects, undrained soil behaviour, and the design of the M.V.-piles at the Amazonehaven. This could all be done with the use of a 3D FEM software such as Plaxis 3D. Research should be carried out into the effective length of anchor elements of quay structures that make use of RPs. It should also be verified if the anchor elements of structures that have been constructed in the same period as the Amazonehaven have a sufficient length. The effect of the surcharges on the geotechnical bearing capacity of the M.V.-piles should be researched further.

List of tables

Table 2-1 - Relevant soil parameters	3
Table 2-2 - The effect of surcharges on soil stresses	5
Table 3-1 - Specifications of the structural elements of the Amazonehaven structure.....	11
Table 3-2 - Water levels corresponding to the Amazonehaven structure [18].....	13
Table 3-3 - Soil parameters at the Amazonehaven structure [17]	13
Table 3-4 - Loads on the Amazonehaven structure.....	14
Table 3-5 - Construction stages of the Amazonehaven structure.....	15
Table 3-6 - Specifications of the structural elements of the SIF structure	16
Table 3-7 - Design water levels [m+NAP] [11]	18
Table 3-8 - Soil layer properties [12].....	20
Table 3-9 - Characteristics of the soil zones [14].....	20
Table 3-10 - Predicted corrosion over 50 years for SIF [11].....	20
Table 3-11 - Loads on the structure	21
Table 3-12 - Construction stages of the SIF structure	21
Table 4-1 - Possible modifications of the local conditions	22
Table 4-2 - Soil profile characteristics	23
Table 4-3 - Soil characteristics belonging to soil profile 6.....	26
Table 4-4 - Soil characteristics belonging to soil profile 5.....	27
Table 4-5 - Level of the top of the soil layers [m+NAP]	28
Table 4-6 - Relevant scenarios in regard to the water levels in m+NAP	29
Table 4-7 - Soil characteristics belonging to zone B.....	30
Table 4-8 - Soil characteristics belonging to zone C	31
Table 5-1 - Representative values of the unknowns according to Blum for Amazonehaven 1	34
Table 5-2 - Representative values of the unknowns according to Blum for Amazonehaven 2	35
Table 5-3 - Representative values of the unknowns according to Blum for SIF 1	36
Table 5-4 - Representative values of the unknowns according to Blum for SIF 2.....	37
Table 6-1 - Characteristics of varying cross sections at Amazonehaven 1	39
Table 6-2 - D-Sheet results of Amazonehaven 1a & 1b	40
Table 6-3 - D-Sheet results of Amazonehaven 2a & 2b	40
Table 6-4 - Characteristics of the varying cross sections at SIF 1a & 1b	41
Table 6-5 - D-Sheet results of SIF 1a & 1b.....	41
Table 6-6 - Characteristics of the varying cross sections at SIF 2a & 2b	42
Table 6-7 - D-Sheet results of SIF 2a & 2b.....	42
Table 7-1 - Soil layering and characteristics for SIF 2	43
Table 7-2 -Structural forces and displacements of the original SIF model	46
Table 7-3 - Soil characteristics for Amazonehaven 1	47
Table 7-4 - Structural characteristics of Amazonehaven 1	48
Table 7-5 - Plaxis 2D results of Amazonehaven 1.....	50
Table 7-6 - Soil characteristics for Amazonehaven 2	51
Table 7-7 - Structural characteristics of Amazonehaven 2	51
Table 7-8 - Plaxis 2D results of Amazonehaven 2.....	52
Table 7-9 - Additional soil characteristics for SIF.....	53
Table 7-10 - Structural characteristics of SIF 1.....	53
Table 7-11 - Plaxis 2D results of SIF 1	54
Table 7-12 - Soil layer positions for SIF 2.....	55
Table 7-13 - Structural characteristics of SIF 2.....	55

Table 7-14 - Plaxis 2D results of SIF 2	56
Table 8-1 - Results of the different modelling methods for Amazonehaven	57
Table 8-2 - Discussion about the differences for Amazonehaven	58
Table 8-3 - Results of the different modelling methods for SIF	59
Table 8-4 - Discussion about the differences for SIF	60
Table 8-5 - Comparison of the field data and the model results for SIF 2	61
Table 8-6 - Critical assessment of the Plaxis 2D models	64
Table 9-1 - Magnitude of the surcharge per load step for Amazonehaven	68
Table 9-2 - Magnitude of the surcharge per load step for SIF	70
Table 9-3 - Structural characteristics of the M.V.-piles	71
Table 9-4 - Structural characteristics of the combined sheet pile walls	72
Table 9-5 - Structural characteristics of the bearing piles.....	73
Table 9-6 - Structural capacities and acting forces for Amazonehaven	73
Table 9-7 - Structural capacities and acting forces for SIF	74
Table 10-1 - Structural capacities of the structural elements for Amazonehaven	75
Table 10-2 - Structural capacities of the structural elements for SIF	80

List of figures

Figure 2-1 - Soil pressure coefficients in relation to deformations [4].....	5
Figure 2-2 - Effect of an infinite load on the vertical soil stresses [2].....	5
Figure 2-3 - Effect of a finite load on the vertical soil stresses [2]	6
Figure 2-4 - Effect of an infinite load on the vertical soil stresses [2].....	6
Figure 2-5 - Effect of a finite load on the vertical soil stresses [2]	6
Figure 2-6 - The effect of a relieving platform on soil stresses [1]	7
Figure 2-7 - Free and fixed earth support	7
Figure 2-8 - Assumption regarding the soil pressures	8
Figure 2-9 - Simplification soil pressure coefficients.....	8
Figure 2-10 - Boundary conditions Blum method	8
Figure 2-11 - Soil schematization of a beam on elastic foundation	8
Figure 2-12 - Relation between the horizontal soil pressure and the displacement [5].....	9
Figure 3-1 - Position of the quay structures, Source: Google Maps	10
Figure 3-2 - Position of Amazonehaven (right) and SIF (left), Source: Google Maps	10
Figure 3-3 - Top view of the Amazonehaven structure	10
Figure 3-4 - Side view of the saddle, dimensions in mm	11
Figure 3-5 - Top view of the saddle, dimensions in mm	11
Figure 3-6 - Overview of the Amazonehaven structure	12
Figure 3-7 - Overview of the saddle element	12
Figure 3-8 - Area in which CPTs were carried out, Source: Google maps	13
Figure 3-9 - Profile of the soil layering [8]	14
Figure 3-10 - Representation of the acting loads [16].....	15
Figure 3-11 - Top view saddle [10]	17
Figure 3-12 - Side view saddle [10]	17
Figure 3-13 - Side view saddle [10]	17
Figure 3-14 - Connection with the saddle [5]	17
Figure 3-15 - Overview of the structure	18
Figure 3-16 - Illustration of the spud can penetration [20]	19
Figure 3-17 - Overview of the RP compartments and different soil zones of the SIF structure	19
Figure 3-18 - Soil structure along the quay structure [12].....	19
Figure 4-1 - Profile 6, load transfer illustration	24
Figure 4-2 - Projected mobile crane load.....	25
Figure 4-3 - Projected tower crane load.....	25
Figure 4-4 - Projected bridge crane load	25
Figure 4-5 - Schematization superstructure	25
Figure 4-6 - Amazonehaven 1a	27
Figure 4-7 - Amazonehaven 1b	27
Figure 4-8 - Amazonehaven 2a	28
Figure 4-9 - Amazonehaven 2b	28
Figure 4-10 - Reaction forces of the superstructure	29
Figure 4-11 - SIF 1a	30
Figure 4-12 - SIF 1b	30
Figure 4-13 - SIF 2a	32
Figure 4-14 - SIF 2b	32
Figure 5-1 - Simplification of the surcharge	33
Figure 5-2 - Determination of the horizontal stress distribution at Amazonehaven 1	34

Figure 5-3 - Blum schematization Amazonehaven 1	34
Figure 5-4 - Blum schematization Amazonehaven 2	35
Figure 5-5 - Blum schematization SIF 1a.....	36
Figure 5-6 - Blum schematization SIF 1b.....	36
Figure 5-7 - Blum schematization SIF 2a.....	36
Figure 5-8 - Blum schematization SIF 2b.....	36
Figure 6-1 - D-Sheet model of Amazonehaven 1a	39
Figure 6-2 - D-Sheet model of Amazonehaven 1b	39
Figure 6-3 - D-Sheet results Amazonehaven 1a	39
Figure 6-4 - D-Sheet results Amazonehaven 1b	39
Figure 6-5 - D-Sheet model of Amazonehaven 2a	40
Figure 6-6 - D-Sheet model of Amazonehaven 2b	40
Figure 6-7 - D-Sheet results Amazonehaven 2a	40
Figure 6-8 - D-Sheet results Amazonehaven 2b	40
Figure 6-9 - D-Sheet model of SIF 1a	41
Figure 6-10 - D-Sheet model of SIF 1b.....	41
Figure 6-11 - D-Sheet results of SIF 1a	41
Figure 6-12 - D-Sheet results of SIF 1b.....	41
Figure 6-13 - D-Sheet model of SIF 2a.....	42
Figure 6-14 - D-Sheet model of SIF 2b.....	42
Figure 6-15 - D-Sheet results of SIF 2a.....	42
Figure 6-16 - D-Sheet results of SIF 2b.....	42
Figure 7-1 - Original Plaxis 2D model for SIF 2	43
Figure 7-2 - Mesh of the original SIF 2 model.....	45
Figure 7-3 - Result of the model input sensitivity analysis.....	46
Figure 7-4 - Plaxis 2D model of Amazonehaven 1	47
Figure 7-5 - Mesh of Amazonehaven 1.....	49
Figure 7-6 - Deformed mesh of Amazonehaven 1a, scaled up 20 times	50
Figure 7-7 - Deformed mesh of Amazonehaven 1b, scaled up 20 times	50
Figure 7-8 - Deformed mesh of Amazonehaven 2a, scaled up 20 times	52
Figure 7-9 - Deformed mesh of Amazonehaven 2b, scaled up 20 times	52
Figure 7-10 - Plaxis 2D model of SIF 1.....	53
Figure 7-11 - Deformed mesh of SIF 1a, scaled up 50 times.....	54
Figure 7-12 - Deformed mesh of SIF 1b, scaled up 50 times.....	54
Figure 7-13 - Deformed mesh of SIF 2a, scaled up 50 times.....	56
Figure 7-14 - Deformed mesh of SIF 2b, scaled up 50 times.....	56
Figure 8-1 - Effective length of the M.V.-piles.....	59
Figure 8-2 - Loading due to the bearing piles	59
Figure 8-3 - Comparison of the field measurements to the model output of SIF 2.....	61
Figure 8-4 - Modified model for the M.V.-pile load testing for Amazonehaven.....	62
Figure 8-5 - Comparison of the M.V.-pile load testing for Amazonehaven.....	62
Figure 8-6 - Modified model for the M.V.-pile load testing for SIF	63
Figure 8-7 - Comparison of the M.V.-pile load testing for SIF	63
Figure 9-1 - Final Plaxis 2D model for Amazonehaven	67
Figure 9-2 - Test loading set-up for Amazonehaven	68
Figure 9-3 - Final Plaxis 2D model for SIF.....	68
Figure 9-4 - Test loading set up for SIF	69

Figure 9-5 - Cross section of an M.V.-pile [16]	70
Figure 10-1 - Calculation phases of the Amazonehaven model	75
Figure 10-2 - Structural reactions to the test loading of Amazonehaven.....	76
Figure 10-3 - Horizontal deflections of the CSPW during the test loading of Amazonehaven .	77
Figure 10-4 - Mobilized skin friction along the M.V.-piles	77
Figure 10-5 - Failure points after the 1 st failure of the Amazonehaven model occurred.....	78
Figure 10-6 - Deformed mesh after the 1 st failure of the Amazonehaven model occurred, scaled up 20 times	78
Figure 10-7 - Failure points after the 2 nd failure of the Amazonehaven model occurred.....	78
Figure 10-8 - Deformed mesh after the 2 nd failure of the Amazonehaven model occurred, scaled up 20 times	79
Figure 10-9 - Calculation phases of the SIF model	79
Figure 10-10 - Structural reactions to the test loading of SIF	80
Figure 10-11 - Deflections of the CSPW during the test loading of SIF	81
Figure 10-12 - Bending moment distribution of the M.V.-piles at the first failure mechanism of SIF	81
Figure 10-13 - Failure points after the 1 st failure of the SIF model occurred	82
Figure 10-14 - Deformed mesh after the 1 st failure of the SIF model occurred, scaled up 20 times.....	82
Figure 10-15 - Failure points after the 2 nd failure of the SIF model occurred	83
Figure 10-16 - Deformed mesh after the 2 nd failure of the SIF model occurred, scaled up 20 times.....	83
Figure 10-17 - Failure points after the 3 rd failure of the SIF model occurred.....	84
Figure 10-18 - Deformed mesh after the 3 rd failure of the SIF model occurred, scaled up 20 times.....	84

Abbreviations

B.O.S.	Bottom of structure
C.t.c.	Center to center
ca.	Circa
CPT	Cone penetration test
CSPW	Combined sheet pile wall
e.g.	Exempli gratia – for example
FEA	Finite element analysis
FEM	Finite element method
i.e.	Id est – that is
M.V.	Müller Verpress
NAP	Normaal Amsterdams peil
NGD	Nautical guaranteed depth
OCR	Overconsolidation ratio
POP	Pre overburden pressure
RP	Relieving platform
SAAF	Shape accel array field
SLS	Serviceability limit state
T.O.S.	Top of structure
TSPW	Temporary sheet pile wall

Nomenclature

Symbol	Unit	Description
c	$[\text{kN/m}^2]$	Cohesion
c_u	$[\text{kN/m}^2]$	Undrained shear strength
E_{50}	$[\text{kN/m}^2]$	Tri-axial loading stiffness
E_{oed}	$[\text{kN/m}^2]$	Oedometer loading stiffness
E_{ur}	$[\text{kN/m}^2]$	Tri-axial unloading stiffness
f_y	$[\text{N/mm}^2]$	Yield strength
I_y	$[\text{m}^4]$	Second moment of inertia
G_0^{ref}	$[\text{kN/m}^2]$	Initial shear modulus
G_s	$[\text{kN/m}^2]$	Secant shear modulus
k	$[\text{kN/m}]$	Hydraulic conductivity
K_0	$[-]$	Initial horizontal stress coefficient
K_a	$[-]$	Active horizontal stress coefficient
K_p	$[-]$	Passive horizontal stress coefficient
l_{buckling}	$[\text{m}]$	Buckling length of the system
O	$[\text{m}]$	Circumference of the element in question
p	$[\text{kN/m}^2]$	Pore pressure
q_c	$[\text{kN/m}^2]$	Cone resistance
W_p	$[\text{m}^3]$	Plastic section modulus of elasticity
$\gamma_{0.7}$	$[-]$	Shear strain level where $G_s=0.7G_0^{\text{ref}}$
γ_s	$[\text{kN/m}^3]$	Saturated volumetric weight
γ_{unsat}	$[\text{kN/m}^3]$	Unsaturated volumetric weight
γ_w	$[\text{kN/m}^3]$	Volumetric weight of water
$\bar{\delta}$	$[\text{°}]$	Wall friction angle
ϑ_a	$[\text{°}]$	Load transferring angle
σ	$[\text{kN/m}^2]$	Soil stress
σ'	$[\text{kN/m}^2]$	Effective soil stress
φ	$[\text{°}]$	Angle of internal friction
\emptyset	$[\text{m}]$	Diameter

1 Introduction

1.1 Background

The transport of cargo has been and continues to be of large importance to society. Transport by sea is one of many possibilities that allows society to meet the transportation demand. At the locations where land and water meet each other quay structures are needed to ensure that the safety of both the people and the cargo is not compromised.

Rotterdam has the largest port in all of Europe, the 5th biggest in the world. It manages to keep this position by expanding seawards. The large retaining heights in combination with the dimensions of the vessels that make use of the quay structures create challenges which the designers of quay structures must overcome.

A number of resources and design methodologies can be used to design a quay structure, the most important aspect in the design process is predicting how the soil is going to interact with the structure and the loads that act upon it. A method that deals specifically with this interaction is the Finite Element Method (FEM) or Finite Element Analysis (FEA).

1.2 Problem description

Quay structures are designed to withstand a certain load. In their design process numerous assumptions, conservative approaches, material factors, and safety factors are applied to ensure that the structure will be safe enough. Even though the structures are designed very conservatively, little is known about the actual load capacity of a quay structure. Physical load testing would both be extremely expensive and the loss of a quay structure due to failing would in most cases be unacceptable.

1.3 Objective

The objective of this MSc thesis is to create and validate FEM models for the old Amazonehaven and the current SIF quay structures and use these models to determine what their reaction to extreme loading situations will be. This should result in the maximum load that these structures can withstand without failing and also determine the specific failure mechanisms that are relevant for these structures.

1.4 Research questions

In order to reach the objective the following research questions, and their respective sub-research questions, were formulated:

How should FEM be applied to the specific quay structures?

- To what extent can relevant failure mechanisms occur in FEM?
- What soil model best fits the specific design conditions?
- What is needed to validate the FEM models?

How does FEM compare to conventional design methods?

- What are the differences between FEM and conventional design methods?

What is the maximum load that the specific quay structures can withstand?

- Which loads are critical for the safety?
- What are the critical cross sections of the structures?

- What are the critical failure mechanisms for these type of quay structures?
- Can the quay structures withstand their design loading conditions?

1.5 Structure of this report

The structure of this report is as follows. Chapter 1 contains the introduction and describes the presented problem, the approach which has been applied to this problem, and the desired results. In chapter 2 the results of the literature study are presented, which give a general idea on the topics that will be covered within this thesis. Chapter 3 gives more detailed information on the quay structures that will be analyzed while chapter 4 determines the critical cross sections of each structure. The selected cross sections will then be subjected to the Blum method in chapter 5, modelled in D-Sheet Piling in chapter 6, and modelled in Plaxis 2D in chapter 7. These chapters also present the initial results of these respective methods. The created FEM models are verified, validated, and modified accordingly in chapter 8. Chapter 9 shows how the test loading will take place for the respective quay structures and elaborates on the expected results. The actual results of the test loading are presented and interpreted in chapter 10. Chapter 11 discusses the results, followed by the conclusions in chapter 12 and the recommendations in chapter 13.

2 Literature study

Prior to starting the actual research, a literature study was conducted to get familiar with the different topics that needed to be addressed. This chapter presents the relevant information from that literature study.

2.1 Selected type of quay structure

There are a lot of different types of quay structure. During this thesis the only type that will be discussed is the combined sheet pile wall (CSPW) with a relieving platform (RP).

The functions of this type of structure are:

- Providing berthing facilities;
- Soil retaining;
- Water retaining;
- Load bearing.

The function of the RP is to decrease the load that acts on the CSPW, this will be discussed later in this chapter.

2.2 Failure mechanisms

Possible failure mechanisms are:

- Insufficient horizontal stability – The structure will simply be pushed away due to the resisting forces being smaller than the driving forces;
- Insufficient vertical stability – The vertical soil stress exceeds the bearing capacity of the soil;
- Overall instability – With large retaining heights in relation to the embedded depths and/or large surcharges the entire structure and the soil around it can experience total instability such as a sliding plane;
- Buckling of the CSPW – The normal force that acts on the CSPW becomes too large for the system to regain its equilibrium position after a deformation has occurred;
- Structural failure – The individual structural elements are not able to withstand the load that is exerted on them.

2.3 Soil characteristics

2.3.1 Relevant parameters

The parameters that are of importance to this thesis are presented in Table 2-1.

Table 2-1 - Relevant soil parameters

Parameter	Symbol	Description
Volumetric weight	$\gamma_s / \gamma_{\text{unsat}}$	The weight of a soil body per unit volume. γ_s stand for the saturated volumetric weight (under the groundwater level) while γ_{unsat} stands for the unsaturated volumetric weight (above the groundwater level).
Oedometer modulus of elasticity	E_{oed}	The oedometer modulus of elasticity for primary compression [23].
Hydraulic conductivity	k	A property that describes the ease with which fluids can pass through the soil. A high value of k indicates very permeable soil, while a low value means relatively impermeable soil.

Cohesion	c	The component of shear strength that is independent of friction between particles.
Angle of internal friction	φ	A representation of the ability to withstand shear stress. It is the angle between the normal effective stress and the shear stress just before failure.
Wall friction angle	δ	The largest value that the angle of the resulting stress of the soil pressure can take with the normal stress of a certain surface. This parameter is generally related to the angle of internal friction.

2.3.2 Stresses

2.3.2.1 Normal and shear stresses

Soil can only transfer normal compressive stresses and shear stresses that are small in relation to the normal stress [4].

2.3.2.2 Water pressure

Since soil contains water a certain hydraulic pressure is present, this pressure is hydrostatic. The pore pressure is only dependent of the piezo metric height and the depth. In the formula below, p represents the pore pressure and d is the difference between the depth and the piezo metric level [4].

$$p = \gamma_w * d$$

The soil will become more compacted due to loading, this causes the porosity of the soil to decrease. Because of this decreased porosity the water in the soil has to be transported out of the soil. When a soil has a low hydraulic conductivity in regard to the loading time this can lead to drastically increased pore pressures. This phenomenon is also called undrained soil behavior.

2.3.2.3 Effective stress

The deformations in a soil sample are almost completely determined by the forces in the contact points of the grains. The grains themselves are surrounded by water, thus pore pressure is present everywhere. This results in what Terzaghi described as an effective stress σ' which is equal to the total stress minus the pore pressure [4].

$$\sigma' = \sigma - p$$

2.3.2.4 Horizontal stress

William Rankine (1857) found that there is a relation between the effective vertical stress in a soil and the acting horizontal stress. K_0 is the relation between the initial horizontal and vertical stress under conditions of one-dimensional compression. K_a and K_p are theoretical values that represent the failure stress states in active and passive stress states respectively. This can be expressed as follows [2]:

$$K_0 = 1 - \sin \varphi \quad (J. Jaky, 1948)$$

$$K_a = \frac{1 - \sin \varphi}{1 + \sin \varphi}; \quad K_p = \frac{1 + \sin \varphi}{1 - \sin \varphi} \quad (Rankine, 1857)$$

$$K_a = \frac{\sin^2(\alpha + \varphi)}{\sin^2 \alpha * \sin(\alpha - \delta) \left[1 + \sqrt{\frac{\sin(\varphi + \delta) * \sin \varphi - \beta}{\sin(\alpha - \delta) * \sin(\alpha + \beta)}} \right]} \quad (Coulomb, 1776)$$

$$K_p = \frac{\sin^2(\alpha - \varphi)}{\sin^2 \alpha * \sin(\alpha - \delta) \left[1 - \sqrt{\frac{\sin(\varphi - \delta) * \sin \varphi + \beta}{\sin(\alpha - \delta) * \sin(\alpha + \beta)}} \right]} \quad (\text{Coulomb, 1776})$$

$\alpha = \text{inclination of the wall}; \beta = \text{inclination of the soil level}$

$$\sigma'_{h,0} = K_0 * \sigma'_v; \sigma'_{h,min} = K_a * \sigma'_v - 2 * c * \sqrt{K_a}; \sigma'_{h,max} = K_p * \sigma'_v + 2 * c * \sqrt{K_p}$$

K_0 is valid for the situation in which the soil is undisturbed, its value was proposed by J. Jaky (1948). K_a is valid for situation in which the soil becomes less compacted and K_p for when the soil becomes more compacted. This is also shown in Figure 2-1, the horizontal axis in this figure represents the displacements while the vertical axis represents the horizontal soil pressure coefficient..

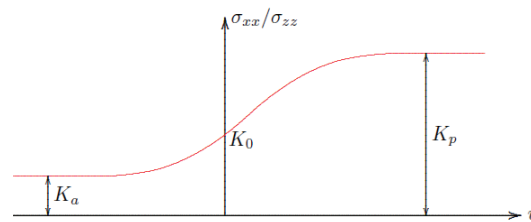


Figure 2-1 - Soil pressure coefficients in relation to deformations [4]

2.3.2.5 The effect of surcharges

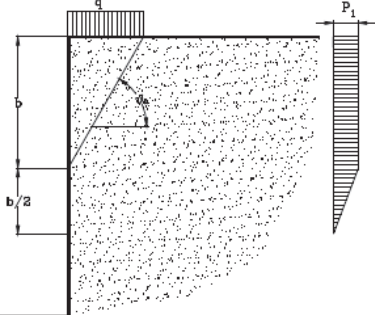
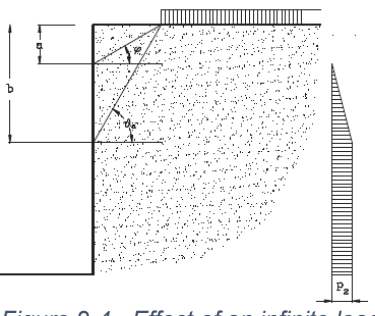
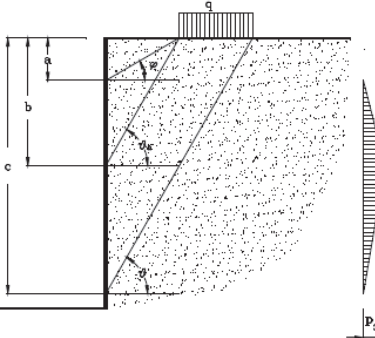
Surcharges affect the stresses that are present in the soil, how these surcharges are transferred in the soil depends on the wall friction angle (δ), the angle of internal friction (φ), and the load transferring angle (ϑ_a). The load transferring angle can be computed with [2]:

$$\tan \vartheta_a = \tan \varphi + \sqrt{\frac{(1 + \tan \varphi^2) * \tan \varphi}{\tan \varphi + \tan \delta}}$$

The different types of surcharges and the theorized way in which they are transferred through the soil are described in Table 2-2.

Table 2-2 - The effect of surcharges on soil stresses

Surcharge	Illustration	Elaboration
Infinite load	<p>Figure 2-2 - Effect of an infinite load on the vertical soil stresses [2]</p>	<p>Here there is a uniformly distributed infinite load which is present everywhere behind the structure. The vertical soil stresses near the structure will increase with a value of P_1. P_1 is equal to the value of the acting load.</p>

<p>Finite load</p>	 <p><i>Figure 2-3 - Effect of a finite load on the vertical soil stresses [2]</i></p>	<p>In this case there is a finite uniformly distributed load. The vertical soil stresses near the structure will increase with a value of P_1 up to a depth of b. P_1 is equal to the value of the acting load. At a depth of 1.5 times b the additional soil stress has diminished again.</p>
<p>Infinite load</p>	 <p><i>Figure 2-4 - Effect of an infinite load on the vertical soil stresses [2]</i></p>	<p>An infinite load at some distance from a structure. The vertical stresses will remain unchanged up to a depth of a, here they will linearly increase up to a depth of b where they will have increased by a value of P_2 which is again equal to that of the acting load.</p>
<p>Finite load</p>	 <p><i>Figure 2-5 - Effect of a finite load on the vertical soil stresses [2]</i></p>	<p>A finite load at some distance from a structure. Over a depth of a, the horizontal soil stresses will remain unchanged, then they will linearly increase up to an increase of P_3 which is at a depth of b. After this they will again linearly decrease to their initial condition. P_3 can be calculated using the following formulas [2]:</p> $P_3 = \frac{2 * q * s * \theta}{c - a}$ $\theta = \frac{\sin(\vartheta_a - \varphi) * \cos \delta}{\cos(\vartheta_a - \varphi - \delta)}$

2.3.2.6 The effect of a relieving platform

The effect that a RP has is shown in Figure 2-6. The platform essentially shields the underlying structure from the stresses that are present above it.

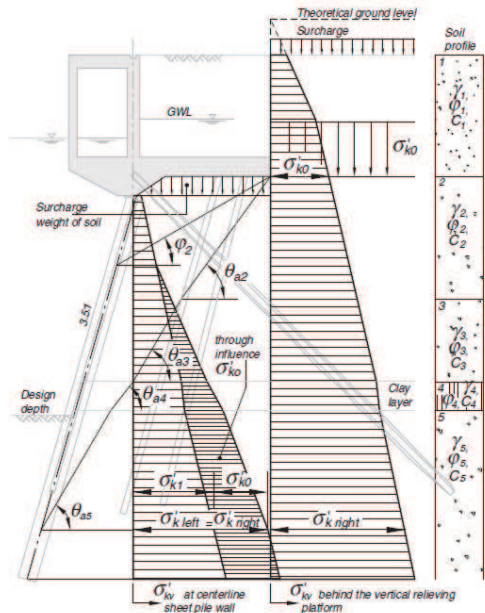


Figure 2-6 - The effect of a relieving platform on soil stresses [1]

$$\tan \theta_a = \frac{1 + \frac{1}{\cos \alpha} \sqrt{\frac{\sin(\varphi + \delta) \cdot \cos(\alpha + \beta)}{\cos(\delta - \alpha) \cdot \sin(\varphi - \beta)}} \cdot \sin \varphi}{\tan \alpha + \frac{1}{\cos \alpha} \sqrt{\frac{\sin(\varphi + \delta) \cdot \cos(\alpha + \beta)}{\cos(\delta - \alpha) \cdot \sin(\varphi - \beta)}} \cdot \cos \varphi}$$

- θ_a = The load transferring angle
- β = The slope of the ground surface
- φ = The angle of internal friction
- δ = The wall friction angle
- α = The inclination of the sheet pile wall

2.4 Different modelling methods

Three different approaches have been analyzed in regard to modelling a quay wall structure:

- Classical method;
- Beam on elastic foundation method;
- Finite Element Method.

2.4.1 Classical method

When designing a sheet pile wall the first thing that needs to be determined is the embedded depth, this can be done in various ways. The two classical methods that will be discussed here are:

- The American method – Free earth support;
- The European method – Fixed earth support.

The free earth support method assumes that the lower end of the sheet piling can freely rotate and does not have any internal moments. Fieldwork has shown that the true moments and anchor forces are lower than the ones predicted by this method, the method is therefore on the conservative side.

The fixed earth support method assumes that the toe of the structure is fully fixed and has no bending moments. Even though this method results in a larger penetration depth, it is usually preferred over the free earth support method because the bending moments have been reduced, resulting in a more slender profile. Both methods are calculating at which depth the equilibrium between the anchor force, the active and passive earth pressures, and the water pressure is first reached [3].

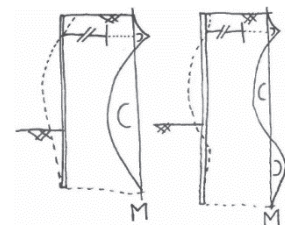


Figure 2-7 - Free and fixed earth support

2.4.1.1 Blum

A relatively simple and often used method is the Blum method. This method assumes a fixed earth support. Blum schematizes the earth pressures as is shown in Figure 2-8, force R in this figure is the “Ersatzkraft” (fixing force), which is the resulting force that ensures that the sheet piling is completely fixed.

The second assumption that the Blum method uses is the use of constant values for both the active and the passive soil pressure coefficients rather than the actual relation between displacements and the pressure coefficients, this is shown in Figure 2-9.

The last assumptions that are needed to solve the problem using this method is that the bending moment at the toe of the structure is zero and the displacement at the location of the anchor is also zero, this is shown in Figure 2-10.

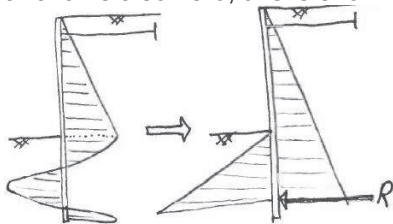


Figure 2-8 - Assumption regarding the soil pressures

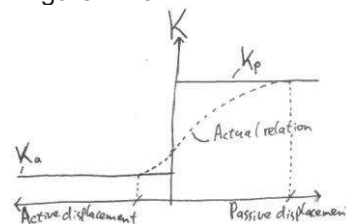


Figure 2-9 - Simplification soil pressure coefficients

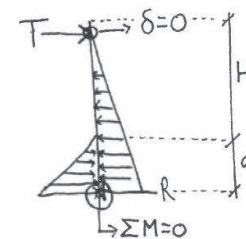


Figure 2-10 - Boundary conditions Blum method

Using theory on the bending of beams the system of equations can be solved, resulting in the needed embedded depth d , the anchor force T , and the fixing force R .

It is essential to understand that the fixing force R is a resulting force that follows from earth pressure underneath the toe of the sheet piling, the embedded depth should therefore be increased by 10 to 20% [4].

2.4.2 Beam on elastic foundation method

When the system becomes more complex due to for instance a large number of different soil layers or multiple anchors, the Blum method becomes increasingly more difficult.

The beam on an elastic foundation method models the soil and water that surrounds the sheet piling system as a set of uncoupled elasto-plastic springs that are connected to the sheet pile wall, the stiffness of the springs is locally determined depending on the displacements. Most systems use a multi-linear relation between the displacement and the soil pressure coefficients [1].

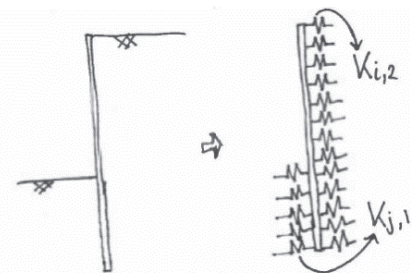


Figure 2-11 - Soil schematization of a beam on elastic foundation

The way that this type of model schematizes the soil is shown in Figure 2-11.

2.4.2.1 D-Sheet Piling

In the Netherlands the software D-Sheet Piling is often used to verify a sheet pile wall design. This software is based on the theory of a beam on elastic foundation. The following elements are modeled in this software:

- The sheet piling;
- Anchors and struts;
- Soil;
- Loads and supports;

- Staged construction;
- Design optimization.

Because of this, more complex boundary conditions can be implemented.

The multilinear relation between the soil and the horizontal effective stress is shown in Figure 2-12.

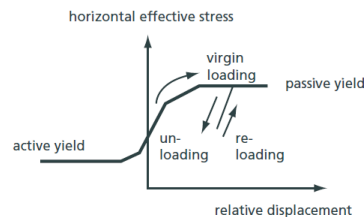


Figure 2-12 - Relation between the horizontal soil pressure and the displacement [5]

Despite the numerous advantages that this software offers it also has some restrictions [5]:

- Only vertical pile systems can be calculated;
- Soil layers need to be horizontal;
- Only soil retaining walls can be calculated.

2.4.3 Finite Element Method

In this method the behavior of the structural elements and the surrounding soil are integrated. The soil behavior is modelled as follows. The entire model is divided into a finite amount of finite elements which are connected to one another through nodes. Compatibility of displacements applies at the boundaries of the elements. At the integration points of different elements, stress-strain relations are included. The stress-strain relations are used to compose the global stiffness matrix, which is in turn used to determine the individual displacements of the nodes by solving the system of equations $K u = f$, in which K is the stiffness matrix, u is the vector with displacement components, and f is the vector with force components. Through the displacements of the nodes, the displacements of the elements is determined which then result in the strains at the integration points. Through stress-strain relations the stresses are determined.

In this thesis Plaxis 2D will be used to model the different structures.

2.4.3.1 Plaxis 2D

Plaxis is the most commonly used finite element software in geo-engineering. It takes multiple theories into consideration, such as:

- Deformation theory of soil;
- Groundwater flow theory;
- Consolidation theory;
- Element formulations.

Within the software there are a number of material models/constitutive models. The stress-strain relations are defined within these models, in principle they are a qualitative description of the mechanical soil behavior. The soil parameters further quantifies this behavior.

3 Quays of interest

This master thesis focusses on two different quay structures. The first one is the old quay structure of the Amazonehaven, which was located on the Maasvlakte. The second structure is the SIF quay structure, which is located on the Maasvlakte 2. In this chapter the designs of the structures will be further elaborated on.

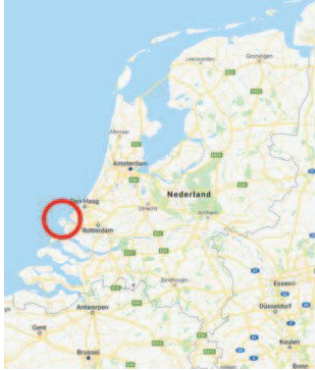


Figure 3-1 - Position of the quay structures, Source: Google Maps



Figure 3-2 - Position of Amazonehaven (right) and SIF (left), Source: Google Maps

3.1 Amazonehaven

This quay structure was constructed in 1990 and was demolished from 2011-2013 due to the expansion of the port. Because this structure was going to be demolished it was briefly discussed to physically apply test loading onto the structure. This would however be very expensive and would take a lot of material to actually exert the load onto the structure. It was therefore decided not to follow through with the physical test loading.

3.1.1 Structural elements

The structure consists of a CSPW with a reinforced concrete RP. It also makes use of concrete bearing piles and Müller Verpress-piles (M.V.-piles). The CSPW is connected to the RP with a cast iron saddle. The total length of the structure is 937 m. The specifications of all the structural elements are included in Table 3-1.

To ensure a safe transfer of forces from the saddle to the CSPW, two plates are connected to the primary pile, one on the inner and one on the outer side. These plates have a thickness of 15.7 mm and a length of 1200 mm. An overview of the structure is shown in Figure 3-6. The integration of the saddle structure can be seen in Figure 3-7.

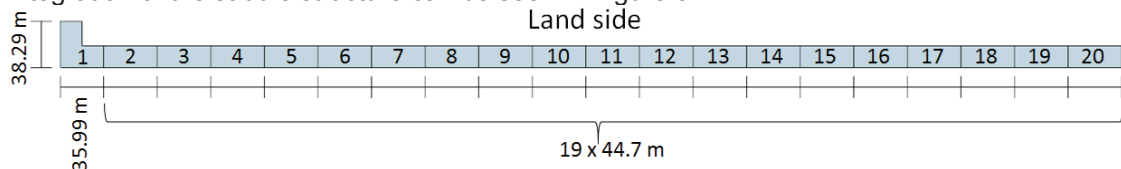


Figure 3-3 - Top view of the Amazonehaven structure

Table 3-1 - Specifications of the structural elements of the Amazonehaven structure

Structural element	Amount	Dimensions	Quality	Additional information
Relieving platform	20	Height = 11 m Length = 18 m Width = 44.7 m	B30	Reinforced concrete T.O.S. = NAP+5.0 m B.O.S. = NAP-6.1 m Figure 3-3, Figure 3-6
Primary tubular piles	306 (+7)	Ø1420 mm (Ø1220 mm) Length = 30-32 m (30 m) t = 15.4-22 mm (16-22 mm)	X-70	Inclination = 5:1 Wall thickness varies along the pile (top, middle, bottom) C.t.c. distance = 2980 mm
Secondary sheet piles	305 (+7)	Larssen IIIs Length = 24 m (20 m) Height = 380 mm t = 14.1 / 10.0 mm Width = 1500 mm	Fe 510.B	Inclination = 5:1 Triple U-profiles
Concrete bearing piles	843	Length = 22-28 m Width = 450 mm (square piles)	B55 [7]	Inclination = 3.5:1 (front row) = 4:1 (back row) C.t.c. distance = 2060 mm
M.V.-piles	332	PSt370/153 Length = 30-36 m	S355	Inclination = 42.5° / 47.5° C.t.c. distance = 2060 mm
Saddle	313	Height = 280 mm Length = 600 mm Width = 620 mm		Cast iron Figure 3-4, Figure 3-5, Figure 3-7

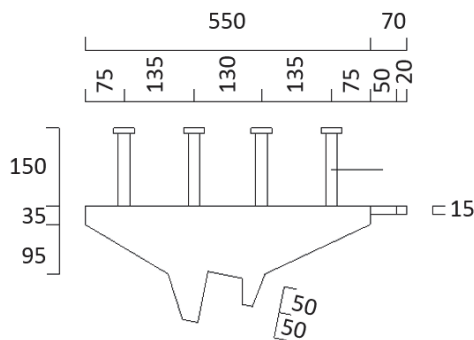


Figure 3-4 - Side view of the saddle, dimensions in mm

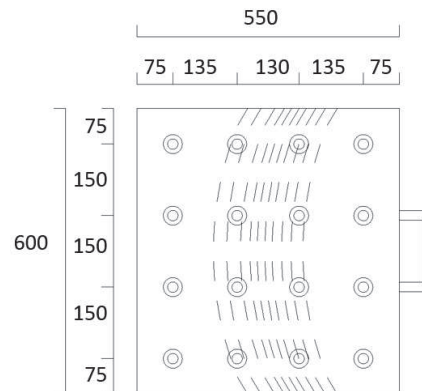


Figure 3-5 - Top view of the saddle, dimensions in mm

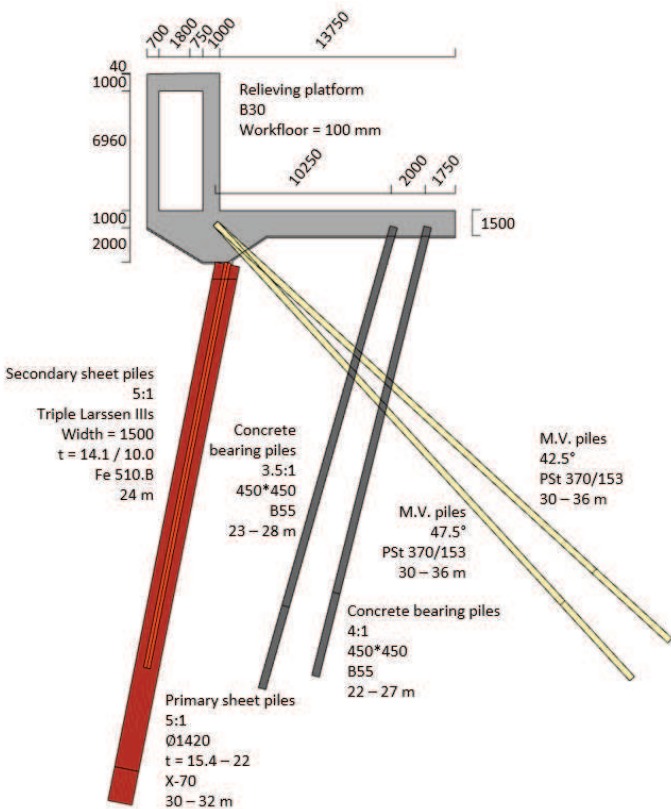


Figure 3-6 - Overview of the Amazonehaven structure

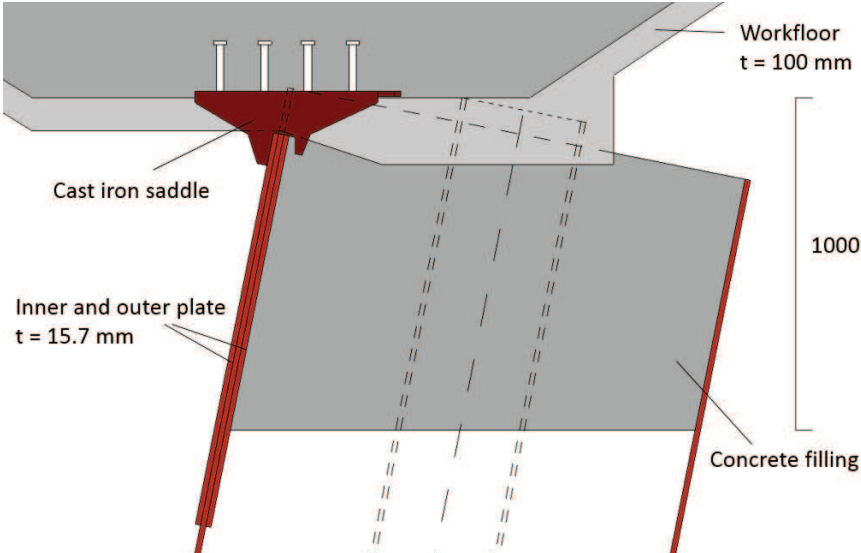


Figure 3-7 - Overview of the saddle element

3.1.2 Local conditions

3.1.2.1 Water levels

The water levels that were used in this design are presented in Table 3-2, they are based on the EAU 1985.

Table 3-2 - Water levels corresponding to the Amazonehaven structure [18]

Situation	Water side	Land side
Lastfall 1 – Low	NAP-1 m	NAP+0 m
Lastfall 1 – High	NAP+0 m	NAP+1 m
Lastfall 3	NAP-2 m	NAP+0 m
Lastfall 2	NAP+0.5 m	NAP+2.5 m

3.1.2.2 Soil conditions

To determine the structure of the soil a total of 123 CPTs (Cone Penetration Tests) and 4 soil borings were carried out, the area marked in red in Figure 3-8 shows the area in which these took place [8]. In light of this, the soil surrounding the Amazonehaven was categorized into 9 different soil profiles.



Figure 3-8 - Area in which CPTs were carried out, Source: Google maps

The top of the soil lies at NAP+5.0 m. The results of the tests are shown in Figure 3-9. The initial contract depth was NAP-21.65 m, which would later be expanded to NAP-24.00 m. The construction depth was therefore set at NAP-25.50 m.

The parameters belonging to the normative soil profile are presented in Table 3-3.

Table 3-3 - Soil parameters at the Amazonehaven structure [17]

Top of the Layer	ϕ	δ	c	γ
m+NAP	°	°	kN/m ²	kN/m ³
-6 m	30	20	0	20
-9.5 m	20	10	15	18
-13 m	30	20	0	20
-20 m	22.5	11	15	18
-24.5 m	35	20	0	20

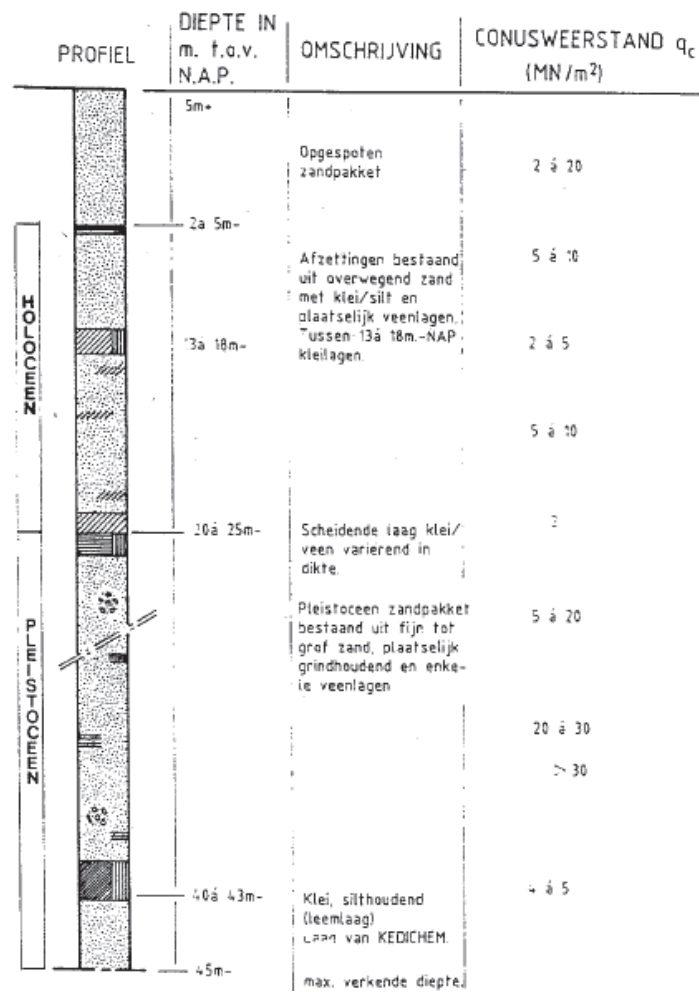


Figure 3-9 - Profile of the soil layering [8]

3.1.2.3 Corrosion

Within this design 3 scenarios were taken into account in regard to corrosion [17]:

1. No occurring corrosion.
2. A corrosion speed of 0.068 mm/year on the waterside of the piles only, 0 mm/year on the landside.
3. A corrosion of 0.13 mm/year from NAP-6 to NAP-13.5 m, and 0.06 mm/year from NAP-13.5 to NAP-25.5 m, again only on the waterside.

3.1.2.4 Loads

The loads that act on the Amazonehaven structure are shown in Table 3-4, they are based on [16] and [19]. Figure 3-10 illustrates the different loads that have been described, in reality the triangular surcharge consists of a pile of ore, this pile would create shear stresses on the top of the soil and would also positively contribute to the overall stability of the quay structure. These effects have however not been taken into consideration within this MSc thesis.

Table 3-4 - Loads on the Amazonehaven structure

Load	Description
Surcharge	20 kN/m ² until 38 m land inwards. 90 kN/m ² increasing linearly to 450 kNm ⁻² over 28.5 m. 450 kN/m ² for 12 m. 450 kN/m ² decreasing linearly to 90 kNm ⁻² over 28.5 m.

Bollard	50 kN/m ¹ (maximum bollard force is 1750 kN).
Mobile crane	2*2700 kN over 21 m → 257.1 kN/m ¹ 3.25 m and 14.25 m land inwards.
Tower crane	12,500 kN vertical and 3330 kN horizontal over 37*4.25 m ² →79.5 kN/m ² and 21.2 kN/m ² 3.25 m and 27.25 m land inwards.
Bridge crane	12,200 kN over 8.5 m → 1435.3 kN/m ¹ 3.25 m and 73.25 m land inwards.

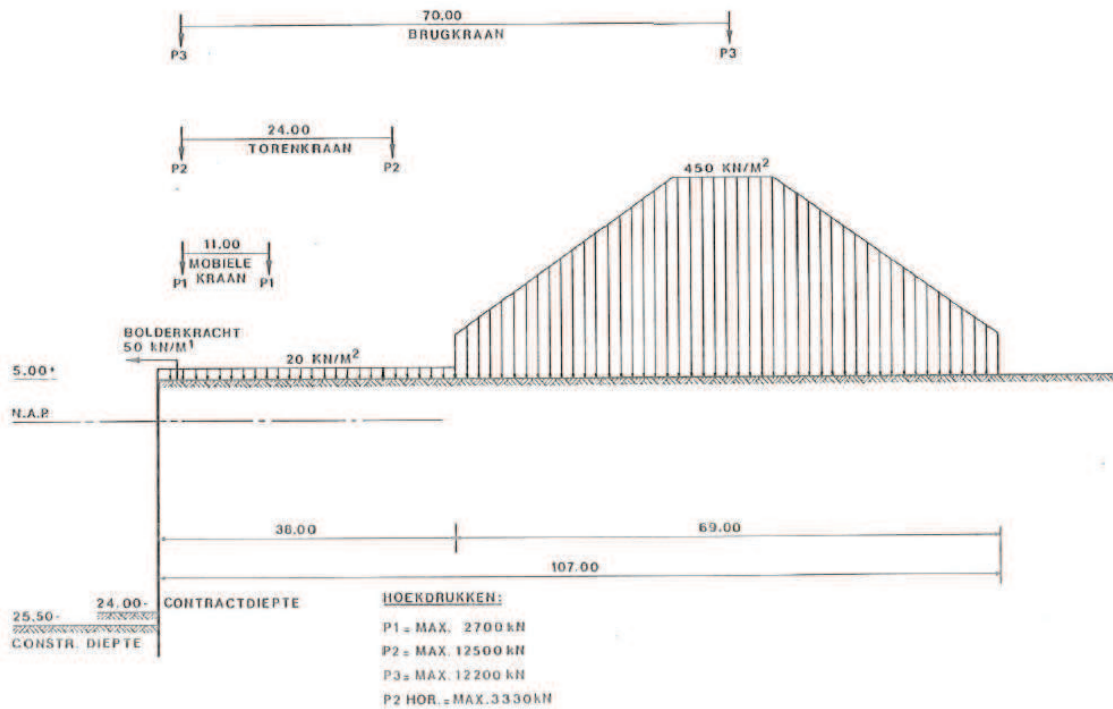


Figure 3-10 - Representation of the acting loads [16]

3.1.3 Construction stages

The construction stages of the Amazonehaven structure is presented in Table 3-5, the stages are based on [7].

Table 3-5 - Construction stages of the Amazonehaven structure

1 st stage: Excavating the trench in which the structure will be constructed.		5 th stage: Placing the saddle and casting the concrete blinding.	
2 nd stage: Installing the CSPW		6 th stage: Casting the RP.	
3 rd stage: Installing the M.V.-piles.		7 th stage: Backfilling the quay structure.	
4 th stage: Installing the concrete bearing piles.		8 th stage: Dredging on the waterside of the structure.	

3.2 SIF

The construction of this quay structure was finished in 2017. The vessels that would make use of this quay structure played an important role in the design process, mainly in the different construction stages. The structure is relevant for this study because it is the most recent and the largest quay structure of Rotterdam. The function, and thus loading conditions, of this structure changes after 50 years. This thesis however focusses mainly on the initial conditions, i.e. the first 50 years.

3.2.1 Structural elements

This quay structure also consists of a CSPW with a RP of reinforced concrete. The RP makes use of M.V.-piles and screw injection bearing piles. The CSPW is connected to the RP by a cast iron saddle.

The structure is separated into 20 compartments, the total length of the structure is 461 m. The characteristics of the structural elements are presented in Table 3-6.

Table 3-6 - Specifications of the structural elements of the SIF structure

Structural element	Amount	Dimensions	Quality	Additional information
Relieving platform	20	Height = 7.1 m Length = 18.1 m Width = 23.06 m Thickness wall = 2.2 m Thickness floor = 1.75 m	C35/45	Reinforced concrete T.O.S. = NAP+5.1 m B.O.S. = NAP-2.0 m
Primary tubular piles	140+7	Ø1420 mm Length = 32-37 m Thickness = 21/23 mm	X-70	At the connection with the saddle part of the primary pile is replaced by a steel plate of 1,025*1,266*60 mm ³ C.t.c. distance = 3,294 mm
Secondary sheet piles	147	PU28 – triple Length = 25.85-29 m Height = 454 mm Thickness = 15.2/10.1 mm Width = 1,800 mm	S355	Triple U-profiles
Concrete bearing piles	320+6	Ø609/850 Length = 29-35 m Thickness wall = 10 mm	C35/45 Casing: S355J2H	Inclination = 3.5:1/4:1 C.t.c. distance = 2,882 mm
M.V.-piles	111+2	HEB600 Length = 52.2-58.5 m	S355	Inclination = 42.5° / 47.5° C.t.c. distance = 2,882 mm /5,765 mm
Saddle	140+7	Height = 380 mm Length = 630 mm Width = 530 mm		Cast iron Figure 3-11, Figure 3-12, Figure 3-13

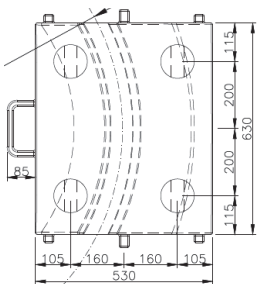


Figure 3-11 - Top view saddle [10]

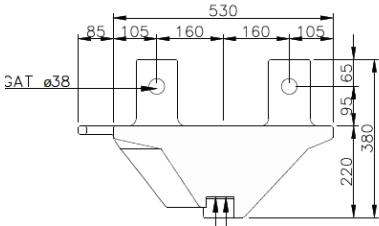


Figure 3-12 - Side view saddle [10]

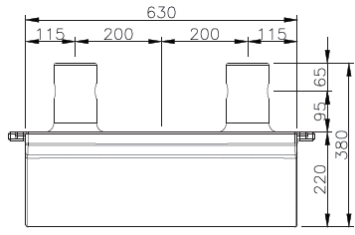


Figure 3-13 - Side view saddle [10]

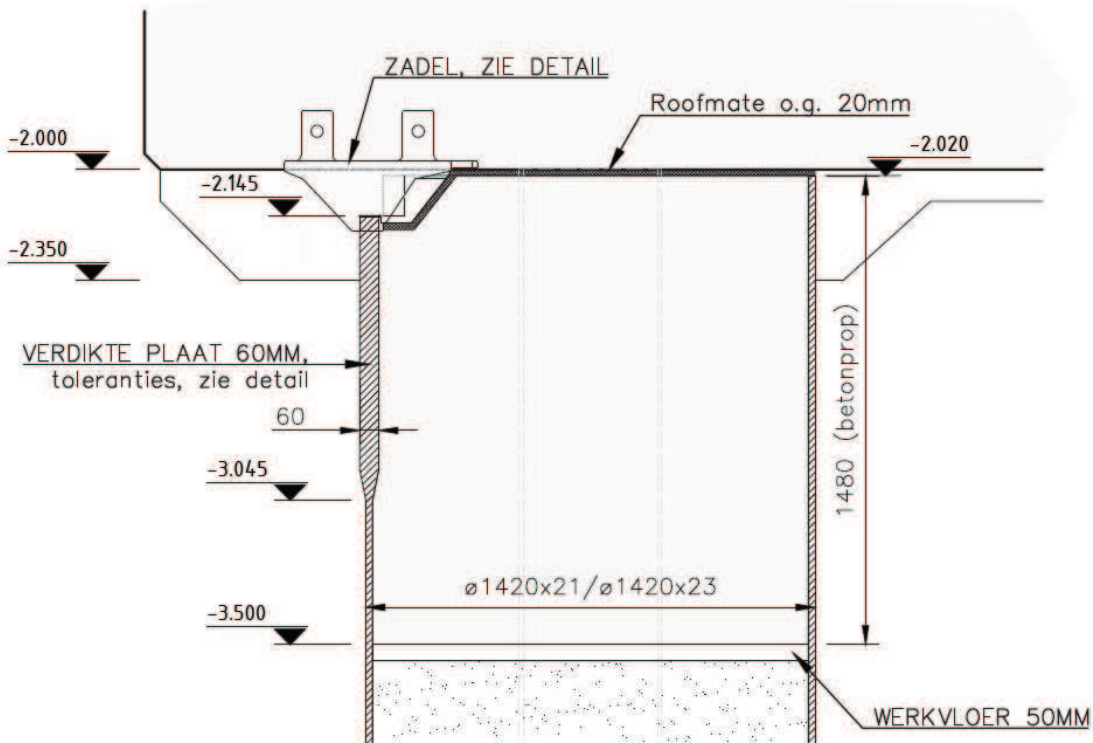


Figure 3-14 - Connection with the saddle [5]

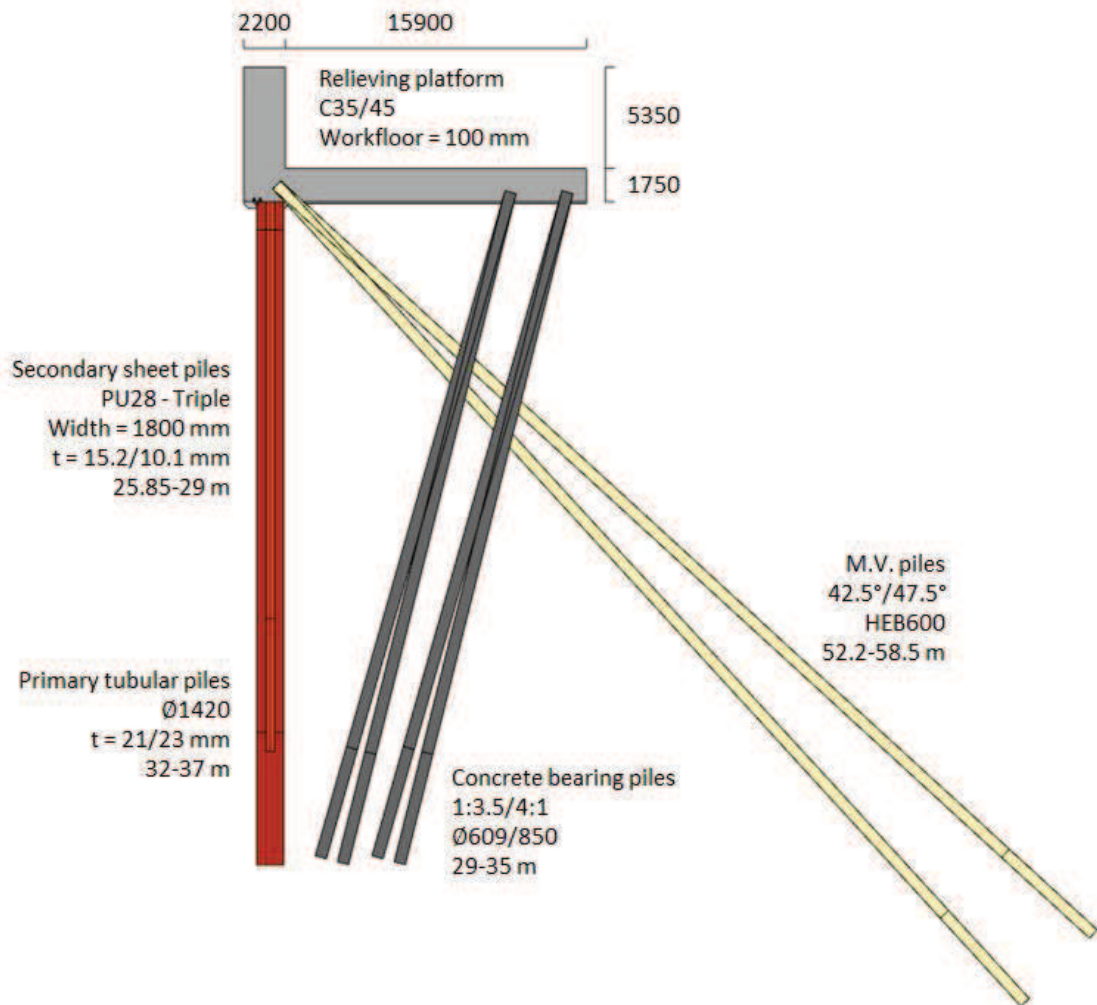


Figure 3-15 - Overview of the structure

3.2.2 Local conditions

3.2.2.1 Water levels

The water levels which should be taken into account during the design process are presented in Table 3-7.

Table 3-7 - Design water levels [m+NAP] [11]

Combination	Water side	Land side	Land side underneath clay layer
	[m+NAP]	[m+NAP]	[m+NAP]
Fundamental	-0.84	-0.34	-0.84
Accidental_{Flooding}	+1.40	+2.30	+1.40
Accidental_{Extreme low water}	-2.29	-2.45	-2.29
Accidental_{Relieving floor}	-2.29	-2.29	-2.29
Accidental_{Failure drainage 1}	-1.50	+0.05	-1.50
Accidental_{Failure drainage 2}	+0.05	+1.22	+0.05

3.2.2.2 Soil conditions

The soil level on the landside is located at NAP+5.10 m. On the waterside the Nautical Guaranteed Depth (NGD) is set at NAP-17.60 m, the design depth is equal to NAP-18.40 m. Due to spud can penetration the construction depth was set to NAP-25.00 m in combination with a surcharge of 55% of the remolded soil, Figure 3-16 illustrates why this addition was needed. The bottom level slopes upwards over the last 8 m closest to the structure under a 1:4 slope.

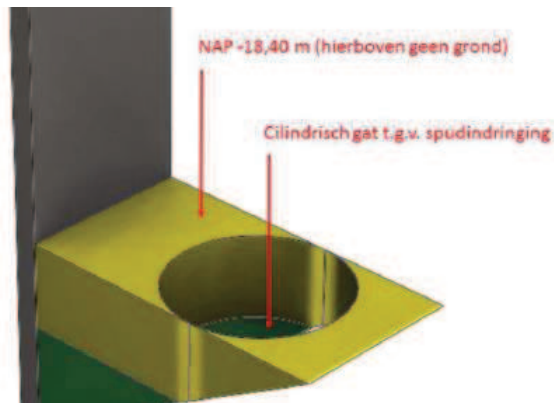


Figure 3-16 - Illustration of the spud can penetration [20]

The structure of the soil has been determined through a large amount of CPTs and soil borings. The result of these surveys is shown in Figure 3-18. Due to large variations in the soil structure the area was divided into different zones, this is shown in Figure 3-17.

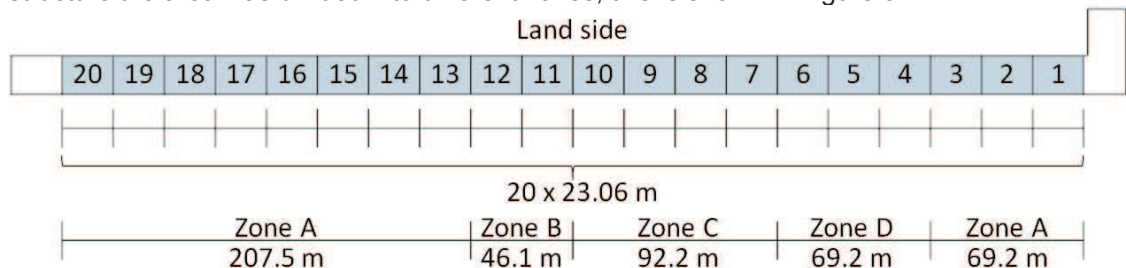


Figure 3-17 - Overview of the RP compartments and different soil zones of the SIF structure

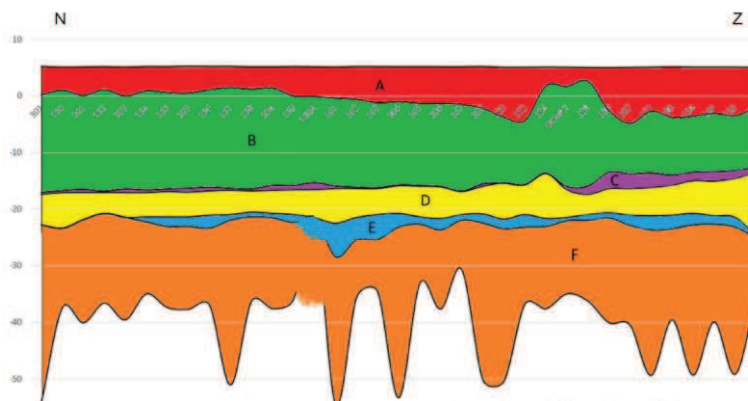


Figure 3-18 - Soil structure along the quay structure [12]

The properties that belong to the different soil layers are presented in Table 3-8.

Table 3-8 - Soil layer properties [12]

Layer	Description	γ_{unsat}	γ_{sat}	ϕ'	c'	c_u
		kN/m ³	kN/m ³	°	kN/m ²	kN/m ²
A	Backfill, mostly densely packed sand	19	21	36	0	-
B	Backfill, mostly moderately packed sand	18.5	20	33.5	0	-
C	Incompletely removed sludge layer	16.5	16.5	26	0	90
D	Fine sand layer with clay	18	20	27	0	-
E	Wijchense clay layer	18	18	25	0	90
F	Coarse sand, moderately to densely packed	18.5	20	36	0	-

Due to the varying thickness and depth of layer E and the load that would be applied on the soil due to the spud cans, it was necessary to replace the soil layer in some of the soil zones. The depth that needed to be excavated for the soil replacement and other properties of the different soil structure zones are shown in Table 3-9.

Table 3-9 - Characteristics of the soil zones [14]

Zone	Description	CPT
A	The thickness of layer E is smaller than 2.50 m. No excavation needed. Due to the relatively shallow position of layer F an inclination of 3.5:1 is possible for the bearing piles.	DKMP 206
B	The same qualities as zone A, this zone is needed to ensure a smooth transition to zone C. Excavation till NAP-22.0 m. To enable a deeper bearing point an inclination of 4:1 is used for the bearing piles.	DKMP 206
C	Very thick layer E, up to 9 m. Excavation till NAP-30.0 m. Inclination of the bearing piles of 4:1.	DKMP 175
D	Relatively thick layer E. Excavation till NAP-27.0 m. Inclination of the bearing piles of 4:1.	DKMP 163

3.2.2.3 Corrosion

The lifetime of this structure is 100 years. The function of the structure changes to a less normative situation after 50 years, the corrosion is therefore only taken into account over the first 50 years. Cathodic protection was used to prevent corrosion from occurring. The resulting corrosion over a period of 50 years is shown in Table 3-10.

Table 3-10 - Predicted corrosion over 50 years for SIF [11]

Position relative to the CSPW	Corrosion over 50 years [mm]
Waterside	0.5
Landside	0
Inside	0

3.2.2.4 Loads

There are three loading scenarios which have been explored. The intended use scenario, the future use scenario, and the partial excavation scenario. In the partial excavation scenario the soil above the RP will be removed up to a final depth of NAP+3.5 m, this is not to be confused with the replacement of the clay layer on the water side.

The loads that are present in each scenario are presented in Table 3-11 [11].







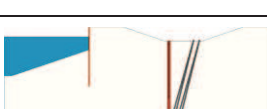
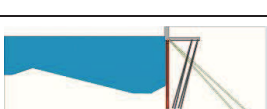
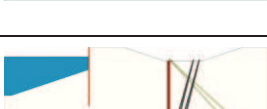
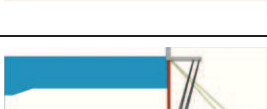

Table 3-11 - Loads on the structure

Load	Intended use	Future use	Partial excavation
Surcharge	100 kN/m ² Everywhere	40 kN/m ² Everywhere	90 kN/m ² Only behind the RP
Bollard	2,000 kN → 130 kN/m	2,000+1,400 kN → 221 kN/m	2,000 kN → 130 kN/m
Recessed bollard	300 kN NAP+1.50 m NAP+3.25 m	300 kN NAP+1.50 m NAP+3.25 m	300 kN NAP+1.50 m NAP+3.25 m
Permanent crane	-	1,002 kN/m	-

3.2.3 Construction stages

The construction stages of the SIF structure are shown in Table 3-12.

Table 3-12 - Construction stages of the SIF structure

1 st stage: Initial situation.		7 th stage: Casting the concrete RP.	
2 nd stage: Installing a temporary retaining structure.		8 th stage: Backfilling the quay structure.	
3 rd stage: Installing the screw injection piles.		9 th stage: Removing the temporary structure and dredging.	
4 th stage: Installing the CSPW.		10 th stage: Lowering the groundwater level and dredging the clay layer.	
5 th stage: Installing the M.V.-piles.		11 th stage: Restoring the design bottom level with sand.	
6 th stage: Placing the saddle and casting the concrete blinding.			

4 Selection of the critical cross sections

This chapter presents the scenarios that will be explored further. It does so by elaborating on the different elements that are taken into consideration and selecting the most critical conditions for each respective structure in relation to the structural safety.

4.1 Modifiable elements

The modifiable areas can broadly be divided into two categories:

- Structure;
- Local conditions.

For this MSc thesis it was decided to use the actual structural characteristics of the structures as a boundary condition. Modifications in regard to the structural characteristics and structural dimensions will therefore not be explored further.

It is however plausible that the local conditions around a structure are misrepresented or that a wrong normative situation has been selected. Table 4-1 presents the parameters that can be modified and the theorized expected effect that this would have on the structure.

Table 4-1 - Possible modifications of the local conditions

Parameter	Modification	Expected effect
Soil		
	Using a profile with more less permeable soil layers (i.e. more “weak” layers).	The effect of this modification is fourfold. Due to the smaller permeability larger pressure difference are likely to occur (undrained soil conditions). Second the direct load that acts on the CSPW, due to the weight of the soil, decreases. Third the surcharge gets transferred under a smaller angle, which makes the surcharge reach the CSPW at a higher position. Lastly, the passive soil pressure coefficient will be smaller while the active soil pressure coefficient will be larger. This will likely result in an increased needed embedded depth, a larger bending moment, and an increase of the anchor force.
	Increasing the internal angle of friction.	The passive horizontal stress coefficients will increase while the active ones decrease, causing the direct loads on the CSPW to decrease. The surcharge will also reach the wall at a lower position.
Water		
	Lowering the low water level.	The load on the CSPW will increase.
	Increasing the water level difference between the outer water level and the groundwater level.	The load on the CSPW will increase.

4.2 Amazonehaven

The water levels were considered to be relatively stable, they were therefore not extensively treated in this MSc thesis.

The parameters that were explored further for modification are the structure of the soil (soil layering) and the different loading situations.

4.2.1 Soil profiles

In §3.1.2.2 it was stated that the soil around the Amazonehaven was categorized into 9 different soil profiles. These profiles were analyzed in regard to their self-weight and their ability to transfer the surcharge towards the CSPW.

The ability to transfer the surcharge was determined by drawing the transfer lines according to the theory presented in §2.3.2. The point of engagement represents the depth at which the surcharge first reaches the CSPW, the point of full loading represents the point at which the surcharge has been fully transferred. Figure 4-1 shows how these depths have been calculated.

The self-weight of the soil profile was averaged over the length of the CSPW, the same was done for the angle of internal friction.

Table 4-2 - Soil profile characteristics

Soil profile	Point of engagement	Point of full loading	Average self-weight γ_s	Average angle of internal friction ϕ
	m+NAP	m+NAP	kN/m ³	°
1	-13.08	-26.12	19.34	30.25
2	-12.33	-26.01	19.57	30.34
3	-12.33	-26.59	19.66	30.90
4	-12.85	-26.34	19.67	30.78
5	-13.08	-27.35	19.90	31.89
6	-11.66	-25.24	19.48	29.71
7	-11.66	-26.23	19.64	30.74
8	-13.08	-27.61	19.93	32.13
9	-13.08	-26.89	19.75	31.31

Table 4-2 shows that soil profile 6 is the normative one in regard to the surcharge, this is the same profile as the one that has been presented earlier in this report. In regard to the self-weight in combination with the angle of internal friction, soil profile 6 is again the normative one. This is due to the larger active soil pressure coefficient. The least conservative profile is profile 5.

The soil profile that was modelled to determine the structural safety of the Amazonehaven structure are soil profiles 5 and 6. Soil profile 6 has been selected because it is the normative one, soil profile 5 has been taken into consideration to determine the effect of a larger internal angle of friction.

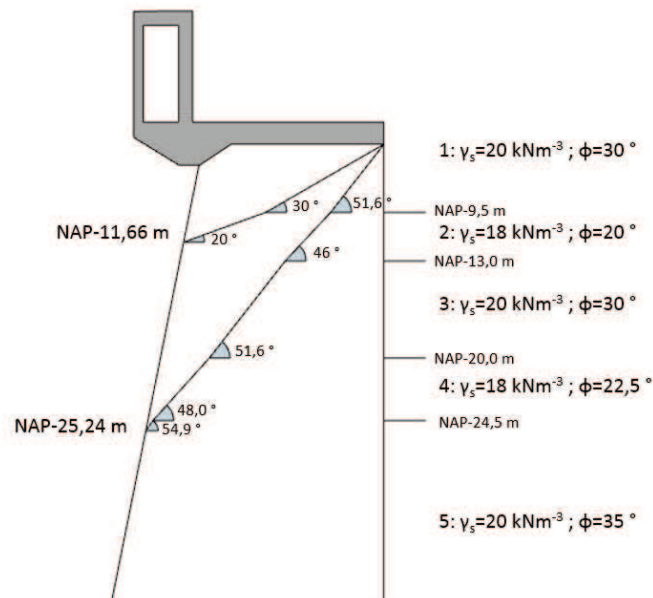


Figure 4-1 - Profile 6, load transfer illustration

4.2.2 Water

In §3.1.2.1 4 different scenarios have been described. The variable of interest is of course the difference in the presented water levels. The water level difference in Lastfall 2 and 3 are the same and larger than that of Lastfall 1, they are however about ultimate states in which a lot of partial factors are applied. The scope of this thesis lies more in the serviceability state. For this reason Lastfall 1 has been selected for the normative water levels in this thesis, which corresponds to a water level difference of 1 m.

4.2.3 Loads

The variable loads in this case are the different crane loads. To decide which loads are the normative ones, the load that they exert on the CSPW has been predicted. The following assumptions have been used in the predictions:

- The RP absorbs all loads that act upon it;
- The average angle of internal friction is 30° ;
- The average "load transferring" angle is 51.5° ;
- The average "load completion" angle is 62.1° ;
- The average wall friction angle is 17.5° .

These assumptions are based on the theory and results that were used in §4.2.1 and §2.3.2.

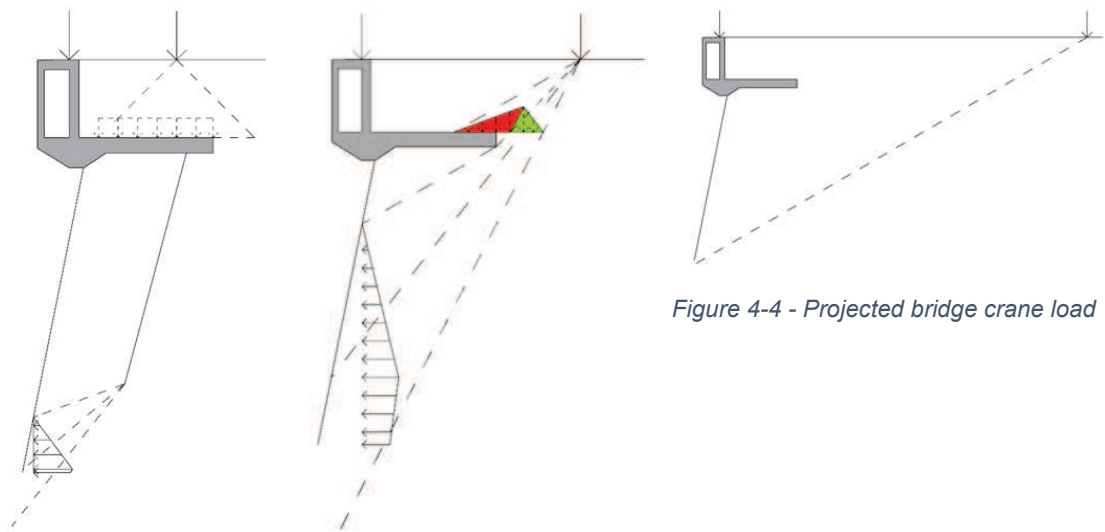


Figure 4-2 - Projected mobile crane load

Figure 4-3 - Projected tower crane load

Figure 4-4 - Projected bridge crane load

From Figure 4-2, Figure 4-3, and Figure 4-4 it can be seen that the scenario in which the tower crane load is present is the normative one in regard to the bending moment of the CSPW.

The superstructure itself plays a large role in the force distribution along the different structural elements. Figure 4-5 shows a schematization of the superstructure and the loads that act on it, the effective weight of the structure was used in determining the magnitude and location of the self-weight. Using the equilibrium of bending moments, horizontal forces, and vertical forces in combination with the direction in which the different reaction forces act, the unknown forces could be calculated. The calculation of the reaction forces can be found in Appendix A.

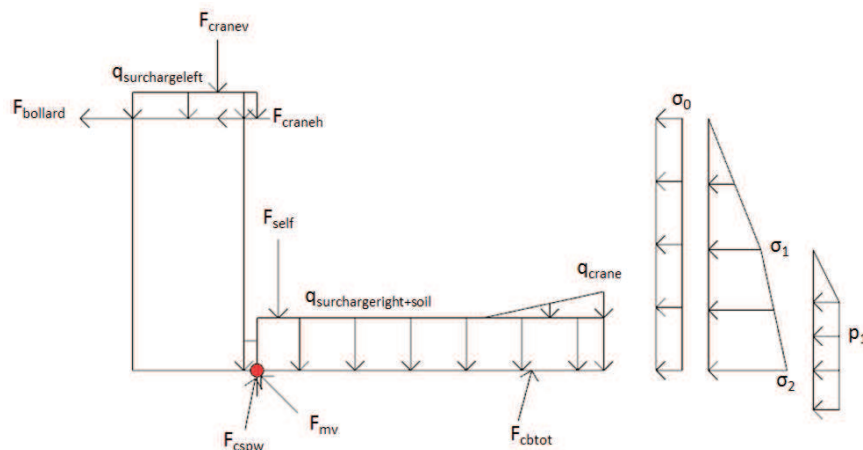


Figure 4-5 - Schematization superstructure

4.2.4 Selected scenarios

Four scenarios have been selected for further modelling. The main difference lies in the soil profiles that were used. The scenarios will now be elaborated on separately, the dimensions of the structural elements were determined based on the locations of the selected soil profiles.

4.2.4.1 Amazonehaven 1a

The local conditions are as follows:

- The entire surcharge is present;
- The tower crane load is present;
- The bollard load is present;
- Soil profile 6;
- The outer water level is NAP-1.00 m;
- The groundwater level is NAP+0.00 m;
- The ground level on the land side is NAP+5.00 m;
- The initial contract depth is NAP-21.65 m, the final one is NAP-24.00 m;
- The construction depth is NAP-25.50 m;
- A corrosion speed of 0.068 mm/year on the waterside of the piles only, 0 mm/year on the landside.

The characteristics of the structural elements are:

- Primary tubular piles: length = 32 m (bottom at NAP-37.5 m);
- Secondary sheet piles: length = 24 m (bottom at NAP-29.57 m);
- M.V.-piles: length = 34.5 m (inclination alternating between 42.5 ° and 47.5 ° at every pile);
- Concrete bearing piles: length of the first row = 27 m (bottom at NAP-29.71 m), length of the second row = 26 m (bottom at NAP-28.97 m).

The soil characteristics belonging to soil profile 6 are presented in Table 4-3.

Table 4-3 - Soil characteristics belonging to soil profile 6

Top of the soil layer	ϕ	δ	c	γ_s	ϑ_a
m+NAP	°	°	kN/m ²	kN/m ³	°
+5.0	30	20	0	20 ($\gamma_{\text{unsat}} = 18$)	51.6
-9.5	20	10	15	18	46.5
-13.0	30	20	0	20	51.6
-20.0	22.5	11	15	18	48.0
-24.5	35	20	0	20	54.9

4.2.4.2 Amazonehaven 1b

This is the scenario in which the force in the M.V.-piles is maximized. The difference with scenario Amazonehaven 1a is as follows:

- No surcharge left of the CSPW;
- No tower crane load;
- The outer water level is NAP+0.00 m;
- The groundwater level is NAP+1.00 m.

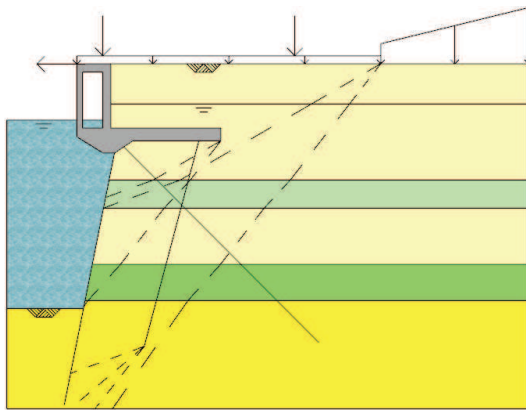


Figure 4-6 - Amazonehaven 1a

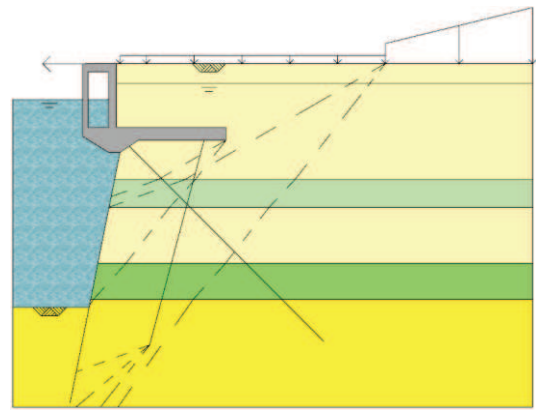


Figure 4-7 - Amazonehaven 1b

4.2.4.3 Amazonehaven 2a

The local conditions are as follows:

- The entire surcharge is present;
- The tower crane load is present;
- The bollard load is present;
- Soil profile 5;
- The outer water level is NAP-1.00 m;
- The groundwater level is NAP+0.00 m;
- The ground level on the land side is NAP+5.00 m;
- The initial contract depth is NAP-21.65 m, the final one is NAP-24.00 m;
- The construction depth is NAP-25.50 m.

The characteristics of the structural elements are:

- Primary tubular piles: length = 31 m (bottom at NAP-36.5 m);
- Secondary sheet piles: length = 24 m (bottom at NAP-29.57 m);
- M.V.-piles: length = 33 m (inclination alternating between 42.5 ° and 47.5 ° at every pile);
- Concrete bearing piles: length of the first row = 25 m (bottom at NAP-27.99 m), length of the second row = 24 m (bottom at NAP-27.235 m).

The soil characteristics belonging to soil profile 5 are presented in Table 4-4.

Table 4-4 - Soil characteristics belonging to soil profile 5

Top of the soil layer	ϕ	δ	c	γ_s	ϑ_a
m+NAP	°	°	kN/m ²	kN/m ³	°
+5.0	30	20	0	20 ($\gamma_{\text{unsat}} = 18$)	51.6
-20.0	22.5	11	15	18	48.0
-21.5	32.5	20	0	20	53.3
-24.0	35	20	0	20	54.9

4.2.4.4 Amazonehaven 2b

Just as scenario Amazonehaven 1b, this scenario looks at the M.V.-piles. The differences with Amazonehaven 2a are:

- No surcharge left of the CSPW;
- No tower crane load;
- The outer water level is NAP+0.00 m;
- The groundwater level is NAP+1.00 m.

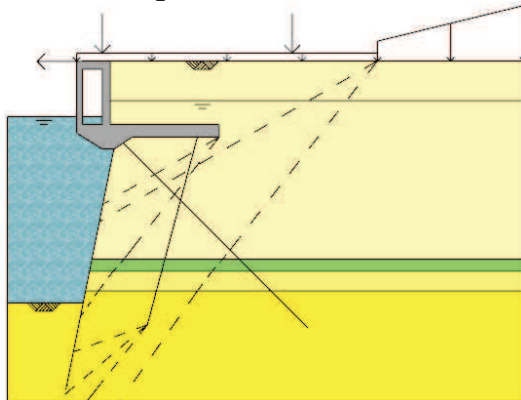


Figure 4-8 - Amazonehaven 2a

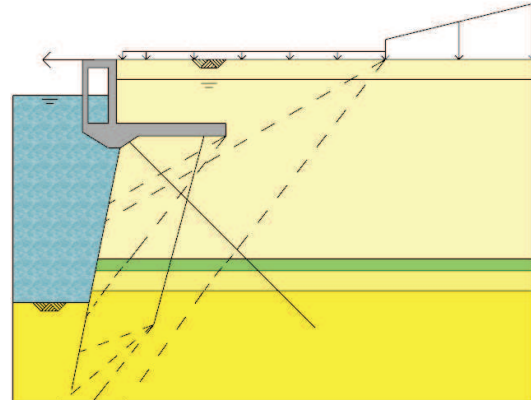


Figure 4-9 - Amazonehaven 2b

4.3 SIF

Earlier in this report it was mentioned that this quay structure has been selected because it is the largest and most recent quay structure of Rotterdam. Regarding this quay structure the construction stages were of importance, more specifically the soil replacement on the water side. In the case of the Amazonehaven the focus was on the projection of the loads behind the RP, in this case the focus was on the effect of the construction stages. The variables that were analyzed will now be presented.

4.3.1 Soil profiles

In §3.2.2.2 it was stated that the structure of the soil was divided into 4 different zones, the main differences of these zones lies in the thickness of the clay layer. Table 4-5 shows the structure of the soil in the different zones, the excavation depth regarding the soil replacement is also presented. The values are based on [14], a tolerance of 1 m needs to be taken into account regarding the excavation depth.

Table 4-5 - Level of the top of the soil layers [m+NAP]

Zone	Layer A	Layer B	Layer C	Layer D	Layer E	Layer F	Excavation depth
A	+5.1	-1.3	-15.5	-16.3	-21.7	-24.2	-
B	+5.1	-1.3	-15.5	-16.3	-21.7	-24.2	-22.0
C	+5.1	-2.0	-16.4	-16.8	-21.9	-29.8	-30.0
D	+5.1	-0.5	-16.0	-16.5	-21.0	-25.5	-27.0

Zone B is used as a transitional zone, it ensures a smooth transition from zone A to zone C. In essence it has the same characteristics as zone A. It was therefore more interesting to look at zone B than at zone A. Zone C experiences the largest excavation for soil replacement, it was therefore more interesting than zone D.

The zones that were selected for further exploration were zones B and C.

4.3.2 Water

In Table 3-7 the design water levels were presented. During the construction stages the water level will be set to the fundamental levels, for the bending moments the failure drainage 1 scenario will be applicable. Table 4-6 shows the described scenarios and their respective water levels.

Table 4-6 - Relevant scenarios in regard to the water levels in m+NAP

Combination	Water side	Land side	Land side underneath clay layer
	[m+NAP]	[m+NAP]	[m+NAP]
Fundamental	-0.84	-0.34	-0.84
Accidental Failure drainage 1	-1.50	+0.05	-1.50

4.3.3 Loads

In this case there are quite some different loads that can vary, in short there is a uniform surcharge of 100 kN/m^2 and a variety of cranes. The largest crane load that can be exerted on the structure is $10,000 \text{ kN}$ which is divided over $13 \times 18.3 \text{ m}^2$, this would result in a uniformly distributed surcharge of 42 kN/m^2 . It was decided to neglect the crane loads in this MSc thesis and use the uniformly distributed surcharge only.

The reaction forces of the superstructure have been determined with the help of a maple sheet. The sheet can be found in Appendix A and is based on Figure 4-10.

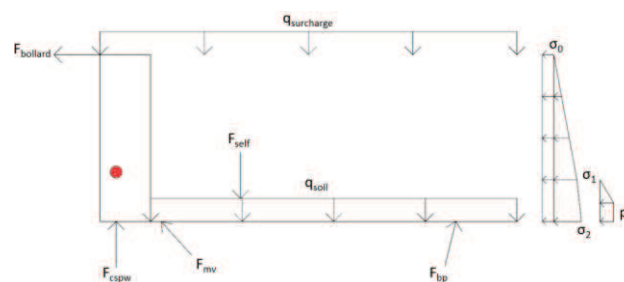


Figure 4-10 - Reaction forces of the superstructure

It is interesting to see that the relation between the surcharge and the force in the M.V.-piles is different than it was in the case of the Amazonehaven. This is due to the fact that the CSPW is vertical in this case.

4.3.4 Selected scenarios

For this case 4 scenarios were explored as well. The difference here, as was mentioned earlier, mainly lies in the amount of soil that needs to be replaced. The scenarios will now be elaborated on.

4.3.4.1 SIF 1a

- Soil structure belonging to zone B;
- Uniformly distributed surcharge present everywhere;
- Bollard load present;
- Contract depth = NAP-18.4 m;
- Construction depth = NAP-25.0 m;
- 55% of the remolded soil on the waterside as surcharge;
- Water level = NAP-1.50 m;
- Groundwater level = NAP+0.05 m;
- Ground level = NAP+5.10 m;

- Corrosion = 0.5 mm in 50 years, waterside only.

The dimensions of the structural elements belonging to the above described conditions are:

- Toe of the primary sheet piles = NAP-34.00 m;
- Thickness of the primary tubular piles = 21 mm;
- Toe of the secondary sheet piles = NAP-27.85 m;
- Toe of the bearing piles = NAP-33.5 m;
- Inclination of the bearing piles = 4:1;
- Length of the M.V.-piles = 52.9 m.

4.3.4.2 SIF 1b

The same as scenario SIF 1a, only during the excavation stage. This is realized by changing the following conditions:

- No surcharge present;
- No bollard load present;
- No surcharge on the waterside;
- Water level = NAP-0.84 m;
- Groundwater level = NAP-6.0 m;
- Construction depth = NAP-23.0 m.

Table 4-7 - Soil characteristics belonging to zone B

Top of the soil layer	ϕ	δ	c	γ_s (γ_{unsat})	ϑ_a
m+NAP	°	°	kN/m ²	kN/m ³	°
+5.1	36	20	0	21 (19)	60.0
-1.3	33.5	20	0	20 (18.5)	58.4
-15.5	26	13	0	16.5	54.5
-16.3	27	18	0	20	54.2
-21.7	25	12.5	0	18	54.0
-24.2	36	20	0	20	60.0

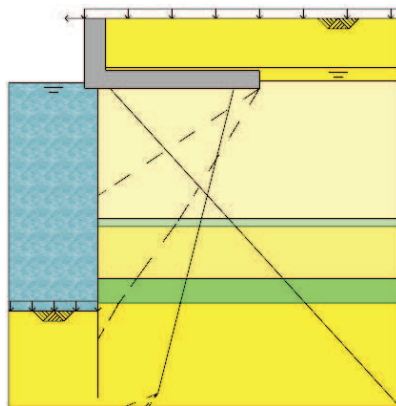


Figure 4-11 - SIF 1a

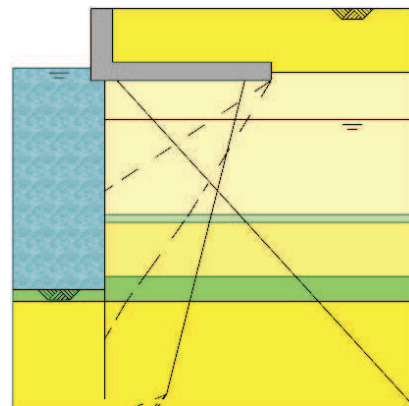


Figure 4-12 - SIF 1b

4.3.4.3 SIF 2a

- Soil structure belonging to zone C;
- Uniformly distributed surcharge present everywhere;
- Bollard load present;
- Contract depth = NAP-18.4 m;
- Construction depth = NAP-25.0 m;
- 55% of the remolded soil on the waterside as surcharge;
- Water level = NAP-1.50 m;
- Groundwater level = NAP+0.05 m;
- Ground level = NAP+5.10 m;
- Corrosion = 0.5 mm in 50 years, waterside only.

The dimensions of the structural elements belonging to the above described conditions are:

- Toe of the primary tubular piles = NAP-39.00 m;
- Thickness of the primary tubular piles = 23 mm;
- Toe of the secondary sheet piles = NAP-31.00 m;
- Toe of the bearing piles = NAP-36.0 m;
- Inclination of the bearing piles = 4:1;
- Length of the M.V.-piles = 58.5 m.

4.3.4.4 SIF 2b

The same as scenario SIF 1a, only during the excavation stage. This is realized by changing the following conditions:

- No surcharge present;
- No bollard load present;
- No surcharge on the waterside;
- Water level = NAP-0.84 m;
- Groundwater level = NAP-6.0 m;
- Construction depth = NAP-31.0 m.

Table 4-8 - Soil characteristics belonging to zone C

Top of the soil layer	ϕ	δ	c	γ_s (γ_{unsat})	ϑ_a
m+NAP	°	°	kPa ²	kN/m ³	°
+5.1	36	20	0	21 (19)	60.0
-2.0	33.5	20	0	20 (18.5)	58.4
-16.4	26	13	0	16.5	54.5
-16.8	27	18	0	20	54.2
-21.9	25	12.5	0	18	54.0
-29.8	36	20	0	20	60.0

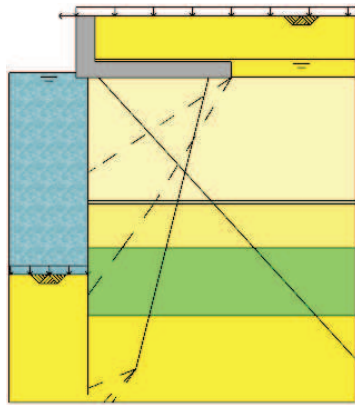


Figure 4-13 - SIF 2a

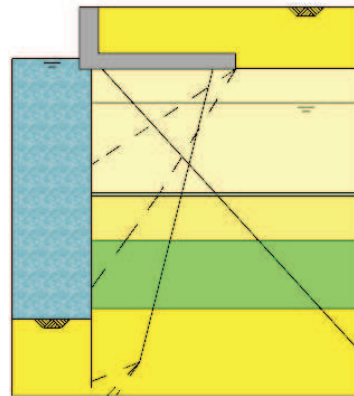


Figure 4-14 - SIF 2b

5 Blum calculation

This chapter contains the Blum calculation of the selected scenarios. First it elaborates on the approach, after this the scenarios and their unknowns will be modelled and computed. The scenarios in which the force of the M.V.-piles will be maximized was only explored according to the reactions of the superstructures, the stresses on the CSPW were not adjusted accordingly.

5.1 Amazonehaven 1

The Blum method for an anchored wall consists of the following steps:

1. Compute the embedded depth;
2. Determine the anchor force using the equilibrium of moments;
3. Compute the fixing force using the equilibrium of forces;
4. Compute the required section modulus of the wall.

This method uses the following assumptions/boundary conditions:

1. The displacement at the anchor point is 0;
2. The displacement at the toe is 0;
3. The bending moment at the top is 0;
4. The bending moment at the toe is 0;
5. An additional length of 10-20% of the embedded depth is needed for the clamping force to develop.

In Figure 4-4 it can be seen that the area where the surcharge reaches its maximum value has little effect on the soil stresses near the CSPW. In light of that, the simplification presented in Figure 5-1 was used for the Blum calculation.

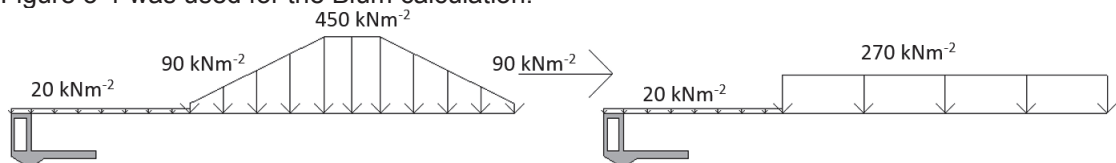


Figure 5-1 - Simplification of the surcharge

To determine the needed length of the CSPW, the horizontal stress distribution along the wall needed to be determined. The components that influence this stress distribution are:

- The water level difference;
- The structure of the soil adjacent to the wall;
- The surcharge;
- The crane load;
- The reaction force of the concrete bearing piles.

The individual contributions to the horizontal stress distribution were determined as follows. The vertical stresses of the adjacent soil, the stress directly behind the RP, and the high surcharge were added together. Then they were multiplied with the corresponding horizontal soil pressure coefficient. The next step was adding the contribution of the water pressure, crane load, and the effect of the concrete bearing piles. The total stress distribution was now found, this distribution was simplified to a triangular distribution with a rectangular component. The described process is shown in Figure 5-2.

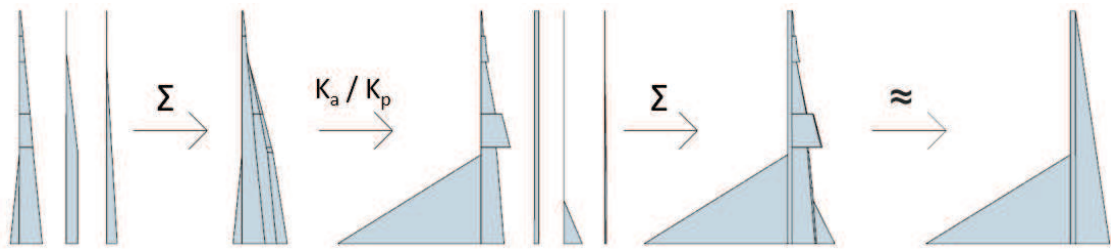


Figure 5-2 - Determination of the horizontal stress distribution at Amazonehaven 1

Figure 5-3 was used for the Blum method, it is based on the stress distribution belonging to the current design.

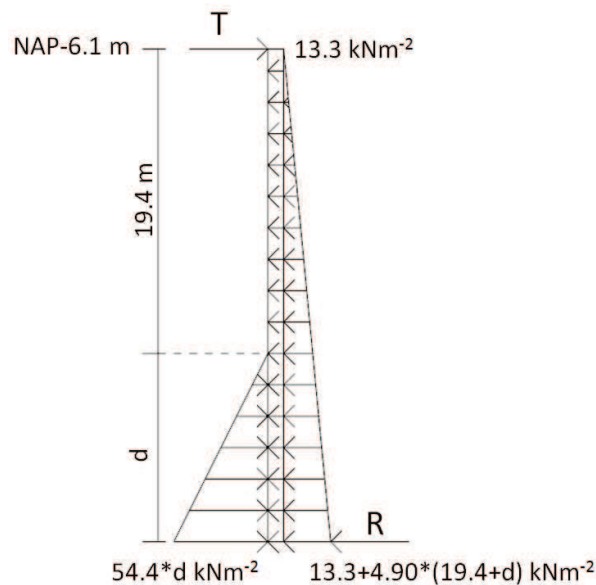


Figure 5-3 - Blum schematization Amazonehaven 1

The presented input parameters together with the boundary conditions were used for the Blum calculation. The shielding effect of the concrete bearing piles and the arching effect of the soil have been implemented by applying a reduction factor of 0.75 over the field bending moment and 0.9 over the fixed bending moment in combination with an increase of the anchor force of 15% [18]. Appendix B shows the entire calculation. The results are as follows:

Table 5-1 - Representative values of the unknowns according to Blum for Amazonehaven 1

T	R	d	Δd_{\min}	$M_{\text{field,CSPW}}$	$M_{\text{fixed,CSPW}}$
kN/m	kN/m	m	m	kNm/m	kNm/m
583.9	1,660.8	12.14	1.21	2,137.5	-2,021.9

The added embedded depth is necessary for the fixing force R to develop. Earlier it was stated that this depth is generally 10-20% of the embedded depth. Due to the obliqueness of the CSPW, which results in a larger passive horizontal stress coefficient on the landward side, the value of 10% has been chosen. T represents the needed anchor force, this should not be confused with the force in the M.V.-piles.

The reaction forces in the superstructure have been determined using the maple sheet that is shown in Appendix A. Assuming that force T would only be transferred to the M.V.-piles, the force in the M.V.-piles was calculated as follows:

$$F_{M.V.\text{total}} = F_{M.V.\text{superstructure},1b} + \sqrt{2} * T = 783.3 \text{ kN/m}$$

5.2 Amazonehaven 2

The same approach was used as in the previous section. The individual contributions to the stress distribution were determined, combined, and schematized. Figure 5-4 shows the values that were used in the Blum calculation.

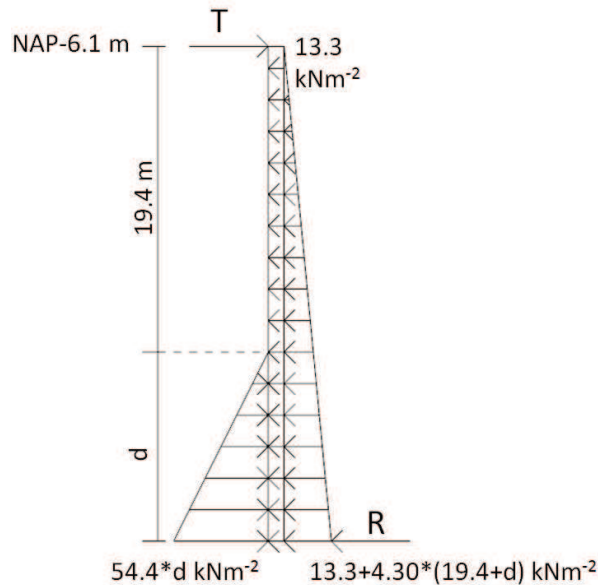


Figure 5-4 - Blum schematization Amazonehaven 2

Using the calculated stress characteristics, the unknown variables could again be determined. The results are shown in Table 5-2.

Table 5-2 - Representative values of the unknowns according to Blum for Amazonehaven 2

T	R	d	Δd_{\min}	$M_{\text{field,CSPW}}$	$M_{\text{fixed,CSPW}}$	$F_{\text{M.V.-piles}}$
kN/m	kN/m	m	m	kNm/m	kNm/m	kN/m
516.8	1,526.8	11.38	1.14	1,757.1	-1,692.4	688.6

5.3 SIF 1

The following simplifications and assumptions were used in the design calculations:

- The same water pressure difference is present over the entire length of the CSPW;
- Instead of a surcharge of 55% of the remolded soil, 55% of the remolded soil itself is present;
- The contribution of the concrete bearing piles to the stress distribution on the CSPW is negligible.

After this the individual stress contributions were again determined and. In Figure 5-5 and Figure 5-6 the values which were used for the Blum maple sheet can be found.

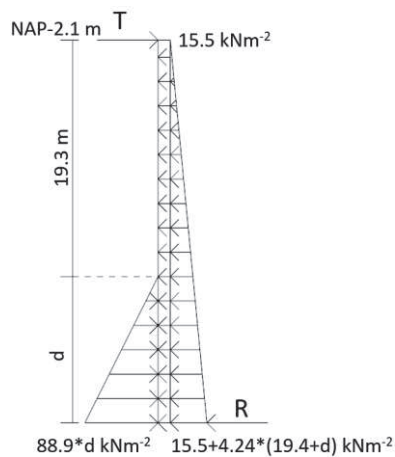


Figure 5-5 - Blum schematization SIF 1a

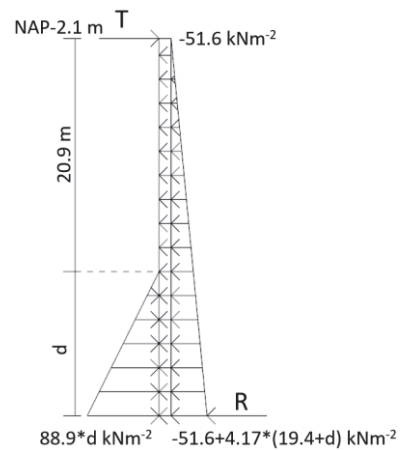


Figure 5-6 - Blum schematization SIF 1b

The results of the Blum calculation are presented in Table 5-3.

Table 5-3 - Representative values of the unknowns according to Blum for SIF 1

Scenario	T	R	d	Δd_{\min}	$M_{\text{field,CSPW}}$	$M_{\text{fixed,CSPW}}$	$F_{\text{M.V.-piles}}$
	kN/m	kN/m	m	m	kNm/m	kNm/m	kN/m
SIF 1a	481.9	1,724.7	8.76	1.75	1,441.0	-1,601.7	980.0
SIF 1b	-215.7	453.2	-3.05	-	-	-	-388.4

Some values for scenario SIF 1b have been left blank. This due to the fact that the maple sheet gave a negative value for the needed embedded depth, which is of course not feasible. For this reason the other variables have not been determined with this method.

5.4 SIF 2

The same simplifications and assumptions that were used for the SIF 1 scenario were applied here. The Blum schematizations can be seen in Figure 5-7 and Figure 5-8.

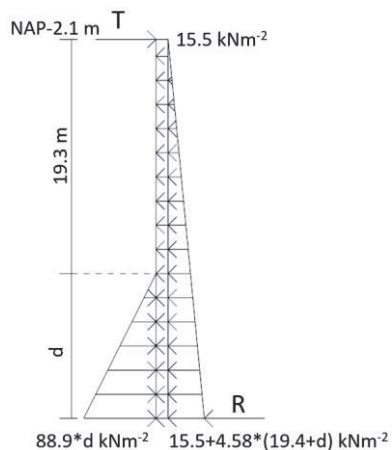


Figure 5-7 - Blum schematization SIF 2a

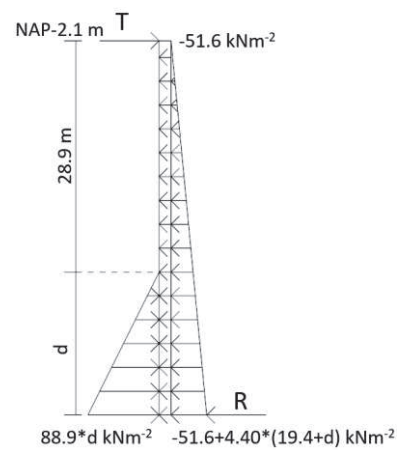


Figure 5-8 - Blum schematization SIF 2b

The results of the Blum calculations can be found in Table 5-4.

Table 5-4 - Representative values of the unknowns according to Blum for SIF 2

Scenario	T	R	d	Δd_{\min}	$M_{\text{field,CSPW}}$	$M_{\text{fixed,CSPW}}$	$F_{\text{M.V.-piles}}$
	kN/m	kN/m	m	m	kNm/m	kNm/m	kN/m
SIF 2a	512.8	1,804.3	9.05	1.81	1,602.6	-1,760.5	1,024.0
SIF 2b	-168.7	1,430.0	7.70	1.54	835.4	-1,237.9	-411.4

It is interesting to see that the Blum method does give a plausible result with scenario SIF 2b, this is due to the fact that the retaining height was far larger in this case, thus more active soil pressure could develop on the landward side.

6 D-Sheet calculation

This chapter contains the D-Sheet Piling calculations. First the challenges within this model and the way that these have been overcome will be elaborated on. Then, the individual scenarios and their outcomes will be presented.

6.1 Challenges

Relieving platform

Within the D-Sheet Piling software it is not possible to model a structure other than a retaining wall. To recreate the function of the RP the soil that would be supported by the RP has been left out. At the edge of the RP the soil is reapplied under the load distribution angle until the original soil surface has been reached again. The loads that would be on the removed “chunk” of soil have also been removed.

Reaction forces of the superstructure

The presence of the superstructure results in a number of reaction forces: a normal force in the concrete bearing piles, the M.V.-piles and the CSPW.

The force that is present on top of the CSPW is added to the model as a normal force in combination with a bending moment (due to the eccentricity of the normal force). Since the anchor force contributes to the magnitude of the normal force and the bending moment, the values that followed from the Blum method were used as an initial value which was corrected after the first calculation.

The force due to the concrete bearing piles is projected on the CSPW as was described in §4.2.3, this has been done with a set of horizontal loads.

Inclination of the combined sheet pile wall

Within the D-Sheet Piling software it is only possible to calculate vertical retaining walls, one way to go about this would be to alter the horizontal soil pressure coefficients. When using this K_a , K_0 , K_p method it is however only possible to use flat surfaces in combination with uniformly distributed loading. This was not an option for the quay structures that needed to be analyzed. It was therefore decided to model the CSPW as vertical. The driving force due to K_a on the landward side is larger than that of the situation with an inclined wall, K_p on the waterside is also larger. It was assumed that the effect of the larger driving force and that of the larger resisting force would cancel each other out in regard to the needed embedded depth.

Varying cross sections

The cross sections of the CSPW vary along the length of the wall due to corrosion, shorter length of the secondary sheet piles, and a varying thickness of the primary tubular pile elements. Within the software this was included by using different cross sections over the length of the CSPW.

6.2 Amazonehaven 1

The characteristics of the different cross sections are presented in Table 6-1. They were determined using the following formulas:

$$I_{yy,primary} = \pi R^3 t$$

$$I_{yy,cspw} = \frac{I_{yy,primary} + I_{yy,secondary}}{c.t.c.primary}$$

As a simplification the average wall thickness of the primary piles has been used in the calculation of the bending stiffness.

Table 6-1 - Characteristics of varying cross sections at Amazonehaven 1

Bottom of cross section	Average wall thickness	$I_{yy,primary}$	$I_{yy,secondary}$	$I_{yy,cspw}$
m+NAP	mm	m ⁴	m ⁴	m ⁴ /m
-15.5	16.3	0,0177	0,00043	0,006086
-25.5	16.3	0,0177	0,00043	0,006086
-29.57	15.7	0,0171	0,00057	0,005921
-37.5	15.7	0,0171	-	0,00573

The M.V.-piles were modelled as a translational spring support, its stiffness was decided based on load tests that were carried out. In normal loading conditions the load that will be supported by a single M.V.-pile will be ca. 2,000 kN, the corresponding deformations were ca. 7.5 mm. The stiffness could now be determined:

$$k_{M.V.-piles,normal} = \frac{F}{\Delta l * ctC_{M.V.-piles}} = \frac{2,000}{7.5 * 10^{-3} * 2.06} = 121,359.2 \frac{kN}{m} / m$$

To get to the effective stiffness of the anchor the transfer of the anchor force T into the M.V.-piles and the lengthening of the M.V.-piles due to the horizontal displacement have to be considered. The force in the M.V.-piles is equal to $T * \sqrt{2}$, the lengthening of the M.V.-piles is equal to the horizontal displacement divided by $\sqrt{2}$. The horizontal stiffness could now be determined.

$$k_{M.V.-piles,horizontal} = \frac{k_{M.V.-piles,normal}}{\sqrt{2}} = 60,679.6 \frac{kN}{m} / m$$

The models that were used within D-Sheet Piling are shown in Figure 6-1 and Figure 6-2.

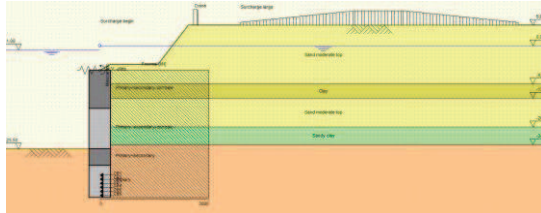


Figure 6-1 - D-Sheet model of Amazonehaven 1a

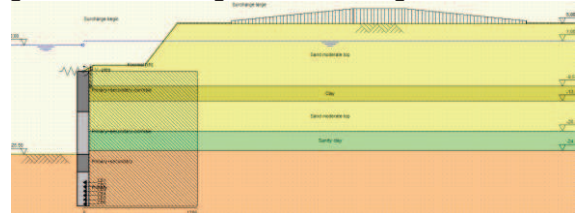


Figure 6-2 - D-Sheet model of Amazonehaven 1b

The analysis resulted in the bending moment distribution, shear force distribution, and deformations. The results are presented in Figure 6-3 and Figure 6-4.

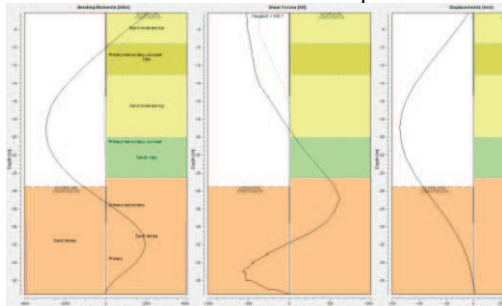


Figure 6-3 - D-Sheet results Amazonehaven 1a

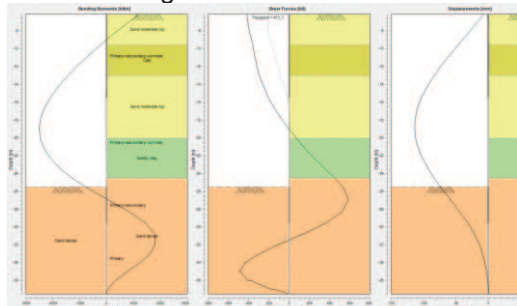


Figure 6-4 - D-Sheet results Amazonehaven 1b

After applying the reduction factors due to arching of the soil and shielding of the bearing piles, the following values were found:

Table 6-2 - D-Sheet results of Amazonehaven 1a & 1b

Scenario	$M_{field,CSPW}$	$M_{fixed,CSPW}$	T	$F_{M.V.-piles}$
	kNm/m	kNm/m	kN/m	kN/m
Amazonehaven 1a	2,025.9	-1,668.7	572.0	690.9
Amazonehaven 1b	1,833.1	-1,583.7	496.3	659.6

6.3 Amazonehaven 2

The described scenarios were modelled in the D-Sheet Piling software, the final models are shown in Figure 6-5 and Figure 6-6.

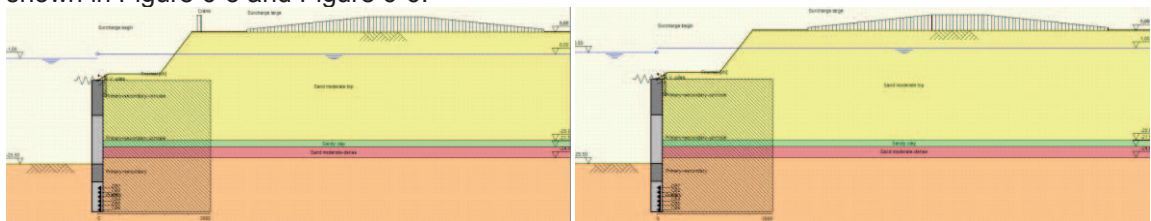


Figure 6-5 - D-Sheet model of Amazonehaven 2a Figure 6-6 - D-Sheet model of Amazonehaven 2b

The results of the two models can be found in Figure 6-7 and Figure 6-8.

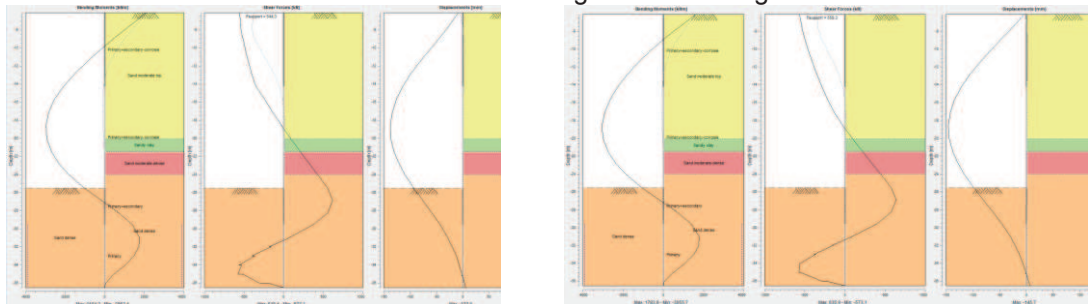


Figure 6-7 - D-Sheet results Amazonehaven 2a

Figure 6-8 - D-Sheet results Amazonehaven 2b

After applying the reduction factors due to arching of the soil and shielding of the bearing piles the following values were found:

Table 6-3 - D-Sheet results of Amazonehaven 2a & 2b

Scenario	$M_{field,CSPW}$	$M_{fixed,CSPW}$	T	$F_{M.V.-piles}$
	kNm/m	kNm/m	kN/m	kN/m
Amazonehaven 2a	2,060.2	-1,550.2	600.9	731.8
Amazonehaven 2b	1,841.9	-1,479.0	520.7	694.0

6.4 SIF 1

The same approach that was used for the Amazonehaven scenarios was applied to the SIF scenarios.

First, the varying cross sections were determined, these are presented in Table 6-4. The fact that corrosion has not yet occurred in scenario SIF 1b has been neglected here.

Table 6-4 - Characteristics of the varying cross sections at SIF 1a & 1b

Bottom of cross section	Average wall thickness	$I_{yy,primary}$	$I_{yy,secondary}$	$I_{yy,cspw}$
m+NAP	mm	m ⁴	m ⁴	m ⁴ /m
-25.0	20.75	0.0223	0.0010	0.00784
-27.85	21	0.0226	0.0011	0.00794
-34.0	21	0.0226	0	0.00758

The M.V.-piles were again modelled as translational spring supports. With the Blum method it was found that the load within an M.V.-pile is ca. 1,000 kN/m¹. One section of the RP has 5 M.V.-piles that are connected to it, making the “effective span” of the M.V.-piles 23.06/5=4.61 m. Based on this the acting load of a single M.V.-pile would approximately be 4,600 kN, test loading of the M.V.-piles gave insight into the displacements in relation to the acting force. The stiffness was determined as follows, the coefficient C stands for the transforming of the normal stiffness of the M.V.-piles to the horizontal stiffness:

$$k_{M.V.-piles, horizontal} = \frac{F}{\Delta l * ct c_{M.V.-piles} * C} = \frac{4,600}{21 * 10^{-3} * 4.61 * 2} = 23,757.9 \frac{kN}{m} / m$$

The D-Sheet models and their results in the SLS for SIF 1a and SIF 1b are depicted in Figure 6-9 to Figure 6-12.

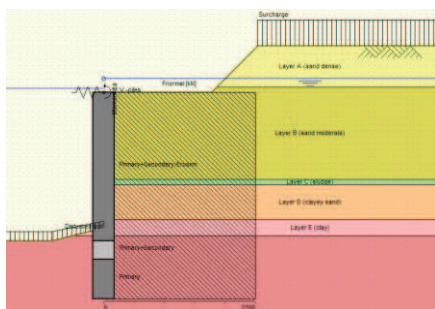


Figure 6-9 - D-Sheet model of SIF 1a

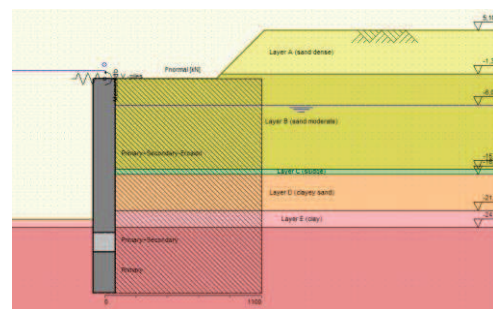


Figure 6-10 - D-Sheet model of SIF 1b

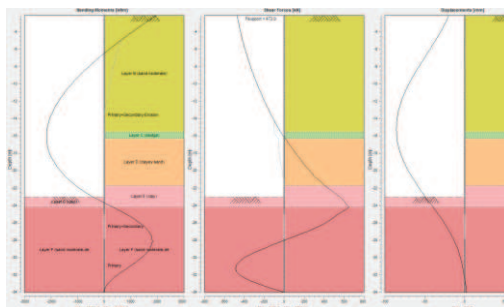


Figure 6-11 - D-Sheet results of SIF 1a

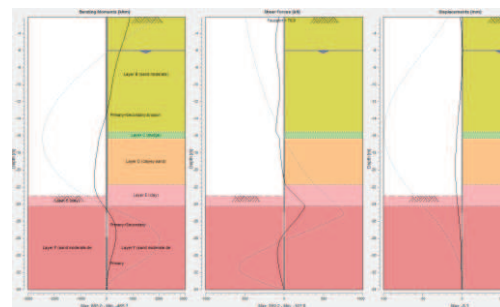


Figure 6-12 - D-Sheet results of SIF 1b

After applying the reduction factors due to arching of the soil and shielding of the bearing piles the values presented in Table 6-5 are found.

Table 6-5 - D-Sheet results of SIF 1a & 1b

Scenario	$M_{field,CSPW}$	$M_{fixed,CSPW}$	T	$F_{M.V.-piles}$
	kNm/m	kNm/m	kN/m	kN/m
SIF 1a	1,630.4	-1,645.4	542.8	1,066.2
SIF 1b	349.4	-339.8	77.65	-63.0

6.5 SIF 2

The different cross sections are presented in Table 6-6.

Table 6-6 - Characteristics of the varying cross sections at SIF 2a & 2b

Bottom of cross section	Average wall thickness	$I_{yy,primary}$	$I_{yy,secondary}$	$I_{yy,cspw}$
m+NAP	mm	m ⁴	m ⁴	m ⁴ /m
-25.0	22.75	0.02437	0.00103	0.008524
-31.0	23	0.024625	0.001065	0.008621
-39.0	23	0.024625	0	0.008263

There are 7 M.V.-piles per RP section, making the “effective span” of the M.V.-piles $23.06/7=3.29$ m, the acting load of a single M.V.-pile will approximately be 3,300 kN, based on M.V.-pile test loading the stiffness was determined as follows:

$$k_{M.V.-piles} = \frac{F}{\Delta l * ctC_{M.V.-piles} * C} = \frac{3,300}{14 * 10^{-3} * 3.29 * 2} = 35,822.8 \frac{kN}{m} / m$$

The D-Sheet models and their results for SIF 2a and SIF 2b are depicted in Figure 6-13 to Figure 6-16.

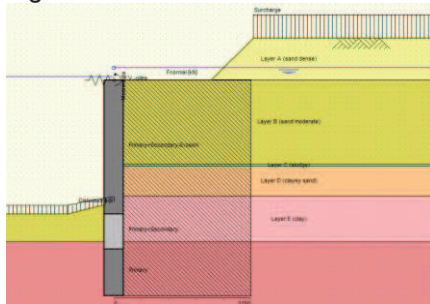


Figure 6-13 - D-Sheet model of SIF 2a

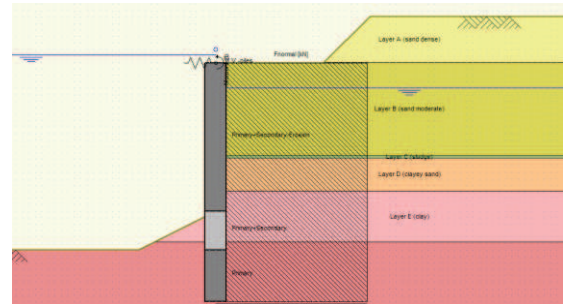


Figure 6-14 - D-Sheet model of SIF 2b

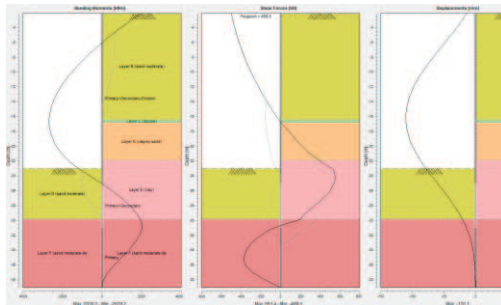


Figure 6-15 - D-Sheet results of SIF 2a

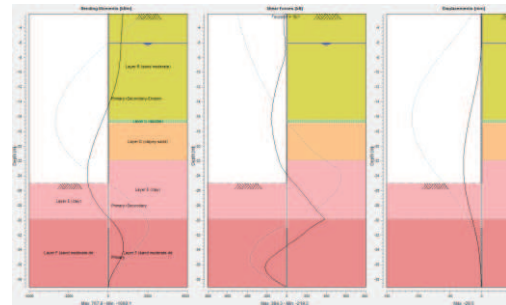


Figure 6-16 - D-Sheet results of SIF 2b

After applying the reduction factors due to arching of the soil and shielding of the bearing piles the following values are found:

Table 6-7 - D-Sheet results of SIF 2a & 2b

Scenario	$M_{field,CSPW}$	$M_{fixed,CSPW}$	T	$F_{M.V.-piles}$
	kNm/m	kNm/m	kN/m	kN/m
SIF 2a	2,035.4	-1,827.2	573.7	1,109.9
SIF 2b	801.1	-736.9	22.0	-141.6

7 Plaxis 2D calculation

This chapter presents the Plaxis 2D calculations. It starts by giving an overview of what the models consist of and what parameters were used. After this the individual scenarios and their results to the FEM modelling are presented.

7.1 Modelling of the original model of SIF 2

The original model for the SIF 2 scenario is shown in Figure 7-1. A systematic breakdown of the model is shown below.

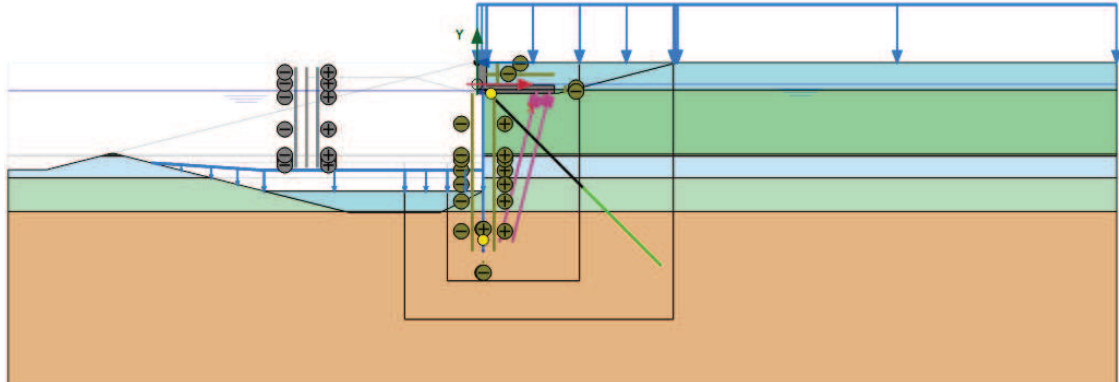


Figure 7-1 - Original Plaxis 2D model for SIF 2

7.1.1 Soil layering

The characteristics of the soil layering are presented in Table 7-1. All soil layers use the soil model Hardening Soil in combination with drained soil conditions.

Table 7-1 - Soil layering and characteristics for SIF 2

Soil type	Top of soil layer	$\gamma_{\text{unsat}} / \gamma_{\text{sat}}$	E_{50}	E_{oed}	E_{ur}	c'	ϕ'	ψ	R_{inter}	OCR
	m+NAP	kN/m^3	kN/m^2	kN/m^2	kN/m^2	kN/m^2	$^\circ$	$^\circ$	-	-
Layer A	5.1	19/21	$50 \cdot 10^3$	$50 \cdot 10^3$	$200 \cdot 10^3$	0	36	6	0.8	1
Layer B	-1.3	18.5/20	$30 \cdot 10^3$	$30 \cdot 10^3$	$120 \cdot 10^3$	0	33.5	3.5	0.8	1.7
Layer C	-16.4	16.5/16.5	$10 \cdot 10^3$	$5 \cdot 10^3$	$40 \cdot 10^3$	0	26	0	0.5	1.7
Layer D	-16.8	18/20	$30 \cdot 10^3$	$30 \cdot 10^3$	$120 \cdot 10^3$	0	27	0	0.8	1.7
Layer E	-21.9	18/18	$10 \cdot 10^3$	$5 \cdot 10^3$	$40 \cdot 10^3$	0	25	0	0.5	2.5
Layer F	-29.8	18.5/20	$50 \cdot 10^3$	$50 \cdot 10^3$	$200 \cdot 10^3$	0	36	6	0.8	2.5

7.1.2 Structural elements

Combined sheet pile wall

For this model the characteristics of the CSPW were the same over the entire length of the CSPW. In the improved models the CSPW consisted of a as a series of coupled plate elements to account for corrosion and the secondary sheet pile elements. The characteristics of the plate element were: $EI = 1.51 \cdot 10^6 \text{ kN m}^2/\text{m}$ and $EA = 6.16 \cdot 10^6 \text{ kN/m}$.

A plate element with the same structural characteristics as the saddle was used at the toe of the piles to simulate the end bearing of the piles. The length of the end bearing plate was estimated using the assumption that plugging of the CSPW would occur.

Saddle

The saddle consisted of two very stiff plate elements. One connected perpendicularly to the CSPW with a fixed connection and one fixed to the RP. The two plates were connected to

each other by means of a hinge. The characteristics were: $EI = 1 \cdot 10^{12} \text{ kN m}^2/\text{m}$ and $EA = 1 \cdot 10^{12} \text{ kN/m}$.

Relieving platform

A soil polygon was used to model this structural element. It used the Linear Elastic material model. The characteristics were: $\gamma_{\text{unsat}}/\gamma_{\text{sat}} = 24 \text{ kN/m}^3$, $E = 25 \cdot 10^6 \text{ kN/m}^2$, $\nu = 0.15$, and $R_{\text{inter}} = 1$.

Bearing piles

The bearing piles were modelled as embedded beam rows, massive predefined circular piles. The structural characteristics were: $E = 20.5 \cdot 10^6 \text{ kN/m}^2$, $D = 0.8 \text{ m}$, $L_{\text{spacing}} = 2.882 \text{ m}$, $T_{\text{skin,max}} = 418.7 \text{ kN/m}$, $F_{\text{max}} = 6840 \text{ kN}$.

M.V.-piles

A combination was used of a node-to-node anchor and an embedded beam row. The characteristics of the node-to-node anchor were: $EA = 5.67 \cdot 10^6 \text{ kN}$ and $L_{\text{spacing}} = 3.3 \text{ m}$. Those of the embedded beam row were: $E = 210 \cdot 10^6 \text{ kN/m}^2$, $A = 0.027 \text{ m}^2$, $I = 1.711 \cdot 10^{-3} \text{ m}^4$, and $L_{\text{spacing}} = 3.3 \text{ m}$.

7.1.3 Loads

There are three loads that were modelled, the bulk surcharge, the bollard load, and the remolded soil as a result of the spud can loading.

Bulk surcharge

Modelled as a uniformly distributed line load with a magnitude of 100 kN/m^2 .

Bollard load

Modelled as a point load with a magnitude of 130 kN/m .

Remolded soil

Modelled as a combination of line loads. A linear surcharge on the sloping part and a uniform surcharge on the horizontal part. The magnitude is $0.55 \cdot (25 - 18.4) \cdot 10 = 36.3 \text{ kN/m}^2$. This load is located on the water side.

7.1.4 Water conditions

The water levels that were used are:

1. NAP-0.84 m
2. NAP-2.5 m
3. NAP-1.5 m
4. NAP+0.05 m
5. NAP-6 m

In case of a water level difference between the land- and the waterside, the aquitard (layer E) was used to interpolate the water levels.

7.1.5 Meshing

The mesh of the model was set to “very fine”, additionally the mesh was refined in the areas which surround the structure. The created mesh is shown in Figure 2-1.

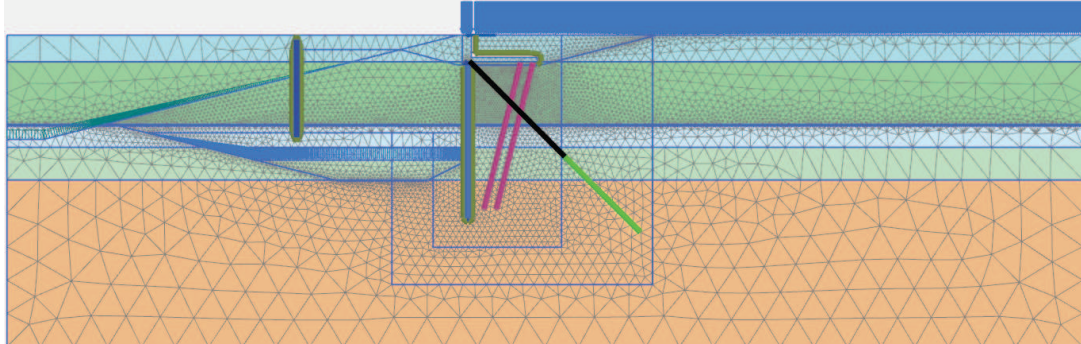


Figure 7-2 - Mesh of the original SIF 2 model

7.1.6 Calculation phases

For the calculation process the model was divided into 15 construction stages. The changes that were made in each calculation step will now be elaborated on.

1. Initial phase – Initial conditions with a sloped surface, $\text{GWL} = \text{NAP}-0.84 \text{ m}$;
2. Zero step to obtain equilibrium – No modifications;
3. Installation of the temporary sheet pile wall – The temporary wall has the structural characteristics of the saddle;
4. Excavation of the soil for the RP – Deactivation of specific soil clusters, $\text{GWL}_{\text{landside}} = \text{NAP}-2.5 \text{ m}$;
5. Installation the CSPW – Activation of the CSPW;
6. Installation of the foundation elements – Activation of the bearing piles and the embedded beam row part of the M.V.-piles;
7. Completion of the RP – Activation of the RP, node-to-node anchor part of the M.V.-piles, and the saddle;
8. Backfill – Activation of the soil behind the RP;
9. Removal of the temporary sheet pile wall – Deactivation of specific soil clusters and the temporary sheet pile wall, $\text{GWL} = \text{NAP}-0.84 \text{ m}$;
10. Initial dredging – Deactivation of the soil clusters up to $\text{NAP}-0.84$;
11. Lowering of the groundwater level – $\text{GWL}_{\text{land side}} = \text{NAP}-6 \text{ m}$;
12. Completion of the dredging (SIF 2b) – Deactivation of soil clusters up to $\text{NAP}-30 \text{ m}$;
13. Replacement of the removed soil – Activation of soil clusters up to $\text{NAP}-18.4 \text{ m}$;
14. Restoration of the normal groundwater level – $\text{GWL} = \text{NAP}-0.84 \text{ m}$;
15. Design conditions (SIF 2a) – $\text{GWL}_{\text{land side}} = \text{NAP}+0.05 \text{ m}$, $\text{GWL}_{\text{water side}} = \text{NAP}-1.5 \text{ m}$, activation of all the loads, deactivation of the remolded soil clusters.

7.2 Sensitivity of the model

The sensitivity of the created model in regard to modifications of the way that structural elements are represented was studied in Appendix C. The goal of this analysis was to see what the effect of specific modifications was on structural forces and the displacements of the CSPW. The results belonging to the original model are presented in Table 7-2. The meaning of the presented variables is presented below:

N_{cspw} = The maximum normal force present in the CSPW

$M_{\text{field,CSPW}}$ = The maximum field bending moment present in the CSPW

- $M_{\text{fixed,CSPW}}$ = The maximum fixed end bending moment present in the CSPW
- $F_{\text{M.V.}}$ = The normal force present in the M.V.-piles
- $N_{\text{BP,left}}$ = The maximum normal force present in the front bearing piles
- $N_{\text{BP,right}}$ = The maximum normal force present in the back bearing piles
- $U_{\text{CSPW,top}}$ = The horizontal displacement of the top of the CSPW
- $U_{\text{CSPW,field}}$ = The maximum horizontal displacement of the CSPW

Table 7-2 -Structural forces and displacements of the original SIF model

N_{CSPW}	$M_{\text{field,CSPW}}$	$M_{\text{fixed,CSPW}}$	$F_{\text{M.V.}}$	$N_{\text{BP,left}}$	$N_{\text{BP,right}}$	$U_{\text{CSPW,top}}$	$U_{\text{CSPW,field}}$
kN/m	kNm/m	kNm/m	kN/m	kN/m	kN/m	mm	mm
2,522.9	1,999.2	-1,539.0	1,024.7	1,573.7	1,168.9	80.2	139.0

The modifications that were considered were as follows:

- Setting the OCR to 1;
- Adding a deep clay layer to the soil layering;
- Modelling the bearing piles as fixed end anchors;
- Modelling the RP as a set of plate elements;
- Using different material models (both with the original values for the OCR as OCR=1).

The results of the analysis are presented in Figure 7-3. The horizontal axis shows the variable which is being considered, the vertical axis presents the relative effect of the modification in regard to the original model.

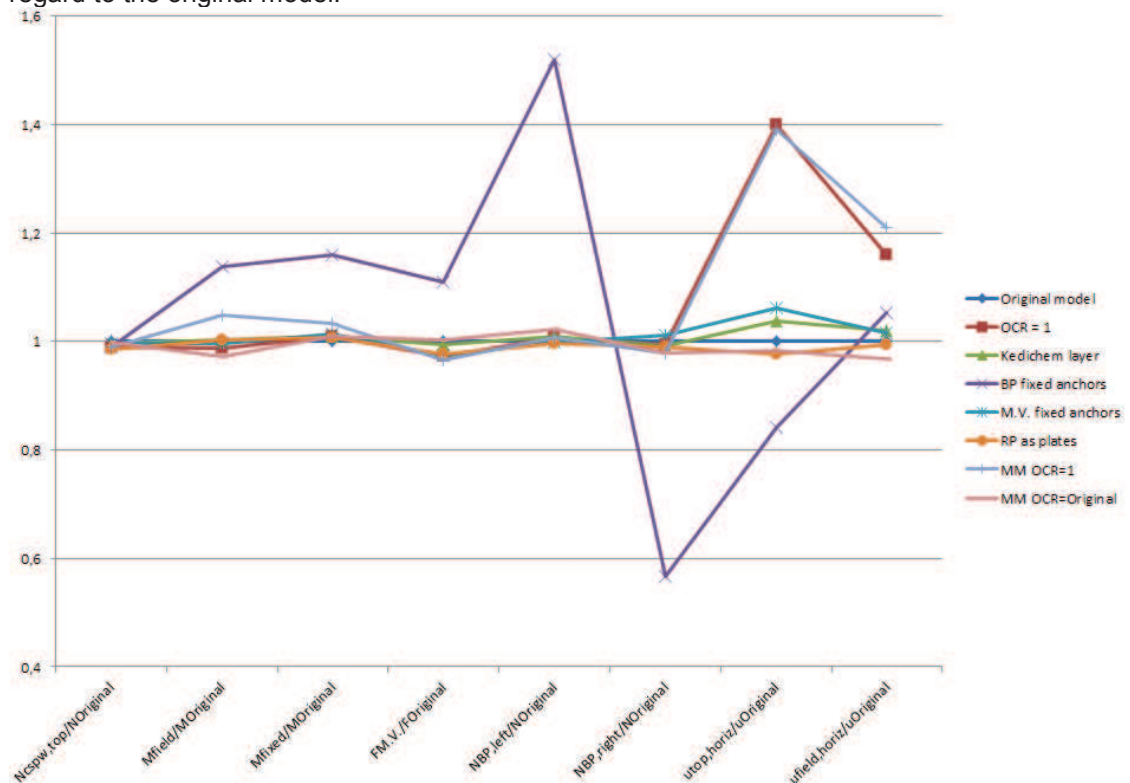


Figure 7-3 - Result of the model input sensitivity analysis

In the figure it can be seen that the OCR mainly affects the displacements of the CSPW, while modelling the bearing piles as fixed end anchors has a large effect on almost all variables. Apart from these 3 models the variations in the results all stay within ca. 5% of the original values.

Based on the analysis that was performed on the model sensitivity it was decided to use the following modelling methods for the final design of the different scenarios:

- All soil layers use the material model Hardening Soil with small-strain stiffness [22];
- The Kedichem clay layer is present, it has the same soil characteristics as the Wijchense clay layer;
- M.V.-piles as a combination of node-to-node anchors and embedded beam rows;
- OCR=1 for the “new” soil, 1.7 for the Holocene soil layers, and 2.5 for the Pleistocene layers;
- Bearing piles as embedded beam rows;
- RP as a soil polygon.

7.3 Amazonehaven 1

The Plaxis 2D model for this quay structure is shown in Figure 7-4. The corresponding structural characteristics have been determined using [2] and [14].

The boundaries of the model were chosen so that they did not create disturbances within the model. After the calculation it was verified that the boundaries were defined correctly.

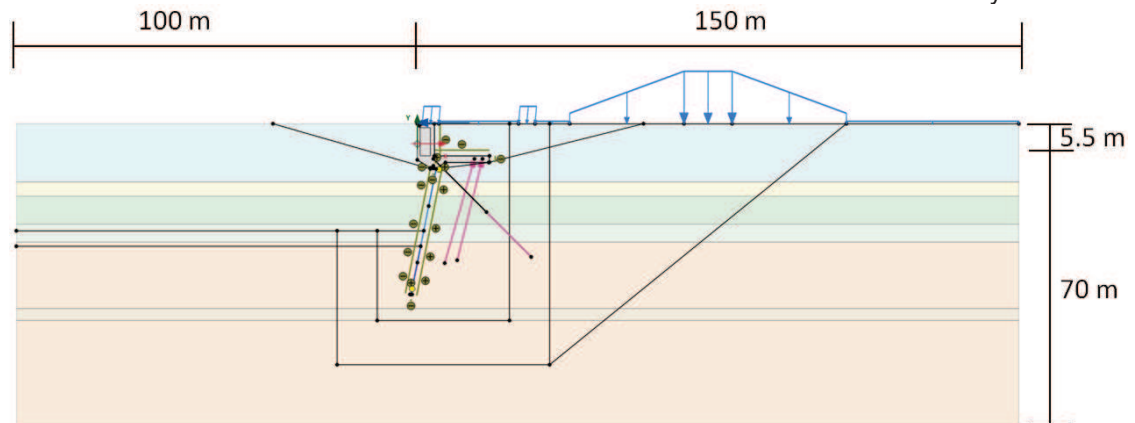


Figure 7-4 - Plaxis 2D model of Amazonehaven 1

7.3.1 Soil layering

The different soil layers all use the Hardening Soil with small-strain stiffness material model in combination with drained soil conditions. The characteristics of the soil layers are presented in Table 7-3.

Table 7-3 - Soil characteristics for Amazonehaven 1

Parameter	Unit	Backfill sand	Silt	Holocene sand	Clay Wijchen	Pleistocene sand	Clay Kedichem
Top of the soil layer	m+NAP	5	-9.5	-13	-20	-24.5 -44	-41
$\gamma_{\text{unsat}}/\gamma_{\text{sat}}$	kN/m ³	18/20	18/18	18.5/20	18/18	18.5/20	18/18
E_{50}	kN/m ²	$50 \cdot 10^3$	$10 \cdot 10^3$	$30 \cdot 10^3$	$10 \cdot 10^3$	$50 \cdot 10^3$	$10 \cdot 10^3$
E_{oed}	kN/m ²	$50 \cdot 10^3$	$5 \cdot 10^3$	$30 \cdot 10^3$	$5 \cdot 10^3$	$50 \cdot 10^3$	$5 \cdot 10^3$
E_{ur}	kN/m ²	$200 \cdot 10^3$	$40 \cdot 10^3$	$120 \cdot 10^3$	$40 \cdot 10^3$	$200 \cdot 10^3$	$40 \cdot 10^3$
c'	kN/m ²	0	15	0	15	0	15
φ'	°	30	20	30	22.5	35	25
ψ	°	0	0	0	0	5	0
R_{inter}	-	0.8	0.5	0.8	0.5	0.8	0.5

OCR	-	1	1.7	1.7	2.5	2.5	2.5
Y_{0.7}	-	1.17*10 ⁻⁴	0.4*10 ⁻³	1.5*10 ⁻⁴	0.4*10 ⁻³	1.17*10 ⁻⁴	0.4*10 ⁻³
G₀^{ref}	kN/m ²	104*10 ³	40*10 ³	86.5*10 ³	40*10 ³	104*10 ³	40*10 ³

7.3.2 Structural elements

The structural elements have been modelled in the same way as was described in the previous paragraph. The characteristics are shown in Table 7-4.

Table 7-4 - Structural characteristics of Amazonehaven 1

Structural element	Characteristics
CSPW	1 st part: top at NAP-6 m, EA = 7.193*10 ⁶ kN/m, EI = 1.278*10 ⁶ kN m ² /m 2 nd part: top at NAP-15.5 m, EA = 7.193*10 ⁶ kN/m, EI = 1.278*10 ⁶ kN m ² /m 3 rd part: top at NAP -25.5 m, EA = 7.009*10 ⁶ kN/m, EI = 1.243*10 ⁶ kN m ² /m 4 th part: top at NAP-29.57 m, EA = 4.881 *10 ⁶ kN/m, EI = 1.203*10 ⁶ kN m ² /m
Saddle	EA = 10*10 ⁹ kN/m, EI = 10*10 ⁹ kN m ² /m
RP	Y _{unsat} /Y _{sat} = 24 kN/m ³ , E = 25*10 ⁶ kN/m ² , ν = 0.15, and R _{inter} = 1
Bearing piles	E = 20*10 ⁶ kN/m ² , b = h = 0.45 m, L _{spacing} = 2.06 m, T _{skin} = 270 kN/m, F _{max} = 3038 kN
M.V.-piles	Node-to-node: EA = 4.095*10 ⁶ kN, L _{spacing} = 2.06 m Embedded beam row: E = 210*10 ⁶ kN/m ² , A = 0.0195 m ² , I = 1*10 ⁻³ , L _{spacing} = 2.06 m, T _{skin} = 383 kN/m, F _{max} = 0 kN

7.3.3 Loads

There are 3 different loads in the model. A bollard load, which is modelled as a point load, its eccentricity in regard to the RP was created by means of a plate element that was connected to the RP. The crane loads were modelled as two line loads at a certain distance from one another. The bulk surcharge was modelled as a combination of two linear line loads and a uniform line load.

7.3.4 Water levels

The water levels that have been used in the model are:

1. NAP+1 m
2. NAP+0 m
3. NAP-1 m
4. NAP-6.5 m

The Wijchense clay layer was used to interpolate the water levels in the case of a water level difference between the land side and the water side.

7.3.5 Meshing

The mesh of the model was set to “very fine”, additionally the mesh was refined in the areas which surround the structure and underneath the bulk surcharge. The created mesh of the model is shown in Figure 7-5.

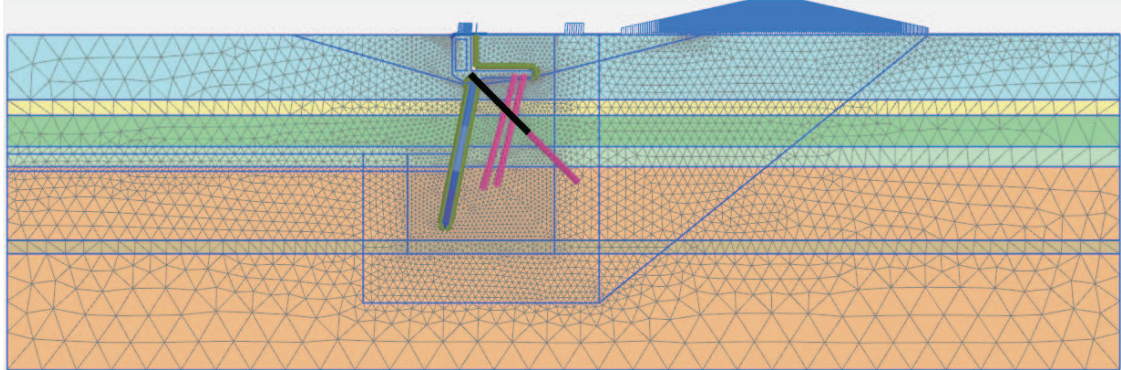


Figure 7-5 - Mesh of Amazonehaven 1

7.3.6 Calculation phases

For the calculation process the model was divided into 9 construction stages. These stages and what they entailed are presented below:

1. Initial phase – Initial conditions with a horizontal soil surface, $GWL = NAP+0$ m;
2. Zero step to obtain equilibrium – No modifications;
3. Excavation of the soil for the RP – Deactivation of specific soil clusters, $GWL = NAP-6.5$ m;
4. Installation of the CSPW – Activation of the CSPW;
5. Completion of the RP – Activation of the bearing piles, the M.V.-piles, the saddle, and the RP;
6. Backfill – Activation of the soil behind the RP, $GWL = NAP+0$ m;
7. Dredging – Deactivation of soil clusters on the waterside up to a depth of $NAP-25.5$ m, $GWL = NAP-1$ m;
8. Design conditions (Amazonehaven 1a) – Activation of all the loads, $GWL_{\text{landside}} = NAP+0$ m;
9. Design conditions (Amazonehaven 1b) – Starting from step 7, partial activation of the normal surcharge (behind the RP), activation of the bulk surcharge, $GWL_{\text{waterside}} = NAP+0$ m, $GWL_{\text{landside}} = NAP+1$ m.

7.3.7 Results

The scaled up deformed meshes of construction stages 8 and 9 are presented in Figure 7-6 and Figure 7-7.

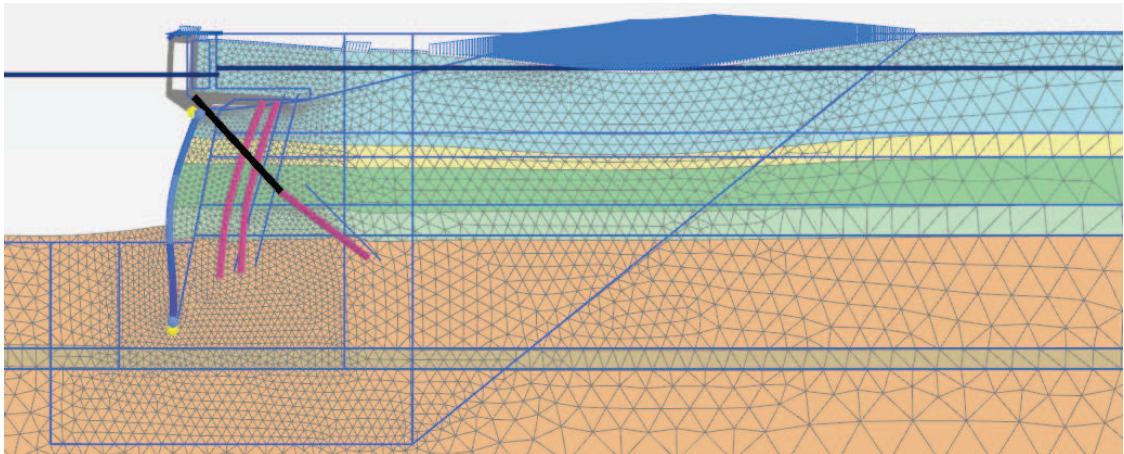


Figure 7-6 - Deformed mesh of Amazonehaven 1a, scaled up 20 times

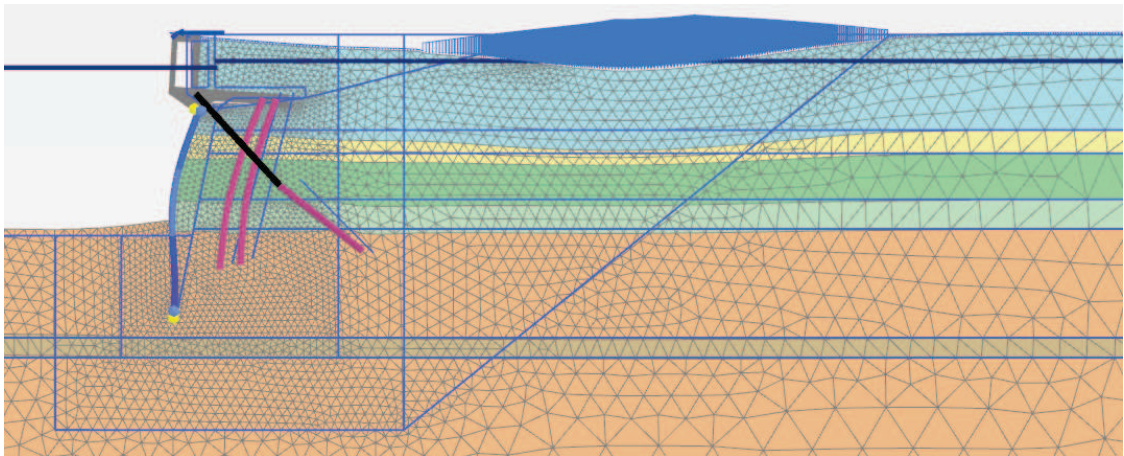


Figure 7-7 - Deformed mesh of Amazonehaven 1b, scaled up 20 times

When looking at the boundaries of the model it can be seen that both the deformations and the stresses have become constant, thus the boundaries have been chosen correctly. The results of the calculation are presented in Table 7-5. The values in this table have not been altered to account for the shielding effect in combination with the arching of the soil, this has been decided because the shielding effect has already been implemented by the use of embedded beam rows for the bearing piles, the individual effects could however not be determined.

Table 7-5 - Plaxis 2D results of Amazonehaven 1

Scenario	N	$M_{\text{field,CSPW}}$	$M_{\text{fixed,CSPW}}$	$F_{\text{M.V.-piles}}$	$U_{\text{CSPW,top}}$	$U_{\text{CSPW,field}}$
	kN/m	kNm/m	kNm/m	kN/m	mm	mm
Amazonehaven 1a	2,694.8	2,314.6	-1,240.1	1,109.8	161.2	225.7
Amazonehaven 1b	2,234.8	2,174.4	-1,297.7	1,192.0	143.8	206.6

7.4 Amazonehaven 2

This structure was modelled in the same way as that of Amazonehaven 1a. The approach is shown below.

7.4.1 Soil layering

The characteristics of the soil are shown in Table 7-6.

Table 7-6 - Soil characteristics for Amazonehaven 2

Parameter	Unit	Backfill sand	Holocene sand	Clay Wijchen	Pleistocene top sand	Pleistocene sand	Clay Kedichem
Top of the soil layer	m+NAP	5	-9.5	-20	-21.5	-24 -44	-41
$\gamma_{\text{unsat}}/\gamma_{\text{sat}}$	kN/m ³	18/20	18/20	18/18	18.5/20	18.5/20	18/18
E_{50}	kN/m ²	$50 \cdot 10^3$	$30 \cdot 10^3$	$10 \cdot 10^3$	$50 \cdot 10^3$	$50 \cdot 10^3$	$10 \cdot 10^3$
E_{oed}	kN/m ²	$50 \cdot 10^3$	$30 \cdot 10^3$	$5 \cdot 10^3$	$50 \cdot 10^3$	$50 \cdot 10^3$	$5 \cdot 10^3$
E_{ur}	kN/m ²	$200 \cdot 10^3$	$120 \cdot 10^3$	$40 \cdot 10^3$	$200 \cdot 10^3$	$200 \cdot 10^3$	$40 \cdot 10^3$
c'	kN/m ²	0	0	15	0	0	15
φ'	°	30	30	22.5	32.5	35	25
ψ	°	0	0	0	0	5	0
R_{inter}	-	0.8	0.8	0.5	0.8	0.8	0.5
OCR	-	1	1.7	2.5	2.5	2.5	2.5
$\gamma_{0.7}$	-	$1.17 \cdot 10^{-4}$	$1.17 \cdot 10^{-4}$	$0.4 \cdot 10^{-3}$	$1.17 \cdot 10^{-4}$	$1.17 \cdot 10^{-4}$	$0.4 \cdot 10^{-3}$
G_0^{ref}	kN/m ²	$104 \cdot 10^3$	$104 \cdot 10^3$	$40 \cdot 10^3$	$104 \cdot 10^3$	$104 \cdot 10^3$	$40 \cdot 10^3$

7.4.2 Structural elements

The characteristics of the different structural elements are shown in Table 7-7.

Table 7-7 - Structural characteristics of Amazonehaven 2

Structural element	Characteristics
CSPW	1 st part: top at NAP-6 m, EA = $6.485 \cdot 10^6$ kN/m, EI = $1.107 \cdot 10^6$ kN m ² /m 2 nd part: top at NAP-15.5 m, EA = $7.193 \cdot 10^6$ kN/m, EI = $1.278 \cdot 10^6$ kN m ² /m 3 rd part: top at NAP -25.5 m, EA = $7.009 \cdot 10^6$ kN/m, EI = $1.243 \cdot 10^6$ kN m ² /m 4 th part: top at NAP-29.57 m, EA = $4.881 \cdot 10^6$ kN/m, EI = $1.203 \cdot 10^6$ kN m ² /m
Saddle	EA = $10 \cdot 10^9$ kN/m, EI = $10 \cdot 10^9$ kN m ² /m
RP	$\gamma_{\text{unsat}}/\gamma_{\text{sat}} = 24$ kN/m ³ , E = $25 \cdot 10^6$ kN/m ² , $\nu = 0.15$, $R_{\text{inter}} = 1$
Bearing piles	E = $20 \cdot 10^6$ kN/m ² , b = h = 0.45 m, $L_{\text{spacing}} = 2.06$ m, $T_{\text{skin}} = 270$ kN/m, $F_{\text{max}} = 3038$ kN
M.V.-piles	Node-to-node: EA = $4.095 \cdot 10^6$ kN, $L_{\text{spacing}} = 2.06$ m Embedded beam row: E = $210 \cdot 10^6$ kN/m ² , A = 0.0195 m ² , I = $1 \cdot 10^{-3}$, $L_{\text{spacing}} = 2.06$ m, $T_{\text{skin}} = 383$ kN/m, $F_{\text{max}} = 0$ kN

7.4.3 Remainder

The loads, water levels, meshing, and calculation phases were identical to that of Amazonehaven 1 and will therefore not be elaborated on any further.

7.4.4 Results

Figure 7-8 and Figure 7-9 show the scaled up deformed meshes of Amazonehaven 2. The results of the modelling are presented in Table 7-8.

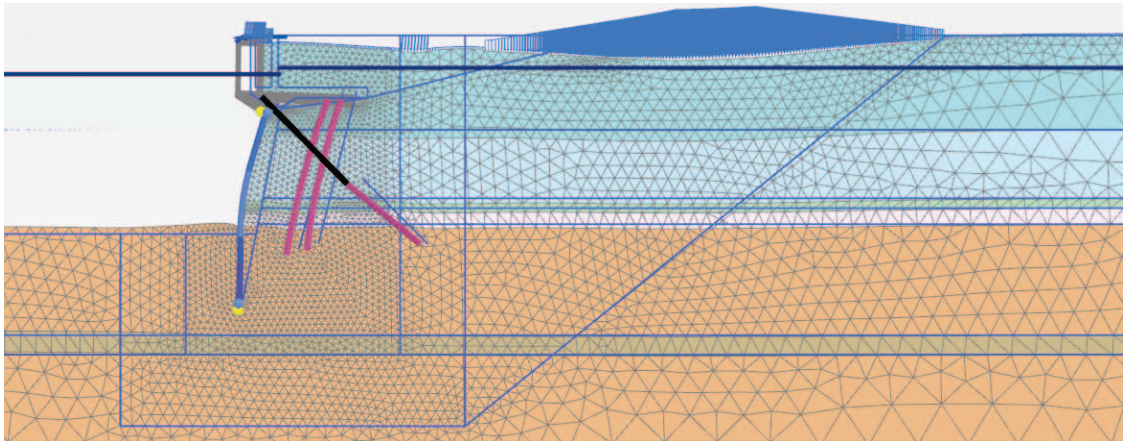


Figure 7-8 - Deformed mesh of Amazonehaven 2a, scaled up 20 times

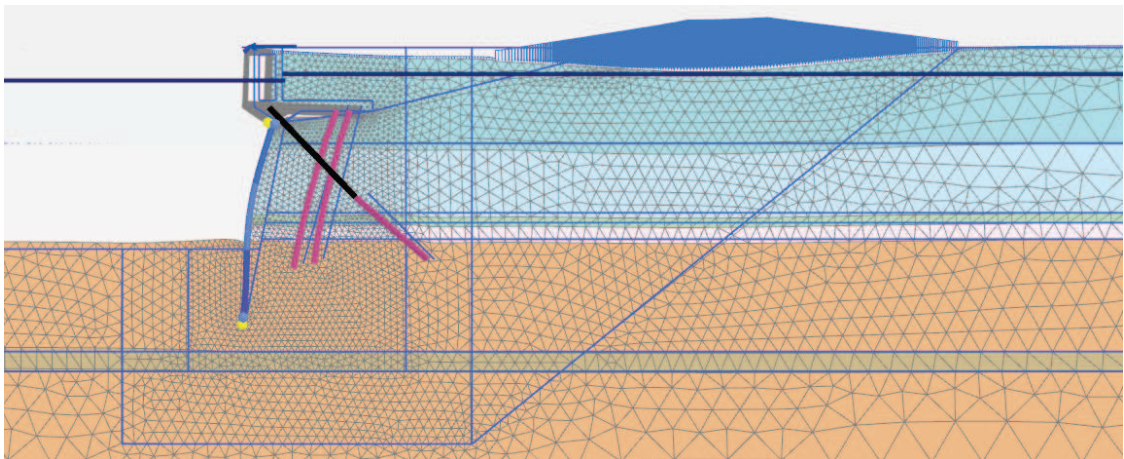


Figure 7-9 - Deformed mesh of Amazonehaven 2b, scaled up 20 times

Table 7-8 - Plaxis 2D results of Amazonehaven 2

Scenario	N	$M_{\text{field,CSPW}}$	$M_{\text{fixed,CSPW}}$	$F_{\text{M.V.-piles}}$	$u_{\text{CSPW,top}}$	$u_{\text{CSPW,field}}$
	kN/m	kNm/m	kNm/m	kN/m	mm	mm
Amazonehaven 2a	2,869.9	1,655.8	-833.7	922.8	120.9	159.0
Amazonehaven 2b	2,109.7	1,481.4	-925.6	886.6	94.6	134.4

7.5 SIF 1

The final Plaxis 2D model for this quay structure is shown in Figure 7-10. The corresponding structural characteristics have been determined based on [14].

The boundaries of the model were chosen as such that they did not create disturbances within the model. After the calculation it was verified that the boundaries were defined correctly.

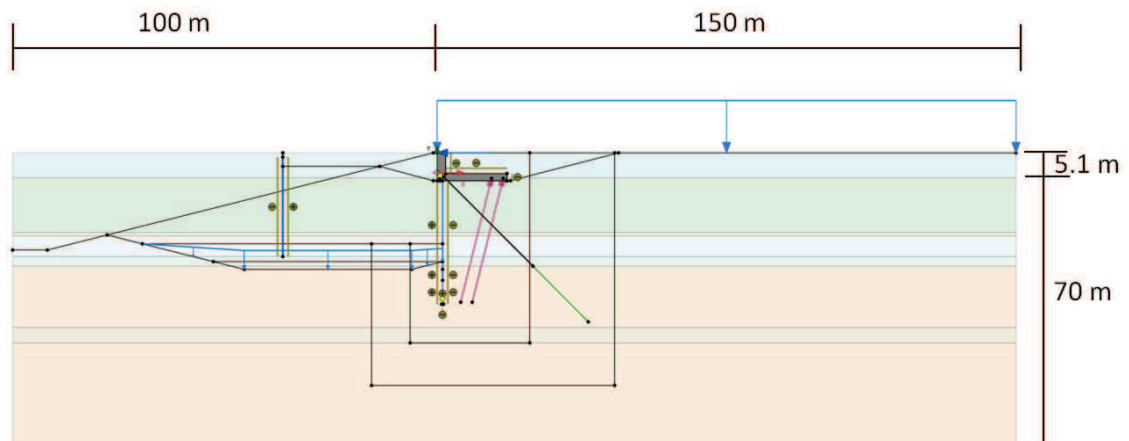


Figure 7-10 - Plaxis 2D model of SIF 1

The same model set up was used as the one that was presented in §7.1 with the modifications that are described below.

7.5.1 Soil layering

The material model Hardening Soil with small-strain stiffness was used for all the soil layers. Table 7-9 shows the additional soil characteristics. Apart from the information in this table an additional soil layer was added, layer G (the clay layer of Kedichem). This layer is positioned from NAP-40 m to NAP-44 m and has the same characteristics as layer E.

Table 7-9 - Additional soil characteristics for SIF

Soil layer	Top of soil layer	$\gamma_{0.7}$	G_0^{ref}
Unit	m+NAP	-	kN/m ²
Layer A	5.1	$1.17 \cdot 10^{-4}$	$104 \cdot 10^3$
Layer B	-1.3	$1.5 \cdot 10^{-4}$	$86.5 \cdot 10^3$
Layer C	-15.5	$0.4 \cdot 10^{-3}$	$40 \cdot 10^3$
Layer D	-16.3	$1.5 \cdot 10^{-4}$	$86.5 \cdot 10^3$
Layer E	-21.7	$0.4 \cdot 10^{-3}$	$40 \cdot 10^3$
Layer F	-24.4	$1.17 \cdot 10^{-4}$	$104 \cdot 10^3$
	-44		

7.5.2 Structural elements

The characteristics of the different structural elements are presented in Table 7-10.

Table 7-10 - Structural characteristics of SIF 1

Structural element	Characteristics
CSPW	Top part: top at NAP-2 m, EA = $9.060 \cdot 10^6$ kN/m, EI = $1.650 \cdot 10^6$ kN m ² /m Middle part: top at NAP-25 m, EA = $9.230 \cdot 10^6$ kN/m, EI = $1.670 \cdot 10^6$ kN m ² /m Bottom part: top at NAP -27.85 m, EA = $6.600 \cdot 10^6$ kN/m, EI = $1.590 \cdot 10^6$ kN m ² /m
Saddle	EA = $1 \cdot 10^{12}$ kN/m, EI = $1 \cdot 10^{12}$ kN m ² /m
RP	$\gamma_{\text{unsat}} / \gamma_{\text{sat}} = 24$ kN/m ³ , E = $25 \cdot 10^6$ kN/m ² , $\nu = 0.15$, $R_{\text{inter}} = 1$
Bearing piles	E = $20.5 \cdot 10^6$ kN/m ² , D = 0.8 m, $L_{\text{spacing}} = 2.882$ m, $T_{\text{skin,max}} = 266.9$ kN/m, $F_{\text{max}} = 6392$ kN.
M.V.-piles	Node-to-node: EA = $5.670 \cdot 10^6$ kN, $L_{\text{spacing}} = 4.612$ m Embedded beam row: E = $210 \cdot 10^6$ kN/m ² , A = 0.027 m ² , I = $1.711 \cdot 10^{-3}$ m ⁴ , $L_{\text{spacing}} = 4.612$ m, $T_{\text{skin}} = 550$ kN/m, $F_{\text{max}} = 0$ kN

7.5.3 Calculation phases

For the calculation process the model was divided into 16 construction stages. The changes that were made in each calculation step will now be elaborated on.

1. Initial phase – Initial conditions with a sloped surface, $GWL = NAP - 0.84$ m;
2. Zero step to obtain equilibrium – No modifications;
3. Installation of the temporary sheet pile wall – The temporary wall has the structural characteristics of the saddle;
4. Excavation of the soil for the RP – Deactivation of specific soil clusters, $GWL_{land\ side} = NAP - 2.5$ m;
5. Installation of the bearing piles – Activation of the bearing piles;
6. Installation the CSPW – Activation of the CSPW;
7. Installation of the foundation elements – Activation of the embedded beam row part of the M.V.-piles;
8. Completion of the RP – Activation of the RP, node-to-node anchor of the M.V.-piles, and the saddle;
9. Backfill – Activation of the soil behind the RP;
10. Removal of the temporary sheet pile wall – Deactivation of specific soil clusters and the temporary sheet pile wall, $GWL = NAP - 0.84$ m;
11. Initial dredging – Deactivation of the soil clusters up to $NAP - 18.4$ m;
12. Lowering of the groundwater level – $GWL_{land\ side} = NAP - 6$ m;
13. Completion of the dredging (SIF 2b) – Deactivation of soil clusters up to $NAP - 23$ m;
14. Replacement of the removed soil – Activation of soil clusters up to $NAP - 18.4$ m;
15. Restoration of the normal groundwater level – $GWL = NAP - 0.84$ m;
16. Design conditions (SIF 2a) – $GWL_{land\ side} = NAP + 0.05$ m, $GWL_{water\ side} = NAP - 1.5$ m, activation of all the loads, deactivation of the remolded soil clusters.

7.5.4 Results

The scaled up deformed meshes of construction stages 13 and 16 are presented in Figure 7-11 and Figure 7-12.

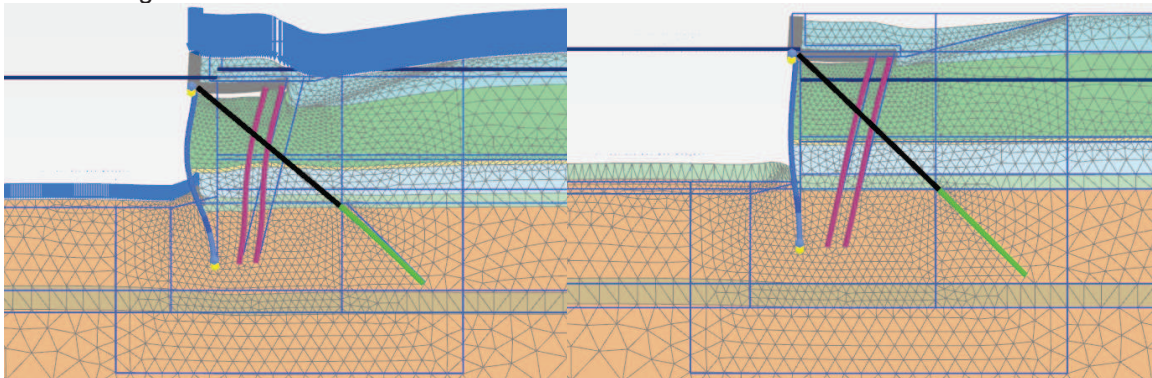


Figure 7-11 - Deformed mesh of SIF 1a, scaled up 50 times

Figure 7-12 - Deformed mesh of SIF 1b, scaled up 50 times

Table 7-11 presents the results of the Plaxis 2D calculation for the SIF 1 scenario.

Table 7-11 - Plaxis 2D results of SIF 1

Scenario	N	$M_{field,CSPW}$	$M_{fixed,CSPW}$	$F_{M.V.-piles}$	$u_{CSPW,top}$	$u_{CSPW,field}$
	kN/m	kNm/m	kNm/m	kN/m	mm	mm
SIF 1a	2,462.0	1,730.1	-1,570.4	951.4	81.0	110.5
SIF 1b	1,238.1	625.6	-725.8	83.6	15.8	32.1

7.6 SIF 2

The same approach was applied to the SIF 2 scenario. The differences in regard to the previous paragraph are discussed below.

7.6.1 Soil layering

The soil layering is shown in Table 7-12.

Table 7-12 - Soil layer positions for SIF 2

Soil layer	Layer A	Layer B	Layer C	Layer D	Layer E	Layer F	Layer G
Top [m+NAP]	5.1	-2	-16.4	-16.8	-21.9	-29.8	-46
						-50	

7.6.2 Structural elements

The structural characteristics for this scenario are shown in Table 7-13.

Table 7-13 - Structural characteristics of SIF 2

Structural element	Characteristics
CSPW	Top part: top at NAP-2 m, EA = $9.690 \cdot 10^6$ kN/m, EI = $1.790 \cdot 10^6$ kN m ² /m Middle part: top at NAP-25 m, EA = $9.850 \cdot 10^6$ kN/m, EI = $1.810 \cdot 10^6$ kN m ² /m Bottom part: top at NAP -31 m, EA = $7.230 \cdot 10^6$ kN/m, EI = $1.740 \cdot 10^6$ kN m ² /m
Saddle	EA = $1 \cdot 10^{12}$ kN/m, EI = $1 \cdot 10^{12}$ kN m ² /m
RP	$\gamma_{unsat}/\gamma_{sat} = 24$ kN/m ³ , E = $25 \cdot 10^6$ kN/m ² , $\nu = 0.15$, $R_{inter} = 1$
Bearing piles	E = $20.5 \cdot 10^6$ kN/m ² , D = 0.8 m, $L_{spacing} = 2.882$ m, $T_{skin,max} = 266.9$ kN/m, $F_{max} = 6392$ kN.
M.V.-piles	Node-to-node: EA = $5.670 \cdot 10^6$ kN, $L_{spacing} = 3.3$ m Embedded beam row: E = $210 \cdot 10^6$ kN/m ² , A = 0.027 m ² , I = $1.711 \cdot 10^{-3}$ m ⁴ , $L_{spacing} = 3.3$ m, $T_{skin} = 550$ kN/m, $F_{max} = 0$ kN

7.6.3 Calculation phases

For the calculation process the model was divided into 16 construction stages. The changes that were made in each calculation step will now be elaborated on.

1. Initial phase – Initial conditions with a sloped surface, GWL = NAP-0.84 m;
2. Zero step to obtain equilibrium – No modifications;
3. Installation of the temporary sheet pile wall – The temporary wall has the structural characteristics of the saddle;
4. Excavation of the soil for the RP – Deactivation of specific soil clusters, $GWL_{landside} =$ NAP-2.5 m;
5. Installation of the bearing piles – Activation of the bearing piles;
6. Installation the CSPW – Activation of the CSPW;
7. Installation of the foundation elements – Activation of the embedded beam row part of the M.V.-piles;
8. Completion of the RP – Activation of the RP, node-to-node anchor of the M.V.-piles, and the saddle;
9. Backfill – Activation of the soil behind the RP;
10. Removal of the temporary sheet pile wall – Deactivation of specific soil clusters and the temporary sheet pile wall, GWL = NAP-0.84 m;
11. Initial dredging – Deactivation of the soil clusters up to NAP-18.4 m;
12. Lowering of the groundwater level – $GWL_{landside} =$ NAP-6 m;

13. Completion of the dredging (SIF 2b) – Deactivation of soil clusters up to NAP-31 m;
14. Replacement of the removed soil – Activation of soil clusters up to NAP-18.4 m;
15. Restoration of the normal groundwater level – $\text{GWL} = \text{NAP}-0.84 \text{ m}$;
16. Design conditions (SIF 2a) – $\text{GWL}_{\text{land side}} = \text{NAP}+0.05 \text{ m}$, $\text{GWL}_{\text{water side}} = \text{NAP}-1.5 \text{ m}$, activation of all the loads, deactivation of the remolded soil clusters.

7.6.4 Results

The scaled up deformed meshes are presented in Figure 7-13 and Figure 7-14. The results are shown in Table 7-14.

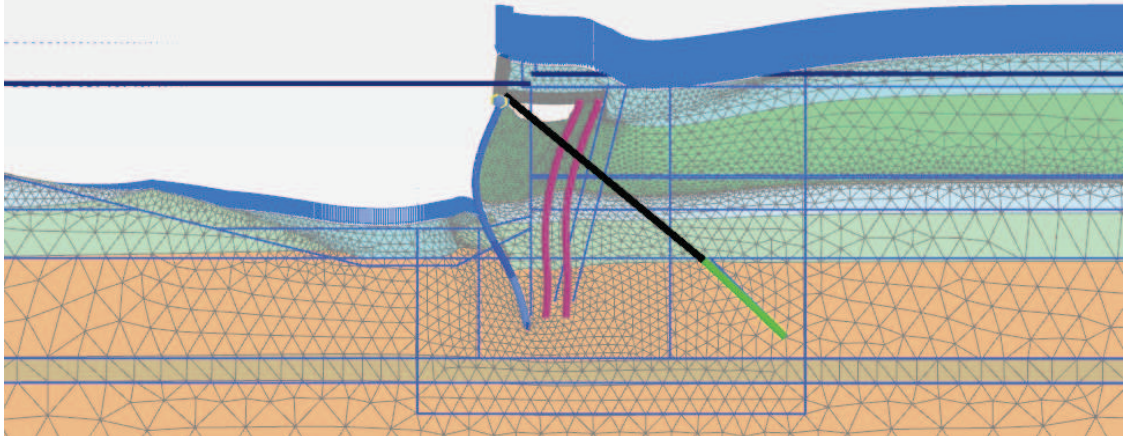


Figure 7-13 - Deformed mesh of SIF 2a, scaled up 50 times

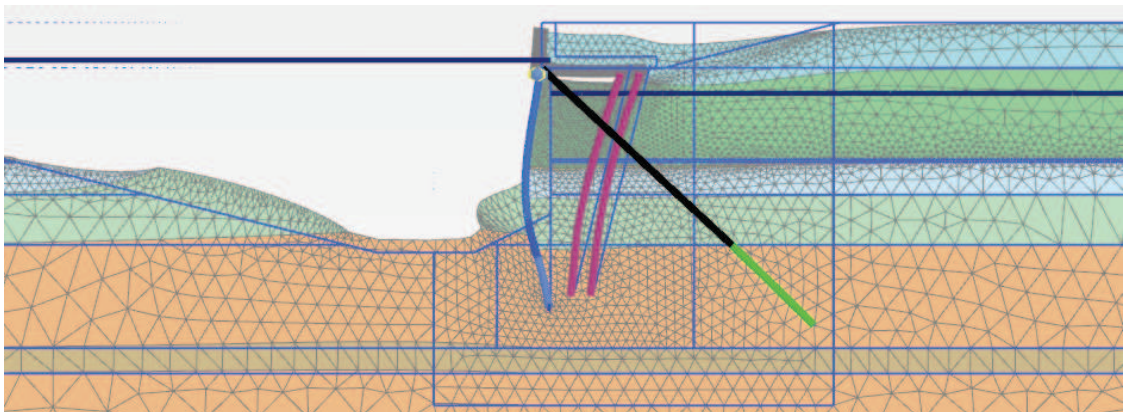


Figure 7-14 - Deformed mesh of SIF 2b, scaled up 50 times

Table 7-14 - Plaxis 2D results of SIF 2

Scenario	N	$M_{\text{field,CSPW}}$	$M_{\text{fixed,CSPW}}$	$F_{\text{M.V.-piles}}$	$u_{\text{CSPW,top}}$	$u_{\text{CSPW,field}}$
	kN/m	kNm/m	kNm/m	kN/m	mm	mm
SIF 2a	2,598.8	2,529.2	-1,580.3	1,132.2	95.9	179.2
SIF 2b	1,315.4	1,251.0	-784.9	254.8	35.8	79.3

8 Model verification and validation

This chapter discusses the models that were presented in chapter 7. The models will be compared to the conventional design methods and to actual field measurements. Lastly, the final models will be subjected to a critical assessment.

8.1 Comparison to other modelling methods

This paragraph compares the results from the different modelling methods. The elements that will be compared are:

- The normal force on top of the CSPW;
- The maximum bending field moment;
- The fixed end bending moment;
- The horizontal displacement of the top of the CSPW;
- The maximum horizontal displacement of the CSPW;
- The normal force in the M.V.-piles.

The Blum method does not give insight into the displacements, therefore these have not been considered for this modelling method.

8.1.1 Amazonehaven

In chapters 5, 6, and 7 the different modelling methods were applied and the respective results were presented, Table 8-1 shows these initial results again.

Table 8-1 - Results of the different modelling methods for Amazonehaven

	$N_{\text{top,CSPW}}$	$M_{\text{field,CSPW}}$	$M_{\text{fixed,CSPW}}$	T_{anchor}	$F_{\text{M.V.-piles}}$	$U_{\text{CSPW,top}}$	$U_{\text{CSPW,field}}$
	kN/m	kNm/m	kNm/m	kN/m	kN/m	mm	mm
1a							
Blum	2,883.6	2,137.5	-2,021.9	583.9	707.7	-	-
D-Sheet	2,871.4	2,025.9	-1,668.7	572.0	690.9	8.8	121.2
Plaxis 2D	2,694.8	2,314.6	-1,240.1	669.3	1,109.8	161.2	225.7
1b							
Blum	2,306.2	2,137.5	-2,021.9	583.9	783.3	-	-
D-Sheet	2,216.8	1,833.1	-1,583.7	496.3	659.6	7.7	108.7
Plaxis 2D	2,234.8	2,174.4	-1,297.7	601.8	1,192.0	143.8	206.6
2a							
Blum	2,815.14	1,757.1	-1,692.4	516.8	612.9	-	-
D-Sheet	2,900.9	2,060.2	-1,550.2	600.9	731.8	8.1	125.0
Plaxis 2D	2,869.9	1,655.8	-833.7	545.4	922.8	120.9	159.0
2b							
Blum	2,237.7	1,757.1	-1,692.4	516.8	688.6	-	-
D-Sheet	2,241.7	1,841.9	-1,479.0	520.7	694.0	7.1	111.9
Plaxis 2D	2,109.7	1,481.4	-925.6	464.4	886.6	94.6	134.4

From the table it can be seen that even though the results are varying between the different modelling methods, they show similarities as well. The Blum method varies from the modelled results with on average 8.5% in regard to $M_{\text{field,CSPW}}$ and 8.1% in regard to T_{anchor} . For the D-Sheet Piling method it is 19.2% for $M_{\text{field,CSPW}}$ and 13.6% for T_{anchor} .

The major differences per modelling method are discussed in Table 8-2. Apart from the elaborations on the differences that are mentioned in this table, some of the differences are partly caused by the modelling decision that the water level difference is present over the entire length of the CSPW in the Blum and D-Sheet Piling methods. This also holds for the SIF scenario.

Table 8-2 - Discussion about the differences for Amazonehaven

Difference	Discussion
Blum	
Larger $M_{\text{fixed,CSPW}}$	The Blum method assumes that the CSPW is completely fixed at the lower end. This causes the fixed end bending moment to increase in regard to the situation where the lower end is less fixed.
Smaller $F_{\text{M.V.-piles}}$	Even though the anchor force (T_{anchor}) has been predicted fairly accurate, the force in the M.V.-piles varies greatly. This is most likely due to the fact that the reaction forces of the superstructure behave differently than assumed.
D-Sheet Piling	
Larger $M_{\text{fixed,CSPW}}$	In D-Sheet Piling it is only possible to model vertical retaining walls. Due to this the passive horizontal stress coefficient on the water side is larger than that of an inclined wall, causing the fixed bending moment to be larger than that of an inclined wall.
Smaller $F_{\text{M.V.-piles}}$	The origin of this difference is the same as that of the Blum method.
Smaller $U_{\text{CSPW,top}}$	The D-sheet Piling software only takes horizontal displacements into account. Due to the loading the structure will settle a certain amount, which will cause the M.V.-piles to lose tension. To make up for this loss of tension the top of the CSPW must deflect the same amount (due to the inclination of the M.V.-piles). Another element that plays a role is the determination of the stiffness of the M.V.-piles. It was assumed that a larger length of the piles would be used to convey the reaction force to the soil (only the top 9 m was disbonded during the M.V.-piles load testing), while in the model the effective part of the piles lies underneath the weaker soil layers. Figure 8-1 illustrates this. A third factor is the fact that the maximum force that the M.V.-piles can exert on the structure is almost reached, this is about the geotechnical holding force of the piles.
Smaller $U_{\text{CSPW,field}}$	Due to the fact that the displacement at the top becomes larger, the one in the field also increases. In the field above it was mentioned that the M.V.-piles had almost reached their critical load, this causes the bearing piles to experience a larger shear force, which due to bending of the pile would partly be exerted back on the soil and then back on the wall again. This process is shown in Figure 8-2.

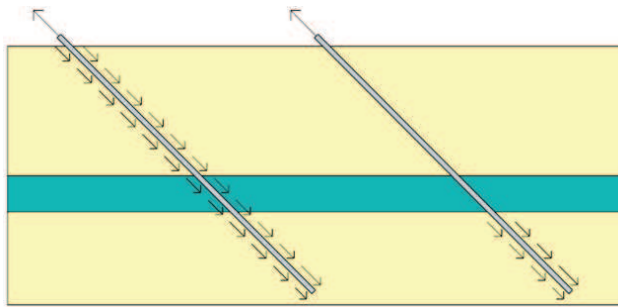


Figure 8-1 - Effective length of the M.V.-piles

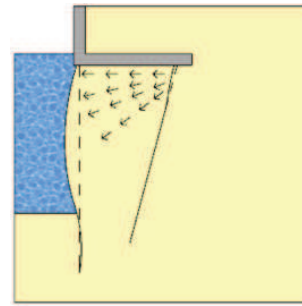


Figure 8-2 - Loading due to the bearing piles

8.1.2 SIF

The results of the different modelling methods regarding the SIF structure are presented in Table 8-3.

Table 8-3 - Results of the different modelling methods for SIF

	$N_{top,CSPW}$	$M_{field,CSPW}$	$M_{fixed,CSPW}$	T_{anchor}	$F_{M.V.-piles}$	$U_{CSPW,top}$	$U_{CSPW,field}$
	kN/m	kNm/m	kNm/m	kN/m	kN/m	mm	mm
1a							
Blum	2,693.8	1,441.0	-1,601.7	481.9	980.0	-	-
D-Sheet	2,754.7	1,630.4	-1,645.4	542.8	1,066.2	20.0	85.7
Plaxis 2D	2,462.0	1,730.1	-1,570.4	554.6	951.4	81.0	110.5
1b							
Blum	908.6	-	-	-215.9	-388.4	-	-
D-Sheet	1,192.0	349.4	-339.8	67.5	-63.0	3.5	8.3
Plaxis 2D	1,238.1	625.6	-725.8	94.6	83.6	15.8	32.1
2a							
Blum	2,724.7	1,602.6	-1,760.5	512.8	1,024.0	-	-
D-Sheet	2,785.6	2,035.4	-1,827.2	573.7	1,109.9	14.1	110.1
Plaxis 2D	2,598.8	2,529.2	-1,580.3	591.3	1,132.2	95.9	179.2
2b							
Blum	955.8	835.4	-1,237.9	-168.7	-411.4	-	-
D-Sheet	1,146.5	801.1	-736.9	22.0	-141.6	10.0	28.5
Plaxis 2D	1,315.4	1,251.0	-784.9	176.5	254.8	35.8	79.3

The Blum method varies from the modelled results with on average 26.7% in regard to $M_{field,CSPW}$ and 13.2% in regard to T_{anchor} , only scenarios SIF 1a and SIF 2a have been taken into consideration for the Blum method since it was already concluded that it did not result in accurate results for the other two scenarios. For the D-Sheet Piling method it is 26.3% for $M_{field,CSPW}$ and 30.3% for T_{anchor} .

The differences between the modelling methods are discussed in Table 8-4.

Table 8-4 - Discussion about the differences for SIF

Difference	Discussion
Blum	
Smaller $M_{\text{field,CSPW}}$	The soil on the waterside was assumed to consist solely of dense sand. Given the fact that a large portion of clay still remains there the passive horizontal soil stress coefficient would be smaller, effectively increasing the “span” of the field moment. This would explain the difference in the field bending moment.
T_{anchor}	The value of the needed anchor force in the SIF 1b and SIF 2b scenarios is relatively inaccurate. The Blum method assumes an active and a passive soil side, in these scenarios they can however not be divided that easily. The inaccuracy of this parameter also influences the values of $N_{\text{top,CSPW}}$ and $F_{\text{M.V.-piles}}$, since they are connected to one another through the reaction forces of the superstructure.
D-Sheet Piling	
Smaller $M_{\text{field,CSPW}}$	The D-sheet Piling software is less applicable when it comes to sloped surfaces on the waterside of a structure. A test with the removal of sloped parts from the model showed results that were closer to that of the Plaxis 2D model in regard to the displacements, it however drastically increased the bending moments, which was deemed implausible.
Smaller $U_{\text{CSPW,top}}$	The reason most likely lies in the settlement of the superstructure. Another feature of interest is the horizontal displacement of the toe of the CSPW and the soil behind it.
Smaller $U_{\text{CSPW,field}}$	The reason most likely lies in the inability to accurately model sloping surfaces on the waterside of the structure within the D-Sheet Piling software.

8.2 Comparison to field data

Field data was available for two different structural elements, for the deflections of the CSPW of the SIF 2 scenario and for the head displacements of the M.V.-piles of both structures. The field data and how the models compare to it will now be elaborated on.

8.2.1 Deformations of the combined sheet pile wall

To gain insight into the actual displacements of a CSPW, field measurements were carried out. The measurements were carried out for soil zones A, C, and D. For this thesis only the measurements belonging to soil zone C (SIF 2) were relevant.

The measurements were carried out with SAAF (Shape Accel Array Field). To make sure that the situations that would be compared to one another were the same, or at the very least similar, some modifications had to be made to the model, these modifications were based on observations that were made during the actual construction of the structure [21]:

- The groundwater level during the dredging process was set at NAP-10 m;
- The top of soil level on the waterside was set at NAP-16.4 m;
- The final dredging level was set to NAP-30.0 m;
- Modified characteristics for the CSPW (no corrosion has occurred yet);
- No water level difference.

The blue line in Figure 8-3 represents the field measurements [21] while the red line shows the output of the Plaxis 2D model. The horizontal axis represents the horizontal displacement of the CSPW in mm, the vertical axis shows the depth profile of the CSPW in m+NAP. The differences and similarities are discussed in Table 8-5.

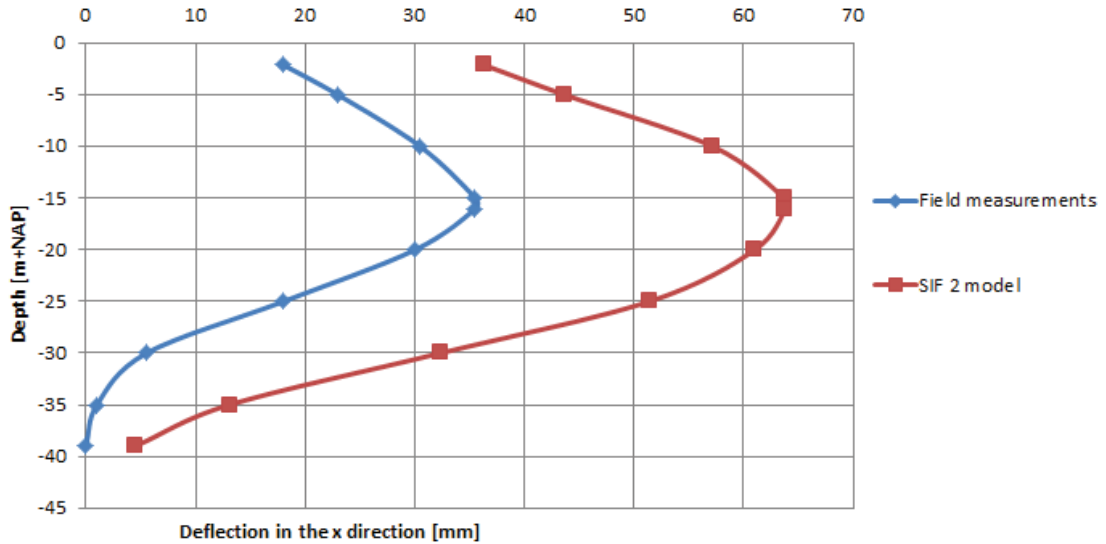


Figure 8-3 - Comparison of the field measurements to the model output of SIF 2

Table 8-5 - Comparison of the field data and the model results for SIF 2

Differences	Possible explanation
Strongly different deflections, ca. a factor 2	<ul style="list-style-type: none"> The deflection at the bottom of the CSPW has not been taken into account; The direction of the toe of the CSPW is taken as vertical instead of as inclined; The vertical displacement of the top of the CSPW is relatively big. To compensate for this vertical displacement it needs to displace an additional amount in the horizontal direction (otherwise the M.V.-piles would lose tension); The soil properties are characteristic values (conservative estimates) of the actual soil properties.
Direction of the toe of the CSPW	The SAAF measuring equipment needs a fixed point to fit the rest of the data to. The measurements were probably made under the assumption that the toe of the CSPW remained in place and vertical.
Similarities	
Shape of the deflection line	-
Position of the maximum deflection	-

8.2.2 Head displacement of the M.V.-piles

The reaction of the M.V.-piles to a certain normal force was tested by placing a certain load on the piles and measuring the response of the piles in terms of head displacement. This was done for several piles for both the Amazonehaven and the SIF structures.

8.2.2.1 Amazonehaven

This comparison was only performed on Amazonehaven 1. The model was altered in the following way:

- Removal of all the structural elements except the CSPW and the embedded beam row part of the M.V.-piles;
- Replacement of the node-to-node anchor part of the M.V.-piles with a fixed end anchor;
- Adjusting the maximum skin friction over the first 9 m of the M.V.-piles to 0 kN/m to account for the disbonding between the M.V.-piles and the surrounding soil;
- Different areas for mesh improvement.

The test loading was carried out by applying a prestressing force to the fixed end anchor and increasing the magnitude of this prestressing force per calculation phase. The modified model is shown in Figure 8-4.

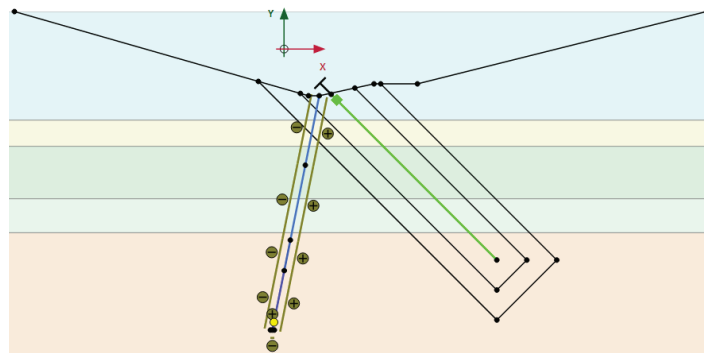


Figure 8-4 - Modified model for the M.V.-pile load testing for Amazonehaven

The results of the model were compared to 5 actual tests [16]. The results are shown in Figure 8-5. The red line represents the results of the original model, in which the first 9 m was disbonded from the soil. The black line shows what the corresponding displacements would be in case the disbonding would not be applied/was not applied correctly. The green lines represent the 5 field tests that were carried out. The horizontal axis in this figure shows the load that acts on the M.V.-pile in kN, the vertical axis shows the accompanying head displacements in the normal direction of that pile in mm.

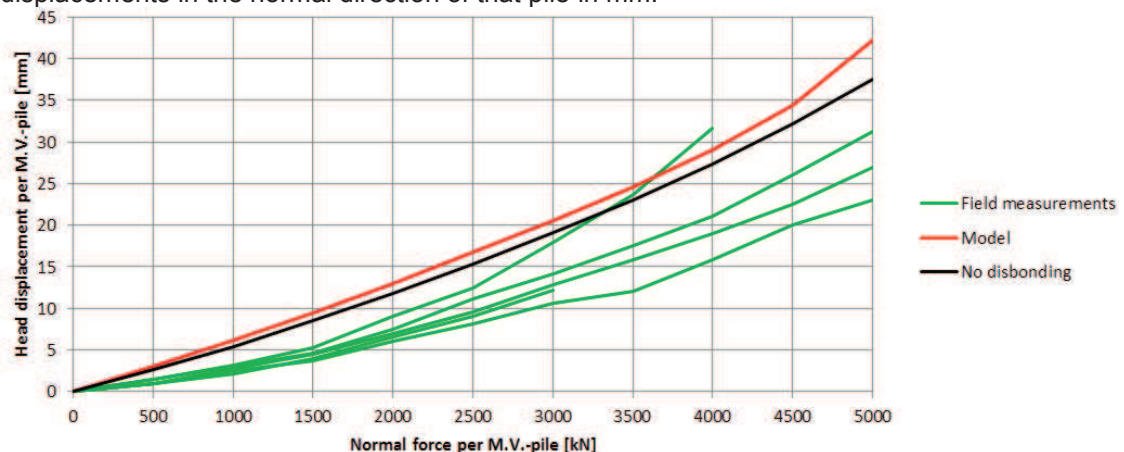


Figure 8-5 - Comparison of the M.V.-pile load testing for Amazonehaven

The results show that the model fails at a load of 5000 kN while the actual test loading resulted in a minimal failure load of 4,000 kN, which is smaller than the modelled load. From the figure it can be seen that the modelled deformations are larger than that of the field measurements,

this most likely originated from the used cone resistances per soil layer since the soil profile that has been used contained the weakest layers.

8.2.2.2 SIF

This comparison was only carried out for the SIF 2 scenario. To make the results of the model compatible to that of the field tests the model was altered in the following way:

- Elongation of the embedded beam row part of the M.V.-piles;
- Placement of a fixed end anchor on top of the M.V.-piles;
- Modifying the maximum skin friction over the length of the M.V.-piles (see Table 9-3);
- Removal of all the unnecessary structural elements;
- Redefining the areas for mesh refinement.

The test loading was carried out by applying a prestressing force to the fixed end anchor and increasing its magnitude per calculation step. The modified model is shown in Figure 8-6.

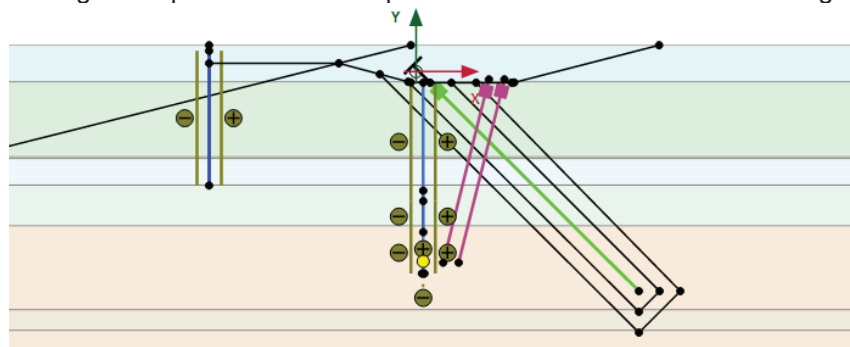


Figure 8-6 - Modified model for the M.V.-pile load testing for SIF

5 M.V.-piles were subjected to physical test loading, the results of these tests (green lines) and that of the model (red line) are presented in Figure 8-7. During the physical tests it was observed that the top part of the M.V.-piles had not sufficiently been disbonded from the soil, this was concluded based on cracks that formed outside of the casing that was used for the disbonding. For this reason the model also ran a simulation in which the M.V.-piles were in their original condition (black line), i.e. friction along the entire length of the M.V.-piles. The horizontal axis in the figure shows the load that acts on a single M.V.-pile in kN, the vertical axis shows the accompanying head displacements in the normal direction of that pile in mm.

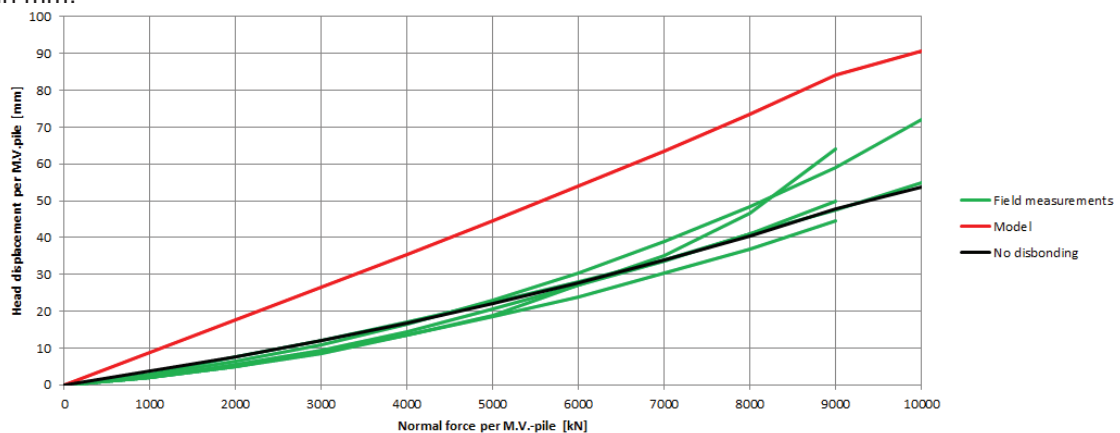


Figure 8-7 - Comparison of the M.V.-pile load testing for SIF

If the M.V.-piles had been properly disbonded they would theoretically consist of two parts, a part that only transports the normal force from one end of the pile to the other and a part that

transmits the force from the pile to the soil. The translational stiffness could then be determined as follows:

$$\frac{1}{k_{total}} = \frac{1}{k_1} + \frac{1}{k_2}$$

In which k_1 and k_2 represent the translational stiffness of parts 1 and 2 respectively. Per definition k_{total} cannot be larger than k_1 or k_2 . The disbonded length for the SIF 2 scenario was approximately 40 m, the area of a single M.V.-pile was 0.027 m², and the Young's modulus was 210 GPa. k_1 was determined as follows:

$$\frac{\Delta l}{l} = \varepsilon = \frac{\sigma}{E} = \frac{N/A}{E} \rightarrow k_1 = \frac{N}{\Delta l} = \frac{EA}{l} \approx 140,000 \text{ kN/m}$$

Based on this, the displacement at a normal force of 5000 kN should at least be larger than 35.7 mm. All the physical tests show displacements that are at least 10 mm smaller than this value. It was therefore concluded that the M.V.-piles were in fact not fully disbonded. In the figure it can also be seen that the model which assumes no disbonding of the M.V.-pile gives extremely similar results to that of the actual tests.

8.3 Critical assessment

In this paragraph the created models will be subjected to knowledge and experience regarding the aspects which have been included and the response of the model. Table 8-6 shows the critical assessment of the Plaxis 2D models, as part of this assessment the SIF 2 model was adjusted for some of these objections to see whether or not the area of interest had been incorporated into the models correctly. For more elaboration on this critical assessment, please take a look at Appendix D.

Table 8-6 - Critical assessment of the Plaxis 2D models

Area of interest	Discussion
Undrained soil behavior	<p>Due to its high permeability, sandy soils will almost always behave as drained soils. Softer soils such as clay and silt however are less permeable. Especially for thicker clay layers, such as the Wijchense clay layer, undrained behavior becomes an issue. Appendix D shows more insight in when drained or undrained models should be applied, this is based on [24] where a relation is given between the soil behavior that should be used and the properties belonging to the soil layer in question.</p> <p>Due to the function of the quay structures, which is mainly the storage of goods, it was initially assumed that the soil would behave as drained. Appendix D showed that the silt layers would indeed behave as drained materials. For the clay layers it was difficult to determine whether they would behave as drained or undrained material due to limited knowledge on the loading time and the actual hydraulic conductivity of the soil.</p>
Overconsolidation	<p>Over consolidation has been taken into account. In Figure 7-3 it could be seen that over consolidation mainly affected the displacements. Since SIF and Amazonehaven have the same geographical location the OCRs have been assumed to be equal as well.</p>
Installation effect of the	<p>This has partially been dealt with. The models use different</p>

structural elements	construction stages to ultimately arrive at their design conditions. The forces that accompany these construction stages, such as the driving of piles and heavy installation equipment, have not been taken into consideration.
Hydraulic level through the soil layers	This has been incorporated into the models through the interpolation of water levels at the Wijchense clay layer. In reality the water level difference at the location of the RP would be zero due to the installed drainage. This thesis however assumes that the drainage has failed, leading to a water level difference that will be present at the location of the RP as well.
Shielding of the bearing piles and arching of the soil	The shielding of the bearing piles has been incorporated in the models through the modelling of the piles as embedded beam rows. In Figure 7-13 it can be seen that the inclination of the bearing piles increases with increasing depth over the first few meters, this is the response of the bearing piles to the load that the soil exerts on them. The effect of the arching of the soil has not been incorporated in the models, there was too little knowledge about the contributions of the shielding and the arching individually. This results in the actual bending moments being somewhat smaller while the anchor forces will be somewhat larger.
Behavior of the superstructure	The superstructure has been modelled as a soil polygon, in this way the properties of the structural element have all been maintained. The connections with the foundation elements have been modelled in the same way as they were connected in reality.
Different failure mechanisms	Appendix D shows the results of the modification of the model to trigger certain failure mechanisms. It shows that the model does fail after a certain failure mechanism has been reached.
Failure of the relieving platform itself	Given the dimensions of the RP itself, it was deemed unlikely that this would fail. The failure mechanism of this structural element itself has therefore not been taken into consideration. Should the RP be modelled as a plate element, this would be relatively easy to implement, the downside of this modelling decision was however larger than the advantages of it.
ϕ reduction due to high stresses	The internal angle of friction of sandy soils decreases under higher loading conditions. Seeing as how the values that have been used for the soil characteristics were characteristic ones, it was assumed that even with this reduction the properties of the model would still create a somewhat conservative representation of the reality. For that reason it was decided that the reduction of this parameter would not be taken into consideration any further.

Out of plane spacing	<p>The model is a 2D schematization of a 3D structure. All the different structural elements were checked to see whether their characteristics were transformed appropriately.</p> <p>CSPW: The input variables were specified per running meter. They were computed by manually dividing the original values with the system length.</p> <p>Bearing piles: The input variables were specified per pile element. The out of plane direction was taken into account through the definition of the system length L_{spacing}.</p> <p>M.V.-piles: The input variables were specified per pile element. The out of plane direction was taken into account through the definition of the system length L_{spacing}.</p> <p>More information on the determining of the input variables is given in chapter 9.</p>
-----------------------------	---

8.4 Conclusion

The results in regard to $M_{\text{field,CSPW}}$ and T_{anchor} showed a deviation of ca. 20% for Amazonehaven and ca. 30% for SIF, most of these deviations could however be explained through the limitations of the conventional design methods. The results of the Plaxis model were deemed to be a more accurate representation of the reality.

The comparison to field data showed some interesting insights. In regard to the deflection of the CSPW it was seen that even though the values of the actual deflection and that of the model differed by ca. a factor 2, the differences could all be explained. A test run with increased values for φ showed deflections that were much closer to that of the field measurements. For the M.V.-piles the modelled results were comparable to that of the field measurements, it was therefore concluded that the M.V.-piles were modelled correctly.

The critical assessment reflected the completeness of the models. There are still a few areas in which the model can be improved on. The most important aspect would be the use of drained or undrained material for the clay layers in the models.

A review of the initial results showed that the M.V.-piles of the Amazonehaven were already at their geotechnical limit, it was decided to model these structural elements more accurately in the final model. It was also discovered that the soil underneath the RP was close to collapsing. To prevent this trivial failure mechanism from occurring, part of the soil was modelled as a line load.

In light of these findings, the models were deemed to be an accurate representation of the reality and were therefore validated. It was also verified that the models correctly implement several areas of interest. The verification however comes with a side note that more research is needed on the undrained behavior of the clay layers.

9 Test loading set-up

This chapter gives insight in the way that the different quay structures are subjected to their test loading scenarios and what these scenarios entail. The different failure mechanisms that will be evaluated are also discussed.

9.1 Respective scenarios

At this point it was clear that certain scenarios were normative over others. Because of that for both the Amazonehaven and the SIF structures, only one scenario was selected for the test loading. The two scenarios that were selected for the test loading were Amazonehaven 1a and SIF 2a. These scenarios have been selected after reviewing the initial results, which can partly be seen in Table 8-1 and Table 8-3.

The model set up of the selected scenarios was the same as presented in chapter 7 with the exception of the calculation phases and further specification of the structural characteristics. The calculation phases will now be elaborated on while the modifications in regard to the structural elements will be discussed in §9.2.

9.1.1 Amazonehaven

The main purpose of this quay structure was to serve as a storage yard, this was taken into account in deciding the test loading set-up. It was assumed that the only thing that would change was the magnitude of the bulk surcharge. The final Plaxis 2D model is shown in Figure 9-1.

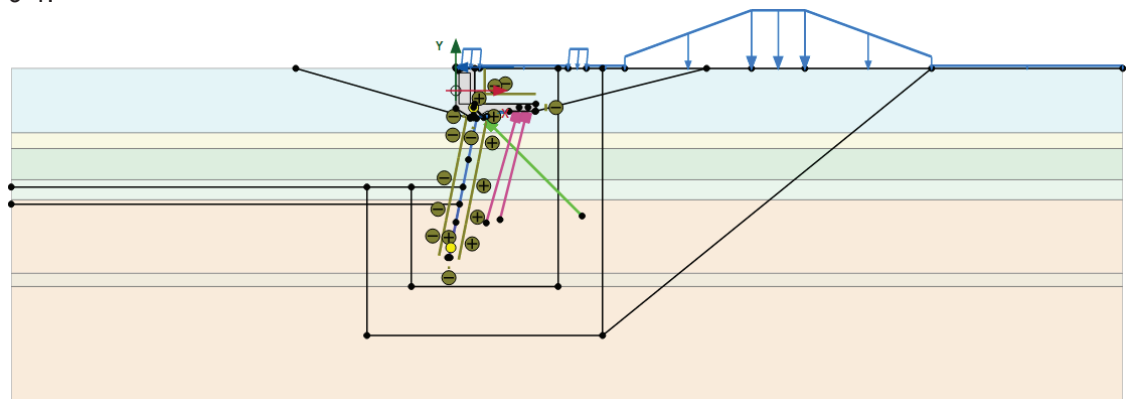


Figure 9-1 - Final Plaxis 2D model for Amazonehaven

The calculation phases are shown below.

1. Initial phase – Initial conditions with a horizontal soil surface, $\text{GWL} = \text{NAP}+0 \text{ m}$;
2. Zero step to obtain equilibrium – No modifications;
3. Excavation of the soil for the RP – Deactivation of specific soil clusters, $\text{GWL} = \text{NAP}-6.5 \text{ m}$;
4. Installation of the CSPW – Activation of the CSPW;
5. Completion of the RP – Activation of the bearing piles, the M.V.-piles, the saddle, and the RP;
6. Backfill – Activation of the soil behind the RP, $\text{GWL} = \text{NAP}+0 \text{ m}$;
7. Dredging – Deactivation of soil clusters on the waterside up to a depth of $\text{NAP}-25.5 \text{ m}$, $\text{GWL} = \text{NAP}-1 \text{ m}$;
8. Start test loading – Activation of the bollard load, the crane loads, and the normal surcharge, $\text{GWL}_{\text{landside}} = \text{NAP}+0 \text{ m}$;

9. Load step 1 – Activation of the bulk surcharge, magnitude equal to that of load step 1 in Table 9-1, see also Figure 9-2;
10. Load step X – Adjusting the magnitude of the bulk surcharge, magnitude equal to that of load step X in Table 9-1.

The magnitude of the bulk surcharge was increased until a failure mechanism occurred. After that, the model was adjusted by increasing the resistance to that specific failure mechanism. The load advancement was then reset and started again until the next failure mechanism occurred, this process was repeated until total instability occurred.

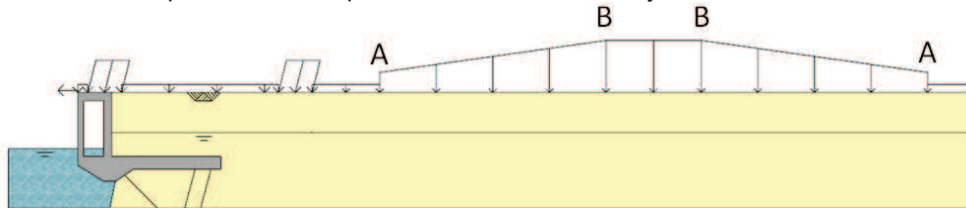


Figure 9-2 - Test loading set-up for Amazonehaven

Table 9-1 - Magnitude of the surcharge per load step for Amazonehaven

Load step	A	B
	kN/m ²	kN/m ²
0	0	0
1	45	45
2	90	90
3	90	135
4	90	180
5	90	225
6	90	270
7	90	315
8	90	360
9	90	405
10	90	450
10+i	90+10i	450+10i

9.1.2 SIF

Similar to the Amazonehaven, this structure is mainly used for the storage of certain goods. It was again assumed that the only varying part would be the magnitude of the surcharge. The final Plaxis 2D model is shown in Figure 9-3.

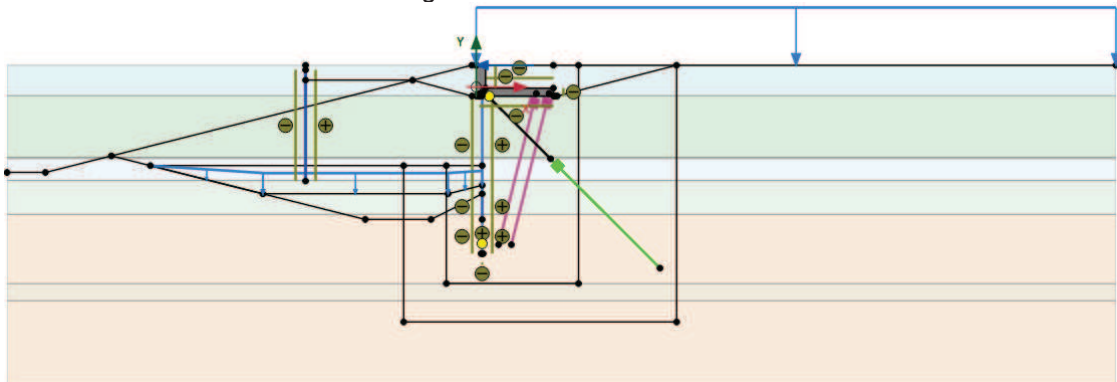


Figure 9-3 - Final Plaxis 2D model for SIF

The calculation phases are presented below.

1. Initial phase – Initial conditions with a sloped surface, $\text{GWL} = \text{NAP}-0.84 \text{ m}$;
2. Zero step to obtain equilibrium – No modifications;
3. Installation of the temporary sheet pile wall – The temporary wall has the same structural characteristics as the saddle;
4. Excavation of the soil for the RP – Deactivation of specific soil clusters, $\text{GWL}_{\text{land side}} = \text{NAP}-2.5 \text{ m}$;
5. Installation of the bearing piles – Activation of the bearing piles;
6. Installation the CSPW – Activation of the CSPW;
7. Installation of the foundation elements – Activation of the embedded beam row part of the M.V.-piles;
8. Completion of the RP – Activation of the RP, node-to-node anchor of the M.V.-piles, and the saddle;
9. Backfill – Activation of the soil behind the RP;
10. Removal of the temporary sheet pile wall – Deactivation of specific soil clusters and the temporary sheet pile wall, $\text{GWL} = \text{NAP}-0.84 \text{ m}$;
11. Initial dredging – Deactivation of the soil clusters up to $\text{NAP}-18.4 \text{ m}$;
12. Lowering of the groundwater level – $\text{GWL}_{\text{land side}} = \text{NAP}-6 \text{ m}$;
13. Completion of the dredging – Deactivation of soil clusters up to $\text{NAP}-31 \text{ m}$;
14. Replacement of the removed soil – Activation of soil clusters up to $\text{NAP}-18.4 \text{ m}$;
15. Restoration of the normal groundwater level – $\text{GWL} = \text{NAP}-0.84 \text{ m}$;
16. Start test loading – $\text{GWL}_{\text{land side}} = \text{NAP}+0.05 \text{ m}$, $\text{GWL}_{\text{water side}} = \text{NAP}-1.5 \text{ m}$, activation of the bollard load and the load due to the remolded soil, deactivation of the remolded soil clusters.
17. Load step 1 – Activation of the bulk surcharge, magnitude equal to that of load step 1 in Table 9-2, see also Figure 9-4;
18. Load step X – Adjusting the magnitude of the bulk surcharge, magnitude equal to that of load step X in Table 9-2.

The magnitude of the bulk surcharge was increased until a failure mechanism occurred. After that, the model was adjusted by increasing the resistance to that specific failure mechanism. The load advancement was then reset and started again until the next failure mechanism occurred, this process was repeated until total instability occurred.

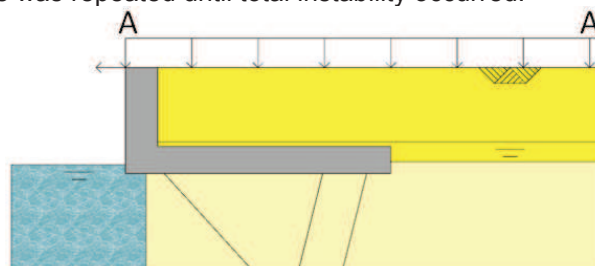


Figure 9-4 - Test loading set up for SIF

Table 9-2 - Magnitude of the surcharge per load step for SIF

Load step	A
	kN/m ²
0	0
1	25
2	50
3	75
4	100
4+i	100+25i

9.2 Relevant failure mechanisms

The relevant failure mechanisms and the conditions at which they occur are presented below. Some of these mechanisms are about structural failure while others concern geotechnical stability. If relevant, the parameters belonging to the structural element in question are also presented. Through post processing of the results, it can be determined if the structure will fail and/or what caused this.

9.2.1 Failure of the M.V.-piles

This failure mechanism can occur in multiple ways. By yielding of the structural element, by insufficient geotechnical bearing capacity, by instability of the anchor, and by failing of the connection to the RP. In this thesis only the first three mechanisms were taken into consideration.

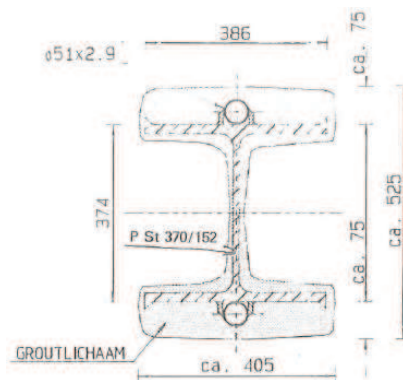


Figure 9-5 - Cross section of an M.V.-pile [16]

The cross-section of a typical M.V.-pile is shown in Figure 9-5.

The parameters that needed to be determined are the skin friction of the effective part of the M.V.-piles and the maximum tensile force that will result in yielding of the M.V.-piles. According to CUR166 [6], the maximum skin friction of a single M.V.-pile per running meter is equal to:

$$T_s = \alpha_s * O * q_{c;z;a}$$

Where: α_s = factor that takes the influence of the installation into account (0.014 for M.V.-piles)

O = the circumference of the grout element

$q_{c;z;a}$ = the cone resistance ($\alpha_s * q_{c;z;a} \leq 250 \text{ kPa}$)

The maximum normal force that a single M.V.-pile can withstand is equal to:

$$N_{max} = A_{M.V.-piles} * f_y$$

Table 9-3 shows the structural characteristics of the M.V.-piles. The values in the 4th and 6th column represent the values of the cone resistance (averaged per soil layer) and maximum skin friction in the individual soil layers where the M.V.-piles are present, from top to bottom.

Table 9-3 - Structural characteristics of the M.V.-piles

Scenario	$A_{M.V.-piles}$	O	$q_{c:z;a}$	f_v	T_s	N_{max}
	m ²	m	MPa	N/mm ²	kN/m	kN
Amazonehaven	0.0195	1.72	9	355	216.7	6,922.5
			2		48.2	
			9		216.7	
			2		48.2	
			18		430	
SIF	0.0270	2.2	10	355	308.0	9,585.0
			1		30.8	
			18		550.0	

For the SIF scenario the plastic bending moment of the M.V.-piles has also been determined, this was equal to ca. 2000 kNm per pile. This value has been determined to analyze the effect of combined bending and normal loading (see the next paragraph).

9.2.2 Failure of the combined sheet pile wall

The CSPW can fail by exceedance of the bending moment capacity, exceedance of the normal force capacity, exceedance of the shear force capacity, buckling, insufficient length, or a combination of the mechanisms.

The capacities that were determined for the CSPW are the bending moment capacity, the normal force capacity, the shear force capacity, and the buckling load. For the shear force capacity it was assumed that only the tubular piles contributed to the capacity.

$$M_p = \frac{\sum(W_p * f_y)}{\text{system length}}$$

$$N_p = \frac{\sum(A * f_y)}{\text{system length}}$$

$$V_p = \frac{\frac{A_v * f_y}{\sqrt{3}}}{\text{system length}}$$

$$F_{buckling} = \frac{\frac{\pi^2 * E * I_y}{l_{buckling}^2}}{\text{system length}}$$

For tubular profiles the following equations hold:

$$W_p = \frac{D_{outer}^3 - D_{inner}^3}{6}$$

$$A_v = \frac{2 * A_{total}}{\pi} = \frac{2 * D * \pi * t_{average}}{\pi} = 2 * D * t_{average}$$

The structural characteristics of the CSPWs are presented in Table 9-4.

Table 9-4 - Structural characteristics of the combined sheet pile walls

Scenario	EI	EA	M _p	N _p	V _p	F _{buckling}
	kN m ² /m	kN/m	kNm/m	kN/m	kN/m	kN/m
Amazonehaven						
Top	1.27*10 ⁶	6.67*10 ⁶	5,451.8	14,351.6	4,331.9	
Middle	1.24*10 ⁶	7.01*10 ⁶	5,375.8	14,823.0	4,172.4	25,840.9
Bottom	1.17*10 ⁶	4.88*10 ⁶	5,018.4	11,226.4	4,172.4	
SIF						
Top	1.78*10 ⁶	9.57*10 ⁶	7,614.2	20,469.3	6,046.0	
Middle	1.81*10 ⁶	9.74*10 ⁶	7,710.2	20,795.9	6,112.5	37,187.1
Bottom	1.73*10 ⁶	7.11*10 ⁶	7,276.0	16,360.8	6,112.5	

Failure due to the combined effect of bending and normal loading occurs when plasticity has been reached in the entire cross section. This happens when the following criteria is met:

$$\frac{M_{acting}}{W_p} \pm \frac{N_{acting}}{A_{CSPW}} \geq f_y \rightarrow \frac{M_{acting}}{W_p * f_y} \pm \frac{N_{acting}}{A_{CSPW} * f_y} = \frac{M_{acting}}{M_p} \pm \frac{N_{acting}}{N_p} \geq 1$$

At the location where the maximum bending moment occurs at design conditions, the normal force is at 94.5% of its maximum value for Amazonehaven and at 95.7% for SIF. In the post processing it was, conservatively, assumed that the maximum bending moment and the maximum normal force occur at the same location.

9.2.3 Failure of the bearing piles

The bearing piles can fail by either exceedance of the normal force/bearing capacity, exceedance of the shear force capacity or exceedance of the bending moment capacity. This thesis only focusses on the bearing capacity of the bearing piles since the resistance to the other two mechanisms is assumed to be far larger than the acting forces.

The parameters that are of interest are the maximum skin friction along the length of the bearing piles and the maximum end bearing capacity.

The skin friction was determined with the same formula that was used for the M.V.-piles, with the following differences [2]:

$$\begin{aligned}\alpha_{s;Amazonehaven} &= 0.010 \\ \alpha_{s;SIF} &= 0.009 \\ q_{c;z;a} &\leq 15 \text{ MPa}\end{aligned}$$

The end bearing capacity was determined with the following formula [2]:

$$F_{end} = A_{bearing\ piles} * \frac{1}{2} * \alpha_p * \beta * s * \left(\frac{q_{c;I;avg} + q_{c;II;avg}}{2} + q_{c;III;avg} \right)$$

In which:

- α_p = pile class factor (1 for Amazonehaven, 0.9 for SIF)
- β = factor for the shape of the foot (1 for both scenarios)
- s = factor for the shape of the foot (1 for both scenarios)
- $q_{c;I-III;avg}$ = average values for the cone resistance on specific intervals

Table 9-5 presents the structural characteristics of the bearing piles. The values in the 3rd and 7th column represent the values corresponding to the relevant soil layers from top to bottom.

Table 9-5 - Structural characteristics of the bearing piles

Scenario	O	q _{c,z:a}	q _{c,l:avg}	q _{c,ll:avg}	q _{c,III:avg}	T _{skin}	F _{end}
	m	MPa	MPa	MPa	MPa	kN/m	kN
Amazonehaven	1.8	9	30.0	25.0	15	162.0	4,303.1
		2				36.0	
		9				162.0	
		2				36.0	
		15				270.0	
SIF	2.67	6.0	25.2	20.7	17.3	144.2	10,277.9
		2.0				48.07	
		11.0				264.4	
		1.0				24.03	
		15.0				360.5	

9.2.4 Total instability

Regardless of the individual strength of the structural elements, total instability, such as a slip circle, can occur. This will result in the rotation of the structure, resulting in the failure of it.

9.3 Expected results

9.3.1 Amazonehaven

Table 9-6 shows the structural capacities and the acting structural forces according to the initial results for the Amazonehaven structure. These values represent the internal load at which the specific structural element will fail due to a certain failure mechanism. For the M.V.-piles it was assumed that only the Pleistocene sand and the above positioned clay layer contribute to the structural capacity. For the bearing piles it was assumed that the Holocene sand, Pleistocene sand, and the clay layer in between contribute to the bearing capacity. These assumptions were made based on the initial results.

Table 9-6 - Structural capacities and acting forces for Amazonehaven

Variable	Acting structural force	Structural capacity
M _{field,CSPW}	2,314.6 kNm/m	5,451.8 kNm/m
M _{fixed,CSPW}	1,240.1 kNm/m	5,018.4 kNm/m
N _{CSPW}	2,694.8 kN/m	14,351.6 kN/m
V _{CSPW}	668.3 kN/m	4,331.9 kN/m
N _{bearing piles combined}	1,976.8 kN/m	$2 \cdot (4,303.1 + 270 \cdot 5.02 + 36 \cdot 4.66 + 162 \cdot 7.24) / 2.060 = 6,795.3$ kN/m
F _{M.V.-piles}	1,374.4 kN/m	Geotechnical: $(430 \cdot 5.233 + 48.2 \cdot 6.307) / 2.060 = 1,239.9$ kN/m Yielding: $6,922.5 / 2.060 = 3,360.4$ kN/m

Based on the initial results the M.V.-piles will in all likelihood fail first due to insufficient geotechnical bearing capacity, this will probably occur at a load not much higher than the design load. The structural forces within the CSPW and the bearing piles are still relatively far away from their structural capacities, due to the relatively short length of the M.V.-piles it is not likely that either the CSPW or the bearing piles will fail before a total instability mechanism will occur.

9.3.2 SIF

Table 9-7 presents the structural capacities and the acting structural forces according to the initial results for the SIF structure.

Table 9-7 - Structural capacities and acting forces for SIF

Variable	Acting structural force	Structural capacity
$M_{\text{field,CSPW}}$	2,529.2 kNm/m	7,614.2 kNm/m
$M_{\text{fixed,CSPW}}$	1,580.3 kNm/m	7,276.0 kNm/m
N_{CSPW}	2,598.8 kN/m	20,469.3 kN/m
V_{CSPW}	591.2 kN/m	6,046.0 kN/m
$N_{\text{bearing piles combined}}$	3,713.6 kN/m	$2 \cdot (10,277.9 + 7.319 \cdot 360.5 + 8.143 \cdot 24.03 + 5.257 \cdot 264.4) / 2.882$ = 10,063.9 kN/m
$F_{\text{M.V.-piles}}$	1,132.2 kN/m	Geotechnical: $550.0 \cdot 17.819 / 3.3 = 2,969.8$ kN/m Yielding: $9,585.0 / 3.3 = 2,904.5$ kN/m

In contrary to the Amazonehaven scenario, all of the structural forces are still far away from their structural capacities. Due to the large length of the M.V.-piles however, it is unlikely that a sliding plane will develop. The combined effect of bending and axial loading of the CSPW will probably lead to the first failure mechanism. After this it is likely that either the bearing piles will fail or a sliding plane will develop due to insufficient length of the CSPW.

10 Results of the test loading

This chapter presents the results of the models to their test loading scenarios. The failure mechanisms that caused the models to fail will be presented and more insight will be given into the development of the structural forces and displacements due to the load advancement.

10.1 Amazonehaven

10.1.1 Overview of the test loading

The final model of the Amazonehaven structure experienced two separate failures. The first one occurred at a surcharge of 122.5/482.5 kN/m² and was caused by the exceedance of the geotechnical bearing capacity of the M.V.-piles. The second one occurred at a surcharge of 197.5/557.5 kN/m² due to the total instability of the structure. An illustration of all the calculation phases of the test loading of the Amazonehaven model is shown in Figure 10-1.

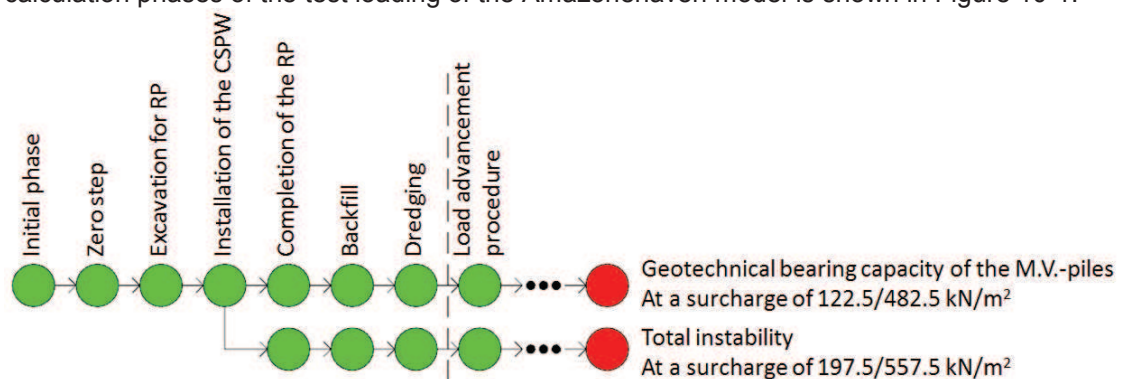


Figure 10-1 - Calculation phases of the Amazonehaven model

The failure of a specific structural element will in most cases lead to the failure of the entire structure, it is therefore interesting to look at the safety of the different structural elements. To effectively present the effect of the test loading on the structural safety, the results of the model have been normalized with respect to the structural capacities of the respective structural elements. These structural capacities are presented in Table 10-1. The structural capacities represent the value of the structural force at which that respective structural element will reach a limit state.

Table 10-1 - Structural capacities of the structural elements for Amazonehaven

Variable	Structural capacity
$M_{\text{field,CSPW}}$	5,451.8 kNm/m
$M_{\text{fixed,CSPW}}$	5,018.4 kNm/m
N_{CSPW}	14,351.6 kN/m
V_{CSPW}	4,331.9 kN/m
$N_{\text{bearing piles combined}}$	6,795.3 kN/m
$F_{\text{M.V.-piles}}$	Geotechnical: 1,239.9 kN/m Yielding: 3,360.4 kN/m

Figure 10-2 presents the normalized structural reactions to the test loading of the Amazonehaven. The horizontal axis shows the magnitude of the bulk surcharge in kN/m², the vertical axis represents the relative magnitude with respect to the structural capacities, e.g. a relative magnitude of 0.5 for $M_{\text{field,CSPW}}$ would mean that the maximum bending moment in the CSPW is equal to half the value at which it would fail (0.5*5,451.8=2,725.9 kNm).

The vertical red dashed lines in the figure represent the point at which the model failed. The other plotted lines are the normalized results of:

- $M_{\text{field,CSPW}}$ = The magnitude of the maximum bending moment in the CSPW
- $M_{\text{fixed,CSPW}}$ = The magnitude of the fixed end bending moment in the CSPW
- N_{CSPW} = The magnitude of the maximum normal force in the CSPW
- N_{bp} = The magnitude of the maximum normal force in the bearing piles (taken as the average between the two pile rows)
- $F_{\text{M.V.-geo}}$ = The magnitude of the maximum normal force in the M.V.-piles with respect to the geotechnical bearing capacity of the piles
- $F_{\text{M.V.-yield}}$ = The magnitude of the maximum normal force in the M.V.-piles with respect to the yielding capacity of the piles
- $\sigma_{\text{normal,CSPW}}$ = The magnitude of the combined effect of bending and normal loading
- V_{CSPW} = The magnitude of the maximum shear force in the CSPW

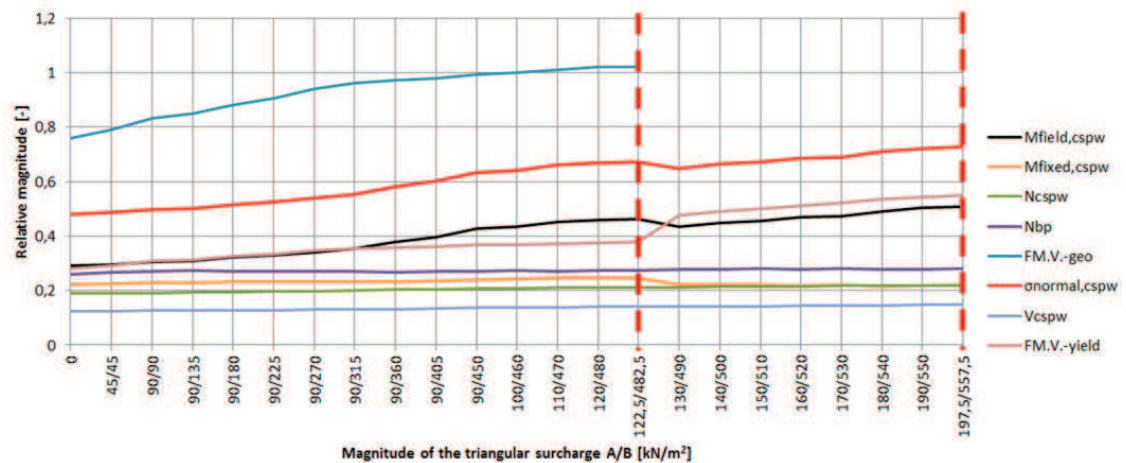


Figure 10-2 - Structural reactions to the test loading of Amazonehaven

From the figure it can be interpreted that the insufficient geotechnical bearing capacity of the M.V.-piles caused the first failure mechanism. At the second failure mechanism it can also be seen that the failure mechanism that occurs is not a structural one, the maximum relative magnitude is that of the normal stress capacity of the CSPW, which is ca. 0.7.

The horizontal displacements of the CSPW are presented in Figure 10-3. The red dashed lines show the loads at which the model failed. The horizontal axis shows the magnitude of the bulk surcharge in kN/m^2 and the vertical axis shows the horizontal displacement of the CSPW in mm.

- $U_{\text{CSPW,top}}$ = The horizontal displacement of the top of the CSPW
- $U_{\text{CSPW,field}}$ = The maximum horizontal displacement of the CSPW

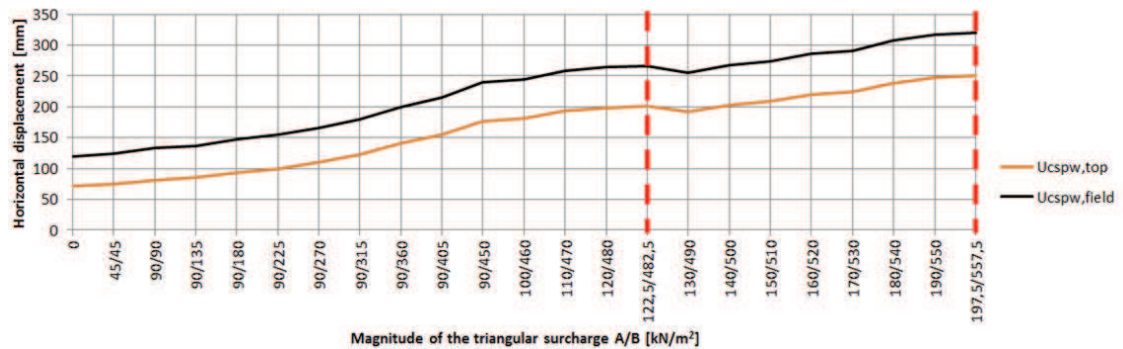


Figure 10-3 - Horizontal deflections of the CSPW during the test loading of Amazonehaven

10.1.2 First failure mechanism

After the load advancement had started it could be seen that the normal force of the M.V.-piles was approaching its geotechnical bearing capacity rather quickly, at load step 7 (where the magnitude of the bulk surcharge was equal to $90/315 \text{ kN/m}^2$) it was seen that the mobilized skin friction in the Pleistocene soil layer was already equal to the maximum one. This is also shown in Figure 10-4.

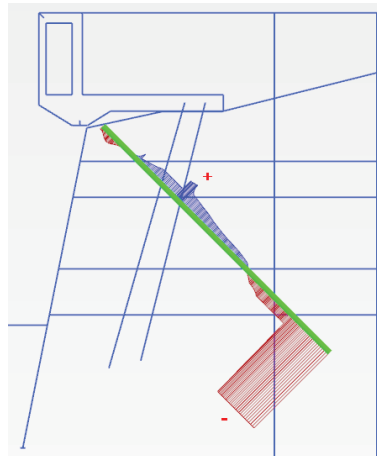


Figure 10-4 - Mobilized skin friction along the M.V.-piles

Even though the geotechnical capacity of the M.V.-piles had already been reached, the system did not yet fail due to the residual strength of other structural members. At a surcharge of $122.5/482.5 \text{ kN/m}^2$ the model failed. Figure 10-5 shows the failure points of the model after the first mechanism had occurred, it can be seen that the soil on the water side of the CSPW fails. Figure 10-6 shows the scaled up deformed mesh at the time of failure.

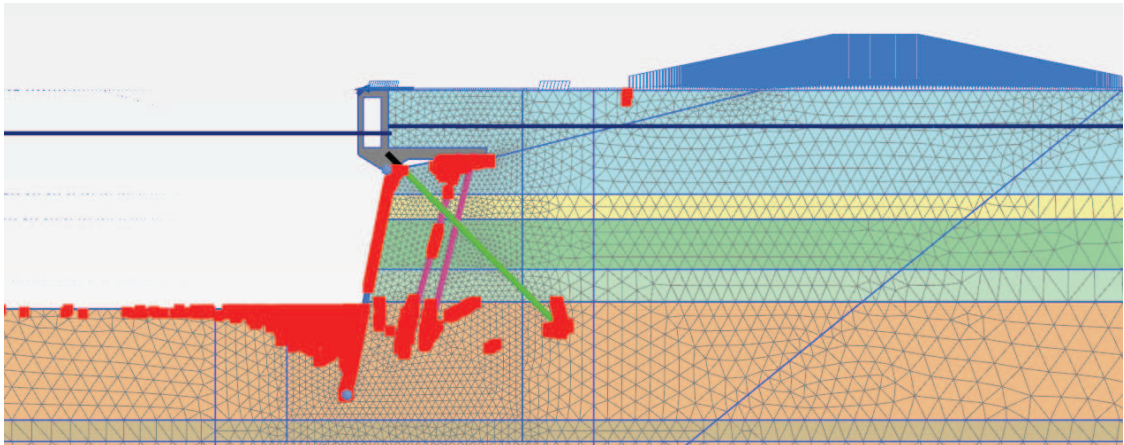


Figure 10-5 - Failure points after the 1st failure of the Amazonehaven model occurred

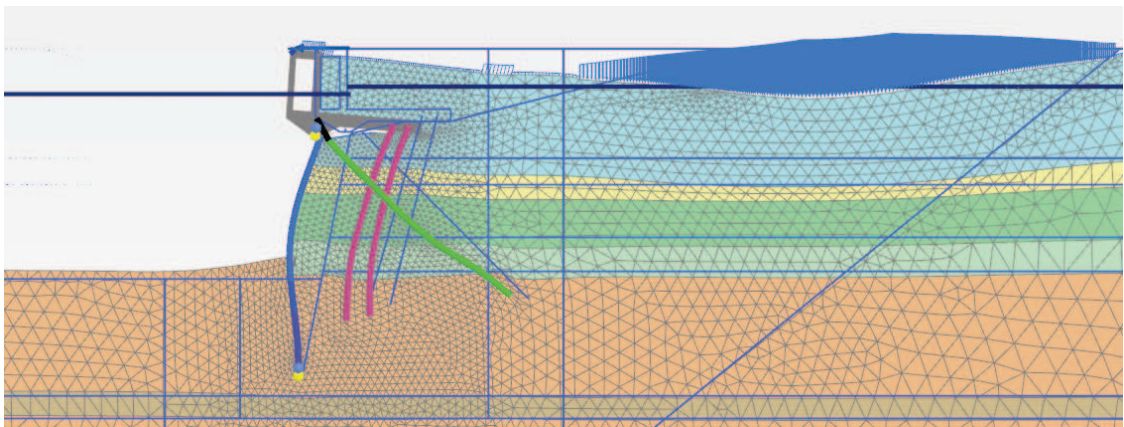


Figure 10-6 - Deformed mesh after the 1st failure of the Amazonehaven model occurred, scaled up 20 times

10.1.3 Second failure mechanism

The resistance to the failing of the M.V.-piles was increased by increasing the maximum value that the skin friction of the M.V.-piles could take, the calculation process was then reset. The model failed at a surcharge of 197.5/557.5 kN/m². Figure 10-7 shows the failure points of the model after the second mechanism had occurred, it can be seen that the soil on the water side of the CSPW and the soil along the end of the M.V.-piles fail. The conclusion that was drawn from this was that a total instability mechanism caused the model to fail. Figure 10-8 shows the scaled up deformed mesh at the time of the second failure mechanism.

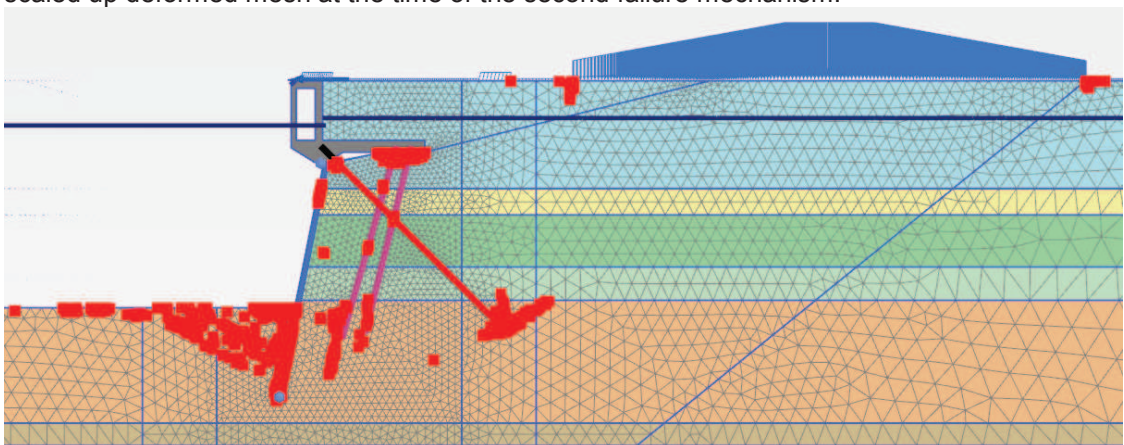


Figure 10-7 - Failure points after the 2nd failure of the Amazonehaven model occurred

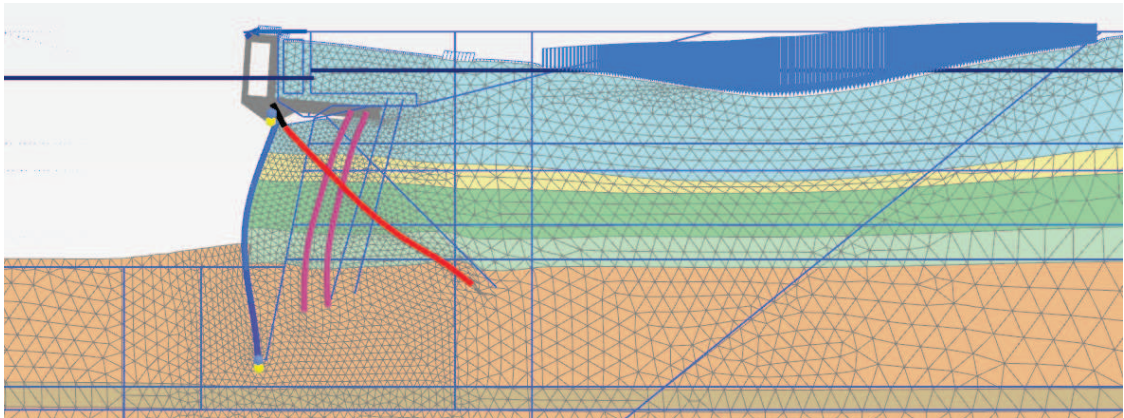


Figure 10-8 - Deformed mesh after the 2nd failure of the Amazonehaven model occurred, scaled up 20 times

10.1.4 Reflection with the expected results

It was expected that the model would fail due to the M.V.-piles at a magnitude of the bulk surcharge that was close to the design conditions. The results in regard to the first mechanism match that of the expected one.

It was further expected that the second mechanism that would occur would be a total instability one, while the safety regarding several structural elements would still be more than sufficient. The results match with this expectation as well.

One of the reason that the expected results and the actual results are very similar to one another is that the final model failed at a surcharge which magnitude was not far from the design conditions. There was already a lot of insight into how the different structural elements would respond to a large surcharge.

10.2 SIF

10.2.1 Overview of the test loading

The final model for the SIF structure experienced three failures. The first one occurred at a surcharge of 430 kN/m², the maximum allowable normal stress of the M.V.-piles caused this mechanism. The next mechanism occurred at a surcharge of 480 kN/m² due to the exceedance of the normal stress capacity of the CSPW. The final mechanism took place at a surcharge of 510 kN/m², this was caused by local geotechnical failure of a soil body on the waterside. An overview of the calculation phases from the test loading of the SIF structure is shown in Figure 10-9.

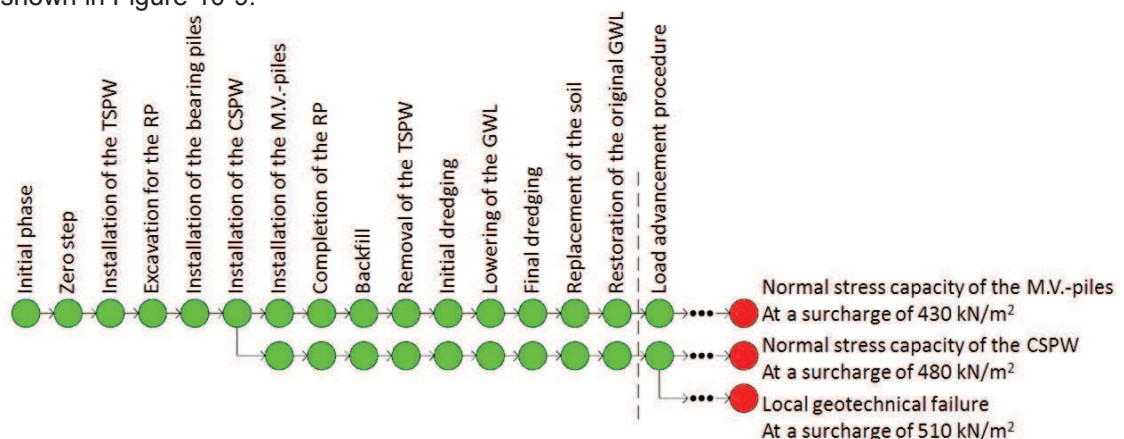


Figure 10-9 - Calculation phases of the SIF model

Just as with the Amazonehaven model, the structural safety of the different structural elements was determined by normalizing the acting structural forces with respect to the respective structural capacity. The structural capacities for the SIF model are presented in Table 10-2. *Table 10-2 - Structural capacities of the structural elements for SIF*

Variable	Structural capacity
$M_{\text{field,CSPW}}$	7,614.2 kNm/m
$M_{\text{fixed,CSPW}}$	7,276.0 kNm/m
N_{CSPW}	20,469.3 kN/m
V_{CSPW}	6,046.0 kN/m
$N_{\text{bearing piles combined}}$	10,063.9 kN/m
$F_{\text{M.V.-piles}}$	Geotechnical: 2,969.8 kN/m Yielding: 2,904.5 kN/m

Since the geotechnical and yielding capacities of the M.V.-piles were almost the same, only the normalized results with respect to yielding have been determined. The normalized structural reactions to the test loading of SIF are presented in Figure 10-10. The horizontal axis shows the magnitude of the bulk surcharge in kN/m^2 , the vertical axis represents the relative magnitude with respect to the structural capacities. The vertical red dashed lines in the figure represent the surcharge at which the model failed. The other plotted lines are the normalized results of:

- $M_{\text{field,CSPW}}$ = The magnitude of the maximum bending moment in the CSPW
- $M_{\text{fixed,CSPW}}$ = The magnitude of the fixed end bending moment in the CSPW
- N_{CSPW} = The magnitude of the maximum normal force in the CSPW
- N_{bp} = The magnitude of the maximum normal force in the bearing piles (taken as the average between the two pile rows)
- $F_{\text{M.V.-yield}}$ = The magnitude of the maximum normal force in the M.V.-piles with respect to the yielding capacity of the piles
- $\sigma_{\text{normal,CSPW}}$ = The magnitude of the combined effect of bending and normal loading
- V_{CSPW} = The magnitude of the maximum shear force in the CSPW

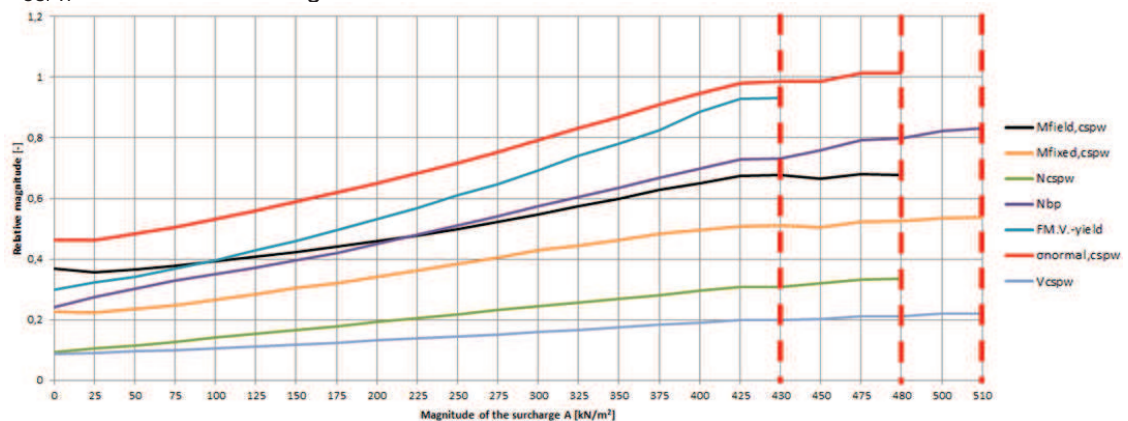


Figure 10-10 - Structural reactions to the test loading of SIF

In the figure above, it looks like the CSPW is the element that causes the model to fail at the first failure mechanism. Further inspection of the results however show that it is in fact the M.V.-piles that have reached their normal stress capacity. It can be seen that the exceedance of the normal stress capacity of the CSPW is the mechanism that causes the second failure of the model. At the time of the final failure, the bearing piles were at ca. 85% of their capacity.

Overall it can be seen that the different structural elements fail at similar surcharge magnitudes, the design is therefore well balanced/economical.

The horizontal displacements of the CSPW are presented in Figure 10-11. The red dashed lines show the magnitudes of the surcharge at which the model failed. The horizontal axis again shows the magnitude of the bulk surcharge in kN/m^2 and the vertical axis shows the horizontal displacement of the CSPW in mm.

$U_{\text{CSPW,top}}$ = The horizontal displacement of the top of the CSPW

$U_{\text{CSPW,field}}$ = The maximum horizontal displacement of the CSPW

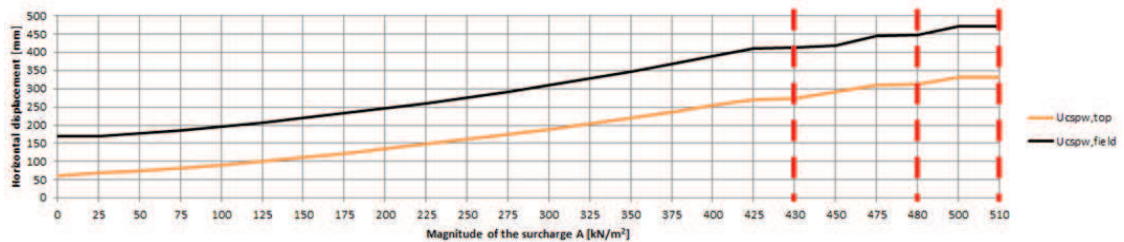


Figure 10-11 - Deflections of the CSPW during the test loading of SIF

10.2.2 First failure mechanism

The load advancement procedure was started, when the surcharge was equal to 350 kN/m^2 the normal stress capacity of the M.V.-piles is first reached, this does however not cause the model to fail yet. The reached values for the bending moment and the normal force at this surcharge are presented below:

$$\frac{M_{\text{acting}}}{M_p} \pm \frac{N_{\text{acting}}}{N_p} = \frac{141.7}{2,000/3.3} + \frac{2,225.5}{9,585/3.3} = 1.00$$

The magnitude of the surcharge is increased further. The model first fails at a surcharge of 430 kN/m^2 . The bending moment distribution of the M.V.-piles is presented in Figure 10-12, its odd shape and the fact that the maximum bending moments have decreased suggest that the exceedance of the normal stress capacity was indeed the mechanism that caused the failure.

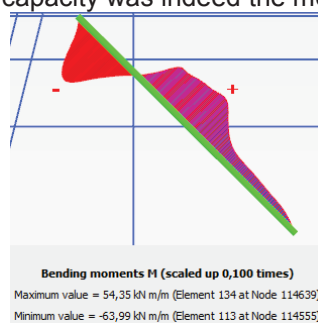


Figure 10-12 - Bending moment distribution of the M.V.-piles at the first failure mechanism of SIF

Figure 10-13 shows the failure points of the model after the first mechanism had occurred, it can be seen that the soil on the water side of the CSPW fails. Figure 10-14 shows the scaled up deformed mesh at the time of failure.

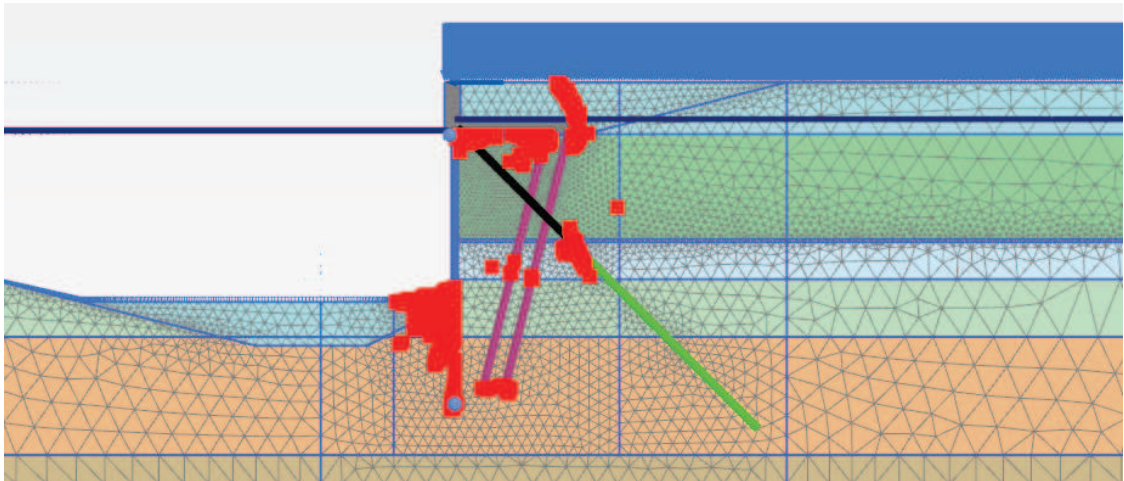


Figure 10-13 - Failure points after the 1st failure of the SIF model occurred

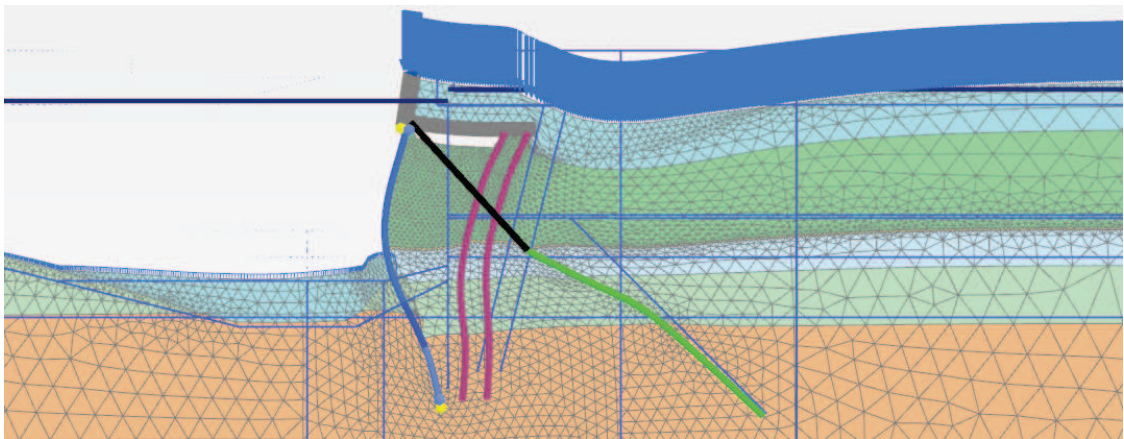


Figure 10-14 - Deformed mesh after the 1st failure of the SIF model occurred, scaled up 20 times

10.2.3 Second failure mechanism

The resistance to the failing of the M.V.-piles was increased by both increasing the maximum allowable skin friction along the piles and changing the material type of the piles from elastoplastic to elastic. This was done because the piles were also close to their geotechnical limit. After resetting and restarting the model, the normal stress capacity of the CSPW is reached at a surcharge of 475 kN/m², the acting structural forces belonging to this surcharge are shown below:

$$\frac{M_{acting}}{M_p} \pm \frac{N_{acting}}{N_p} = \frac{5,175.8}{7,614.2} + \frac{6,561.5}{20,469.3} = 1.00$$

The model fails at a load of 480 kN/m². The failure points are shown in Figure 10-15 and the scaled up deformed mesh in Figure 10-16.

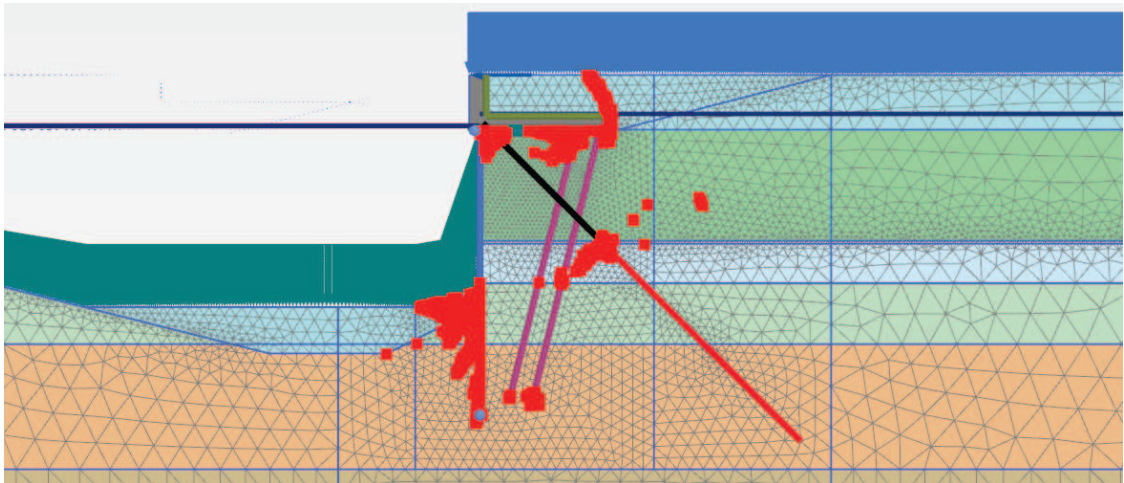


Figure 10-15 - Failure points after the 2nd failure of the SIF model occurred

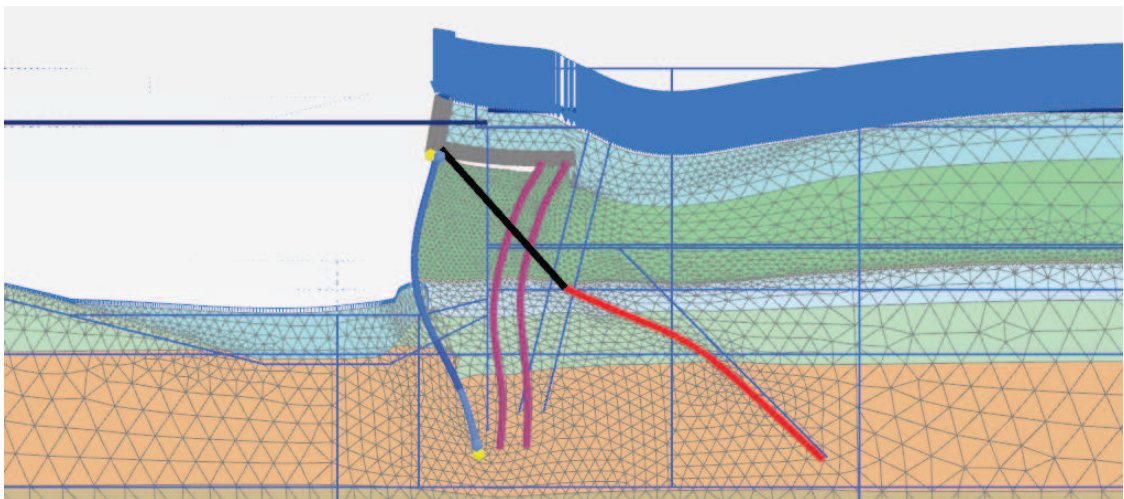


Figure 10-16 - Deformed mesh after the 2nd failure of the SIF model occurred, scaled up 20 times

10.2.4 Third failure mechanism

The resistance in regard to the failing of the CSPW was increased by changing the material type of the CSPW from elastoplastic to elastic. The load advancement was then reset. The final failure of the model occurred at a surcharge of 510 kN/m^2 , it was induced by local geotechnical failure of a soil body on the waterside. The failure points are shown in Figure 10-17 and the scaled up deformed mesh in Figure 10-18.

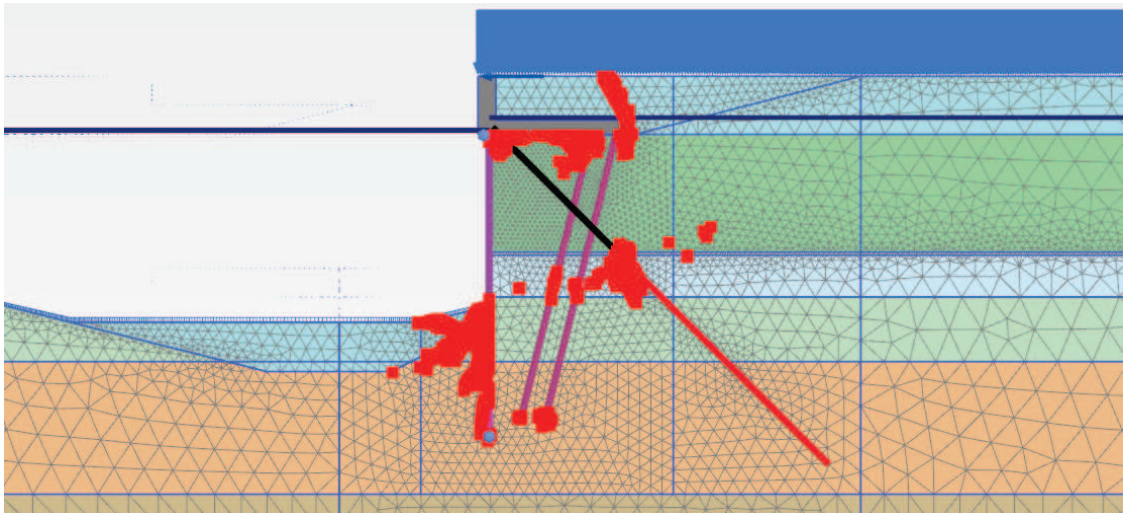


Figure 10-17 - Failure points after the 3rd failure of the SIF model occurred

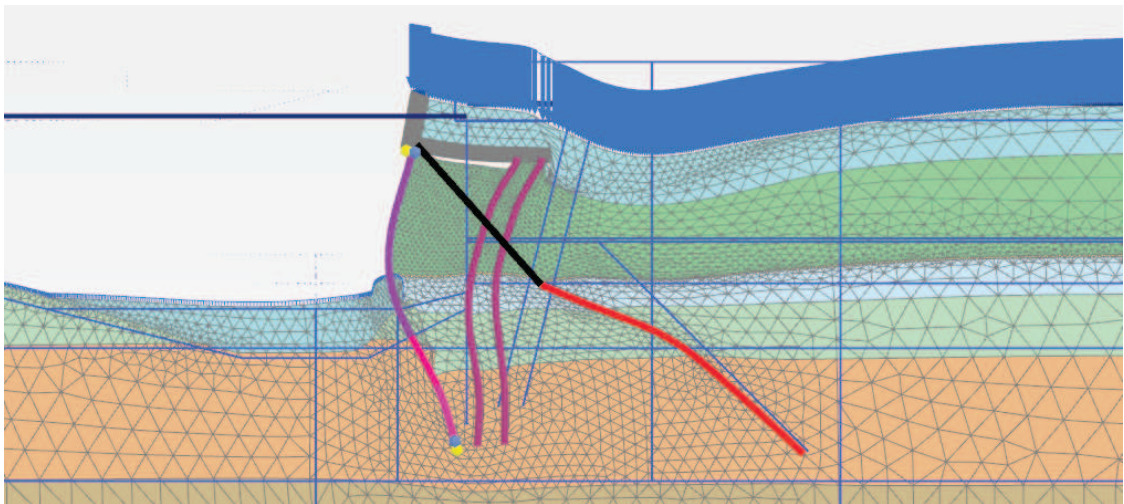


Figure 10-18 - Deformed mesh after the 3rd failure of the SIF model occurred, scaled up 20 times

10.2.5 Reflection with the expected results

It was expected that the model would fail due to the exceedance of the normal stress capacity of the CSPW. The actual results however show that the model fails first due to the same mechanism, but of the M.V.-piles. After this the expected mechanism did cause the model to fail. In line with the expectations a Bishop type of failure did not occur, local geotechnical failure of a soil body caused the model to fail.

Even though the model failed at surcharges that were far larger than the design loading conditions, the expected outcome was fairly accurate.

11 Discussion of the results

In this chapter the results will be discussed. Why certain failure mechanisms occurred and the theory behind the magnitudes of the surcharges at which this happened will be elaborated on. Areas of interest which were not implemented in the models will also be discussed.

11.1 Amazonehaven

The model for the Amazonehaven failed at loads that were relatively close to their design load. The first mechanism that occurred was the geotechnical failure of the M.V.-piles, the final one was due to total instability. Each mechanism will now be elaborated on separately.

In the design of the M.V.-piles of the Amazonehaven, the theorized active sliding plane was used in determining the effective length of the piles. This resulted in the assumption that the M.V.-piles would acquire 50% of their bearing capacity in the Holocene soil layer and 50% in the Pleistocene soil layer. The model however shows that only the Pleistocene sand layer contributes to the bearing capacity, this means that the geotechnical bearing capacity of the M.V.-piles is effectively halved in regard to the predicted one. Another element is the variations in the soil layering, the soil profile that was selected was the most normative one. In reality a there would both be M.V.-piles that are located at positions where the soil is relatively weak, while others are installed in stronger soil. When looking at an entire RP compartment and all the M.V.-piles that are attached to it, the results might show a more promising outcome. This would probably still only marginally improve the effective length of the M.V.-piles.

According to the Blum method the toe of the CSPW needed to be at ca. NAP-38.9 m for the CSPW to be fully fixed at its toe. The toe of the design however was located at NAP-37.5, meaning that the CSPW was not fully fixed into the soil. This results in increased bending moments within the CSPW and a lower resistance against the failure of the soil on the passive side of the CSPW. The relatively short length of the M.V.-piles in combination with the high loads that are present and the not fully fixed CSPW make a total instability failure mechanism very likely.

From the results it can be interpreted that apart from the insufficient length of the M.V.-piles (which resulted in the insufficient geotechnical bearing capacity and contributed to the early total instability plane) the model is still relatively safe in regard to the different structural elements. Should the length of the M.V.-piles have been increased, the design would most likely have been safe enough.

The maximum skin friction that the M.V.-piles could withstand was determined based on CPTs. In reality the high surcharges will have a positive effect on the maximum skin friction that can occur with certain structural elements. In the created models this has not been taken into account, by using the "layer dependent" function within the Plaxis 2D software, this effect could be implemented. The expected result of this implementation would be the increase of the first failure load of the structure. It would however not have an effect on the final failure load. Another area of interest is the construction depth. The design of the Amazonehaven had an initial contract depth of NAP-21.65 m which would later be expanded to NAP-24 m with a construction depth of NAP-25.5 m. This deepening however has never taken place, resulting in an increased embedded depth and a reduced retaining height in regard to the model.

A third area of interest is the bulk surcharge itself. In the models the surcharge has been modelled as a combination of line loads, in reality the surcharge consists of a large pile of coal or iron ore with a high internal angle of friction. On one hand the pile would increase the resistance against a total instability failure mechanism. On the other hand the load would already be transmitted throughout the pile of material itself, effectively increasing the part of the surcharge that would reach the CSPW. It is hard to predict which of these two effects has a larger contribution on the safety.

11.2 SIF

The model for the SIF structure failed at loads that were far larger than the design loading conditions. The first failure occurred due to failure of the M.V.-piles, the second due to failure of the CSPW, and the final one due to geotechnical failure of a soil body. The different failures will now be elaborated on.

Based on the input variables it could already be seen that the geotechnical bearing capacity and the yield strength of the M.V.-piles were almost identical to each other. It was therefore not unexpected that their failures would somewhat coincide. It could also be seen that they were more than sufficient for the design loading conditions. That the combined effect of bending and normal loading proved normative was however not foreseen.

Due to the extremely high normal loads on the CSPW it was expected that this would contribute significantly to the failure of the model. It was therefore expected that the failure would occur at a certain surcharge. The structural response to the design loading conditions however already showed that there was still plenty safety in regard to this mechanism. Within this thesis the effect that the sand within the primary tubular piles had on the plastic bending moment capacity and the residual strength of the structure has not been accounted for.

The Blum method stated that in order to be fully fixed into the soil, the toe of the CSPW needed to be at a depth of at least NAP-31.9 m. The actual position of the toe is NAP-39 m, this is far deeper than the calculated required depth. The Blum method did however have some limitations which resulted in a somewhat optimistic needed embedded depth. Even taking these “optimistic limitations” into account, it seems fair to say that the CSPW should be fully fixed into the soil. This suggests that the resistance against failure of the soil on the waterside should far exceed the design loading conditions, the results are in agreement with this statement.

The high safety of the SIF structure is most likely the result of several conservative approaches, safety and material factors, and other assumptions. The fact that the model could withstand more than 4 times its design bulk surcharge is most likely the result of the assumption that only the magnitude of the bulk surcharge would vary. If other parameters, such as the internal angle of friction of the soil or undrained soil behavior, were to be taken into account, the model could show a different result.

12 Conclusions

To apply FEM to a quay structure, insight should be gained into that specific structure and the local conditions regarding it. By having a clear understanding of the structure and the expected reaction of it to the boundary conditions, the accuracy of the model can be improved.

The FEM software that was used within this MSc thesis is mostly focused on the failure of the soil. Through the interpretation and post processing of the results the failure of the model and what caused this becomes apparent.

Due to the soil types of the soils that were present and the function of the structures at the respective locations, the soil model that was best applicable to all of the soil layers was the Hardening Soil with small-strain stiffness model in combination with drained soil behavior.

To validate a FEM model it is important to be able to assess the results from a critical point of view. Within this MSc thesis this was done by:

- Comparing the FEM results to that of other modelling methods;
- Comparing the FEM results to actual field measurements;
- Assessing the model to determine whether important aspects had been incorporated correctly.

One of the major difference between the FEM software that was applied and the Blum and D-Sheet Piling method was that the entire structure was used in the FEM software while in the other methods it was decoupled. This resulted in far less assumptions being used for the FEM method than for the other methods. The differences in the results could mostly be explained by limitations of the other modelling methods.

Another major difference was that the FEM software applied constitutive models to model the soil behavior.

The Amazonehaven structure collapsed at a bulk surcharge of 122.5/482.5 kN/m² which is only 32.5 kN/m² more than the design loading conditions. For the SIF structure failure occurred at 430 kN/m², which is more than 4 times the magnitude of the design load.

The main function of the considered quay structures was the storage of goods. The critical loads were therefore the bulk surcharges and the loads of the equipment that would be used to apply these surcharges. For the Amazonehaven model the tower crane load proved to be normative, for the SIF model the equipment loads were covered by the magnitude of the bulk surcharge.

Over the length of the quay structures the critical cross sections were the cross sections that contained the most soft soil layers in relation to their retaining height. In this thesis those cross sections have been named Amazonehaven 1 & SIF 2.

According to the FEM analysis the critical failure mechanism for the Amazonehaven model was failure of the M.V.-piles due to the exceedance of the geotechnical bearing capacity, due to the redistribution of structural forces however, the model did not yet fail. After a certain increase in the magnitude of the bulk surcharge the model did however fail due to insufficient length of the CSPW. For the SIF model the results of the FEM analysis show that the first failure mechanism that occurs is the exceedance of the normal stress capacity of the M.V.-piles. After an increase of the magnitude of the surcharge the model fails due geotechnical failure of a soil body on the waterside.

The Amazonehaven model had not yet failed at its design loading conditions, the M.V.-piles however had already reached their maximum geotechnical bearing capacity prior to these conditions. It was therefore concluded that even though the model had not yet failed, the Amazonehaven structure could not withstand its design loading conditions. Should the M.V.-piles have had a larger length, the structure would have been able to withstand it. Implementation of the effect that the surcharge has on the geotechnical bearing capacity of the M.V.-piles would likely result in a higher failure load.

At the design loading conditions of SIF the structural element that was closest to failure was the CSPW due to the exceedance of its normal stress capacity. The structural forces that would incite this mechanism however were only at ca. 55% of the values that were needed for failure. The SIF structure can therefore withstand its design loading conditions.

13 Recommendations

The following recommendations are made to improve the load capacity assessment of the quay structures:

- More research should be done into the way in which the bulk surcharges are applied and the hydraulic conductivity of the clay layers. In this way it becomes clearer whether drained or undrained soil behavior should be applied;
- The shielding effect of the bearing piles in combination with the arching effect of the soil has not been incorporated in the models accurately, a 3D FEM analysis should be carried out to predict the structural forces more accurately;
- A 3D FEM analysis should be carried out on the Amazonehaven in which the structure of the soil is represented over the entire width of a RP compartment. It was also observed that even though the critical soil profile was selected, the corresponding structural cross section did not contain the longest M.V.-piles of the structure, insight should be gained into this decision;
- The predicted effective length of the M.V.-piles of the Amazonehaven was completely different from the length that followed from the FEM models. More research should be carried out into the effective length of anchor elements of structures that apply a RP;
- Research into the effect of the large surcharges on the geotechnical bearing capacity of the M.V.-piles;
- Modelling of the bulk surcharge of the Amazonehaven as a soil body with a high internal angle of friction instead of as a combination of line loads.

Based on the obtained results in regard to the insufficient length of the M.V.-piles in the design of the Amazonehaven structure, it is also recommended to check the designs of other quay structures that were constructed in the same period. It should be checked whether the anchor elements of these structures have a sufficient effective length or not.

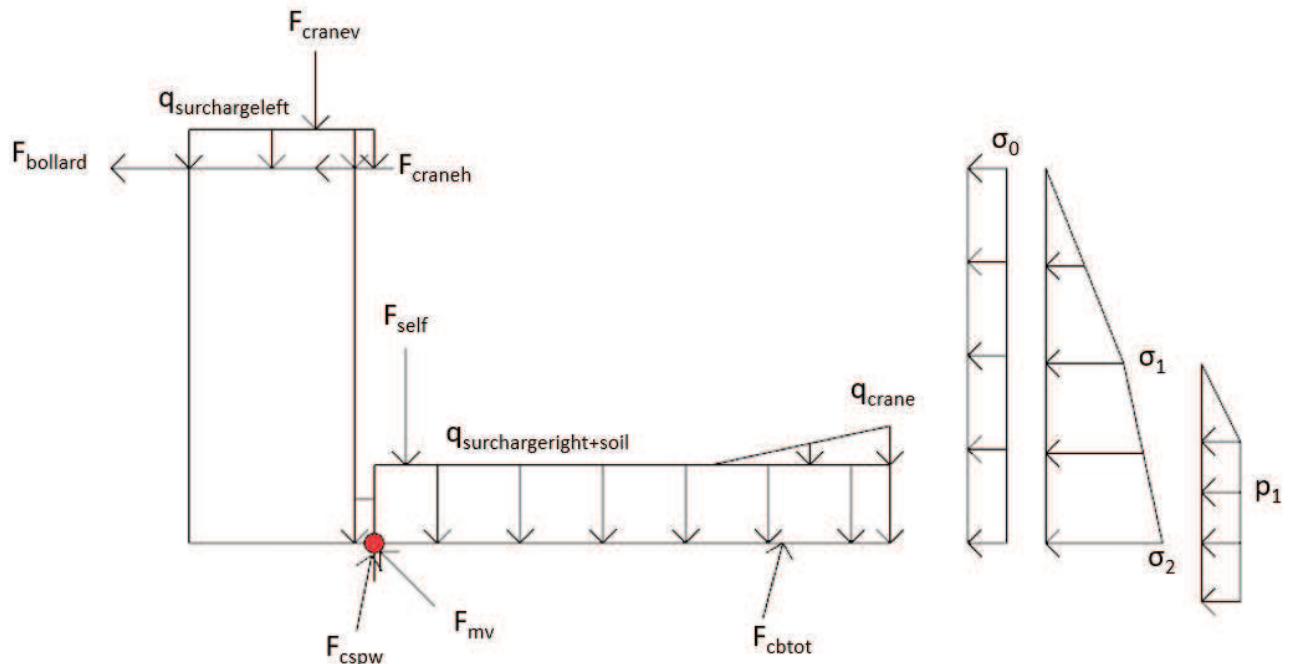
References

- [1] SBRCURnet (2014), Publication 211E 'Quay Walls, Second Edition', SBRCURnet
- [2] Vrijling J.K., Bezuyen K.G., Kuijper H.K.T., van Baars S., Molenaar W.F., Voorendt M.Z. (2015), Manual Hydraulic Structures, TU Delft, Delft
- [3] U. Smolczyk (2002), Geotechnical Engineering Handbook, Ernst & Sohn, Böblingen
- [4] A. Verruijt (2012), Soil Mechanics, TU Delft, Delft
- [5] Deltares (2016), D-Sheet Piling – Design of diaphragm and sheet pile walls – User Manual, Deltares, Delft
- [6] SBRCURnet (2005), CUR-publicatie 166 (vierde druk) – Damwandconstructies, SBRCURnet
- [7] N.K.N. Mourillon (2015), MSc thesis report - Stability analysis quay structure at the Amazonehaven port of Rotterdam
- [8] Municipality of Rotterdam (1988), Bestek 1-071-88, Rotterdam
- [9] MariTeam (2015), Ontwerprapportage – Zeekade Offshore Terminal Rotterdam – Hoofdberekening onderbouw
- [10] MariTeam (2015), Ontwerptekening – DZK-T-BST-0015-B
- [11] MariTeam (2015), Ontwerprapportage – DZK-R-BST-0001 Uitgangspuntennota diepzeekade
- [12] MariTeam (2015), Ontwerprapportage – DZK-R-BST-0002 Grondopbouw en grondparameters
- [13] MariTeam (2015), Ontwerptekening – DZK-T-BST-0010
- [14] MariTeam (2015), Ontwerprapportage – DZK-R-BST-0101 Hoofdberekening onderbouw
- [15] Municipality of Rotterdam (2011), Ontwerprapportage – Amazonehaven – Verbreding Amazonehaven – Geotechnisch lengteprofiel kade A1 en A2, Rotterdam
- [16] M.G. Parent, J.G. de Gijt, H. Brassinga, C.N. Schaik, W. van Ast, R.E. Roelfsema, J.B. Verheul (1990), Diepwaterterminal op de Maasvlakte te Rotterdam 1-6, PT Civiele Techniek, Nummer 2, 3-30
- [17] Municipality of Rotterdam (2002), Ontwerprapportage – Zeekade Zuidzijde – Controle constructieve veiligheid Zeekade Amazonehaven Zuidzijde, Rotterdam
- [18] Gemeentewerken Rotterdam (1988), Ontwerprapportage – Amazonehaven Zuidzijde – Funderingsberekening – Deel A, Rotterdam
- [19] Gemeentewerken Rotterdam (1988), Ontwerprapportage – Diepwater-terminal Frans Swarttouw – Programma van Eisen – Plan “Insteekhaven Maasvlakte”, Rotterdam
- [20] MariTeam (2017), Presentation – Design, construction and operation of a heavy duty deep sea quay wall for offshore wind energy
- [21] MariTeam (2018), Ontwerpmemo – Vervorming kade OTR ter informatie voor HES
- [22] PLAXIS (2018), PLAXIS 2D Material Models Manual 2018
- [23] PLAXIS (2018), PLAXIS 2D Reference Manual 2018
- [24] R.B.J. Brinkgreve (2005), Selection of soil models and parameters for geotechnical engineering application, Proceedings Geo-Frontiers Congress 2005, Austin, 4

Appendices

A. Maple - Reaction forces of the superstructures

[> restart; #Amazonehaven 1a & 2a



- > $F_{cbv} := 'F_{cbv}':$ # Vertical force in the concrete bearing piles
- $F_{cbtot} := 'F_{cbtot}':$ # Normal force in the concrete bearing piles
- $F_{cspw} := 'F_{cspw}':$ # Normal force in the combined sheet pile wall
- $F_{mv} := 'F_{mv}':$ # Normal force in the M.V.-piles
- $F_{bollard} := 50 :$ # Bollard force
- $q_{surchargelleft} := 20 :$ # Surcharge, position relative to the combined sheet pile wall
- $q_{surchargeright} := 20 :$ # Surcharge, position relative to the combined sheet pile wall
- $F_{cranev} := 337.8 :$ # 337.8 or 0, Crane load vertical
- $F_{craneh} := 90 :$ # 90 or 0, Crane load horizontal
- $GWL := 0 :$ # Groundwater level
- $Sig0 := 0.5 \cdot q_{surchargeright} :$ # Vertical soil stress due to the surcharge
- $Sig1 := 0.5 \cdot (5 - GWL) \cdot 18 :$ # Vertical soil stress at the GWL
- $Sig2 := 0.5 \cdot ((5 - GWL) \cdot 18 + (4.6 + GWL) \cdot 10) :$
Vertical soil stress at the bottom of the Relieving Platform floor
- $p1 := 10 :$ # Water pressure difference
- $F_{self} := 869.9 - 1.7 \cdot GWL \cdot 10 :$
Reduction of the self-weight do to the effective volumetric weight, the shift in the position of the centre of gravity is neglected
- $q_{soil} := (5 - GWL) \cdot 18 + (3 + GWL) \cdot 10 :$ # Soil that rests on the R.P.
- $q_{crane} := F_{cranev} \cdot 0.2733 :$ # for the tower crane 0.2733 · F_cranev, for the bridge crane 0
- $rF_{bollard} := -9.85 :$
- $rq_{surchargelleft} := -2.375 :$
- $rq_{surchargeright} := 6.625 :$
- $rF_{cranev} := -1.5 :$
- $rF_{craneh} := -9.6 :$
- $rq_{soil} := 6.375 :$
- $rF_{self} := 0.819 :$
- $rq_{crane} := 11.717 :$

$$rFcbv := -10.5 :$$

$$rsig0 := -\frac{9.6}{2} :$$

$$rp1a := -\left(4.6 + GWL - \frac{2}{3}\right) :$$

$$rp1b := -\left(\frac{(6.1 + GWL - 1)}{2} - 1.5\right) :$$

$$rsig1 := -\left(\frac{(5 - GWL)}{3} + 4.6 + GWL\right) :$$

$$rsig2a := -\frac{(4.6 + GWL)}{2} :$$

$$rsig2b := -\frac{(4.6 + GWL)}{3} :$$

$$\begin{aligned} > eq1 := Fbollard \cdot rFbollard + qsurchargeleft \cdot 4.75 \cdot rqsurchargeleft + qsurchargeright \cdot 13.25 \\ & \cdot rqsurchargeright + Fcranev \cdot rFcranev + Fcraneh \cdot rFcraneh + \frac{Sig1 \cdot (5 - GWL)}{2} \cdot rsig1 \\ & + Sig1 \cdot (4.6 + GWL) \cdot rsig2a + \frac{(Sig2 - Sig1) \cdot (4.6 + GWL)}{2} \cdot rsig2b + \frac{p1 \cdot 2}{2} \cdot rp1a + p1 \\ & \cdot (6.1 + GWL - 2) \cdot rp1b + Fself \cdot rFself + qsoil \cdot 13.75 \cdot rqsoil + \frac{qcrane \cdot 4.6}{2} \cdot rqcrane \\ & + Fcbv \cdot rFcbv + Sig0 \cdot 9.6 \cdot rsig0 = 0 : \# \text{ Sum of the moments} = 0 \end{aligned}$$

$$eq2 := Fcbtot = \frac{(3.75^2 + 1)^{0.5}}{3.75} \cdot Fcbv : \# \text{ average inclination of } 3.75:1$$

$$\begin{aligned} eq3 := & -Fbollard - Fcraneh - Sig0 \cdot 9.6 - \frac{Sig1 \cdot (5 - GWL)}{2} - Sig1 \cdot (4.6 + GWL) \\ & - \frac{(Sig2 - Sig1) \cdot (4.6 + GWL)}{2} - \frac{p1 \cdot 2}{2} - p1 \cdot (6.1 + GWL - 2) + \frac{Fcbv}{3.75} + \frac{Fcspw}{26^{0.5}} \\ & - \frac{Fmv}{2^{0.5}} : \# \text{ Sum of the horizontal forces} = 0 \end{aligned}$$

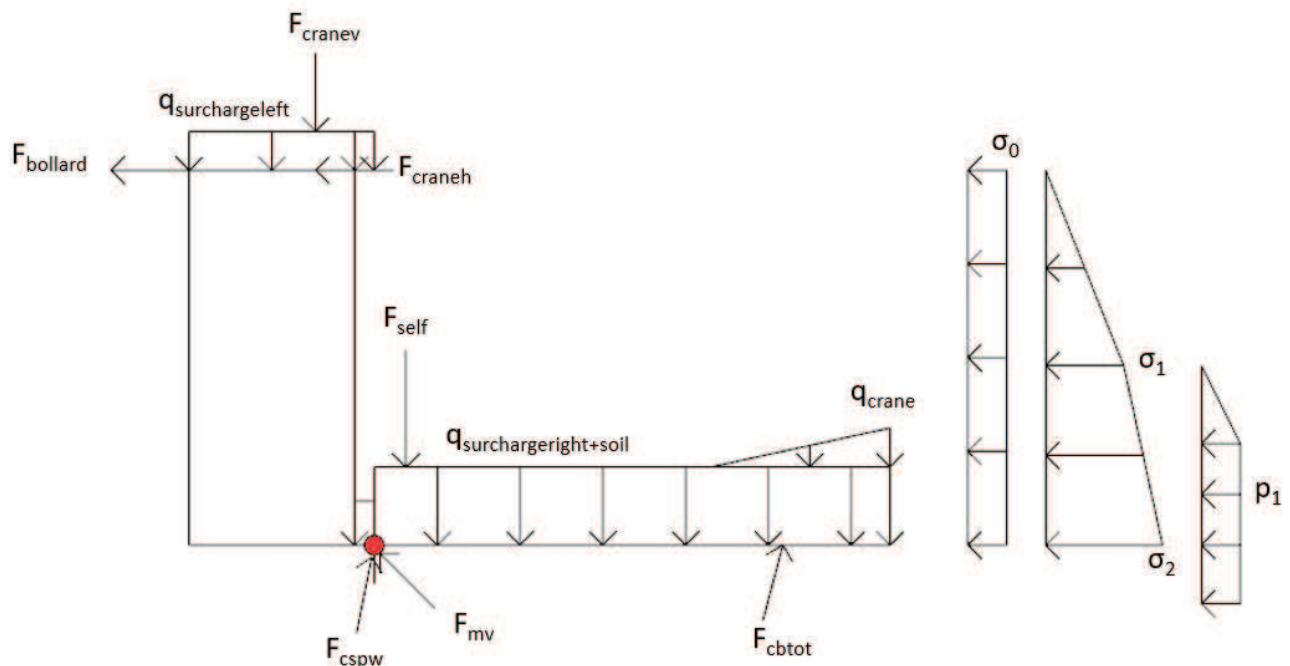
$$\begin{aligned} eq4 := & qsurchargeleft \cdot 4.75 + qsurchargeright \cdot 13.25 + Fcranev + Fself + qsoil \cdot 13.75 \\ & + \frac{qcrane \cdot 4.6}{2} - Fcbv - \frac{Fcspw \cdot 5}{26^{0.5}} - \frac{Fmv}{2^{0.5}} : \# \text{ Sum of the vertical forces} = 0 \end{aligned}$$

$$> S := solve(\{eq1, eq2, eq3, eq4\}, \{Fcbv, Fcbtot, Fmv, Fcspw\});$$

$$S := \{Fcbtot = 1141.451886, Fcbv = 1102.910694, Fcspw = 2288.114886, Fmv = 118.0101349\}$$

(1)

> **restart; #Amazonehaven 1b & 2b**



- $F_{cbv} := 'F_{cbv}':$ # Vertical force in the concrete bearing piles
 $F_{cbtot} := 'F_{cbtot}':$ # Normal force in the concrete bearing piles
 $F_{cspw} := 'F_{cspw}':$ # Normal force in the combined sheet pile wall
 $F_{mv} := 'F_{mv}':$ # Normal force in the M.V.-piles
 $F_{bollard} := 50 :$ # Bollard force
 $q_{surchargelleft} := 0 :$ # Surcharge, position relative to the combined sheet pile wall
 $q_{surchargeright} := 20 :$ # Surcharge, position relative to the combined sheet pile wall
 $F_{cranev} := 0 :$ # 337.8 or 0, Crane load vertical
 $F_{craneh} := 0 :$ # Crane load horizontal
 $GWL := 1 :$ # Groundwater level
 $Sig0 := 0.5 \cdot q_{surchargeright} :$ # Vertical soil stress due to the surcharge
 $Sig1 := 0.5 \cdot (5 - GWL) \cdot 18 :$ # Vertical soil stress at the GWL
 $Sig2 := 0.5 \cdot ((5 - GWL) \cdot 18 + (4.6 + GWL) \cdot 10) :$
 # Vertical soil stress at the bottom of the Relieving Platform floor
 $p1 := 10 :$ # Water pressure difference
 $F_{self} := 869.9 - 1.7 \cdot GWL \cdot 10 :$
 # Reduction of the self-weight do to the effective volumetric weight, the shift in the position of the centre of gravity is neglected
 $q_{soil} := (5 - GWL) \cdot 18 + (3 + GWL) \cdot 10 :$ # Soil that rests on the R.P.
 $q_{crane} := F_{cranev} \cdot 0.2733 :$ # for the tower crane $0.2733 \cdot F_{cranev}$, for the bridge crane 0
 $rF_{bollard} := -9.85 :$
 $rq_{surchargelleft} := -2.375 :$
 $rq_{surchargeright} := 6.625 :$
 $rF_{cranev} := -1.5 :$
 $rF_{craneh} := -9.6 :$
 $rq_{soil} := 6.375 :$
 $rF_{self} := 0.819 :$
 $rq_{crane} := 11.717 :$
 $rF_{cbv} := -10.5 :$
 $rsig0 := -\frac{9.6}{2} :$

$$rp1a := - \left(4.6 + GWL - \frac{2}{3} \right) :$$

$$rp1b := - \left(\frac{(6.1 + GWL - 1)}{2} - 1.5 \right) :$$

$$rsig1 := - \left(\frac{(5 - GWL)}{3} + 4.6 + GWL \right) :$$

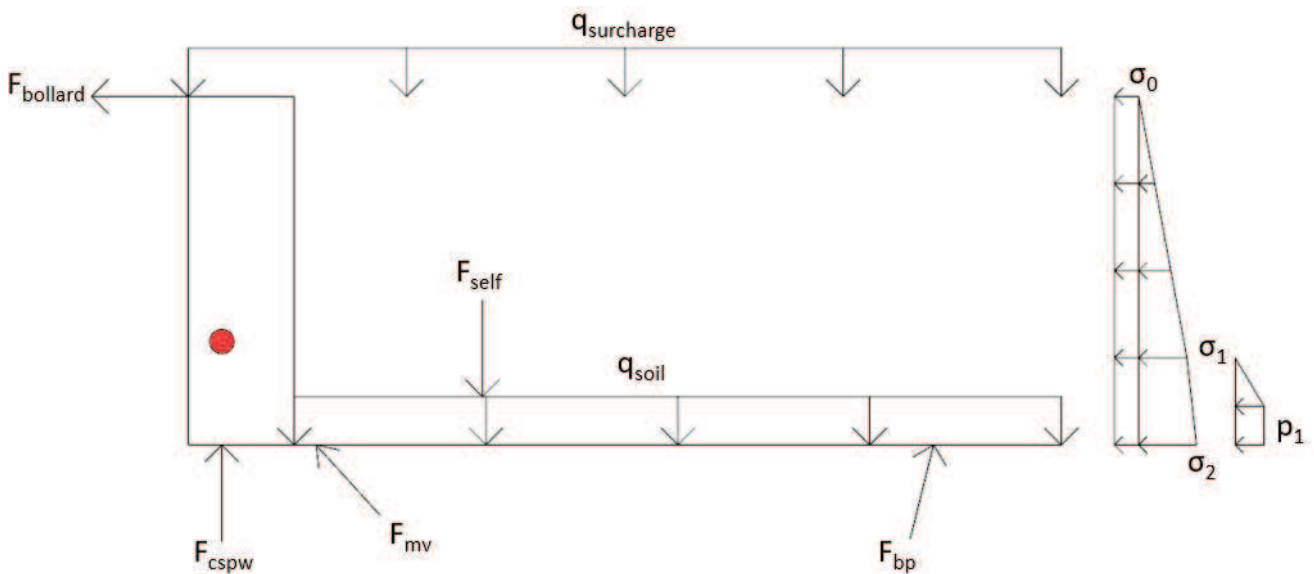
$$rsig2a := - \frac{(4.6 + GWL)}{2} :$$

$$rsig2b := - \frac{(4.6 + GWL)}{3} :$$

$$\begin{aligned} > eq1 := Fbollard \cdot rFbollard + qsurchargeleft \cdot 4.75 \cdot rqsurchargeleft + qsurchargeright \cdot 13.25 \\ & \cdot rqsurchargeright + Fcranev \cdot rFcranev + Fcraneh \cdot rFcraneh + \frac{Sig1 \cdot (5 - GWL)}{2} \cdot rsig1 \\ & + Sig1 \cdot (4.6 + GWL) \cdot rsig2a + \frac{(Sig2 - Sig1) \cdot (4.6 + GWL)}{2} \cdot rsig2b + \frac{p1 \cdot 2}{2} \cdot rp1a + p1 \\ & \cdot (6.1 + GWL - 2) \cdot rp1b + Fself \cdot rFself + qsoil \cdot 13.75 \cdot rqsoil + \frac{qcrane \cdot 4.6}{2} \cdot rqcrane \\ & + Fcbv \cdot rFcbv + Sig0 \cdot 9.6 \cdot rsig0 = 0 : \# \text{ Sum of the moments} = 0 \\ eq2 := Fcbtot = \frac{(3.75^2 + 1)^{0.5}}{3.75} \cdot Fcbv : \# \text{ average inclination of } 3.75:1 \\ eq3 := -Fbollard - Fcraneh - Sig0 \cdot 9.6 - \frac{Sig1 \cdot (5 - GWL)}{2} - Sig1 \cdot (4.6 + GWL) \\ & - \frac{(Sig2 - Sig1) \cdot (4.6 + GWL)}{2} - \frac{p1 \cdot 2}{2} - p1 \cdot (6.1 + GWL - 2) + \frac{Fcbv}{3.75} + \frac{Fcspw}{26^{0.5}} \\ & - \frac{Fmv}{2^{0.5}} : \# \text{ Sum of the horizontal forces} = 0 \\ eq4 := qsurchargeleft \cdot 4.75 + qsurchargeright \cdot 13.25 + Fcranev + Fself + qsoil \cdot 13.75 \\ & + \frac{qcrane \cdot 4.6}{2} - Fcbv - \frac{Fcspw \cdot 5}{26^{0.5}} - \frac{Fmv}{2^{0.5}} : \# \text{ Sum of the vertical forces} = 0 \end{aligned}$$

$$\begin{aligned} > S := solve(\{eq1, eq2, eq3, eq4\}, \{Fcbv, Fcbtot, Fmv, Fcspw\}); \\ S := \{Fcbtot = 983.6846578, Fcbv = 950.4704857, Fcspw = 1710.696162, Fmv = 42.36123406\} \quad (2) \end{aligned}$$

> **restart; # SIF 1a & 2a**



```

> Fbp := 'Fbp': # Normal force in the bearing piles
Fcspw := 'Fcspw': # Normal force in the combined sheet pile wall
Fmv := 'Fmv': # Normal force in the M.V.-piles
Fbollard := 130 : # Bollard force
qsurcharge := 100 : # Uniformly distributed surcharge
GrL := 5.1 : # Ground level
GWL := 0.05 :
    # Groundwater level (minimum value -2.1, otherwise the code would get to complicated)
OWL := -1.5 :
    # Outer water level (minimum value -2.1, otherwise the code would get to complicated)
Sig0 := 0.5 * qsurcharge : # Vertical soil stress due to the surcharge
Sig1 := 0.5 * (GrL - GWL) * 19 : # Vertical soil stress at the GWL
Sig2 := Sig1 + 0.5 * (2.1 + GWL) * 10 :
    # Vertical soil stress at the bottom of the Relieving Platform floor
p1 := (GWL - OWL) * 10 : # Water pressure difference
Fc1 := 15.9 * 1.85 * 24 : # Weight of the concrete R.P.
Fc2 := 2.2 * 7.2 * 24 : # Weight of the concrete R.P.
if GWL >= -2.1 then Fw1 := min(GWL + 2.1, 1.85) * 15.9 * 10 else Fw1 := 0 end if:
    # Upwards water force of the long part of the R.P.
if GWL >= -2.1 and OWL >= -2.1 then Fw2 :=  $\left( \frac{(GWL + OWL)}{2} + 2.1 \right) \cdot 2.2 \cdot 10$  elif GWL >=
    -2.1 and OWL < -2.1 then Fw2 :=  $\frac{GWL}{2} \cdot 2.2 \cdot 10$  else Fw2 := 0 end if:
    # Upwards water force of the high part of the R.P.
Fself := Fc1 + Fc2 - Fw1 - Fw2 : # Effective self-weight of the R.P.
qsoil := min(GrL - GWL, GrL + 0.25) * 19 + max(0.25 + GWL, 0) * 10 :
    # Soil that rests on the R.P.
rFbollard := -5.065 :
rqsurcharge := 8.35 :
rqsoil := 9.45 :
rFc1 := 9.45 : rFc2 := 0.4 : rFw1 := 9.45 : rFw2 := 0.4 :
rFself :=  $\frac{(Fc1 \cdot rFc1 + Fc2 \cdot rFc2 - Fw1 \cdot rFw1 - Fw2 \cdot rFw2)}{Fself}$  :
rFbp := -14.827 :

```

$$rp1a := 2.135 - 2.1 - GWL + 2 \cdot \frac{(GWL - OWL)}{3} :$$

$$rp1b := 2.135 - 2.1 - OWL - \frac{(2.1 + OWL)}{2} :$$

$$rsig0 := 2.135 - \frac{(GrL + 2.1)}{2} :$$

$$rsig1 := -2.1 - GWL + 2.135 - \frac{(GrL - GWL)}{3} :$$

$$rsig2a := 2.135 - \frac{(2.1 + GWL)}{2} :$$

$$rsig2b := 2.135 - \frac{(2.1 + GWL)}{3} :$$

$$\begin{aligned} > eq1 := Fbollard \cdot rFbollard + qsurcharge \cdot 18.1 \cdot rqsurcharge + \frac{Sig1 \cdot (GrL - GWL)}{2} \cdot rsig1 \\ &+ Sig1 \cdot (2.1 + GWL) \cdot rsig2a + \frac{(Sig2 - Sig1) \cdot (2.1 + GWL)}{2} \cdot rsig2b \\ &+ \frac{p1 \cdot (GWL - OWL)}{2} \cdot rp1a + p1 \cdot (2.1 + \min(GWL, OWL)) \cdot rp1b + Fself \cdot rFself + qsoil \\ &\cdot 15.9 \cdot rqsoil + Fbp \cdot rFbp + Sig0 \cdot 7.2 \cdot rsig0 = 0 : \# \text{ Sum of the moments} = 0 \end{aligned}$$

$$\begin{aligned} eq2 := -Fbollard - Sig0 \cdot (GrL + 2.1) - \frac{Sig1 \cdot (GrL - GWL)}{2} - Sig1 \cdot (2.1 + GWL) \\ - \frac{(Sig2 - Sig1) \cdot (2.1 + GWL)}{2} - \frac{p1 \cdot (GWL - OWL)}{2} - p1 \cdot (2.1 + OWL) + \frac{Fbp}{17^{0.5}} \\ - \frac{Fmv}{2^{0.5}} : \# \text{ Sum of the horizontal forces} = 0 \end{aligned}$$

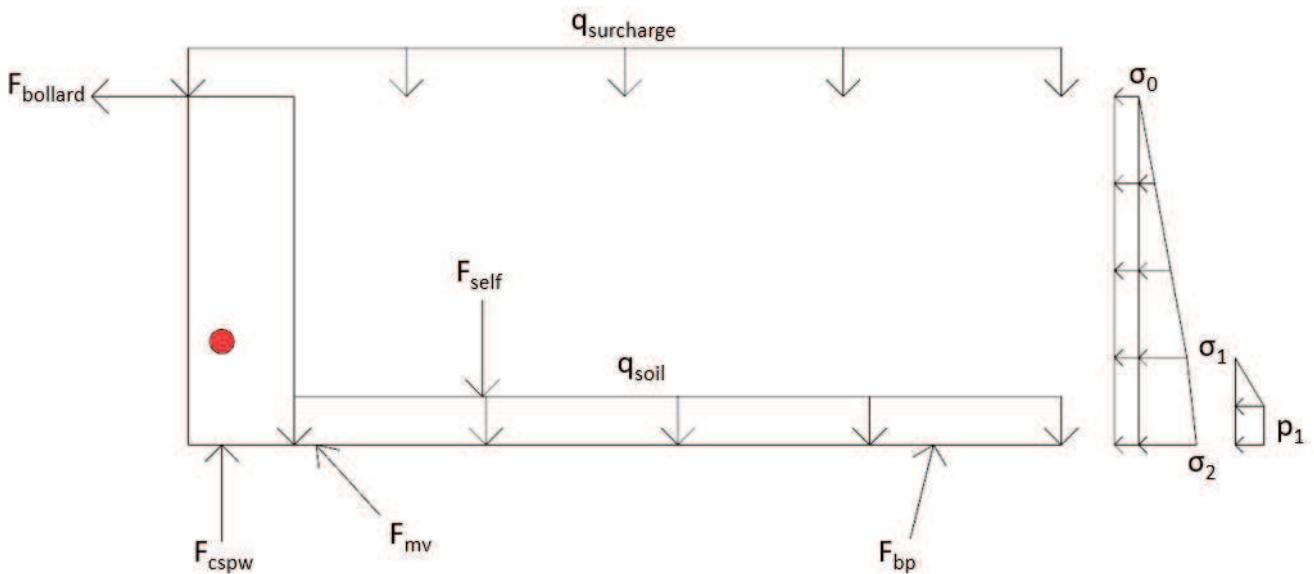
$$eq3 := qsurcharge \cdot 18.1 + Fself + qsoil \cdot 15.9 - \frac{Fbp \cdot 4}{17^{0.5}} - Fcspw - \frac{Fmv}{2^{0.5}} :$$

Sum of the vertical forces = 0

$$\begin{aligned} > solve(\{eq1, eq2, eq3\}, \{Fbp, Fmv, Fcspw\}); \\ \{Fbp = 2210.201917, Fcspw = 2211.913358, Fmv = -298.5393114\} \end{aligned}$$

(3)

> **restart; # SIF 1b & 2b**



```

> Fbp := 'Fbp': # Normal force in the bearing piles
Fcspw := 'Fcspw': # Normal force in the combined sheet pile wall
Fmv := 'Fmv': # Normal force in the M.V.-piles
Fbollard := 0 : # Bollard force
qsurchage := 0 : # Uniformly distributed surcharge
GrL := 5.1 : # Ground level
GWL := -2.1 :
    # Groundwater level (minimum value -2.1, otherwise the code would get to complicated)
OWL := -0.84 :
    # Outer water level (minimum value -2.1, otherwise the code would get to complicated)
Sig0 := 0.5 * qsurchage : # Vertical soil stress due to the surcharge
Sig1 := 0.5 * (GrL - GWL) * 19 : # Vertical soil stress at the GWL
Sig2 := Sig1 + 0.5 * (2.1 + GWL) * 10 :
    # Vertical soil stress at the bottom of the Relieving Platform floor
p1 := (GWL - OWL) * 10 : # Water pressure difference
Fc1 := 15.9 * 1.85 * 24 : # Weight of the concrete R.P.
Fc2 := 2.2 * 7.2 * 24 : # Weight of the concrete R.P.
if GWL >= -2.1 then Fw1 := min(GWL + 2.1, 1.85) * 15.9 * 10 else Fw1 := 0 end if:
    # Upwards water force of the long part of the R.P.
if GWL >= -2.1 and OWL >= -2.1 then Fw2 :=  $\left( \frac{(GWL + OWL)}{2} + 2.1 \right) \cdot 2.2 \cdot 10$  elif GWL >=
    -2.1 and OWL < -2.1 then Fw2 :=  $\frac{GWL}{2} \cdot 2.2 \cdot 10$  else Fw2 := 0 end if:
    # Upwards water force of the high part of the R.P.
Fself := Fc1 + Fc2 - Fw1 - Fw2 : # Effective self-weight of the R.P.
qsoil := min(GrL - GWL, GrL + 0.25) * 19 + max(0.25 + GWL, 0) * 10 :
    # Soil that rests on the R.P.
rFbollard := -5.065 :
rqsurcharge := 8.35 :
rqsoil := 9.45 :
rFc1 := 9.45 : rFc2 := 0.4 : rFw1 := 9.45 : rFw2 := 0.4 :
rFself :=  $\frac{(Fc1 \cdot rFc1 + Fc2 \cdot rFc2 - Fw1 \cdot rFw1 - Fw2 \cdot rFw2)}{Fself}$  :
rFbp := -14.827 :

```

$$rp1a := 2.135 - 2.1 - GWL + 2 \cdot \frac{(GWL - OWL)}{3} :$$

$$rp1b := 2.135 - 2.1 - OWL - \frac{(2.1 + OWL)}{2} :$$

$$rsig0 := 2.135 - \frac{(GrL + 2.1)}{2} :$$

$$rsig1 := -2.1 - GWL + 2.135 - \frac{(GrL - GWL)}{3} :$$

$$rsig2a := 2.135 - \frac{(2.1 + GWL)}{2} :$$

$$rsig2b := 2.135 - \frac{(2.1 + GWL)}{3} :$$

$$\begin{aligned} > eq1 := Fbollard \cdot rFbollard + qsurcharge \cdot 18.1 \cdot rqsurcharge + \frac{Sig1 \cdot (GrL - GWL)}{2} \cdot rsig1 \\ &+ Sig1 \cdot (2.1 + GWL) \cdot rsig2a + \frac{(Sig2 - Sig1) \cdot (2.1 + GWL)}{2} \cdot rsig2b \\ &+ \frac{p1 \cdot (GWL - OWL)}{2} \cdot rp1a + p1 \cdot (2.1 + \min(GWL, OWL)) \cdot rp1b + Fself \cdot rFself + qsoil \\ &\cdot 15.9 \cdot rqsoil + Fbp \cdot rFbp + Sig0 \cdot 7.2 \cdot rsig0 = 0 : \# \text{ Sum of the moments} = 0 \end{aligned}$$

$$\begin{aligned} eq2 := -Fbollard - Sig0 \cdot (GrL + 2.1) - \frac{Sig1 \cdot (GrL - GWL)}{2} - Sig1 \cdot (2.1 + GWL) \\ - \frac{(Sig2 - Sig1) \cdot (2.1 + GWL)}{2} - \frac{p1 \cdot (GWL - OWL)}{2} - p1 \cdot (2.1 + OWL) + \frac{Fbp}{17^{0.5}} \\ - \frac{Fmv}{2^{0.5}} : \# \text{ Sum of the horizontal forces} = 0 \end{aligned}$$

$$eq3 := qsurcharge \cdot 18.1 + Fself + qsoil \cdot 15.9 - \frac{Fbp \cdot 4}{17^{0.5}} - Fcspw - \frac{Fmv}{2^{0.5}} :$$

Sum of the vertical forces = 0

$$\begin{aligned} > solve(\{eq1, eq2, eq3\}, \{Fbp, Fmv, Fcspw\}); \\ &\quad \{Fbp = 1486.227076, Fcspw = 1124.481936, Fmv = 172.7617611\} \end{aligned}$$

(4)

B. Maple - Blum calculations

> restart : # Amazonehaven 1

with(LinearAlgebra) :

> t := 0.02 :

$$r := 0.720 - \frac{t}{2} :$$

$$E := 210000000 :$$

$$ctc := 1.420 + 1.560 :$$

$$> I_{yy} := \frac{\text{evalf}(\text{Pi}) \cdot r^3 \cdot t}{ctc} :$$

> h := 19.4 :

d = d' : # Embedded depth

T = T' : # Anchor force

x1 := 'x1' : # Location of the maximum field moment

x2 := 'x2' : # Centre of moments

y := 'y' : # Location of the maximum fixed end moment

R := 'R' : # Clamping force

Z := 'Z' : # Location along the combined sheet pile wall

$$\text{Mec} := \left(2288 + T \cdot \left(\frac{26}{25} \right)^{\frac{1}{2}} \right) \cdot r : \# \text{ Bending moment due to the eccentricity of the normal force}$$

$$qa := 4.90 \cdot (h + d) :$$

$$qp := 54.4 \cdot d :$$

$$qr := 13.3 :$$

Kpright := 10 : # Passive soil pressure coefficient, a maximum value of 10 has been used

Ytoe := 449 : # The effective vertical soil stress at the toe of the combined sheet pile wall

$$> u1 := \frac{T \cdot (h + d)^3}{3 \cdot E \cdot I_{yy}} : \# \text{ Displacement due to } T$$

$$u2 := \frac{qa \cdot (h + d)^4}{30 \cdot E \cdot I_{yy}} : \# \text{ Displacement due to } qa$$

$$u3 := \frac{qp \cdot d^4}{30 \cdot E \cdot I_{yy}} + \frac{qp \cdot d^3}{24 \cdot E \cdot I_{yy}} \cdot h : \# \text{ Displacement due to } qp$$

$$u4 := \frac{qr \cdot (h + d)^4}{8 \cdot E \cdot I_{yy}} : \# \text{ Displacement due to } qr$$

$$> eq1 := u1 + u3 - u2 - u4 = 0 : \# \text{ No displacement at the top}$$

$$eq2 := T \cdot (h + d) + \frac{qp \cdot d^2}{6} - \frac{qa \cdot (h + d)^2}{6} - \frac{qr \cdot (h + d)^2}{2} = 0 :$$

Bending moment at the toe equals to zero

$$eq3 := T + \frac{qp \cdot d}{2} - qr \cdot (h + d) - \frac{qa \cdot (h + d)}{2} - R = 0 : \# \text{ Sum horizontal forces equal to zero}$$

$$eq4 := T - x1 \cdot qr - \frac{qa \cdot x1^2}{2 \cdot (h + d)} = 0 : \# \text{ Location of } x1$$

$$eq5 := T + \frac{qp}{d} \cdot \frac{y^2}{2} - qr \cdot (h + y) - \frac{qa}{(h + d)} \cdot \frac{(h + y)^2}{2} = 0 : \# \text{ Location of } y$$

$$eq6 := T \cdot x2 + \frac{qp}{d} \cdot \frac{(x2 - h)^3}{6} - \frac{qr \cdot x2^2}{2} - \frac{qa}{h + d} \cdot \frac{x2^3}{6} = 0 : \# \text{ Location of } x2$$

$$eq7 := x2 > h : \# \text{ Equation to limit the solutions}$$

eq8 := x2 - h < y : # Equation to limit the solutions

eq9 := x1 > 0 : # Equation to limit the solutions

eq10 := y > 0 : # Equation to limit the solutions

> S := solve({eq1, eq2, eq3, eq4, eq5, eq6, eq7, eq8, eq9, eq10}, {T, d, R, x1, y, x2}) :

> T := subs(S, T);

R := subs(S, R);

d := subs(S, d);

x1 := subs(S, x1);

y := subs(S, y);

x2 := subs(S, x2);

Mfield := evalf((T·x1 - $\frac{qr \cdot x1^2}{2}$ - $\frac{qa}{(h+d)} \cdot \frac{x1^3}{6}$ - $(1 - \frac{x1}{x2}) \cdot Mec$) · 0.75);

Mfixed := evalf((T·(h+y) + $\frac{qp}{d} \cdot \frac{y^3}{6}$ - $\frac{qr \cdot (h+y)^2}{2}$ - $\frac{qa}{h+d} \cdot \frac{(h+y)^3}{6}$ + $\frac{Mec}{2}$) · 0.9);

w := max($\frac{R}{Kp\text{right} \cdot Y\text{toe}}$, $\frac{d}{10}$);

T := 507.6964974

R := 1660.789048

d := 12.14211085

x1 := 11.93461892

y := 7.842410120

x2 := 21.25834244

Mfield := 2137.501004

Mfixed := -2021.857627

w := 1.214211085

(1)

> Mz := Z → if Z ≥ 0 and Z ≤ h then T·Z - $\frac{qr \cdot Z^2}{2}$ - $\frac{qa}{(h+d)} \cdot \frac{Z^3}{6}$ - $(1 - \frac{Z}{x2}) \cdot Mec$ elif Z

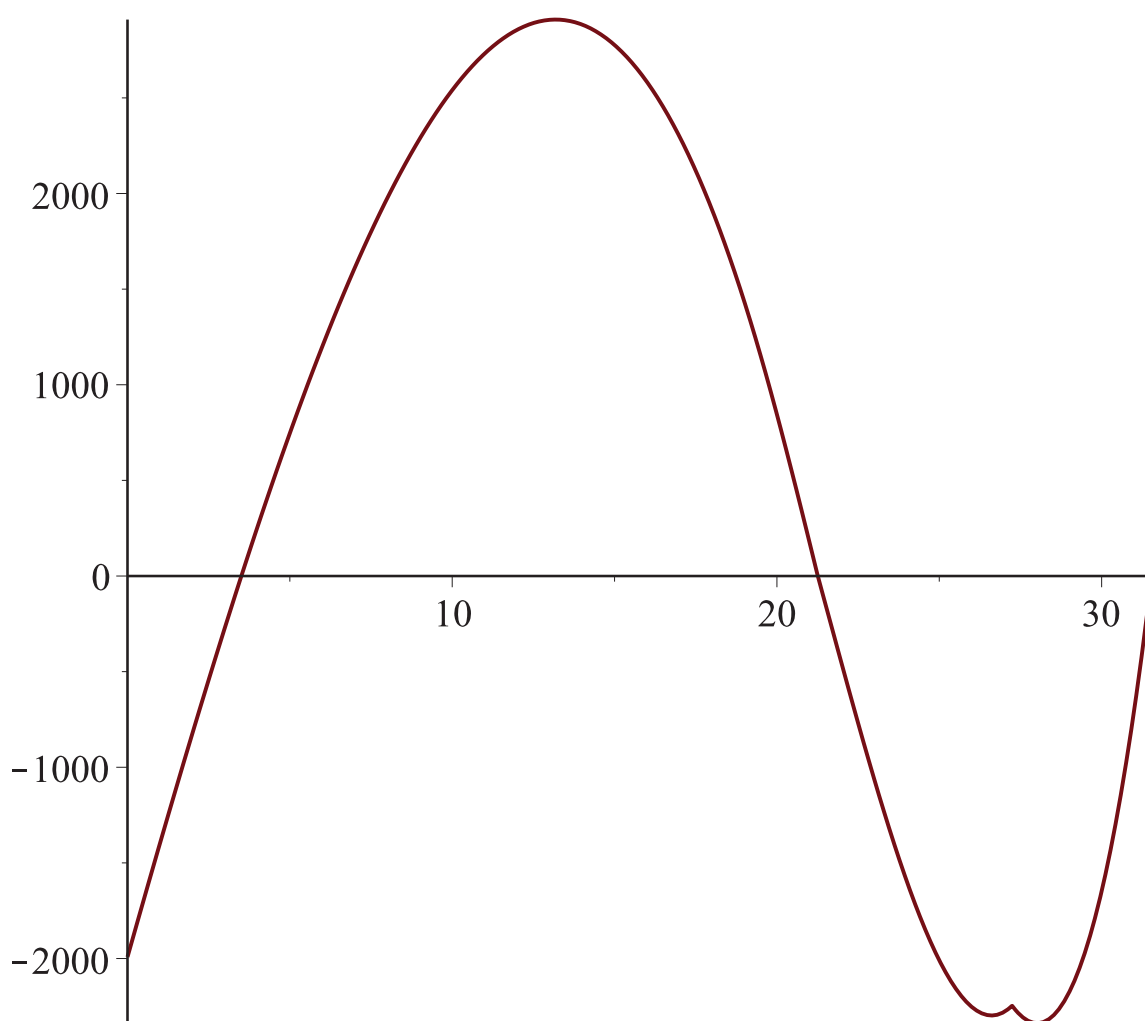
> h and Z ≤ x2 then T·Z + $\frac{qp}{d} \cdot \frac{(Z-h)^3}{6}$ - $\frac{qr \cdot Z^2}{2}$ - $\frac{qa}{h+d} \cdot \frac{Z^3}{6}$ - $(1 - \frac{Z}{x2}) \cdot Mec$ elif Z

> x2 and Z ≤ h + y then T·Z + $\frac{qp}{d} \cdot \frac{(Z-h)^3}{6}$ - $\frac{qr \cdot Z^2}{2}$ - $\frac{qa}{h+d} \cdot \frac{Z^3}{6}$ + $\frac{Mec}{2}$

· $\frac{(Z-x2)}{h+y-x2}$ else T·Z + $\frac{qp}{d} \cdot \frac{(Z-h)^3}{6}$ - $\frac{qr \cdot Z^2}{2}$ - $\frac{qa}{h+d} \cdot \frac{Z^3}{6}$ + $\frac{Mec}{2} \cdot (1 - \frac{Z-h-y}{d-y})$

end if;

> plot(Mz, 0 .. (h + d))



> # The graph illustrates the shape of the bending moment distribution, the field and fixed moments have to be multiplied by 0.75 and 0.9 respectively

> $T := 1.15 \cdot T;$

$T := 583.8509720$

(2)

> **restart** : # *Amazonhaven 2*

with(*LinearAlgebra*) :

> $t := 0.02 :$

$r := 0.720 - \frac{t}{2} :$

$E := 210000000 :$

$ctc := 1.420 + 1.560 :$

> $I_{yy} := \frac{\text{evalf}(\text{Pi}) \cdot r^3 \cdot t}{ctc} :$

> $h := 19.4 :$

$d = d'$: # *Embedded depth*

$T = T'$: # *Anchor force*

$x1 = x1'$: # *Location of the maximum field moment*

$x2 = x2'$: # *Centre of moments*

$y = y'$: # *Location of the maximum fixed end moment*

$R := 'R'$: # Clamping force

$Z := 'Z'$: # Location along the combined sheet pile wall

$$Mec := \left(2288 + T \cdot \left(\frac{26}{25} \right)^{\frac{1}{2}} \right) \cdot r : \# \text{ Bending moment due to the eccentricity of the normal force}$$

$$qa := 4.30 \cdot (h + d) :$$

$$qp := 54.4 \cdot d :$$

$$qr := 13.3 :$$

$Kpright := 10$: # Passive soil pressure coefficient, a maximum value of 10 has been used

$$Ytoe := (h + d + 11.1) \cdot 10 :$$

The An estimate of the vertical soil stress at the toe of the combined sheet pile wall

$$\text{> } u1 := \frac{T \cdot (h + d)^3}{3 \cdot E \cdot Iyy} : \# \text{ Displacement due to } T$$

$$u2 := \frac{qa \cdot (h + d)^4}{30 \cdot E \cdot Iyy} : \# \text{ Displacement due to } qa$$

$$u3 := \frac{qp \cdot d^4}{30 \cdot E \cdot Iyy} + \frac{qp \cdot d^3}{24 \cdot E \cdot Iyy} \cdot h : \# \text{ Displacement due to } qp$$

$$u4 := \frac{qr \cdot (h + d)^4}{8 \cdot E \cdot Iyy} : \# \text{ Displacement due to } qr$$

$$\text{> } eq1 := u1 + u3 - u2 - u4 = 0 : \# \text{ No displacement at the top}$$

$$eq2 := T \cdot (h + d) + \frac{qp \cdot d^2}{6} - \frac{qa \cdot (h + d)^2}{6} - \frac{qr \cdot (h + d)^2}{2} = 0 :$$

Bending moment at the toe equals to zero

$$eq3 := T + \frac{qp \cdot d}{2} - qr \cdot (h + d) - \frac{qa \cdot (h + d)}{2} - R = 0 : \# \text{ Sum horizontal forces equal to zero}$$

$$eq4 := T - x1 \cdot qr - \frac{qa \cdot x1^2}{2 \cdot (h + d)} = 0 : \# \text{ Location of } x1$$

$$eq5 := T + \frac{qp}{d} \cdot \frac{y^2}{2} - qr \cdot (h + y) - \frac{qa}{(h + d)} \cdot \frac{(h + y)^2}{2} = 0 : \# \text{ Location of } y$$

$$eq6 := T \cdot x2 + \frac{qp}{d} \cdot \frac{(x2 - h)^3}{6} - \frac{qr \cdot x2^2}{2} - \frac{qa}{h + d} \cdot \frac{x2^3}{6} = 0 : \# \text{ Location of } x2$$

$$eq7 := x2 > h : \# \text{ Equation to limit the solutions}$$

$$eq8 := x2 - h < y : \# \text{ Equation to limit the solutions}$$

$$eq9 := x1 > 0 : \# \text{ Equation to limit the solutions}$$

$$eq10 := y > 0 : \# \text{ Equation to limit the solutions}$$

$$\text{> } S := \text{solve}(\{eq1, eq2, eq3, eq4, eq5, eq6, eq7, eq8, eq9, eq10\}, \{T, d, R, x1, y, x2\}) :$$

$$\text{> } T := \text{subs}(S, T);$$

$$R := \text{subs}(S, R);$$

$$d := \text{subs}(S, d);$$

$$x1 := \text{subs}(S, x1);$$

$$y := \text{subs}(S, y);$$

$$x2 := \text{subs}(S, x2);$$

$$Mfield := \text{evalf}\left(\left(T \cdot x1 - \frac{qr \cdot x1^2}{2} - \frac{qa}{(h + d)} \cdot \frac{x1^3}{6} - \left(1 - \frac{x1}{x2}\right) \cdot Mec\right) \cdot 0.75\right);$$

$$Mfixed := \text{evalf}\left(\left(T \cdot (h + y) + \frac{qp}{d} \cdot \frac{y^3}{6} - \frac{qr \cdot (h + y)^2}{2} - \frac{qa}{h + d} \cdot \frac{(h + y)^3}{6} + \frac{Mec}{2}\right) \cdot 0.9\right);$$

$$w := \max\left(\frac{R}{K_{pright} \cdot Y_{toe}}, \frac{d}{10}\right);$$

$T := 449.4257628$

$R := 1526.800991$

$d := 11.38244490$

$x1 := 11.69217310$

$y := 7.258614297$

$x2 := 20.86618970$

$M_{field} := 1757.140537$

$M_{fixed} := -1692.357059$

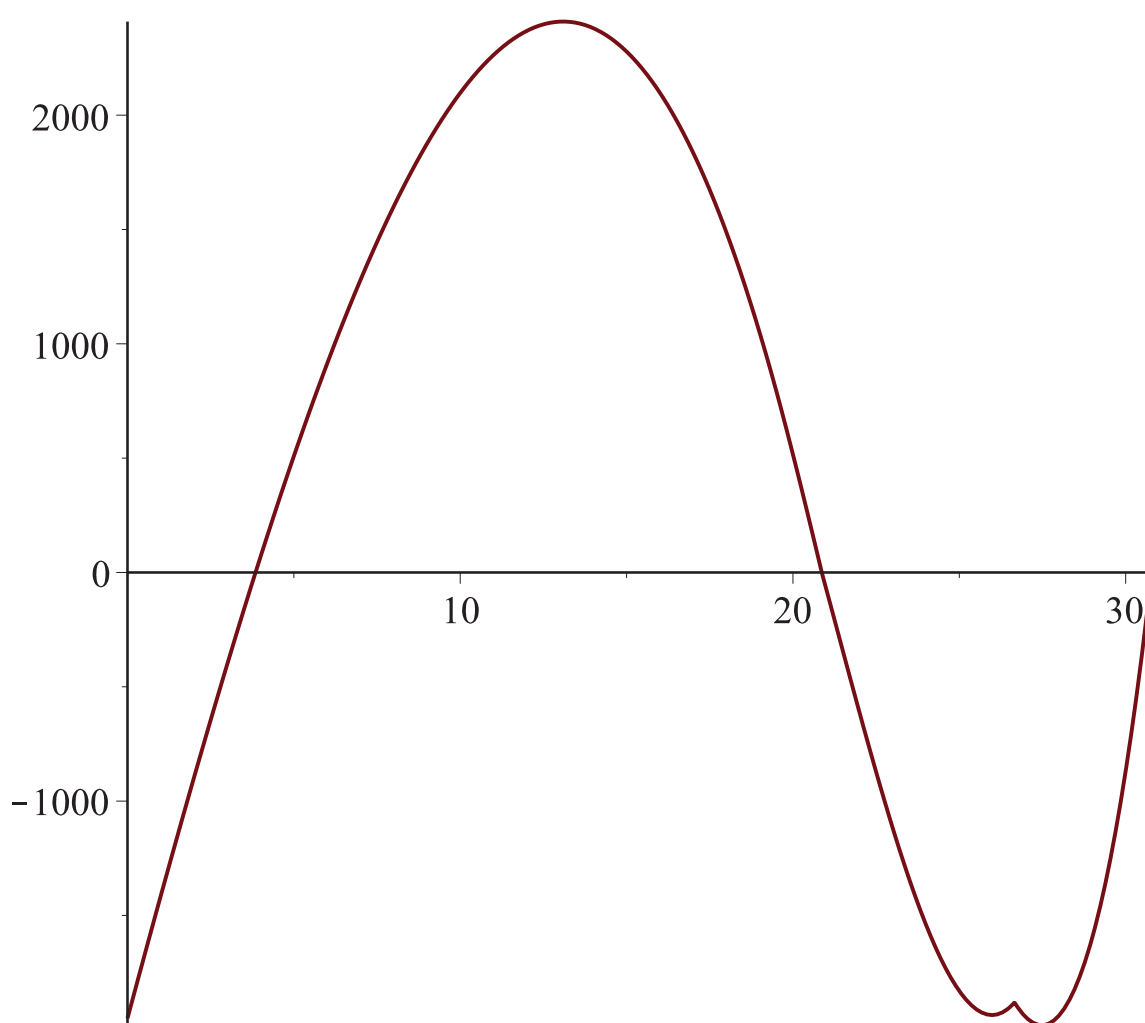
$w := 1.138244490$

(3)

```

> Mz := Z → if Z ≥ 0 and Z ≤ h then T·Z -  $\frac{qr \cdot Z^2}{2} - \frac{qa}{(h+d)} \cdot \frac{Z^3}{6} - \left(1 - \frac{Z}{x2}\right) \cdot Mec$  elif Z
  > h and Z ≤ x2 then T·Z +  $\frac{qp}{d} \cdot \frac{(Z-h)^3}{6} - \frac{qr \cdot Z^2}{2} - \frac{qa}{h+d} \cdot \frac{Z^3}{6} - \left(1 - \frac{Z}{x2}\right) \cdot Mec$  elif Z
  > x2 and Z ≤ h + y then T·Z +  $\frac{qp}{d} \cdot \frac{(Z-h)^3}{6} - \frac{qr \cdot Z^2}{2} - \frac{qa}{h+d} \cdot \frac{Z^3}{6} + \frac{Mec}{2}$ 
  ·  $\frac{(Z-x2)}{h+y-x2}$  else T·Z +  $\frac{qp}{d} \cdot \frac{(Z-h)^3}{6} - \frac{qr \cdot Z^2}{2} - \frac{qa}{h+d} \cdot \frac{Z^3}{6} + \frac{Mec}{2} \cdot \left(1 - \frac{Z-h-y}{d-y}\right)$ 
end if;
> plot(Mz, 0..(h+d))

```



> # The graph illustrates the shape of the bending moment distribution, the field and fixed moments have to be multiplied by 0.75 and 0.9 respectively

> $T := 1.15 \cdot T;$

$T := 516.8396272$

(4)

> **restart : # SIF 1a**

with(LinearAlgebra) :

> $t := 0.02 :$

$r := 0.710 - \frac{t}{2} :$

$E := 210000000 :$

$ctc := 3.294 :$

> $I_{yy} := \frac{\text{evalf}(\text{Pi}) \cdot r^3 \cdot t}{ctc} :$

> $h := 19.3 :$

$d = d'$: # Embedded depth

$T = T'$: # Anchor force

$x1 = x1'$: # Location of the maximum field moment

$x2 = x2'$: # Centre of moments

$y = y'$: # Location of the maximum fixed end moment

$R := 'R'$: # Clamping force
 $Z := 'Z'$: # Location along the combined sheet pile wall
 $Mec := (2200 + T) \cdot r$: # Bending moment due to the eccentricity of the normal force
 $qa := 4.24 \cdot (h + d)$:
 $qp := 88.9 \cdot d$:
 $qr := 15.5$:
 $Kpright := 8.89$: # Passive soil pressure coefficient
 $Ytoe := (h + d + 7.2) \cdot 10$:
 # An estimate of the vertical soil stress at the toe of the combined sheet pile wall

$> u1 := \frac{T \cdot (h + d)^3}{3 \cdot E \cdot Iyy}$: # Displacement due to T
 $u2 := \frac{qa \cdot (h + d)^4}{30 \cdot E \cdot Iyy}$: # Displacement due to qa
 $u3 := \frac{qp \cdot d^4}{30 \cdot E \cdot Iyy} + \frac{qp \cdot d^3}{24 \cdot E \cdot Iyy} \cdot h$: # Displacement due to qp
 $u4 := \frac{qr \cdot (h + d)^4}{8 \cdot E \cdot Iyy}$: # Displacement due to qr
 $> eq1 := u1 + u3 - u2 - u4 = 0$: # No displacement at the top
 $eq2 := T \cdot (h + d) + \frac{qp \cdot d^2}{6} - \frac{qa \cdot (h + d)^2}{6} - \frac{qr \cdot (h + d)^2}{2} = 0$:
 # Bending moment at the toe equals to zero
 $eq3 := T + \frac{qp \cdot d}{2} - qr \cdot (h + d) - \frac{qa \cdot (h + d)}{2} - R = 0$: # Sum horizontal forces equal to zero
 $eq4 := T - x1 \cdot qr - \frac{qa \cdot x1^2}{2 \cdot (h + d)} = 0$: # Location of x1
 $eq5 := T + \frac{qp}{d} \cdot \frac{y^2}{2} - qr \cdot (h + y) - \frac{qa}{(h + d)} \cdot \frac{(h + y)^2}{2} = 0$: # Location of y
 $eq6 := T \cdot x2 + \frac{qp}{d} \cdot \frac{(x2 - h)^3}{6} - \frac{qr \cdot x2^2}{2} - \frac{qa}{h + d} \cdot \frac{x2^3}{6} = 0$: # Location of x2
 $eq7 := x2 > h$: # Equation to limit the solutions
 $eq8 := x2 - h < y$: # Equation to limit the solutions
 $eq9 := x1 > 0$: # Equation to limit the solutions
 $eq10 := y > 0$: # Equation to limit the solutions
 $> S := solve(\{eq1, eq2, eq3, eq4, eq5, eq6, eq7, eq8, eq9, eq10\}, \{T, d, R, x1, y, x2\})$:
 $> T := subs(S, T)$;
 $R := subs(S, R)$;
 $d := subs(S, d)$;
 $x1 := subs(S, x1)$;
 $y := subs(S, y)$;
 $x2 := subs(S, x2)$;
 $Mfield := evalf\left(\left(T \cdot x1 - \frac{qr \cdot x1^2}{2} - \frac{qa}{(h + d)} \cdot \frac{x1^3}{6} - \left(1 - \frac{x1}{x2}\right) \cdot Mec\right) \cdot 0.75\right)$;
 $Mfixed := evalf\left(\left(T \cdot (h + y) + \frac{qp}{d} \cdot \frac{y^3}{6} - \frac{qr \cdot (h + y)^2}{2} - \frac{qa}{h + d} \cdot \frac{(h + y)^3}{6} + \frac{Mec}{2}\right) \cdot 0.9\right)$;
 $w := \max\left(\frac{R}{Kpright \cdot Ytoe}, \frac{d}{5}\right)$;

$T := 419.0201931$

```

R := 1724.733008
d := 8.758241778
x1 := 10.87069110
y := 5.290364968
x2 := 19.47703317
Mfield := 1440.994756
Mfixed := -1601.723724
w := 1.751648356

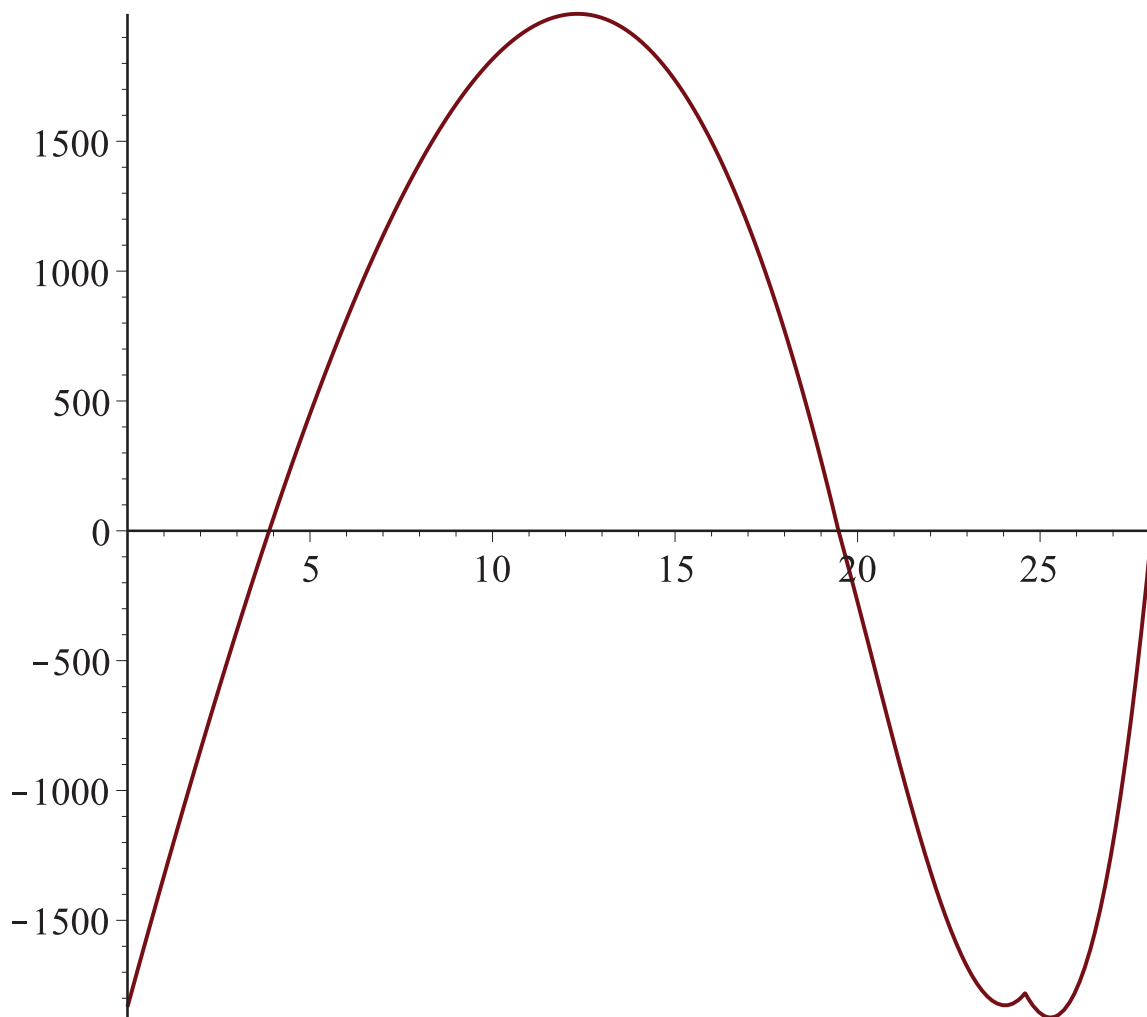
```

(5)

```

> Mz := Z → if Z ≥ 0 and Z ≤ h then T·Z -  $\frac{qr \cdot Z^2}{2} - \frac{qa}{(h+d)} \cdot \frac{Z^3}{6} - \left(1 - \frac{Z}{x2}\right) \cdot Mec$  elif Z
  > h and Z ≤ x2 then T·Z +  $\frac{qp}{d} \cdot \frac{(Z-h)^3}{6} - \frac{qr \cdot Z^2}{2} - \frac{qa}{h+d} \cdot \frac{Z^3}{6} - \left(1 - \frac{Z}{x2}\right) \cdot Mec$  elif Z
  > x2 and Z ≤ h + y then T·Z +  $\frac{qp}{d} \cdot \frac{(Z-h)^3}{6} - \frac{qr \cdot Z^2}{2} - \frac{qa}{h+d} \cdot \frac{Z^3}{6} + \frac{Mec}{2}$ 
  ·  $\frac{(Z-x2)}{h+y-x2}$  else T·Z +  $\frac{qp}{d} \cdot \frac{(Z-h)^3}{6} - \frac{qr \cdot Z^2}{2} - \frac{qa}{h+d} \cdot \frac{Z^3}{6} + \frac{Mec}{2} \cdot \left(1 - \frac{Z-h-y}{d-y}\right)$ 
end if:
> plot(Mz, 0..(h+d))

```



> # The graph illustrates the shape of the bending moment distribution, the field and fixed moments have to be multiplied by 0.75 and 0.9 respectively

> $T := 1.15 \cdot T;$

$T := 481.8732221$

(6)

> **restart : # SIF 1b**

with(LinearAlgebra) :

> $t := 0.02 :$

$r := 0.710 - \frac{t}{2} :$

$E := 210000000 :$

$ctc := 3.294 :$

> $I_{yy} := \frac{\text{evalf}(\text{Pi}) \cdot r^3 \cdot t}{ctc} :$

> $h := 20.9 :$

$d = d'$: # Embedded depth

$T = T'$: # Anchor force

$R = R'$: # Clamping force

$Z = Z'$: # Location along the combined sheet pile wall

$Mec := (1100 + T) \cdot r$: # Bending moment due to the eccentricity of the normal force

$qa := 4.17 \cdot (h + d) :$

$qp := 88.9 \cdot d :$

$qr := -51.6 :$

> $u1 := \frac{T \cdot (h + d)^3}{3 \cdot E \cdot I_{yy}}$: # Displacement due to T

$u2 := \frac{qa \cdot (h + d)^4}{30 \cdot E \cdot I_{yy}}$: # Displacement due to qa

$u3 := \frac{qp \cdot d^4}{30 \cdot E \cdot I_{yy}} + \frac{qp \cdot d^3}{24 \cdot E \cdot I_{yy}} \cdot h$: # Displacement due to qp

$u4 := \frac{qr \cdot (h + d)^4}{8 \cdot E \cdot I_{yy}}$: # Displacement due to qr

> $eq1 := u1 + u3 - u2 - u4 = 0$: # No displacement at the top

$eq2 := T \cdot (h + d) + \frac{qp \cdot d^2}{6} - \frac{qa \cdot (h + d)^2}{6} - \frac{qr \cdot (h + d)^2}{2} = 0 :$

Bending moment at the toe equals to zero

$eq3 := T + \frac{qp \cdot d}{2} - qr \cdot (h + d) - \frac{qa \cdot (h + d)}{2} - R = 0$: # Sum horizontal forces equal to zero

> $S = \text{fsolve}(\{eq1, eq2, eq3\}, \{T, d, R\});$

$S = \{R = 453.2246210, T = -215.6531195, d = -3.045403192\}$

(7)

> $F_{mv} := -215.6531195 - 172.7617611;$

$F_{mv} := -388.4148806$

(8)

> **restart : # SIF 2a**

with(LinearAlgebra) :

> $t := 0.02 :$

$r := 0.710 - \frac{t}{2} :$

$E := 210000000 :$

$ctc := 3.294 :$

> $I_{yy} := \frac{\text{evalf}(\text{Pi}) \cdot r^3 \cdot t}{ctc} :$

> $h := 19.3 :$

$d = d' :$ # Embedded depth

$T = T' :$ # Anchor force

$x1 := x1' :$ # Location of the maximum field moment

$x2 := x2' :$ # Centre of moments

$y := y' :$ # Location of the maximum fixed end moment

$R := R' :$ # Clamping force

$Z := Z' :$ # Location along the combined sheet pile wall

$Mec := (2200 + T) \cdot r :$ # Bending moment due to the eccentricity of the normal force

$qa := 4.58 \cdot (h + d) :$

$qp := 88.9 \cdot d :$

$qr := 15.5 :$

$K_{pright} := 8.89 :$ # Passive soil pressure coefficient

$Y_{toe} := (h + d + 7.2) \cdot 10 :$

An estimate of the vertical soil stress at the toe of the combined sheet pile wall

> $u1 := \frac{T \cdot (h + d)^3}{3 \cdot E \cdot I_{yy}} :$ # Displacement due to T

$u2 := \frac{qa \cdot (h + d)^4}{30 \cdot E \cdot I_{yy}} :$ # Displacement due to qa

$u3 := \frac{qp \cdot d^4}{30 \cdot E \cdot I_{yy}} + \frac{qp \cdot d^3}{24 \cdot E \cdot I_{yy}} \cdot h :$ # Displacement due to qp

$u4 := \frac{qr \cdot (h + d)^4}{8 \cdot E \cdot I_{yy}} :$ # Displacement due to qr

> $eq1 := u1 + u3 - u2 - u4 = 0 :$ # No displacement at the top

$eq2 := T \cdot (h + d) + \frac{qp \cdot d^2}{6} - \frac{qa \cdot (h + d)^2}{6} - \frac{qr \cdot (h + d)^2}{2} = 0 :$

Bending moment at the toe equals to zero

$eq3 := T + \frac{qp \cdot d}{2} - qr \cdot (h + d) - \frac{qa \cdot (h + d)}{2} - R = 0 :$ # Sum horizontal forces equal to zero

$eq4 := T - x1 \cdot qr - \frac{qa \cdot x1^2}{2 \cdot (h + d)} = 0 :$ # Location of x1

$eq5 := T + \frac{qp}{d} \cdot \frac{y^2}{2} - qr \cdot (h + y) - \frac{qa}{(h + d)} \cdot \frac{(h + y)^2}{2} = 0 :$ # Location of y

$eq6 := T \cdot x2 + \frac{qp}{d} \cdot \frac{(x2 - h)^3}{6} - \frac{qr \cdot x2^2}{2} - \frac{qa}{h + d} \cdot \frac{x2^3}{6} = 0 :$ # Location of x2

$eq7 := x2 > h :$ # Equation to limit the solutions

$eq8 := x2 - h < y :$ # Equation to limit the solutions

$eq9 := x1 > 0 :$ # Equation to limit the solutions

$eq10 := y > 0 :$ # Equation to limit the solutions

> $S := \text{solve}(\{eq1, eq2, eq3, eq4, eq5, eq6, eq7, eq8, eq9, eq10\}, \{T, d, R, x1, y, x2\}) :$

> $T := \text{subs}(S, T) ;$

$R := \text{subs}(S, R) ;$

$d := \text{subs}(S, d) ;$

$x1 := \text{subs}(S, x1) ;$

```

y := subs(S, y);
x2 := subs(S, x2);
Mfield := evalf( ( T*x1 -  $\frac{qr \cdot x1^2}{2}$  -  $\frac{qa}{(h+d)} \cdot \frac{x1^3}{6}$  -  $(1 - \frac{x1}{x2}) \cdot Mec$  ) * 0.75 );
Mfixed := evalf( ( T*(h+y) +  $\frac{qp}{d} \cdot \frac{y^3}{6}$  -  $\frac{qr \cdot (h+y)^2}{2}$  -  $\frac{qa}{h+d} \cdot \frac{(h+y)^3}{6}$  +  $\frac{Mec}{2}$  ) * 0.9 );
w := max(  $\frac{R}{Kpight \cdot Ytoe}$ ,  $\frac{d}{5}$  );

```

T := 446.0637180

R := 1804.316878

d := 9.046413873

x1 := 10.97681370

y := 5.506012954

x2 := 19.62513899

Mfield := 1602.549308

Mfixed := -1760.452472

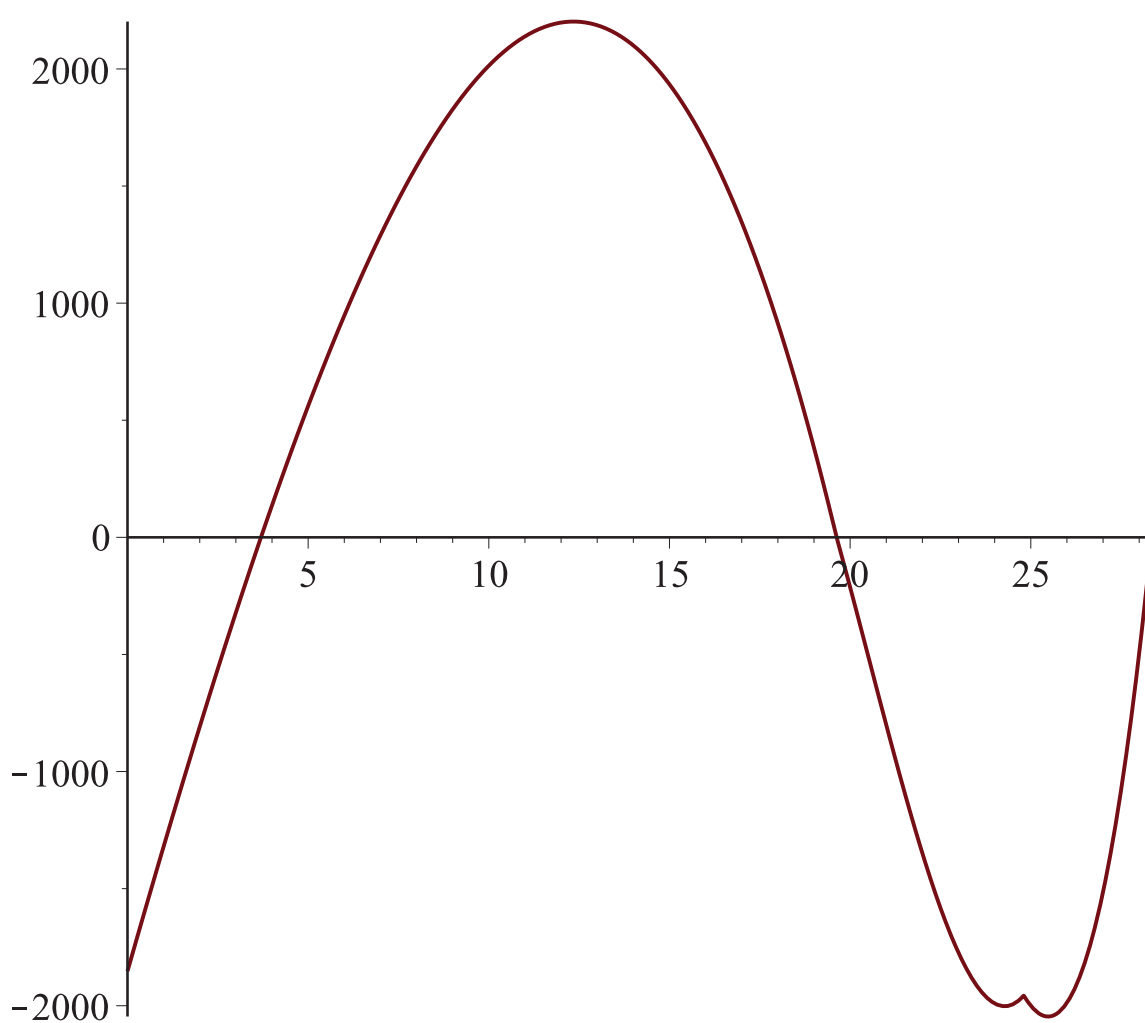
w := 1.809282775

(9)

```

> Mz := Z → if Z ≥ 0 and Z ≤ h then T·Z -  $\frac{qr \cdot Z^2}{2}$  -  $\frac{qa}{(h+d)} \cdot \frac{Z^3}{6}$  -  $(1 - \frac{Z}{x2}) \cdot Mec$  elif Z
  > h and Z ≤ x2 then T·Z +  $\frac{qp}{d} \cdot \frac{(Z-h)^3}{6}$  -  $\frac{qr \cdot Z^2}{2}$  -  $\frac{qa}{h+d} \cdot \frac{Z^3}{6}$  -  $(1 - \frac{Z}{x2}) \cdot Mec$  elif Z
  > x2 and Z ≤ h + y then T·Z +  $\frac{qp}{d} \cdot \frac{(Z-h)^3}{6}$  -  $\frac{qr \cdot Z^2}{2}$  -  $\frac{qa}{h+d} \cdot \frac{Z^3}{6}$  +  $\frac{Mec}{2}$ 
  ·  $\frac{(Z-x2)}{h+y-x2}$  else T·Z +  $\frac{qp}{d} \cdot \frac{(Z-h)^3}{6}$  -  $\frac{qr \cdot Z^2}{2}$  -  $\frac{qa}{h+d} \cdot \frac{Z^3}{6}$  +  $\frac{Mec}{2} \cdot (1 - \frac{Z-h-y}{d-y})$ 
end if;
> plot(Mz, 0 .. (h + d))

```



> # The graph illustrates the shape of the bending moment distribution, the field and fixed moments have to be multiplied by 0.75 and 0.9 respectively

> $T := 1.15 \cdot T;$

$T := 512.9732757$

(10)

> **restart : # SIF 2b**

with(LinearAlgebra) :

> $t := 0.02 :$

$r := 0.710 - \frac{t}{2} :$

$E := 210000000 :$

$ctc := 3.294 :$

> $I_{yy} := \frac{\text{evalf}(\text{Pi}) \cdot r^3 \cdot t}{ctc} :$

> $h := 28.9 :$

$d = d'$: # Embedded depth

$T = T'$: # Anchor force

$x1 = x1'$: # Location of the maximum field moment

$x2 = x2'$: # Centre of moments

$y = y'$: # Location of the maximum fixed end moment

$R := 'R'$: # Clamping force
 $Z := 'Z'$: # Location along the combined sheet pile wall
 $Mec := (2200 + T) \cdot r$: # Bending moment due to the eccentricity of the normal force
 $qa := 4.40 \cdot (h + d)$:
 $qp := 88.9 \cdot d$:
 $qr := -51.6$:
 $Kpright := 8.89$: # Passive soil pressure coefficient
 $Ytoe := (h + d + 7.2) \cdot 10$:
 # An estimate of the vertical soil stress at the toe of the combined sheet pile wall

> $u1 := \frac{T \cdot (h + d)^3}{3 \cdot E \cdot Iyy}$: # Displacement due to T

$u2 := \frac{qa \cdot (h + d)^4}{30 \cdot E \cdot Iyy}$: # Displacement due to qa

$u3 := \frac{qp \cdot d^4}{30 \cdot E \cdot Iyy} + \frac{qp \cdot d^3}{24 \cdot E \cdot Iyy} \cdot h$: # Displacement due to qp

$u4 := \frac{qr \cdot (h + d)^4}{8 \cdot E \cdot Iyy}$: # Displacement due to qr

> $eq1 := u1 + u3 - u2 - u4 = 0$: # No displacement at the top

$eq2 := T \cdot (h + d) + \frac{qp \cdot d^2}{6} - \frac{qa \cdot (h + d)^2}{6} - \frac{qr \cdot (h + d)^2}{2} = 0$:

Bending moment at the toe equals to zero

$eq3 := T + \frac{qp \cdot d}{2} - qr \cdot (h + d) - \frac{qa \cdot (h + d)}{2} - R = 0$: # Sum horizontal forces equal to zero

$eq4 := T - x1 \cdot qr - \frac{qa \cdot x1^2}{2 \cdot (h + d)} = 0$: # Location of x1

$eq5 := T + \frac{qp}{d} \cdot \frac{y^2}{2} - qr \cdot (h + y) - \frac{qa}{(h + d)} \cdot \frac{(h + y)^2}{2} = 0$: # Location of y

$eq6 := T \cdot x2 - \frac{qr \cdot x2^2}{2} - \frac{qa}{h + d} \cdot \frac{x2^3}{6} = 0$: # Location of x2

$eq7 := x2 > 15$: # Equation to limit the solutions

$eq8 := x2 - h < y$: # Equation to limit the solutions

$eq9 := x1 > 5$: # Equation to limit the solutions

$eq10 := y > 0$: # Equation to limit the solutions

> $S := solve(\{eq1, eq2, eq3, eq4, eq5, eq6, eq7, eq8, eq9, eq10\}, \{T, d, R, x1, y, x2\})$:

> $T := subs(S, T)$;

$R := subs(S, R)$;

$d := subs(S, d)$;

$x1 := subs(S, x1)$;

$y := subs(S, y)$;

$x2 := subs(S, x2)$;

$Mfield := evalf\left(\left(T \cdot x1 - \frac{qr \cdot x1^2}{2} - \frac{qa}{(h + d)} \cdot \frac{x1^3}{6} - \left(1 - \frac{x1}{x2}\right) \cdot Mec\right) \cdot 0.75\right)$;

$Mfixed := evalf\left(\left(T \cdot (h + y) + \frac{qp}{d} \cdot \frac{y^3}{6} - \frac{qr \cdot (h + y)^2}{2} - \frac{qa}{h + d} \cdot \frac{(h + y)^3}{6} + \frac{Mec}{2}\right) \cdot 0.9\right)$;

$w := \max\left(\frac{R}{Kpright \cdot Ytoe}, \frac{d}{5}\right)$;

$T := -146.7382557$

```

R := 1430.015223
d := 7.699626098
x1 := 20.14331209
y := 4.425106749
x2 := 28.04760366
Mfield := 835.4216179
Mfixed := -1237.882481
w := 1.539925220

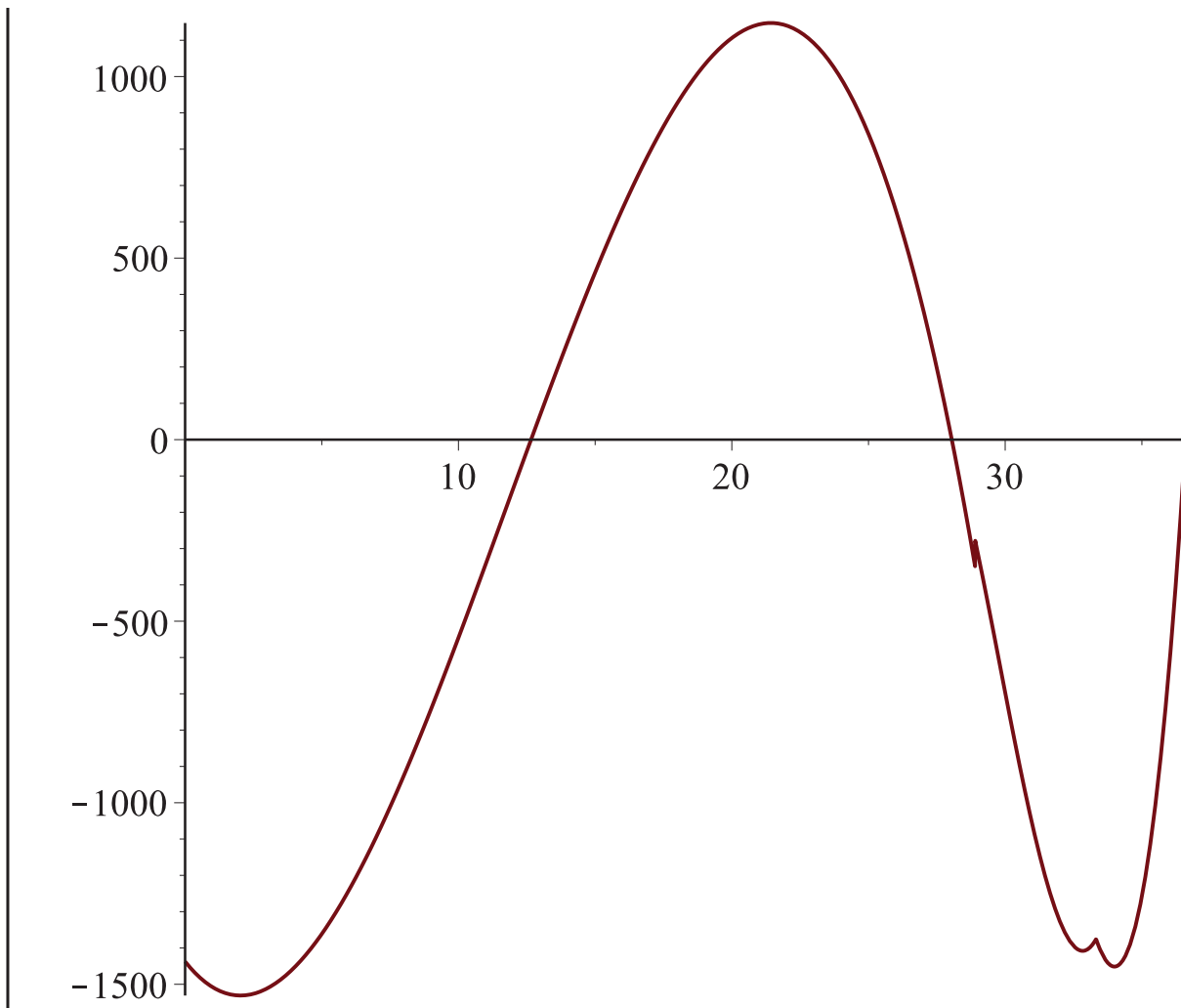
```

(11)

```

> Mz := Z → if Z ≥ 0 and Z ≤ h then T·Z -  $\frac{qr \cdot Z^2}{2} - \frac{qa}{(h+d)} \cdot \frac{Z^3}{6} - \left(1 - \frac{Z}{x2}\right) \cdot Mec$  elif Z
  > h and Z ≤ x2 then T·Z +  $\frac{qp}{d} \cdot \frac{(Z-h)^3}{6} - \frac{qr \cdot Z^2}{2} - \frac{qa}{h+d} \cdot \frac{Z^3}{6} - \left(1 - \frac{Z}{x2}\right) \cdot Mec$  elif Z
  > x2 and Z ≤ h + y then T·Z +  $\frac{qp}{d} \cdot \frac{(Z-h)^3}{6} - \frac{qr \cdot Z^2}{2} - \frac{qa}{h+d} \cdot \frac{Z^3}{6} + \frac{Mec}{2}$ 
  ·  $\frac{(Z-x2)}{h+y-x2}$  else T·Z +  $\frac{qp}{d} \cdot \frac{(Z-h)^3}{6} - \frac{qr \cdot Z^2}{2} - \frac{qa}{h+d} \cdot \frac{Z^3}{6} + \frac{Mec}{2} \cdot \left(1 - \frac{Z-h-y}{d-y}\right)$ 
end if;
# The intervals have not been correctly specified, this does not influence the shape of the
bending moment distribution a lot and has therefore not been corrected
> plot(Mz, 0 .. (h + d))

```



> # The graph illustrates the shape of the bending moment distribution, the field and fixed moments have to be multiplied by 0.75 and 0.9 respectively

> $T := 1.15 \cdot T;$

$T := -168.7489941$

(12)

C. Evaluation of different modelling methods within Plaxis 2D

Appendix C – Modifications within Plaxis 2D

In this appendix some modifications to the Plaxis 2D model will be discussed, their effect on the stability and whether or not their results are plausible will also be determined and compared. The scenario that will be used for the sensitivity analysis regarding the modelling decisions is a combination of SIF 1 and SIF 2.

The different scenarios that will be analyzed are:

- OCR of 1;
- Presence of the layer of Kedichem (deep clay layer);
- Bearing piles as fixed anchors;
- Top of the M.V.-piles as an embedded beam row;
- Relieving platform as a set of plate elements;
- Different soil material models.

For comparisons sake the original model will also be shown. Based on the findings of this appendix this model may however be altered to better simulate the reality.

The modified models will now briefly be discussed along with their characteristics. The mesh was kept the same through all the models. To better see the reaction to the modifications, the surcharge was hidden in the figures that are presented in this appendix, it is however present in all the models.

Original model

This model was composed as follows:

- All soil types as modelled as “Hardening soil”;
- Relieving platform as a soil polygon;
- M.V.-piles as a combination of a node-to-node anchor and an embedded beam row;
- OCR of the Holocene soil layers (B, C, and D) of 1.7, Pleistocene layers (E and deeper) 2.5;
- Bearing piles as embedded beam rows;
- No deeper laying clay layer.

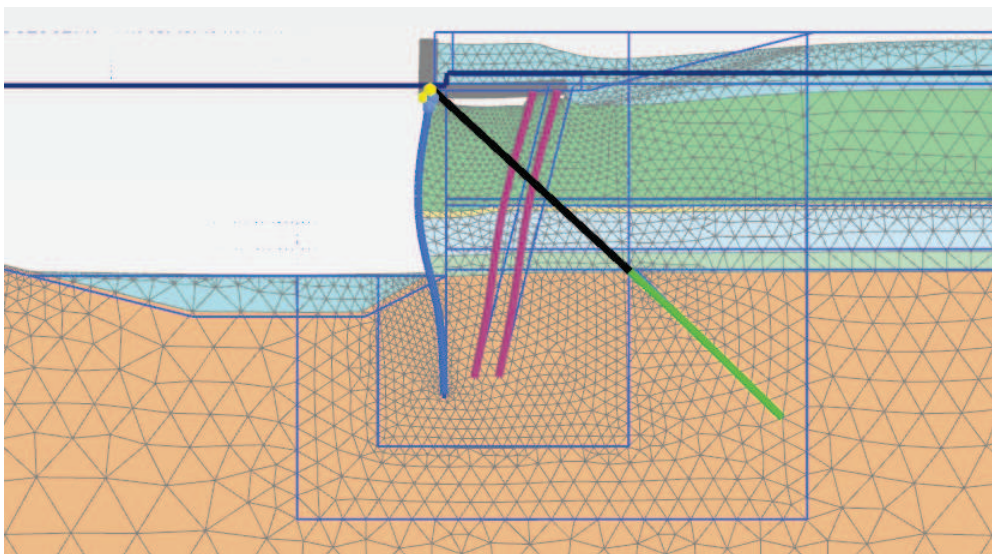


Figure 1 - Deformed mesh of the original SIF 2 model, scaled up 25 times

OCR = 1

The modification that was applied to this model is:

- The OCR of all the soil layers has been set to 1.

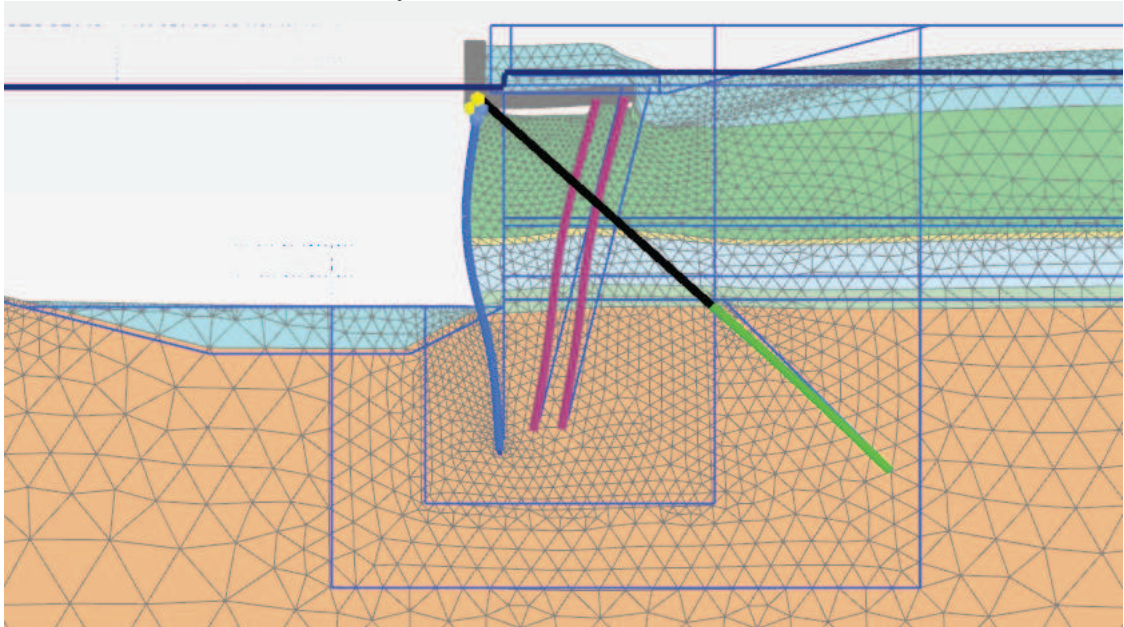


Figure 2 - Deformed mesh of the OCR = 1 model, scaled up 25 times

Kedichem layer

The modification that was applied to this model is:

- The layer of Kedichem has been added.

The characteristics of the clay layer have been copied from layer E (Wijchense clay layer). Should the effect of the clay layer make a substantial difference, then the characteristics will be analysed further. The same goes for the position and thickness of the layer, in this model the layer is present from NAP-43 m to NAP-45 m while in reality this varies greatly per cross section.

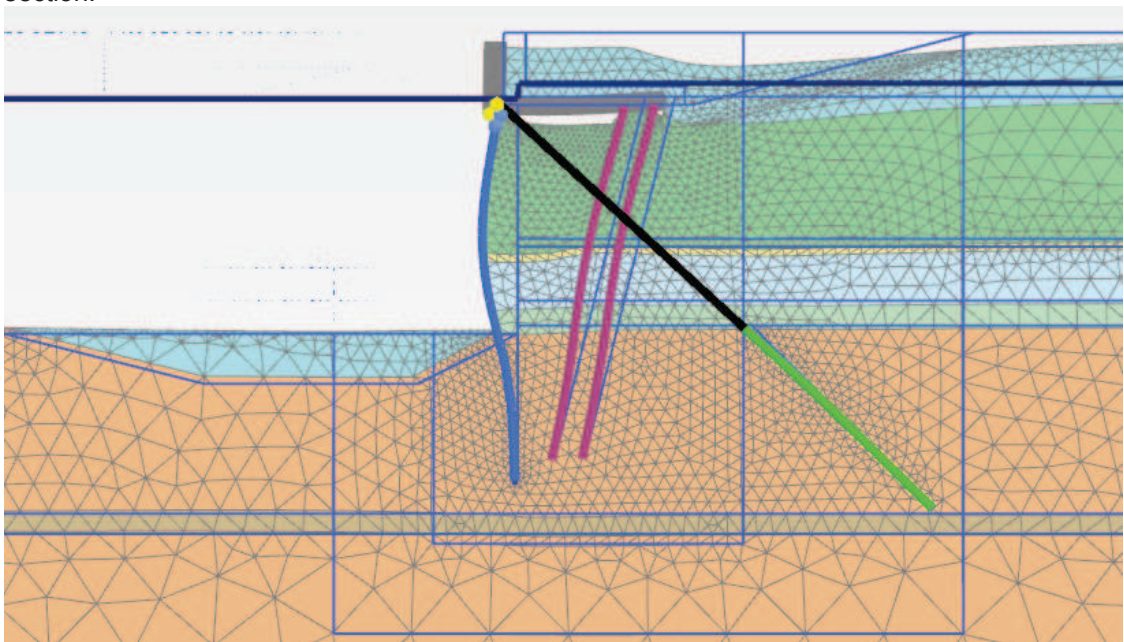


Figure 3 - Deformed mesh of the Kedichem layer model, scaled up 25 times

Bearing piles as fixed anchors

The modification that was applied to this model is:

- The bearing piles have been modelled as fixed end anchors instead of as embedded beam rows.

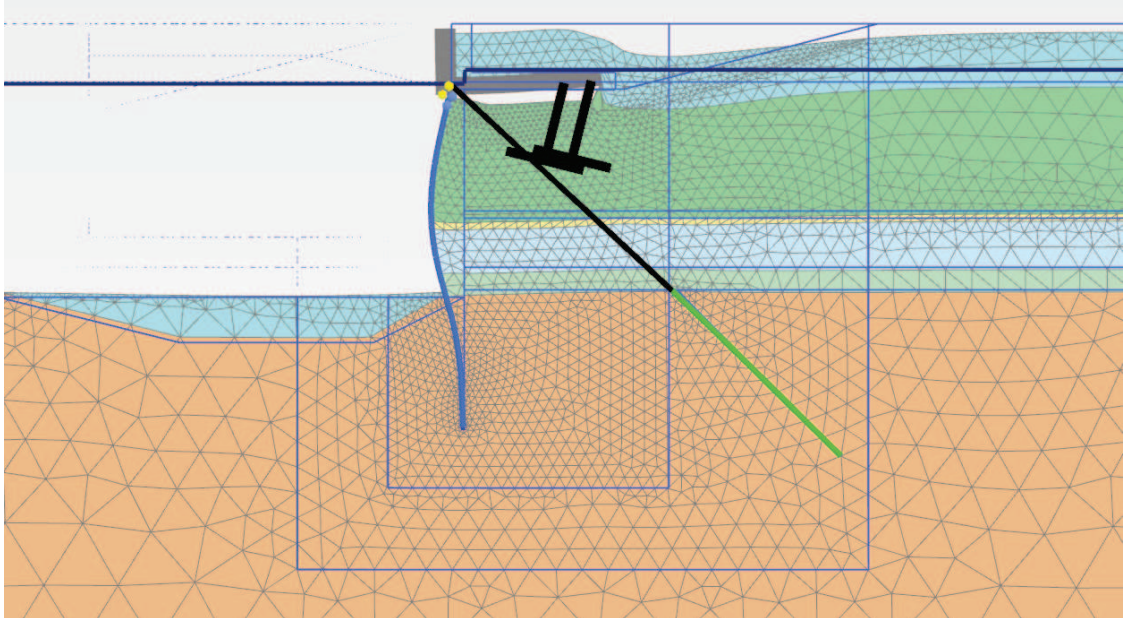


Figure 4 - Deformed mesh of the fixed bearing piles model, scaled up 25 times

M.V.-piles as a fixed anchor

The modification that was applied to this model is:

- The M.V.-piles have been modelled as fixed end anchors instead of a combination of node-to-node anchors and embedded beam rows.

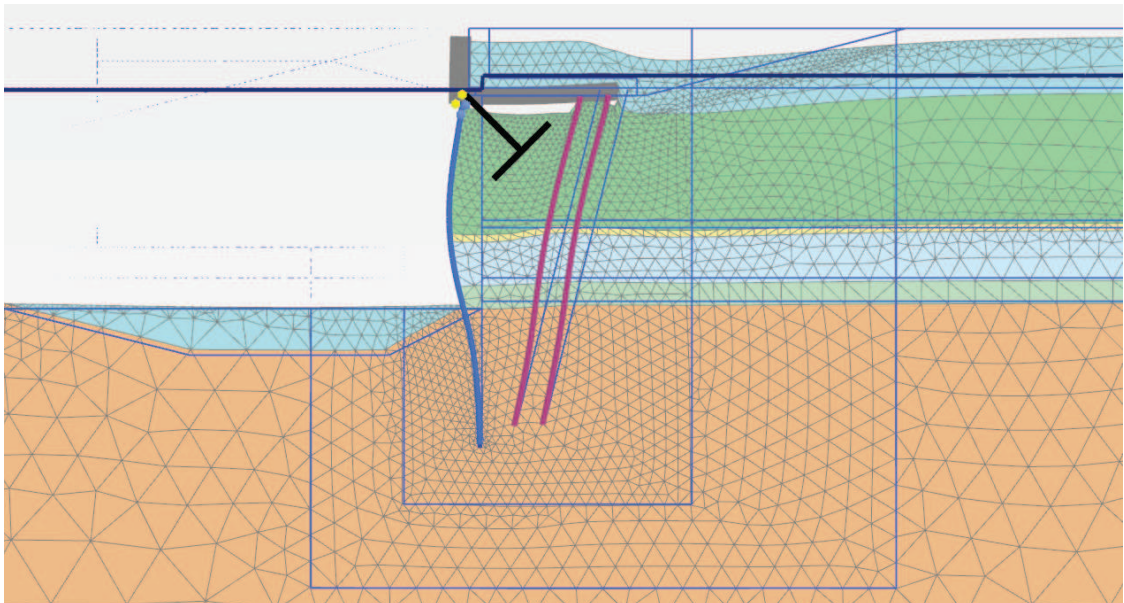


Figure 5 - Deformed mesh of the fixed M.V.-piles model, scaled up 25 times

Relieving platform as plate elements

The modification that was applied to this model is:

- The relieving platform has been modelled as a set of plate elements instead of as a soil polygon.

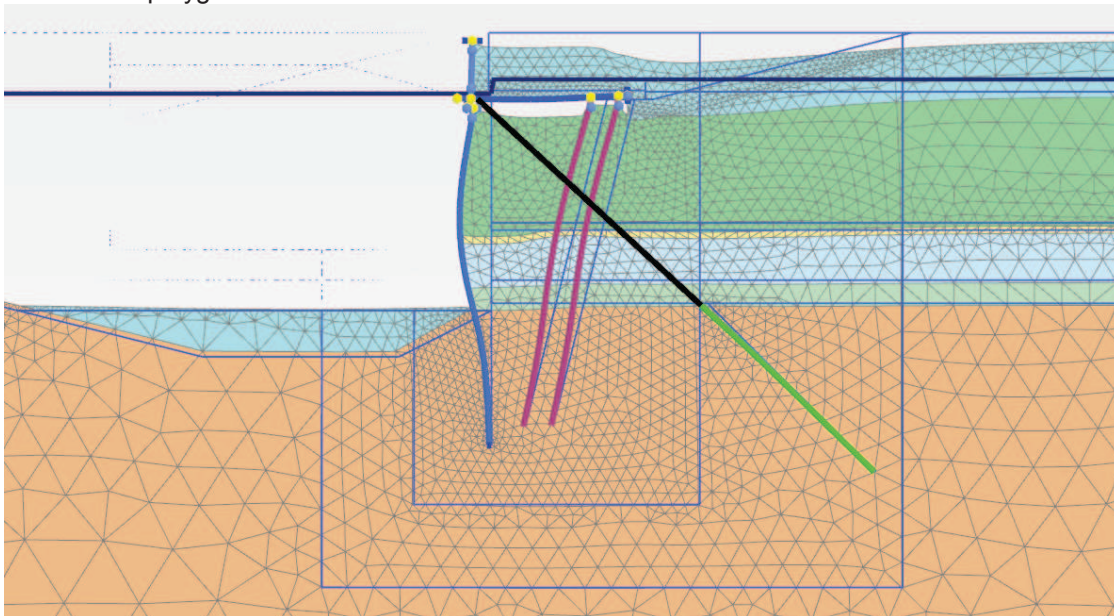


Figure 6 - Deformed mesh of the RP as plates model, scaled up 25 times

Different material models

The modifications that were applied to this model are:

- The soil layers have been modelled with different material models. Table 2 shows which model has been applied to which soil layer.

Table 1 - Material Models that were considered

Material model	Description and limitations
Mohr-Coulomb	<ul style="list-style-type: none"> • Linear elastic perfectly plastic • Does not use all the features of soil • Good as a first approximation of the soil behaviour
Hardening Soil	<ul style="list-style-type: none"> • Advanced soil model • Does not use all the features of the soil (softening and debonding) • Long calculation times • Applicable to soft as well as stiff soil types • Not suitable for very soft soils with a high compressibility ($E_{oed}/E_{50} < 0.5$)
Hardening Soil with small-strain stiffness	<ul style="list-style-type: none"> • Same basic principles as the Hardening Soil model • Applicable to cyclic loading • Even longer calculation times • More accurate un- and reloading modelling
Soft Soil	<ul style="list-style-type: none"> • Primarily used for compression situation • Not applicable for excavation/unloading scenarios • Applicable or near-normally consolidated clays, clayey silts and peat

Soft Soil Creep	<ul style="list-style-type: none"> • Same basic principles as the Soft Soil model • Over-predicts the range of the elastic soil behaviour • Takes creep into consideration
Modified Cam-Clay	<ul style="list-style-type: none"> • Same limitations as Soft Soil Creep • Allows unrealistically high shear stresses • Can't be used in combination with phi-c reduction

Based on the findings that were presented in Table 1 and Appendix B of the Material Model Manual of Plaxis 2D the following decisions were made regarding what Material Model to use for the different soil layers. To be able to accurately determine the effect of the modifications the OCR has been set to both 1 and the original values.

Table 2 - Soil layers and their assigned material model

Soil layer	Selected material model
A – Sand	Hardening Soil with small-strain
B – Sand	Hardening Soil with small-strain
C – Silt	Hardening Soil with small-strain
D – Sand	Hardening Soil with small-strain
E – Clay	OCR = 1: Soft soil (soil parameters copied from tutorial 2 of the Plaxis 2D tutorial manual) OCR = Original: Hardening Soil with small-strain
F – Sand	Hardening Soil with small-strain

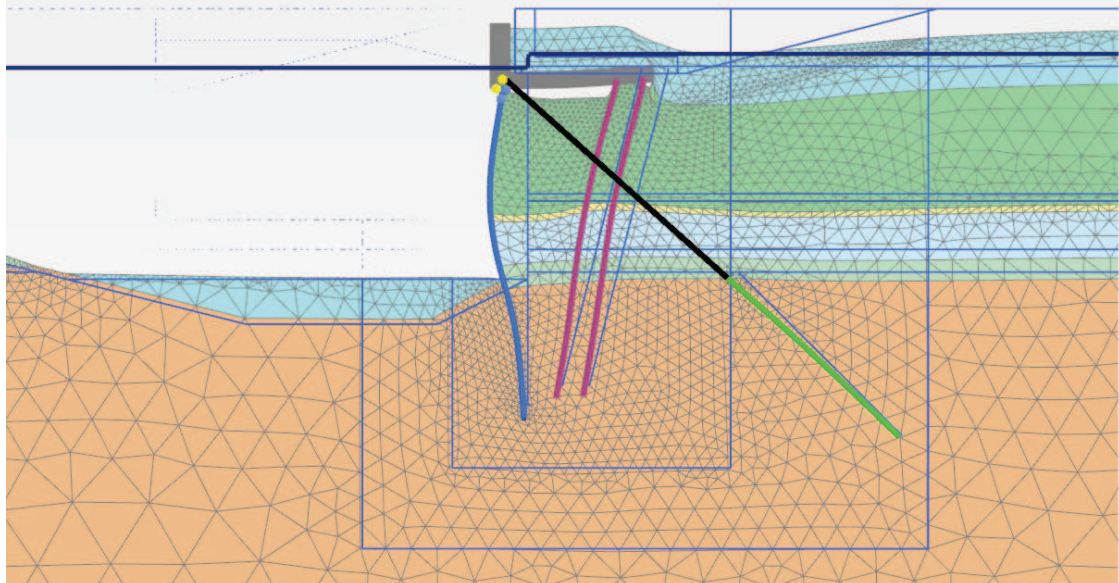


Figure 7 - Deformed mesh of the material model with OCR=1, scaled up 25 times

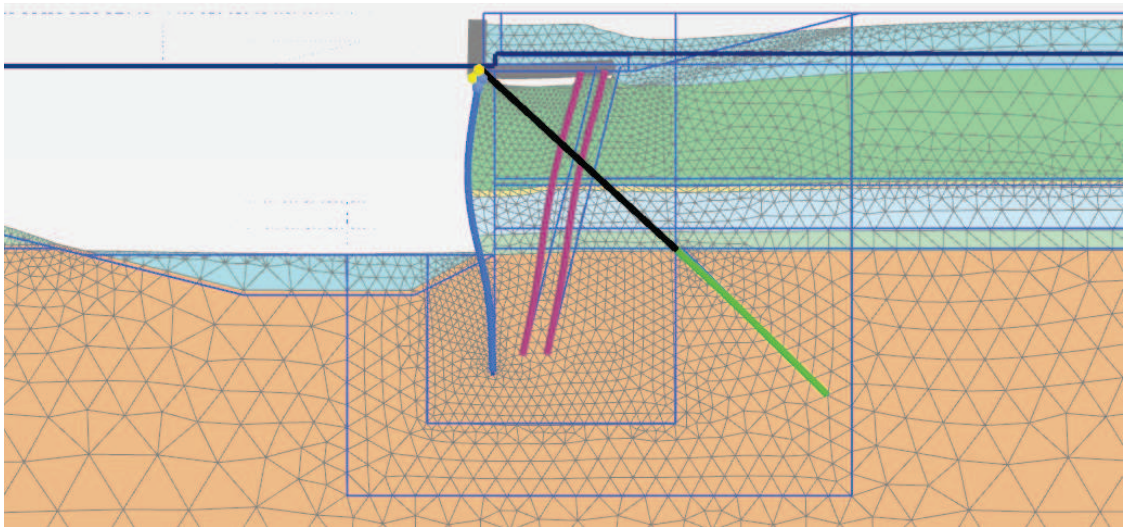


Figure 8 - Deformed mesh of the material model, scaled up 25 times

Evaluation

The results of all the different models are presented in Table 3. The results have also been normalized with respect to the original model, the results of this step are presented in Table 3. The normalized results, with respect to the original situation have also been visualized in , t gain more accuracy presents the same results only without the largely diverging models.

Table 3 - Reactions of the different models

Scenario	$N_{cspw,top}$	M_{field}	M_{fixed}	$F_{M.V.-piles}$	$N_{bp,left}$	$N_{bp,right}$	$U_{top,horiz}$	$U_{field,horiz}$
	kN/m	kNm/m	kNm/m	kN/m	kN/m	kN/m	mm	mm
Original	2,522.9	1,999.2	-1,539.0	1,024.7	1,573.7	1,168.9	80.2	139.0
OCR = 1	2,499.3	1,972.7	-1,552.3	996.0	1,584.1	1,163.0	112.2	161.2
Kedichem	2,515.6	2,004.2	-1,553.4	1,017.9	1,587.4	1,158.6	83.2	141.8
BP fixed	2,495.5	2,273.5	-1,783.6	1,137.0	2,390.6	662.3	67.4	146.5
M.V. fixed	2,512.0	1,991.7	-1,560.3	998.9	1,571.1	1,182.8	85.2	141.1
RP as plates	2,486.5	2,006.5	-1,549.9	1,001.5	1,567.4	1,156.1	78.4	138.1
Material Models_{OCR=1}	2,496.8	2,094.7	-1,589.0	989.9	1,585.6	1,145.2	111.6	168.3
Material Models_{original}	2,516.7	1,945.1	-1,552.0	1,027.8	1,610.4	1,144.3	78.9	134.4

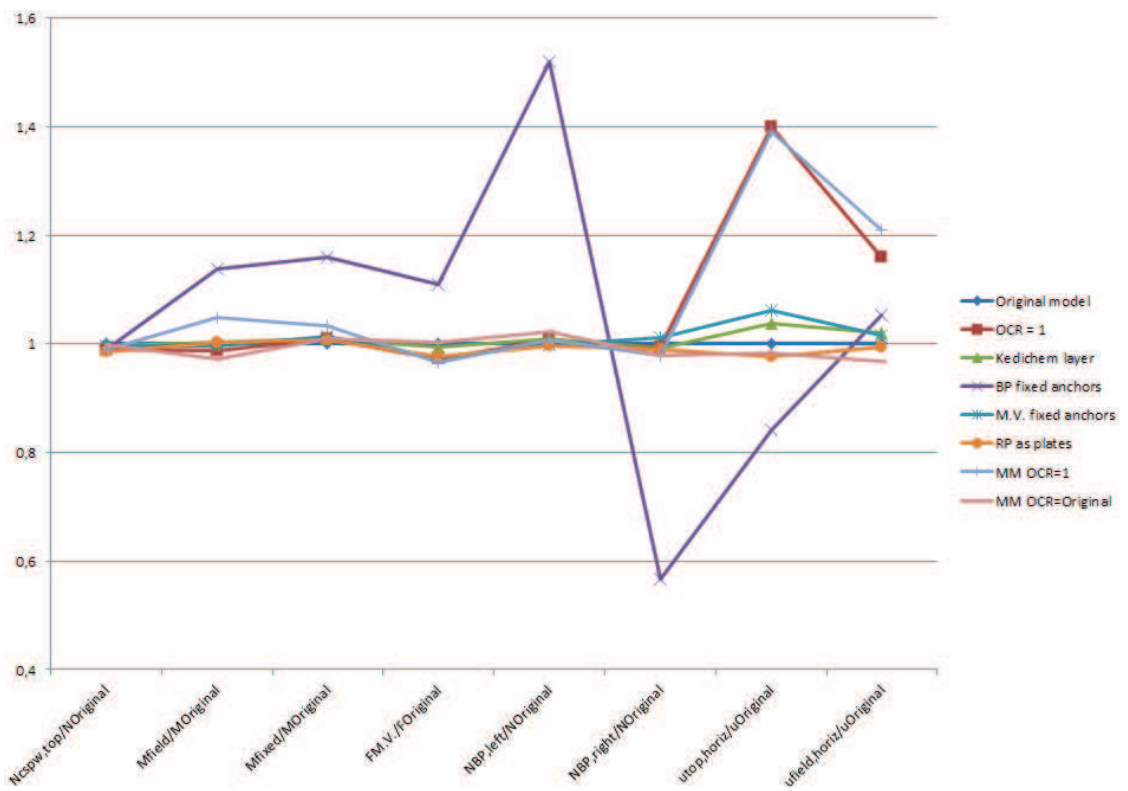


Figure 9 - Normalized result of the modification analysis

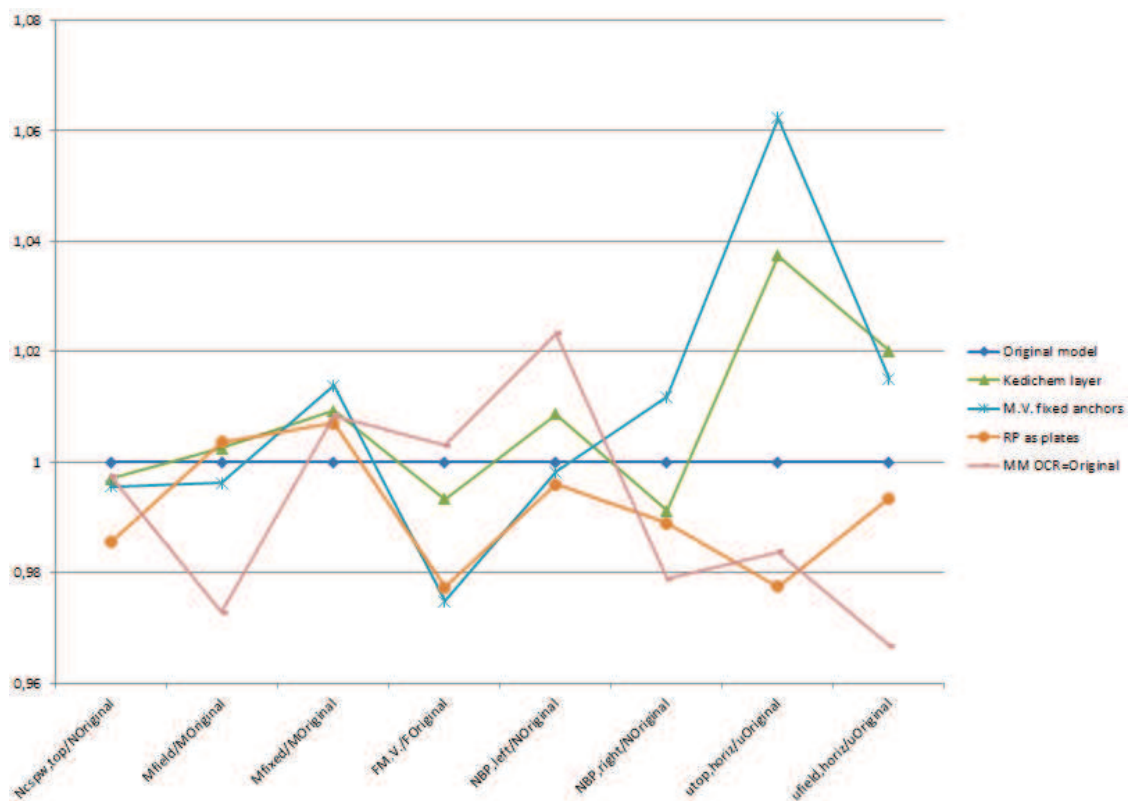


Figure 10 - Normalized results of the modification analysis, excluding the diverging models

D. Critical assessment of the Plaxis 2D models

Appendix D - Critical assessment of the models

In this appendix the created models will be subjected to several tests. The objective of this assessment is to verify whether or not all the relevant areas of interest have been incorporated in the models properly.

Drained or undrained behaviour

In [24] R. Brinkgreve presents a formula to determine whether the soil should be modelled as drained or undrained. The formula is presented below:

$$T = \frac{kE_{oed}}{\gamma_w D^2} t$$

In which:

- T = hydrodynamic period [-]
- k = soil permeability [m/s]
- E_{oed} = oedometer stiffness [kN/m²]
- γ_w = unit weight of water [kN/m³]
- D = drainage length [m]
- t = Construction or loading time [s]

If $T < 0.01$ the soil should be modelled as undrained, if $T > 0.4$ the soil can be modelled as drained since sufficient consolidation can take place during the loading. For the values in between, the least favourable situation should be used: undrained for loading and drained for unloading.

In Table 1 the different weak soil layers have been presented along with their relevant properties, the soil permeability of the different soil types have been estimated based on the range given by A. Verruijt in [4].

Table 1 - Calculation of the needed loading times

Scenario	Soil type	D	k	$t_{undrained}$	$t_{drained}$
	[-]	[m]	[m/s]	[d]	[days]
Amazonehaven 1	Silt	1.75	10^{-7}	<0.0	>0.3
Amazonehaven 1	Clay	2.25	10^{-9}	<1.2	>46.9
Amazonehaven 2	Clay	0.75	10^{-9}	<0.1	>5.2
SIF 1	Silt	0.4	10^{-7}	<0.0	>0.0
SIF 1	Clay	1.25	10^{-9}	<0.4	>14.5
SIF 2	Silt	0.2	10^{-7}	<0.0	>0.0
SIF 2	Clay	3.95	10^{-9}	<3.6	>144.5

The quay structures will be used for the storage of goods, it is very likely that the storing of these goods, i.e. the application of the load, will not be instantaneous but will take at least a few days if not weeks. From the table it follows that the silt layers can be modelled as drained materials, the clay layers however show much larger necessary loading times to qualify as drained material. To be certain of whether the material acts as drained or undrained material, more research is needed about the hydraulic conductivity of the different soil layers and the loading time.

Failure mechanisms

This paragraph presents the findings of the failure mechanism analysis. The design step of the final model of SIF 2 has been modified so that it triggers a certain failure mechanism. The modification that has been applied will be elaborated on, along with the corresponding result.

Exceedance of the bearing capacity of the bearing piles

This check was performed by reducing both the maximum skin friction and the end bearing capacity of the bearing piles.

The expected result was that after the critical load had been reached, the RP would make contact with the soil underneath it and start transferring the excess load towards it. The soil will then transfer it to the CSPW again, resulting in larger deformations and bending moments. The results of the modified model are shown in Figure 1.

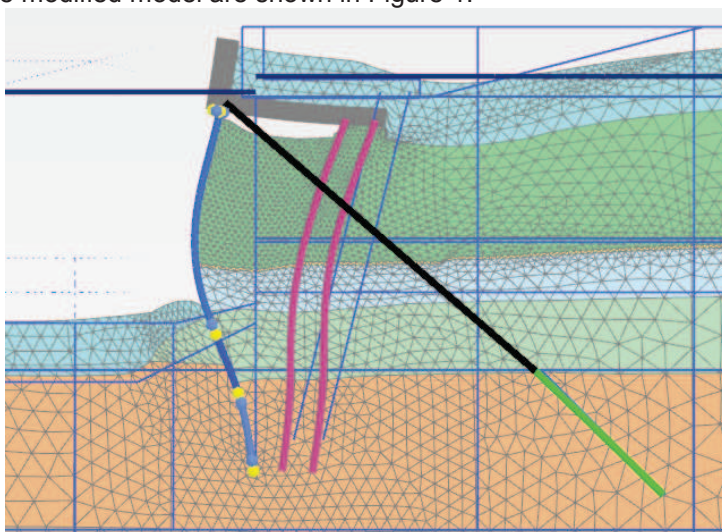


Figure 1 - Deformed mesh of the bearing capacity model, scaled up 25 times

The results of the modified model are in line with the expected results. The model does take this failure mechanism into consideration.

Exceedance of the bending moment capacity of the combined sheet pile wall

The modification was applied by modelling the CSPW as an elastoplastic plate element with a reduced plastic moment.

The expected result was that the CSPW would show a kink at the location of the maximum bending moment, after this initial kink the deflection in the field would grow drastically, resulting in the instability of the soil behind it and the collapse of the RP.

The results of the modified model are shown in Figure 2.

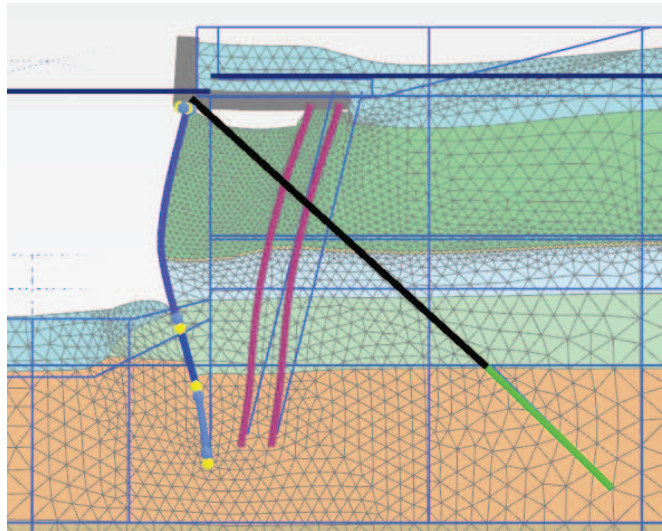


Figure 2 - Deformed mesh of the maximum bending moment model, scaled up 25 times

The results of the modified model are in line with the expected results. The model does take this failure mechanism into consideration.

Insufficient length of the combined sheet pile wall

The modification was applied by reducing the length of the CSPW and removing the surcharge from the waterside of the structure.

The expected result was that the soil on the waterside would not be able to build up enough resistance and would show large deformations, resulting in the collapse of the soil behind the RP.

The results of the modified model are shown in Figure 3.

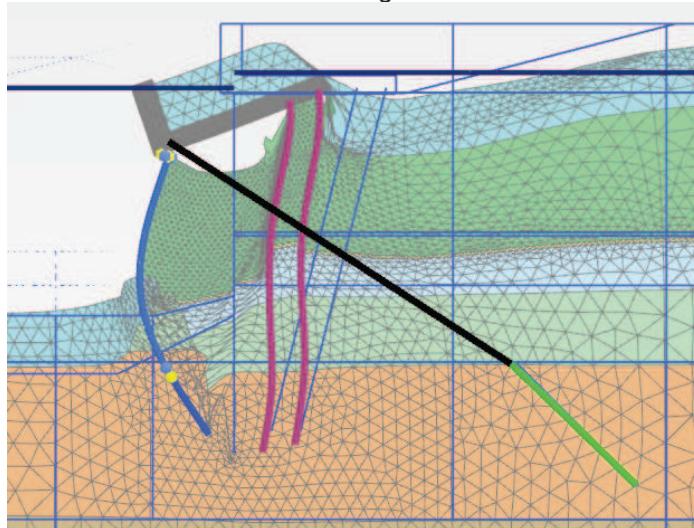


Figure 3 - Deformed mesh of the insufficient length model, scaled up 25 times

The model does take this failure mechanism into consideration. Due to the high vertical load on top of the combined sheet pile wall however, the toe of the combined wall moves both towards the waterside and downwards, resulting in the collapse of the RP before larger horizontal deflection of the toe of the structural element occur.

Yielding of the M.V.-piles

This modification was applied by reducing the EA of the M.V.-piles.

The expected result was that the bearing piles would have to compensate for the lack of horizontal resistance. This would result in larger deflections, larger shear forces in the bearing piles, and larger bending moments in the CSPW.

The results of the modified model are shown in Figure 4.

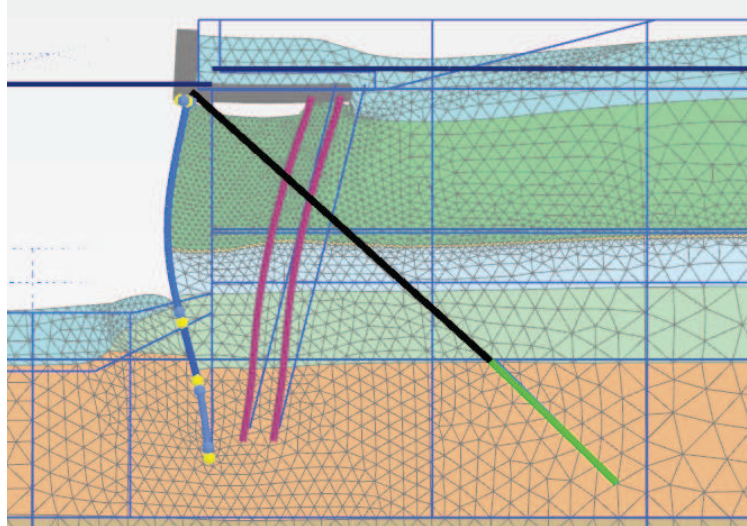


Figure 4 - Deformed mesh of the M.V.-piles yielding model, scaled up 25 times

The results of the modified model are in line with the expected results. The model does take this failure mechanism into consideration.

Exceedance of the geotechnical bearing capacity of the M.V.-piles

This modification was applied by reducing the maximum geotechnical friction of the effective part of the M.V.-piles.

The expected effect was the same as that of the yielding of the M.V.-piles.

The results of the modified model are shown in Figure 5.

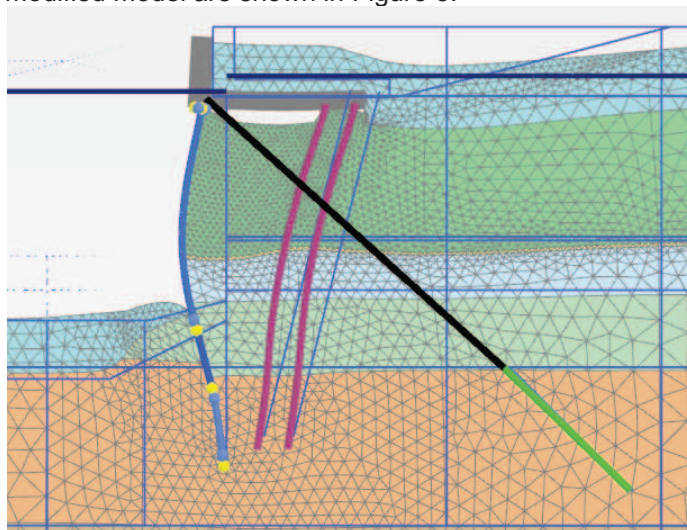


Figure 5 - Deformed mesh of the M.V.-piles geotechnical model, scaled up 25 times

The results of the modified model are in line with the expected results. The model does take this failure mechanism into consideration.